161

CENTRAL RESEARCH LIBRARY
DO

MARTIN MARIETTA ENERGY SYSTEMS LIBRARIES
3 4456 0364415 3

ORNL-3157
UC-80—Reactor Technology

EXPERIMENTAL STRESS ANALYSIS OF EGCR PRESSURE VESSEL

B. L. Greenstreet
R. W. Holland
M. E. LaVerne
R. L. Maxwell
L. R. Shobe
F. J. Witt

CENTRAL RESEARCH LIBRARY
DOCUMENT COLLECTION
LIBRARY LOAN COPY
DO NOT TRANSFER TO ANOTHER PERSON
If you wish someone else to see this document, send in name with document and the library will arrange a loan.

OAK RIDGE NATIONAL LABORATORY
operated by
UNION CARBIDE CORPORATION
for the
U.S. ATOMIC ENERGY COMMISSION

Printed in USA. Price $3.50. Available from the

Office of Technical Services
Department of Commerce
Washington 25, D.C.

LEGAL NOTICE

This report was prepared as an account of Government sponsored work. Neither the United States, nor the Commission, nor any person acting on behalf of the Commission:

A. Makes any warranty or representation, expressed or implied, with respect to the accuracy, completeness, or usefulness of the information contained in this report, or that the use of any information, apparatus, method, or process disclosed in this report may not infringe privately owned rights; or

B. Assumes any liabilities with respect to the use of, or for damages resulting from the use of any information, apparatus, method, or process disclosed in this report.

As used in the above, "person acting on behalf of the Commission" includes any employee or contractor of the Commission, or employee of such contractor, to the extent that such employee or contractor of the Commission, or employee of such contractor prepares, disseminates, or provides access to, any information pursuant to his employment or contract with the Commission, or his employment with such contractor.

ORNL-3157

UC-80—Reactor Technology
TID-4500 (16th ed.)

Contract No. W-7405-eng-26

REACTOR DIVISION

EXPERIMENTAL STRESS ANALYSIS OF EGCR PRESSURE VESSEL

Part 1. Experimental Determination of Stresses in Model

R. W. Holland R. L. Maxwell

Part 2. Interpretation of Experimental Results and Examination for Structural Integrity

F. J. Witt B. L. Greenstreet
L. R. Shobe M. E. LaVerne
R. L. Maxwell

DATE ISSUED

AUG 24 1959

OAK RIDGE NATIONAL LABORATORY
Oak Ridge, Tennessee
operated by
UNION CARBIDE CORPORATION
for the
U. S. ATOMIC ENERGY COMMISSION

MARTIN MARIETTA ENERGY SYSTEMS LIBRARIES

3 4456 0364415 3

CONTENTS

	Page
ABSTRACT	xv
INTRODUCTION	1
PART 1. EXPERIMENTAL DETERMINATION OF STRESSES IN MODEL	7
Description of Model	9
Experimental Procedure	10
Results	13
PART 2. INTERPRETATION OF EXPERIMENTAL RESULTS AND EXAMINATION FOR STRUCTURAL INTEGRITY	31
Nomenclature	31
Introduction	32
Dimensional Analysis	33
Analysis of the Pressure Vessel	34
Internal Pressure and Nozzle Loads	35
Nozzle Analysis	35
Head Analysis	39
Discussion of Results	40
Torsional Loads on the Nozzles	41
Thermal Stresses in the Nozzles and Head	42
Examination for Structural Integrity	43
Stresses and Stress Concentrations	43
Examination of the Design	52
Nozzle A	52
Nozzle B	60
Nozzle K	67
Gas Outlet Nozzle	73
Head Around Nozzle B	75
Conclusions	81
Appendix A. Experimental Results	139
List of Tables	141
Appendix B. Stresses in Full-Scale Pressure Vessel	223
List of Tables	224

Page

Appendix C. Analytical Study and Comparison of Experimental and Theoretical Results 243

List of Figures 247

List of Figures

		Page
Fig. 1.	EGCR Pressure Vessel Elevation.	2
Fig. 2.	EGCR Pressure Vessel Plan and Section.	3
Fig. 3.	EGCR Pressure Vessel Model – Plan View.	15
Fig. 4.	EGCR Pressure Vessel Model – Elevation.	16
Fig. 5.	Photograph of Machined Vessel Ready for Drilling of Holes and Attaching Nozzles.	17
Fig. 6.	Photograph of Outside of Vessel Ready for Attachment of Gages.	18
Fig. 7.	Photograph of Inside of Vessel Ready for Attachment of Gages.	19
Fig. 8.	Instrumented Portion of Shell.	20
Fig. 9.	Gage Locations on Section A of Fig. 8 and Along Cylindrical Portion of Shell.	21
Fig. 10.	Gage Locations on Section B of Fig. 8 and Along Cylindrical Portion of Shell.	22
Fig. 11.	Typical Gage Locations on a Nozzle.	23
Fig. 12.	Gage Locations on Inner Surface of Gas Outlet Nozzle and Its Extension Inside the Head.	24
Fig. 13.	Tangential Stress Distribution Around Hole in Perforated Plate for a/b = 0.27.	25
Fig. 14.	Stresscoat Crack Pattern on Perforated Plate in Bending.	26
Fig. 15.	Photograph of Gages in Place Inside Dome.	27
Fig. 16.	Photograph of Gages in Place Outside Dome with Shell in Frame Ready for Testing.	28
Fig. 17.	Photograph of Gage Installation on and Near Nozzle A.	29
Fig. 18.	Stress Distributions on Outer Surface of Nozzle A from 350-psig Pressure Loading.	82
Fig. 19.	Stress Distributions on Inner Surface of Nozzle A from 350-psig Pressure Loading.	82
Fig. 20.	Stress Distributions on Outer Surface of Nozzle A from Axial Tensile Loading of 1 lb/in. Along Mean Circumference.	83
Fig. 21.	Stress Distributions on Inner Surface of Nozzle A from Axial Tensile Loading of 1 lb/in. Along Mean Circumference.	83

Page

Fig. 22. Stress Distributions on Outer Surface of Nozzle A from Simultaneous Axial Tensile Loadings of 1 lb/in. Along Mean Circumference on Each of the B Nozzles. 84

Fig. 23. Stress Distributions on Inner Surface of Nozzle A from Simultaneous Axial Tensile Loadings of 1 lb/in. Along Mean Circumference on Each of the B Nozzles. 84

Fig. 24. Stress Distributions on Outer Surface of Nozzle B from 350-psig Pressure Loading (Uphill Side). 85

Fig. 25. Stress Distributions on Inner Surface of Nozzle B from 350-psig Pressure Loading (Uphill Side). 85

Fig. 26. Stress Distributions on Outer Surface of Nozzle B from 350-psig Pressure Loading (Downhill Side). 85

Fig. 27. Stress Distributions on Inner Surface of Nozzle B from 350-psig Pressure Loading (Downhill Side). 85

Fig. 28. Stress Distributions on Outer Surface of Nozzle B from Axial Tensile Loading of 1 lb/in. Along Mean Circumference (Uphill Side). 86

Fig. 29. Stress Distributions on Inner Surface of Nozzle B from Axial Tensile Loading of 1 lb/in. Along Mean Circumference (Uphill Side). 86

Fig. 30. Stress Distributions on Outer Surface of Nozzle B from Axial Tensile Loading of 1 lb/in. Along Mean Circumference (Downhill Side). 87

Fig. 31. Stress Distributions on Inner Surface of Nozzle B from Axial Tensile Loading of 1 lb/in. Along Mean Circumference (Downhill Side). 87

Fig. 32. Stress Distributions on Outer Surface of Nozzle B from Simultaneous Axial Tensile Loadings of 1 lb/in. Along Mean Circumference on Each of the B Nozzles (Downhill Side). 88

Fig. 33. Stress Distributions on Inner Surface of Nozzle B from Simultaneous Axial Tensile Loadings of 1 lb/in. Along Mean Circumference on Each of the B Nozzles (Downhill Side). 88

Fig. 34. Stress Distributions on Outer Surface of Nozzle J from 350-psig Pressure Loading (Uphill Side). 89

Fig. 35. Stress Distributions on Inner Surface of Nozzle J from 350-psig Pressure Loading (Uphill Side). 89

Fig. 36. Stress Distributions on Outer Surface of Nozzle J from 350-psig Pressure Loading (Downhill Side). 90

Page

Fig. 37. Stress Distributions on Inner Surface of Nozzle J from 350-psig Pressure Loading (Downhill Side). 90

Fig. 38. Stress Distributions on Outer Surface of Nozzle J from Axial Tensile Loading of 1 lb/in. Along Mean Circumference (Uphill Side). 91

Fig. 39. Stress Distributions on Inner Surface of Nozzle J from Axial Tensile Loading of 1 lb/in. Along Mean Circumference (Uphill Side). 91

Fig. 40. Stress Distributions on Outer Surface of Nozzle J from Axial Tensile Loading of 1 lb/in. Along Mean Circumference (Downhill Side). 92

Fig. 41. Stress Distributions on Inner Surface of Nozzle J from Axial Tensile Loading of 1 lb/in. Along Mean Circumference (Downhill Side). 92

Fig. 42. Stress Distributions on Outer Surface of Nozzle K from 350-psig Pressure Loading (Uphill Side). 93

Fig. 43. Stress Distributions on Inner Surface of Nozzle K from 350-psig Pressure Loading (Uphill Side). 93

Fig. 44. Stress Distributions on Outer Surface of Nozzle K from 350-psig Pressure Loading (Downhill Side). 94

Fig. 45. Stress Distributions on Inner Surface of Nozzle K from 350-psig Pressure Loading (Downhill Side). 94

Fig. 46. Stress Distributions on Outer Surface of Nozzle K from Axial Tensile Loading of 1 lb/in. Along Mean Circumference (Uphill Side). 95

Fig. 47. Stress Distributions on Inner Surface of Nozzle K from Axial Tensile Loading of 1 lb/in. Along Mean Circumference (Uphill Side). 95

Fig. 48. Stress Distributions on Outer Surface of Nozzle K from Axial Tensile Loading of 1 lb/in. Along Mean Circumference (Downhill Side). 96

Fig. 49. Stress Distributions on Inner Surface of Nozzle K from Axial Tensile Loading of 1 lb/in. Along Mean Circumference (Downhill Side). 96

Fig. 50. Stress Distributions on Outer Surface of Nozzle L from 350-psig Pressure Loading (Uphill Side). 97

Fig. 51. Stress Distributions on Inner Surface of Nozzle L from 350-psig Pressure Loading (Uphill Side). 97

Fig. 52. Stress Distributions on Outer Surface of Nozzle L from 350-psig Pressure Loading (Downhill Side). 98

Page

Fig. 53. Stress Distributions on Inner Surface of Nozzle L from 350-psig Pressure Loading (Downhill Side). 98

Fig. 54. Stress Distributions on Outer Surface of Nozzle L from Axial Tensile Loading of 1 lb/in. Along Mean Circumference (Uphill Side). 99

Fig. 55. Stress Distributions on Inner Surface of Nozzle L from Axial Tensile Loading of 1 lb/in. Along Mean Circumference (Uphill Side). 99

Fig. 56. Stress Distributions on Outer Surface of Nozzle L from Axial Tensile Loading of 1 lb/in. Along Mean Circumference (Downhill Side). 100

Fig. 57. Stress Distributions on Inner Surface of Nozzle L from Axial Tensile Loading of 1 lb/in. Along Mean Circumference (Downhill Side). 100

Fig. 58. Stress Distributions on Outer Surface of Nozzle M from 350-psig Pressure Loading (Uphill Side). 101

Fig. 59. Stress Distributions on Inner Surface of Nozzle M from 350-psig Pressure Loading (Uphill Side). 101

Fig. 60. Stress Distributions on Outer Surface of Nozzle M from 350-psig Pressure Loading (Downhill Side). 102

Fig. 61. Stress Distributions on Inner Surface of Nozzle M from 350-psig Pressure Loading (Downhill Side). 102

Fig. 62. Stress Distributions on Outer Surface of Nozzle M from Axial Tensile Loading of 1 lb/in. Along Mean Circumference (Uphill Side). 103

Fig. 63. Stress Distributions on Inner Surface of Nozzle M from Axial Tensile Loading of 1 lb/in. Along Mean Circumference (Uphill Side). 103

Fig. 64. Stress Distributions on Outer Surface of Nozzle M from Axial Tensile Loading of 1 lb/in. Along Mean Circumference (Downhill Side). 104

Fig. 65. Stress Distributions on Inner Surface of Nozzle M from Axial Tensile Loading of 1 lb/in. Along Mean Circumference (Downhill Side). 104

Fig. 66. Stress Distributions on Outer Surface of Burst-Slug-Detection Nozzle from 350-psig Pressure Loading. 105

Fig. 67. Stress Distributions on Inner Surface of Burst-Slug-Detection Nozzle from 350-psig Pressure Loading. 105

Fig. 68. Stress Distributions on Outer Surface of Gas Outlet Nozzle from 350-psig Pressure Loading (Uphill Side). 106

Page

Fig. 69. Stress Distributions on Inner Surface of Gas Outlet Nozzle from 350-psig Pressure Loading (Uphill Side). 106

Fig. 70. Stress Distributions on Outer Surface of Gas Outlet Nozzle from 350-psig Pressure Loading (Downhill Side). 107

Fig. 71. Stress Distributions on Inner Surface of Gas Outlet Nozzle from 350-psig Pressure Loading (Downhill Side). 107

Fig. 72. Stress Distributions on Outer Surface of Gas Outlet Nozzle from 350-psig Pressure Loading (Side 90 deg from Uphill Side). 108

Fig. 73. Stress Distributions on Inner Surface of Gas Outlet Nozzle from 350-psig Pressure Loading (Side 90 deg from Uphill Side). 108

Fig. 74. Stress Distributions on Outer Surface of Gas Outlet Nozzle from Axial Tensile Loading of 1 lb/in. Along Mean Circumference (Uphill Side). 109

Fig. 75. Stress Distributions on Inner Surface of Gas Outlet Nozzle from Axial Tensile Loading of 1 lb/in. Along Mean Circumference (Uphill Side). 109

Fig. 76. Stress Distributions on Outer Surface of Gas Outlet Nozzle from Axial Tensile Loading of 1 lb/in. Along Mean Circumference (Downhill Side). 109

Fig. 77. Stress Distributions on Inner Surface of Gas Outlet Nozzle from Axial Tensile Loading of 1 lb/in. Along Mean Circumference (Downhill Side). 109

Fig. 78. Stress Distributions on Outer Surface of Gas Outlet Nozzle from Axial Tensile Loading of 1 lb/in. Along Mean Circumference (Side 90 deg from Uphill Side). 110

Fig. 79. Stress Distributions on Inner Surface of Gas Outlet Nozzle from Axial Tensile Loading of 1 lb/in. Along Mean Circumference (Side 90 deg from Uphill Side). 110

Fig. 80. Sign Convention for Transverse Loadings and Applied Moments on Gas Outlet Nozzle. 111

Fig. 81. Stress Distributions on Outer Surface of Nozzle B from Transverse Load of 1 lb Directed Toward Nozzle A at a Distance of 139.7 in. Above the Apex (Uphill Side). 111

Fig. 82. Stress Distributions on Outer Surface of Nozzle B from Transverse Load of 1 lb Directed Toward Nozzle A at a Distance of 139.7 in. Above the Apex (Downhill Side). 112

Page

Fig. 83. Stress Distributions on Outer Surface of Nozzle B from Transverse Load of 1 lb Directed Toward Nozzle A at a Distance of 192.3 in. Above the Apex (Uphill Side). 112

Fig. 84. Stress Distributions on Outer Surface of Nozzle B from Transverse Load of 1 lb Directed Toward Nozzle A at a Distance of 192.3 in. Above the Apex (Downhill Side). 113

Fig. 85. Stress Distributions on Outer Surface of Nozzle K from Transverse Load of 1 lb Directed Toward Nozzle A at a Distance of 135.9 in. Above the Apex (Uphill Side). 113

Fig. 86. Stress Distributions on Outer Surface of Nozzle K from Transverse Load of 1 lb Directed Toward Nozzle A at a Distance of 135.9 in. Above the Apex (Downhill Side). 114

Fig. 87. Stress Distributions on Outer Surface of Gas Outlet Nozzle from Transverse Load of 1 lb Directed in $-F_z$ Direction at a Distance of 47.0 in. from the Junction (Uphill Side). 114

Fig. 88. Stress Distributions on Outer Surface of Gas Outlet Nozzle from Transverse Load of 1 lb Directed in $-F_z$ Direction at a Distance of 47.0 in. from the Junction (Downhill Side). 115

Fig. 89. Stress Distributions on Outer Surface of Gas Outlet Nozzle from Transverse Load of 1 lb Directed in F_y Direction at a Distance of 47.0 in. from the Junction (Side 90 deg from Uphill Side). 115

Fig. 90. Stress Distributions on Outer Surface of Gas Outlet Nozzle from an Applied Moment of 1 in.-lb Directed in M_z Direction (Uphill Side). 116

Fig. 91. Stress Distributions on Outer Surface of Gas Outlet Nozzle from an Applied Moment of 1 in.-lb Directed in M_z Direction (Downhill Side). 116

Fig. 92. Stress Distributions of Outer Surface of Gas Outlet Nozzle from an Applied Moment of 1 in.-lb Directed in M_y Direction (Side 90 deg from Uphill Side). 117

Fig. 93. Maximum Stresses (Absolute) for Nozzle A as a Function of Axial Load While Vessel Is Subjected to 350-psig Pressure Loading. 117

Fig. 94. Maximum Stresses (Absolute) for Nozzle A as a Function of Axial Loads Simultaneously Applied to Four B Nozzles While Vessel Is Subjected to 350-psig Pressure Loading. 118

Page

Fig. 95. Maximum Stresses (Absolute) for Nozzle B as a Function of Axial Load While Vessel is Subjected to 350-psig Pressure Loading (Downhill Side). 118

Fig. 96. Maximum Stresses (Absolute) for Nozzle B as a Function of Axial Load While Vessel Is Subjected to 350-psig Pressure Loading (Downhill Side). 119

Fig. 97. Maximum Stresses (Absolute) for Nozzle B as a Function of Axial Loads Simultaneously Applied to Four B Nozzles While Vessel is Subjected to 350-psig Pressure Loading (Downhill Side). 119

Fig. 98. Maximum Stresses (Absolute) for Nozzle J as a Function of Axial Load While Vessel is Subjected to 350-psig Pressure Loading (Uphill Side). 120

Fig. 99. Maximum Stresses (Absolute) for Nozzle J as a Function of Axial Load While Vessel Is Subjected to 350-psig Pressure Loading (Downhill Side). 120

Fig. 100. Maximum Stresses (Absolute) for Nozzle K as a Function of Axial Load While Vessel Is Subjected to 350-psig Pressure Loading (Uphill Side). 121

Fig. 101. Maximum Stresses (Absolute) for Nozzle K as a Function of Axial Load While Vessel Is Subjected to 350-psig Pressure Loading (Downhill Side). 121

Fig. 102. Maximum Stresses (Absolute) for Nozzle L as a Function of Axial Load While Vessel Is Subjected to 350-psig Pressure Loading (Uphill Side). 122

Fig. 103. Maximum Stresses (Absolute) for Nozzle L as a Function of Axial Load While Vessel Is Subjected to 350-psig Pressure Loading (Downhill Side). 122

Fig. 104. Maximum Stresses (Absolute) for Nozzle M as a Function of Axial Load While Vessel Is Subjected to 350-psig Pressure Loading (Uphill Side). 123

Fig. 105. Maximum Stresses (Absolute) for Nozzle M as a Function of Axial Load While Vessel Is Subjected to 350-psig Pressure Loading (Downhill Side). 123

Fig. 106. Maximum Stresses (Absolute) for Gas Outlet Nozzle as a Function of Axial Load While Vessel Is Subjected to 350-psig Pressure Loading (Uphill Side). 124

Fig. 107. Maximum Stresses (Absolute) for Gas Outlet Nozzle as a Function of Axial Load While Vessel Is Subjected to 350-psig Pressure Loading (Downhill Side). 124

Page

Fig. 108. Maximum Stresses (Absolute) for Gas Outlet Nozzle as a Function of Axial Load While Vessel Is Subjected to 350-psig Pressure Loading (Side 90 deg from Uphill Side). 124

Fig. 109. Circumferential and Meridional or Axial Stresses on Outer Surface of Head, Gas Outlet Nozzle, and Nozzles A and M on a Diametral Section Through Gas Outlet Nozzle. 125

Fig. 110. Circumferential and Meridional or Axial Stresses on Inner Surface of Head, Gas Outlet Nozzle, and Nozzles A and M on a Diametral Section Through Gas Outlet Nozzle. 126

Fig. 111. Circumferential and Meridional or Axial Stresses on Outer Surface of Head and Nozzles B and K on a Diametral Section Through Nozzles A, B, D, G, and K. 127

Fig. 112. Circumferential and Meridional or Axial Stresses on Inner Surface of Head and Nozzles B and K on a Diametral Section Through Nozzles A, B, D, G, and K. 128

Fig. 113. Circumferential and Meridional or Axial Stresses on Outer Surface of Head, BSD Nozzle, and Nozzle L on a Diametral Section Through BSD Nozzle. 129

Fig. 114. Circumferential and Meridional or Axial Stresses on Inner Surface of Head, BSD Nozzle, and Nozzle L Along a Diametral Section Through BSD Nozzle. 130

Fig. 115. Thermal Stresses (Theoretical) in Exterior Control Rod or Large Experimental Loop Nozzles Assuming a Single Nozzle-to-Shell Attachment. 131

Fig. 116. Thermal Stresses (Theoretical) in Interior Control Rod or Large Experimental Loop Nozzle Assuming a Single Nozzle-to-Shell Attachment. 131

Fig. 117. Thermal Stresses (Theoretical) in Exterior Special Plug or Small Experimental Loop Nozzle Assuming a Single Nozzle-to-Shell Attachment. 132

Fig. 118. Thermal Stresses (Theoretical) in the Interior Special Plug or Small Experimental Loop Nozzle Assuming a Single Nozzle-to-Shell Attachment. 132

Fig. 119. Theoretical Stresses in the Spherical Head from Axial Temperature Gradient Along Control Rod Nozzle. 133

Fig. 120. Theoretical Stresses in the Spherical Head from Axial Temperature Gradient Along Special Plug Nozzle. 133

Page

Fig. 121.	Principal Stresses Versus Time for the Outer Surface of Nozzle A.	134
Fig. 122.	Principal Stress Differences Versus Time for the Outer Surface of Nozzle A.	134
Fig. 123.	Fatigue Diagram for the Outer Surface of Nozzle A.	135
Fig. 124.	Principal Stresses Versus Time for the Outer Surface of Nozzle B on the Downhill Side.	135
Fig. 125.	Principal Stress Differences Versus Time for the Outer Surface of Nozzle B on the Downhill Side.	136
Fig. 126.	Fatigue Diagram for the Outer Surface of Nozzle B on the Downhill Side.	136
Fig. 127.	Fatigue Diagram for the Gas Outlet Nozzle.	137

ABSTRACT

Structural evaluations of the upper head of the EGCR pressure vessel were made using the procedures outlined in "Tentative Structural Design Basis for Reactor Pressure Vessels and Directly Associated Components," PB 151987, 1 December 1958 Revision, Department of Commerce, Office of Technical Services. The configuration throughout the cluster region in the vessel was found to be structurally adequate. The primary and primary-plus-secondary stress intensities for the burst-slug detection and gas outlet nozzles were found to be within the allowable limits. However, the complete design evaluations of these units cannot be made until the temperature distributions are known.

INTRODUCTION

The pressure vessel for the Experimental Gas-Cooled Reactor[1] (EGCR) is a cylindrical shell having hemispherical top and bottom heads. The vessel has an over-all height of 46 ft 4 in., an inside diameter of 20 ft 0 in., and a minimum wall thickness of 2 3/4 in. (see Fig. 1). The hemispherical heads are 4.0 in. thick. The entire vessel is constructed of carbon steel, type SA 212, grade B. The design pressure is 350 psig and the design temperature is 650°F, whereas the normal operating pressure will be 300 psig and the vessel cooling system will maintain the vessel wall at a temperature below 650°F.

As shown in Fig. 1, the upper head of the pressure vessel has numerous nozzle penetrations which make this a crucial region from a structural standpoint. The large number of nozzles in close proximity makes an accurate theoretical analysis difficult, and the use of nozzles which are alined vertically rather than being attached normal to the shell adds to the complexity of any analytical study. Hence, an experimental stress analysis was considered to be necessary in order to assess the structural adequacy of the design.

The control rod, special plug, and experimental loop nozzles in the upper head form a closely spaced cluster. At the time the experimental program was initiated there were 53 nozzles in the cluster, and the design of the test vessel was based on this number. Later, 12 special plug nozzles were eliminated. The nozzles removed are shown dotted in Fig. 2. Although the structural integrity evaluations were made using the data derived from the earlier configuration, the conclusions reached are equally applicable to the final vessel design.

A description of the nozzles in the vessel is given in Table 1. Since the large and small experimental loop nozzle stubs are identical to those of the control rod and special plug nozzles, respectively, only two types are represented in the cluster region of the upper head. Each size is

---

[1]Experimental Gas-Cooled Reactor Preliminary Hazards Summary Report, ORO-196 (May 1959).

UNCLASSIFIED
ORNL-LR-DWG 59232

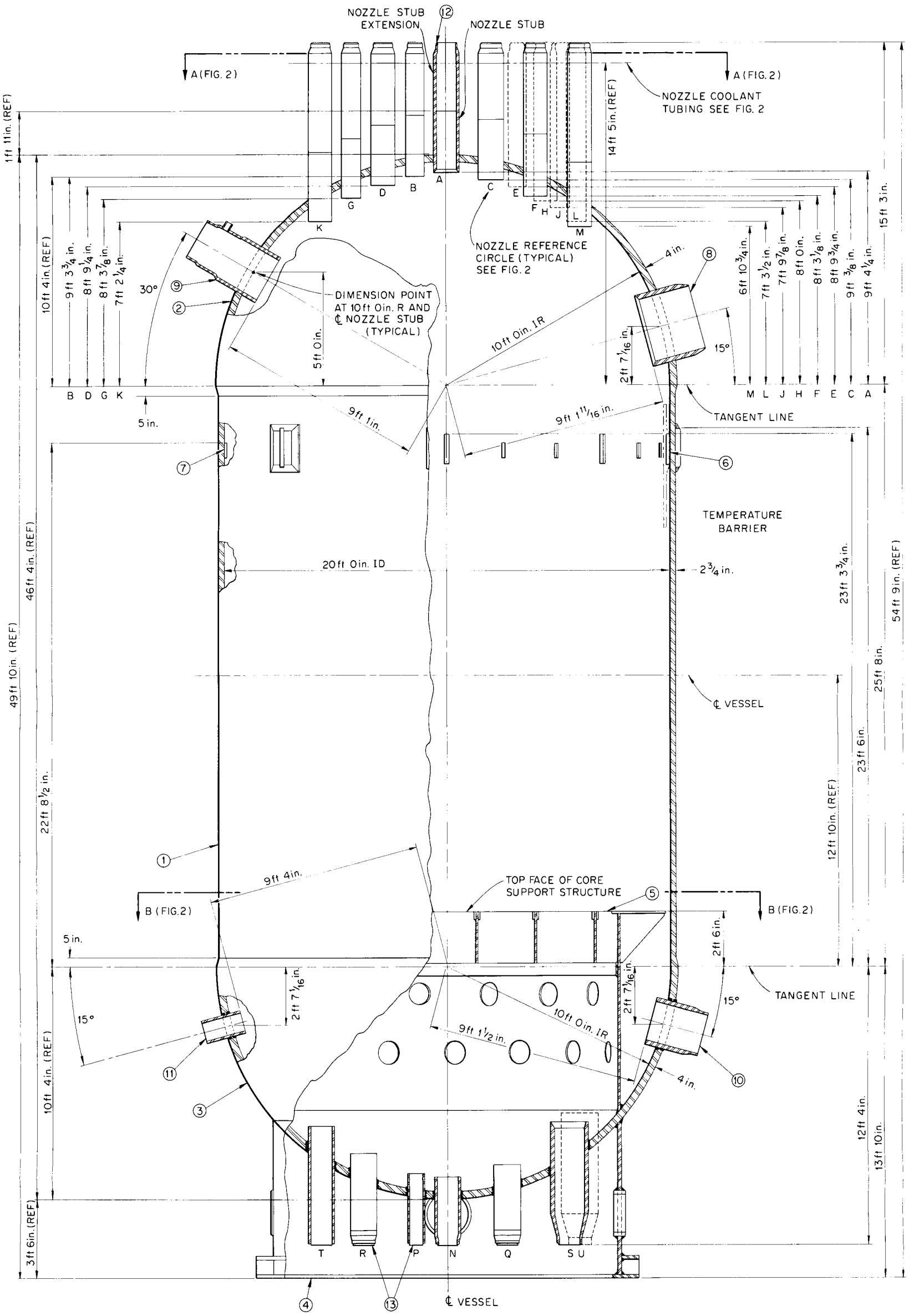

BILL OF MATERIAL			
ITEM	REQ'D	DESCRIPTION	MATERIAL
1	1	PRESSURE VESSEL CYLINDER	SA 212 GRADE B
2	1	PRESSURE VESSEL TOP HEAD	SA 212 GRADE B
3	1	PRESSURE VESSEL BOTTOM HEAD	SA 212 GRADE B
4	1	VESSEL SUPPORT	
5	1	CORE SUPPORT STRUCTURE	
6	8	LATERAL RESTRAINT LUGS	
7	16	BARRIER SUPPORT LUG	
8	2	GAS OUTLET NOZZLE STUB	
9	2	B.S.D. AND TC NOZZLE STUB AND EXTENSION	
10	2	GAS INLET NOZZLE STUB	
11	4	THERMOCOUPLE NOZZLE STUB AND EXTENSION	
12	41	TOP HEAD NOZZLE STUBS AND EXTENSIONS	
13	29	BOTTOM HEAD NOZZLE STUBS	

Fig. 1. EGCR Pressure Vessel Elevation.

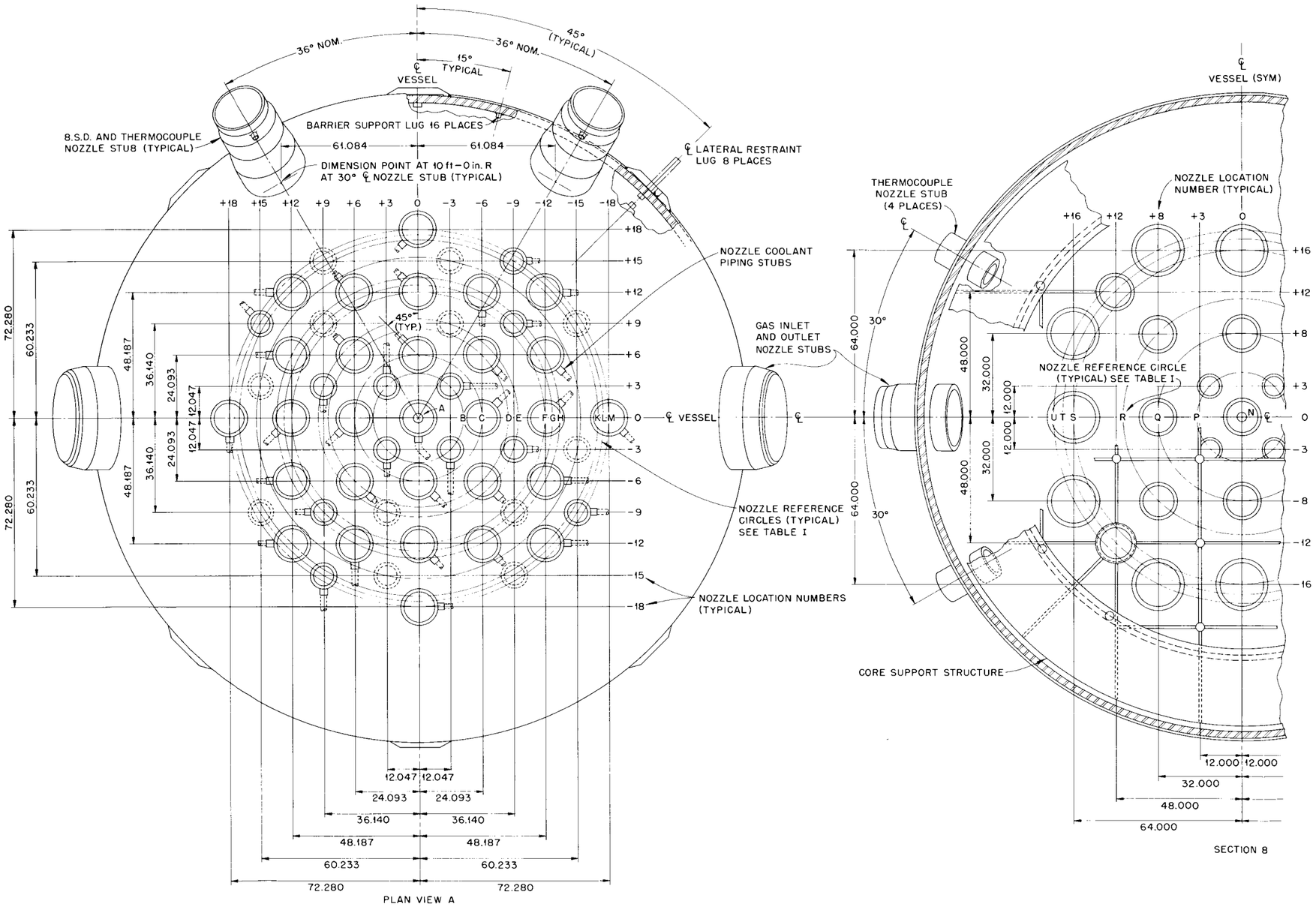

TABLE I

NOZZLE REF. CIRCLE	NOZZLE REF. CIRCLE R (REF. DIM. FOR ORIENTATION ONLY)	NOZZLE TYPE	REQ'D	REMARKS
A	0	CONTROL ROD	1	
B	17.037 in.	SMALL THRU-LOOP	4	
C	24.093 in.	CONTROL ROD	4	
D	34.073 in.	CONTROL ROD	4	
E	38.095 in.	SPECIAL PLUG	2	
F	48.187 in.	CONTROL ROD	4	
G	51.110 in.	SPECIAL PLUG	2	
H	53.875 in.	CONTROL ROD	8	
K	68.147 in.	9½-in-DIA NOM THRU-LOOP	4	
L	70.244 in.	SPECIAL PLUG	4	
M	72.280 in.	CONTROL ROD	4	
N	0	FUEL CHARGE	1	
P	16.970 in.	5¼-in.-DIA NOM THRU-LOOP	4	
Q	32.000 in.	FUEL CHARGE	4	
R	45.255 in.	FUEL CHARGE	4	
S	64.000 in.	FUEL CHARGE	4	
T	67.882 in.	LARGE THRU-LOOP	4	
U	71.554 in.	FUEL CHARGE	8	

Fig. 2. EGCR Pressure Vessel Plan and Section.

Table 1. Nozzles in EGCR Pressure Vessel

Nozzle Location	Purpose	Number	Inside Diameter (in.)	Wall Thickness (in.)	Pitch (in.)
Top head	Burst-slug-detection tube and thermocouple	2	28[a]	2	
	Control rod	25	11 1/8	1 3/16	24
	Experimental loop				
	Large	4	11 1/8	1 3/16	
	Small	4	7 3/4	7/8	
	Special plug	20[b]	7 3/4	7/8	24
	Gas outlet	2	34	2 1/2	
Bottom head	Experimental loop				
	Large	4	14[c]		
	Small	4	7	1	24
	Fuel charging				
	Large	12	16 1/2	1 3/4	32
	Small	9	12	1 1/4	32
	Gas inlet	2	22	2	
	Thermocouple	2	11 1/2	1 1/4	

[a]Diameter used for scale model was based on a 22-in.-diam prototype rather than the final 28-in.-diam nozzle.

[b]Reduced to eight in final design.

[c]Outside diameter.

spaced on a 24-in. square pitch that gives an effective spacing of 12 in. and a minimum distance between the nozzles of 5.47 in. All the nozzles extend through the pressure vessel to provide added reinforcement around the openings, and full penetration welds are used throughout.

A description of the methods used in fabricating the 1/5.533-scale model of the upper portion of the pressure vessel is given in Part 1. The model was fabricated from 6061 aluminum and instrumented with bonded wire strain gages. The complete experimental stress analysis program is also discussed in Part 1. A description of the strain gage locations, the experimental techniques employed, and the loads applied to the vessel are included.

The model was subjected to an internal pressure loading, and forces and moments were applied to the nozzles in the top head. A summary of the nozzle loadings is given in Table 2. Each load was applied singly so that stresses for various combined loads could be obtained by superposition.

The second phase of the experimental investigation of the EGCR pressure vessel is described in Part 2. This phase consisted of translating the experimental data into quantities applicable to the full-scale vessel and utilizing the results in making design evaluations.

Table 2. Loads Applied to Nozzles in Top Head

Nozzle Type	Reference Circle	Reference Circle Radius (in.)	Load
Control rod	A	16.991	Axial Normal
	M	72.085	Axial Normal
Special plug	J	61.259	Axial Normal
	L	70.052	Axial Normal
Small experimental loop	B	16.991	Axial Normal
Large experimental loop	K	67.960	Axial Normal
Gas outlet			Axial Transverse moment Meridional moment Transverse normal Meridional normal Torsional moment

PART 1. EXPERIMENTAL DETERMINATION OF STRESSES IN MODEL

R. W. Holland[2] R. L. Maxwell[2]

The experimental study was conducted by the Mechanical Engineering Department under Subcontract 1441 between Union Carbide Nuclear Company and the University of Tennessee Engineering Experiment Station. The purpose of this investigation was to determine experimentally the stresses produced in the shell and in the nozzles of the top head of the EGCR pressure vessel.

The stresses were determined with the use of bonded-wire strain gages attached to an aluminum model of the reactor head which was loaded by internal pressure and other loads applied to the various nozzles in simulation of the loads that were expected to act upon the reactor vessel during operation. Scale drawings of the completed model are presented in Figs. 3 and 4. In the tests the following loads were applied (the nozzle designations correspond to those shown in Fig. 3):

1. Internal pressure loading of 60 psig.
2. Axial load of 2000 lb on nozzle A.
3. Axial load of 1500 lb on nozzle B_2.
4. Axial load of 2000 lb on nozzle M_3.
5. Axial load of 1500 lb on nozzle J_2.
6. Axial load of 1500 lb on nozzle L_4.
7. Axial load of 2000 lb on nozzle K_2.
8. Combined load of 60-psig internal pressure and axial load of 2000 lb on nozzle A.
9. Normal load of 50 lb on nozzle A at a distance of 34 3/4 in. above the apex of the dome.
10. Normal load of 150 lb on nozzle A at a distance of 13 3/16 in. from the apex of the dome.
11. Normal load of 30 lb on nozzle B_2 at a distance of 34 3/4 in. from the apex of the dome.

---

[2]Mechanical Engineering Department, University of Tennessee.

12. Normal load of 40 lb on nozzle B_2 at a distance of 25 1/4 in. from the apex of the dome.
13. Normal load of 50 lb on nozzle M_3 at a distance of 34 3/4 in. above the apex of the dome.
14. Normal load of 150 lb on nozzle M_3 at a distance of 13 3/16 in. from the apex of the dome.
15. Normal load of 30 lb on nozzle J_2 at a distance of 34 3/4 in. from the apex of the dome.
16. Normal load of 80 lb on nozzle J_2 at a distance of 13 3/16 in. from the apex of the dome.
17. Normal load of 30 lb on nozzle L_4 at a distance of 34 3/4 in. from the apex of the dome.
18. Normal load of 80 lb on nozzle L_4 at a distance of 13 3/16 in. from the apex of the dome.
19. Normal load of 75 lb on nozzle K_2 at a distance of 24 9/16 in. from the apex of the dome.
20. Axial load of 1500 lb applied simultaneously to each of the four small experimental loop nozzles (nozzles B_1, B_2, B_3, and B_4).
21. Axial load of 5000 lb on gas outlet.
22. Normal load of 2000 lb on gas outlet in transverse plane at a distance of 8 1/2 in. from dome surface.
23. Normal load of 2000 lb on gas outlet in axial plane at a distance of 8 1/2 in. from dome surface.
24. Pure moment of 19 200 in.-lb on gas outlet in transverse plane.
25. Pure moment of 19 200 in.-lb on gas outlet in axial plane.
26. Torsional load of 32 000 in.-lb on gas outlet.

All the normal loads given above, except that on nozzle A and the gas outlet nozzle, were applied in the axial plane containing nozzle A with the load applied in a direction toward nozzle A. The normal load on nozzle A was in an axial plane passing through the gas outlet nozzles. The distances above the apex for normal load applications correspond to the locations of the upper and lower surfaces of the biological shield in the cases of both the control rod and special plug nozzles A, M_3, B_2, J_2, and L_4.

For the experimental loop nozzles B_2 and K_2 the distances correspond to the locations of the external piping attachment points.

DESCRIPTION OF MODEL

A model of the top head of the reactor pressure vessel and adjacent cylindrical section was fabricated of 6061 aluminum plate. The spherical portion of the head was cold formed on a male die. The cylindrical portion and the flange at the bottom were cold rolled to shape. The spherical section and the other parts were then welded into the completed vessel shape by heliarc welding techniques. This gave a weld joint between the spherical and cylindrical sections, a weld joint between the cylindrical section and the flange, and one axial weld along the cylindrical section. These joints were all radiographically inspected. This work was done by Combustion Engineering Company in Chattanooga, Tennessee.

This fabricated shell was then machined to size on both inside and outside surfaces by C. L. Gougler Company of Kent, Ohio. The finished model was machined to a scale of 1/5.533. This scale was necessitated by the available male die for forming the spherical portion of the head. The machined model is shown in Fig. 5 ready for attachment of nozzles.

The nozzles were attached by boring holes in the head and welding the nozzles in place by the heliarc process. The welds around the nozzles were hand ground to provide a 1/16-in. radius fillet at the inner and outer surfaces of the shell, and then all welds were inspected by radiography. The nozzles were attached in order from the center of the cluster, progressing outward one concentric circle of nozzles at a time. Each group of nozzles was welded in and the fillets ground to size before the next group of holes was drilled. This was necessary in order to allow working room for finishing the fillets. Also, this procedure prevented excessive warpage in the head as a result of the welding. The completed model is shown in Figs. 6 and 7 ready for attachment of the strain gages.

EXPERIMENTAL PROCEDURE

Strain gages were attached at the locations indicated in Figs. 8 through 12. The locations of the gages on the outer surface of the shell and the gages inside nozzle A are indicated in Figs. 9 and 10. All gages on the outer surfaces of the spherical head and cylindrical section were matched with corresponding gages on the inner surfaces so that total strains at both surfaces could be determined and the membrane and bending stress components at each gage position could be calculated. Corresponding gages on the inner and outer surfaces were designated with the same gage number.

Since the stress distribution around any nozzle in the cluster is influenced by the neighboring nozzles, distributions similar to those in a perforated plate were expected to exist. The interaction between holes is illustrated in Fig. 13, where the tangential stresses around the edge of a hole under biaxial tension have been plotted. From this figure it may be seen that the highest stresses exist along lines joining the centers of the holes. In addition, the pattern of cracks obtained in a Stress-coat test on a perforated plate in bending is shown in Fig. 14; the principal stress directions and regions of high stress may be seen. Using this evidence, the gages on the spherical shell were positioned to measure these peak stresses. In some cases, however, the locations and orientations were chosen to coincide with the circumferential and meridional directions of the shell.

The typical gage locations on a nozzle are shown in Fig. 11. Dimensions of the gage locations for each nozzle are tabulated in Table 3, referenced to Fig. 11. Bonded-wire SR-4 strain gages, type A-7, with a gage length of 1/4 in. were used in all cases.

The gages are shown in Fig. 15 completely installed on the inside of the dome. The lead wires of these gages were brought out through the gas outlet nozzles and the burst-slug-detection outlets. The gages on the outside of the shell are shown in Fig. 16 with the shell in the loading frame ready for testing. A large-scale photograph showing the manner in which the gages were attached at the fillet between the dome and the gas outlet nozzle is presented in Fig. 17. The gages were attached in a similar manner at all fillets.

Table 3. Location of Gages on Nozzles with Reference to Figure 11

Nozzle	Side of Nozzle	Gage Number		Location Dimensions (in.)			
		Axial	Tangential	a	b	c	d
A	Toward gas outlet No. 2	533	534	1/4			
		535	536		15/16		
		537	538			1 11/16	
		539	540				2 11/16
	Toward gas outlet No. 1	541	542	1/4			
		543	544		1		
		545	546			1 7/8	
		547	548				2 7/8
B_2	Opposite nozzle A, downhill side	581	582	7/32			
		583	584		7/8		
		585	586			1 9/16	
		587	588				2 3/8
	Toward nozzle A, uphill side	589	590	7/32			
		591	592		23/32		
		593	594			1 11/32	
		595	596				2 9/32
J_2	Opposite nozzle A, downhill side	565	566	3/16			
		567	568		7/8		
		569	570			1 2/132	
		571	572				2 9/16
	Toward nozzle A, uphill side	573	574	1/4			
		575	576		15/16		
		577	578			1 3/4	
		579	580				2 3/4
K_2	Opposite nozzle A, downhill side	613	614	3/16			
		615	616		7/8		
		617	618			1 3/4	
		619	620				2 13/16
	Toward nozzle A, uphill side	621	622	1/4			
		623	624		15/16		
		625	626			1 21/32	
		627	628				2 3/8
L_4	Opposite nozzle A, downhill side	597	598	3/16			
		599	600		13/16		
		601	602			1 11/16	
		603	604				2 25/32
	Toward nozzle A, uphill side	605	606	7/32			
		607	608		29/32		
		609	610			1 23/32	
		611	612				2 1/2
M_3	Opposite nozzle A, downhill side	549	550	3/16			
		551	552		13/16		
		553	554			1 23/32	
		555	556				2 3/4

Table 3 (continued)

Nozzle	Side of Nozzle	Gage Number		Location Dimensions (in.)			
		Axial	Tangential	a	b	c	d
	Toward nozzle A, uphill side	557	558	1/4			
		559	560		15/15		
		561	562			1 13/16	
		563	564				2 11/16
BSD-1	Opposite nozzle A, downhill side	629	630	3/16			
		631	632		13/16		
		633	634			1 5/8	
		635	636				2 11/16
	Toward nozzle A, uphill side	637	638	1/8			
		639	640		3/4		
		641	642			1 3/8	
		643	644				2 7/16
Gas outlet No. 1	Opposite nozzle A, downhill side	501	502	1/8			
		503	504		3/4		
		505	506			1 9/16	
		507	508				2 9/16
	Toward nozzle A, uphill side	509	510	3/16			
		511	512		13/16		
		513	514			1 5/8	
		515	516				2 9/16
Gas outlet No. 1	In transverse plane on side opposite BSD nozzles	517	518	3/16			
		519	520		3/4		
		521	522			1 9/16	
		523	524				2 1/2
	In transverse plane on side toward BSD nozzles	525	526	1/8			
		527	528		9/16		
		529	530			1 9/16	
		531	532				2 9/16

As seen from the figures, the gages were placed on one-half the dome and evenly spaced in two axial rows along the cylindrical section of the shell so that a duplicate strain reading could be obtained at each point on the hemispherical dome and cylindrical section. These duplicate strain readings served as a check of the results.

At all gage positions, two gages oriented at 90 deg to each other were installed so that the stresses in the two directions could be determined. The gages were alined in the anticipated directions of the principal strains at each location. Stresscoat lacquer was used to check the directions of the principal stresses caused by an axial load on one of

the nozzles. The cracks in the Stresscoat indicated that the principal directions were in the directions of the strain gages for that nozzle.

In conducting the tests, gage readings were recorded at zero load, at one-half load, and at full load, and then again at zero load after the load had been removed. Thus the linearity and drift of the gages could be checked. Each gage was checked for grounding and air bubbles in the cement after the lead wires had been connected. The strain readings were made with SR-4 Strain Indicators, and SR-4 Switching Units were used for switching gages.

The magnitudes of all the loadings were made as large as possible so that maximum strain readings could be obtained. The limiting value of the load was determined in each case by the strain value at the yield-point stress. A maximum allowable strain of approximately 400 μin. was used, corresponding to a stress of 4000 psi. (The yield-point stress for annealed 6061 aluminum is approximately 5000 psi.)

Concentrated loads were applied to the nozzles by means of hydraulic jacks working through SR-4 Load Cells. Air pressure was used for the pressure loading. Difficulty was encountered in the pressure tests with the gages located inside the dome. The gage readings were not linear and considerable drift was found between the initial reading and the final zero reading. It was found that the moisture in the compressed air used for loading was reducing the resistance between the inside gages and the model, which was grounded. This difficulty was eliminated by drying the air before it entered the dome.

RESULTS

The results of the tests are tabulated in Tables A.1 through A.52 of Appendix A. Tables A.1 through A.26, which are numbered in the order of the loadings as given in the introduction, give the maximum value of the strain at each gage position for the various loadings.

Tables A.27 through A.52 give the stresses corresponding to the strains tabulated in Table A.1 through A.26. These tables are also arranged in the order of loading as given in the introduction. In determining the stresses the following elastic constants were used: modulus

of elasticity, $E = 10.0 \times 10^6$ psi; Poisson's ratio, $\mu = 0.3$. The equations used in determining the stresses are given in Appendix A.

In some cases the gage numbers do not appear in the tables, indicating bad gages for those gage numbers. For the concentrated loads only those gages are listed that gave significant stresses. Plots of the pressure stresses along various sections of the dome are given in Part II of this report (Figs. 109 through 114, pp. 125–130).

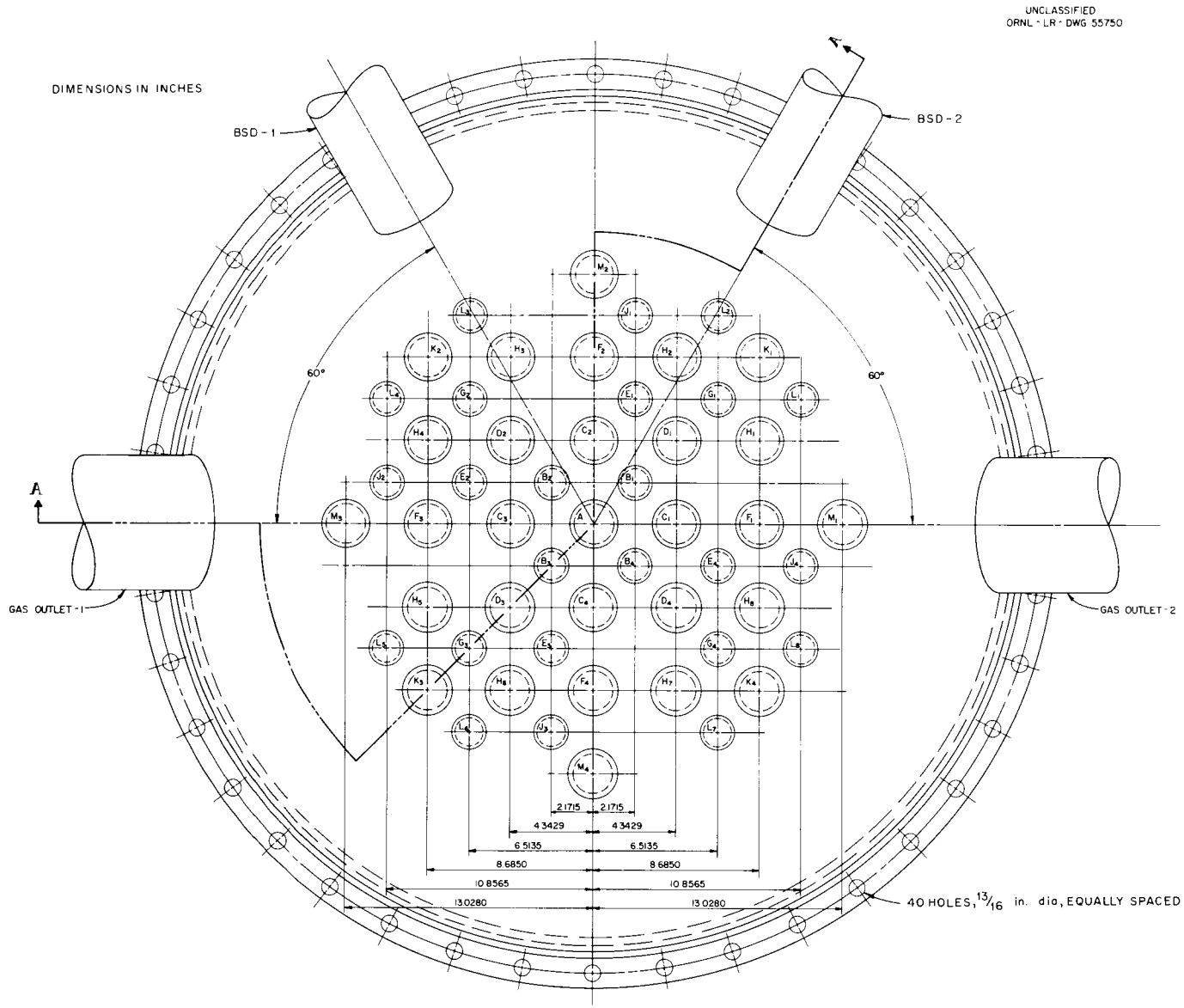

Fig. 3. EGCR Pressure Vessel Model — Plan View.

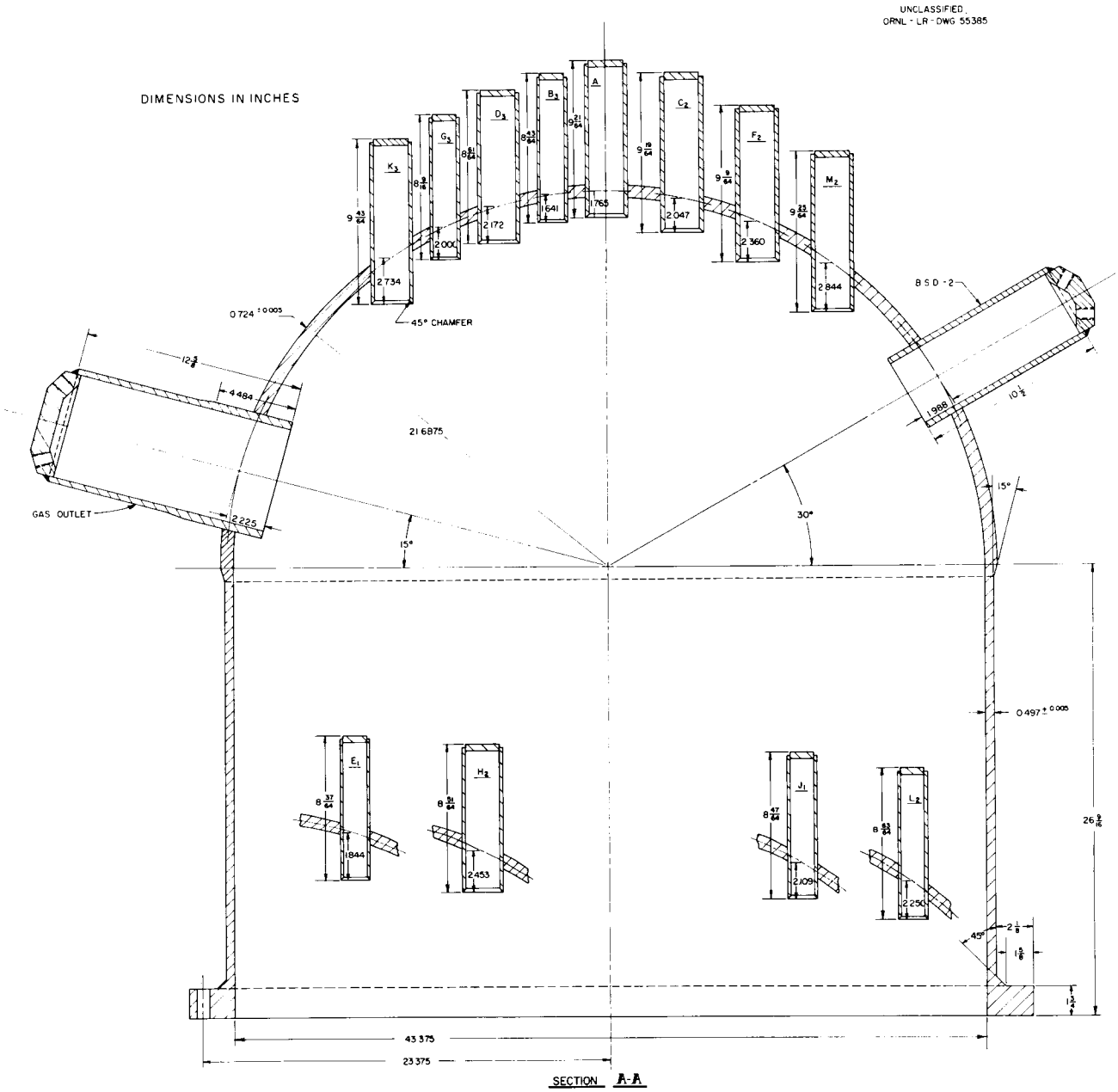

Fig. 4. EGCR Pressure Vessel Model — Elevation.

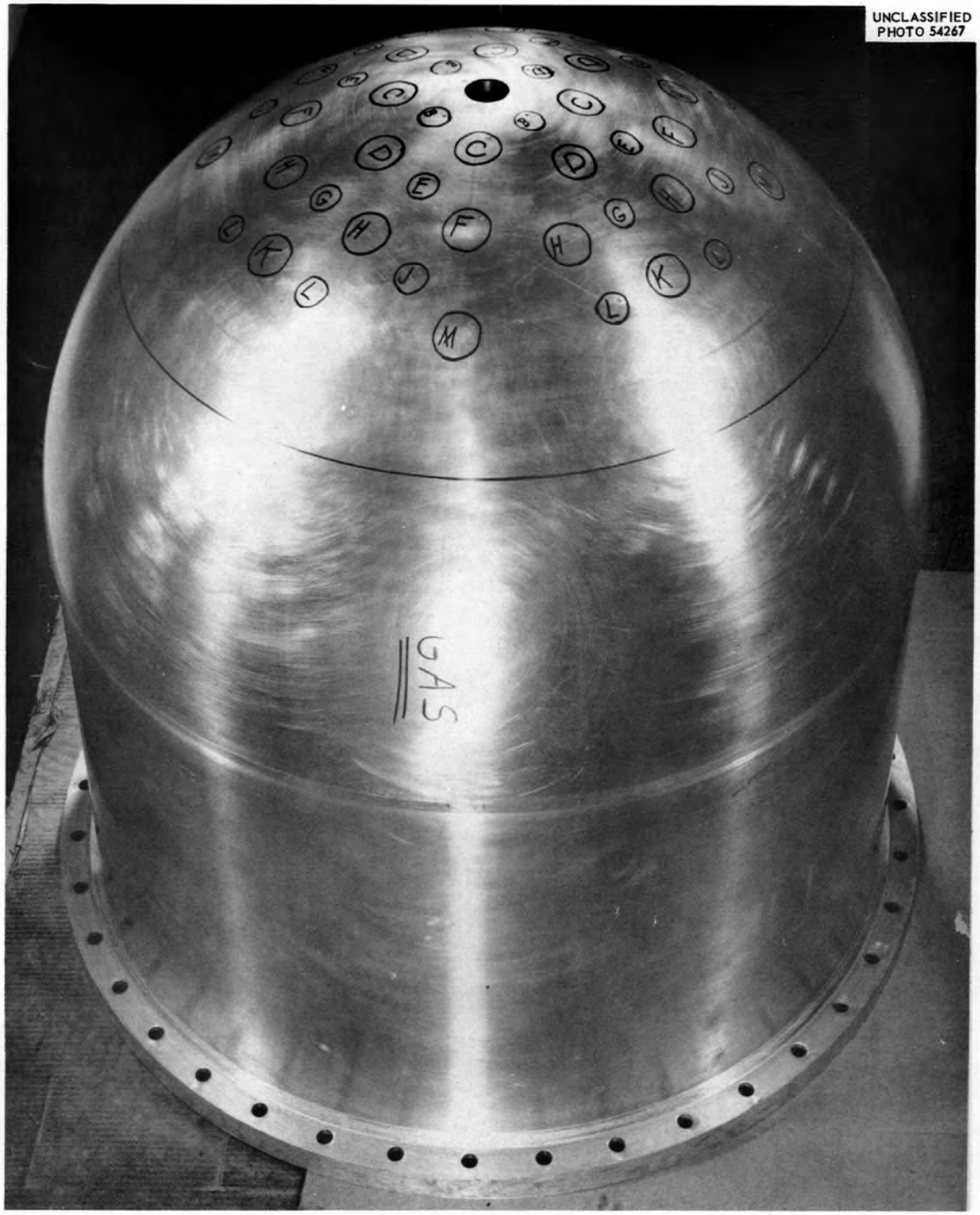

Fig. 5. Photograph of Machined Vessel Ready for Drilling of Holes and Attaching Nozzles.

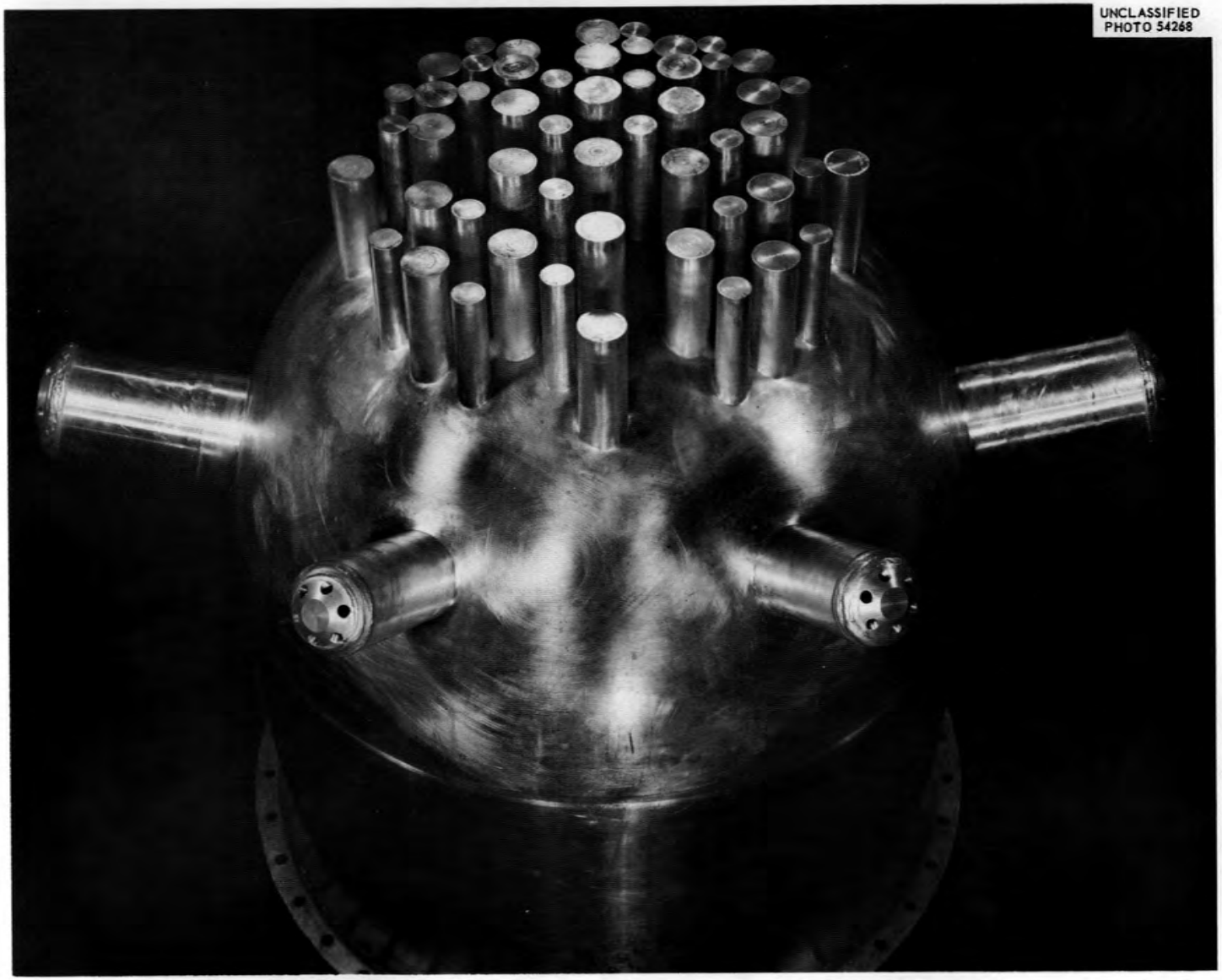

Fig. 6. Photograph of Outside of Vessel Ready for Attachment of Gages.

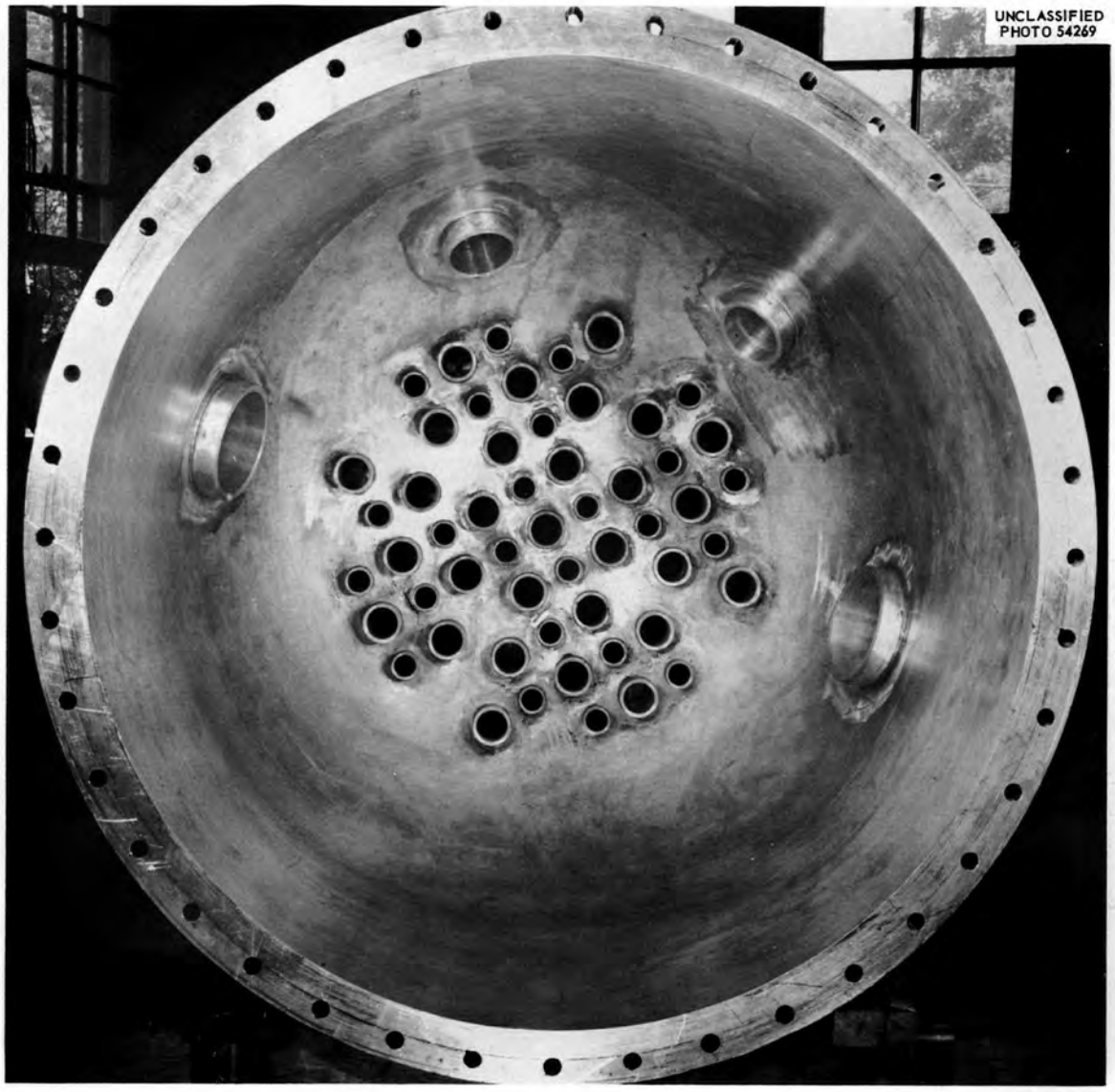

Fig. 7. Photograph of Inside of Vessel Ready for Attachment of Gages.

UNCLASSIFIED
ORNL - LR - DWG 54622

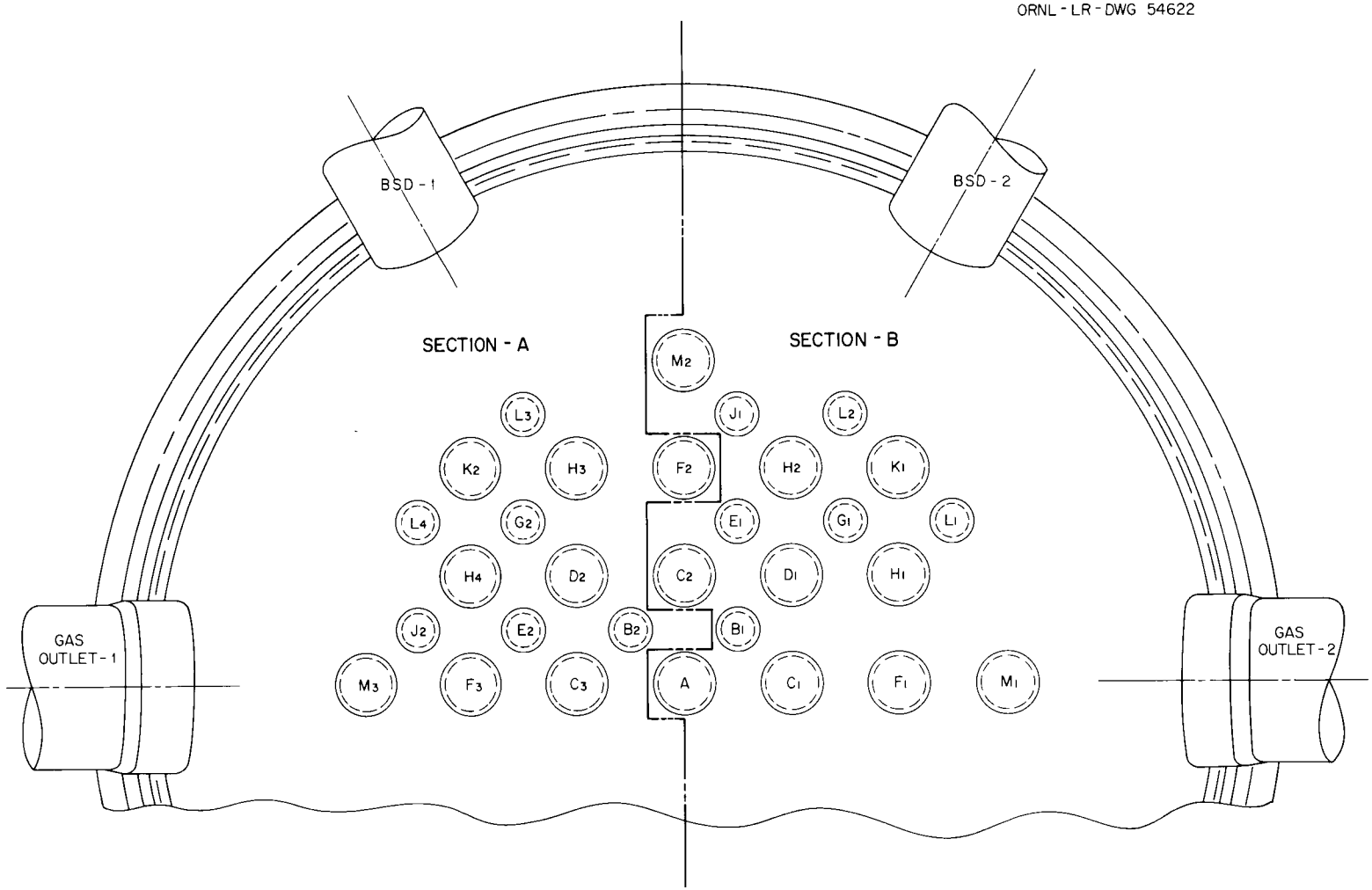

Fig. 8. Instrumented Portion of Shell.

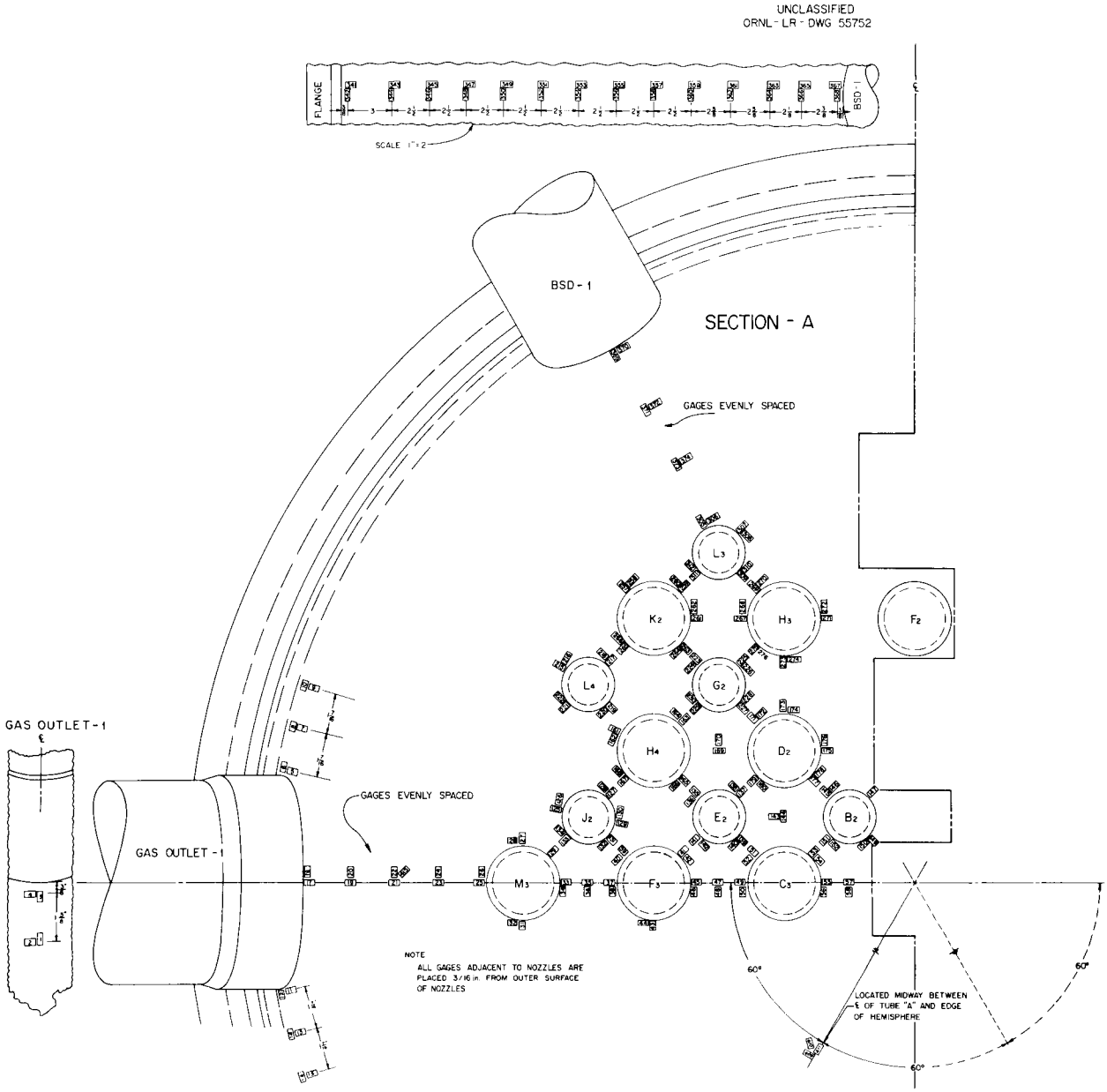

Fig. 9. Gage Locations on Section A of Fig. 8 and Along Cylindrical Portion of Shell.

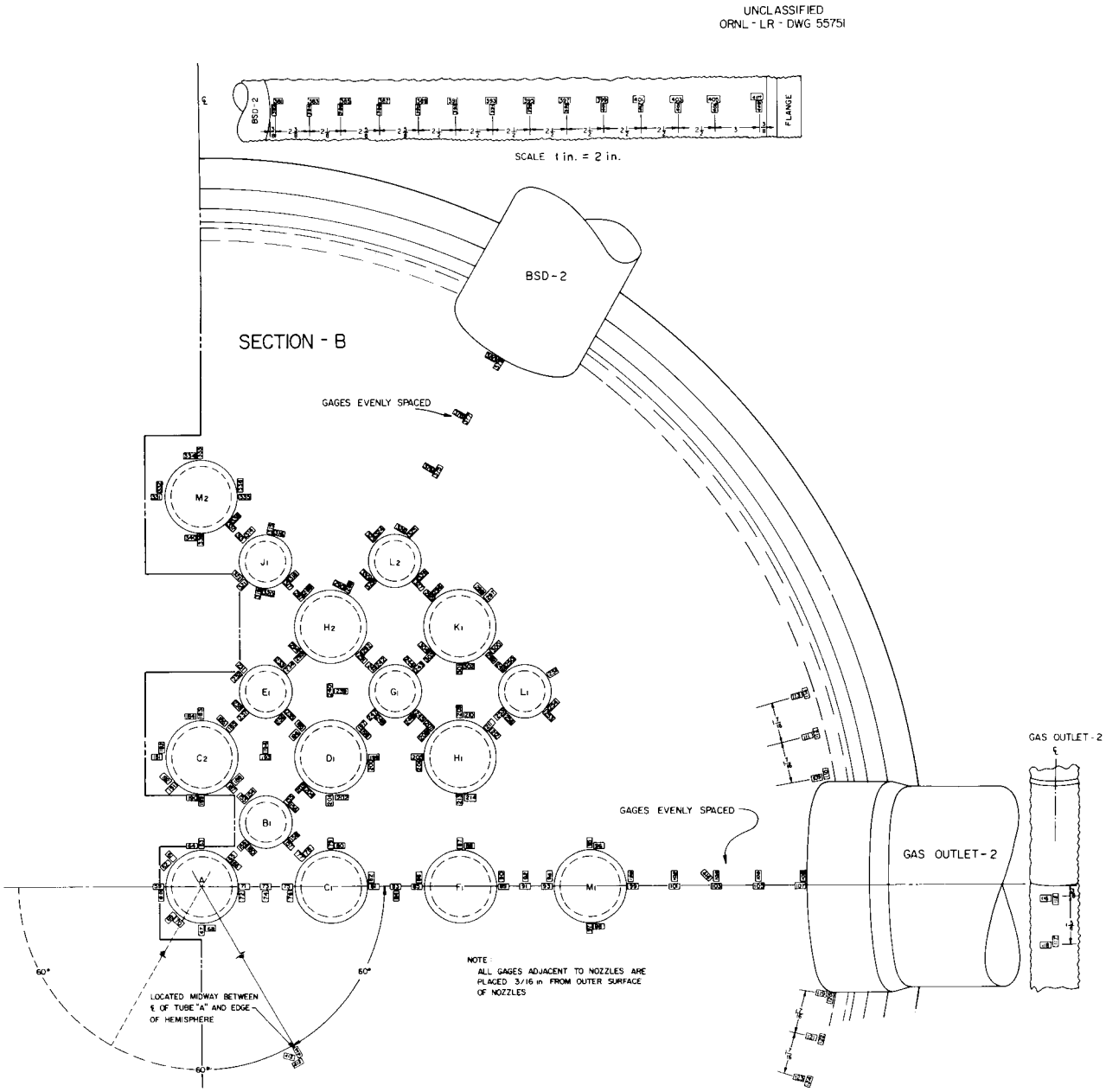

Fig. 10. Gage Locations on Section B of Fig. 8 and Along Cylindrical Portion of Shell.

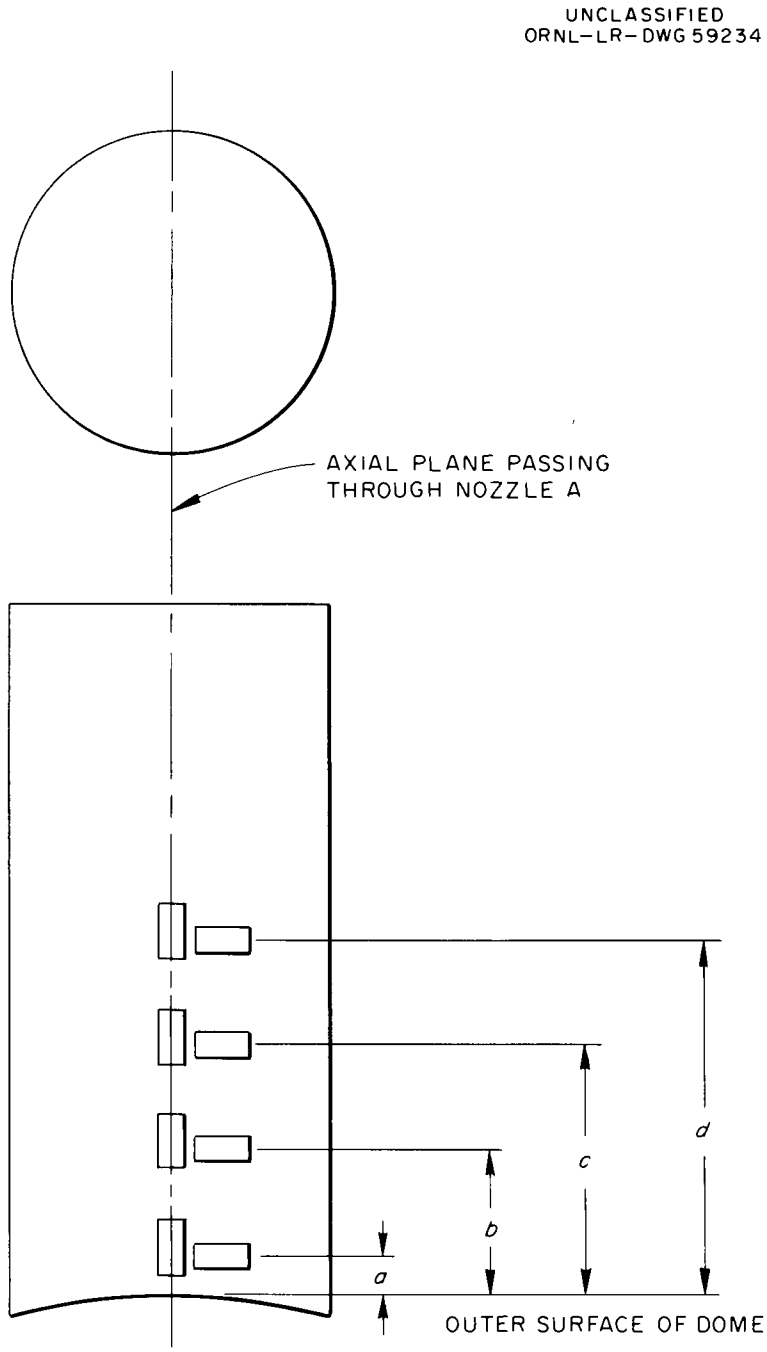

Fig. 11. Typical Gage Locations on a Nozzle.

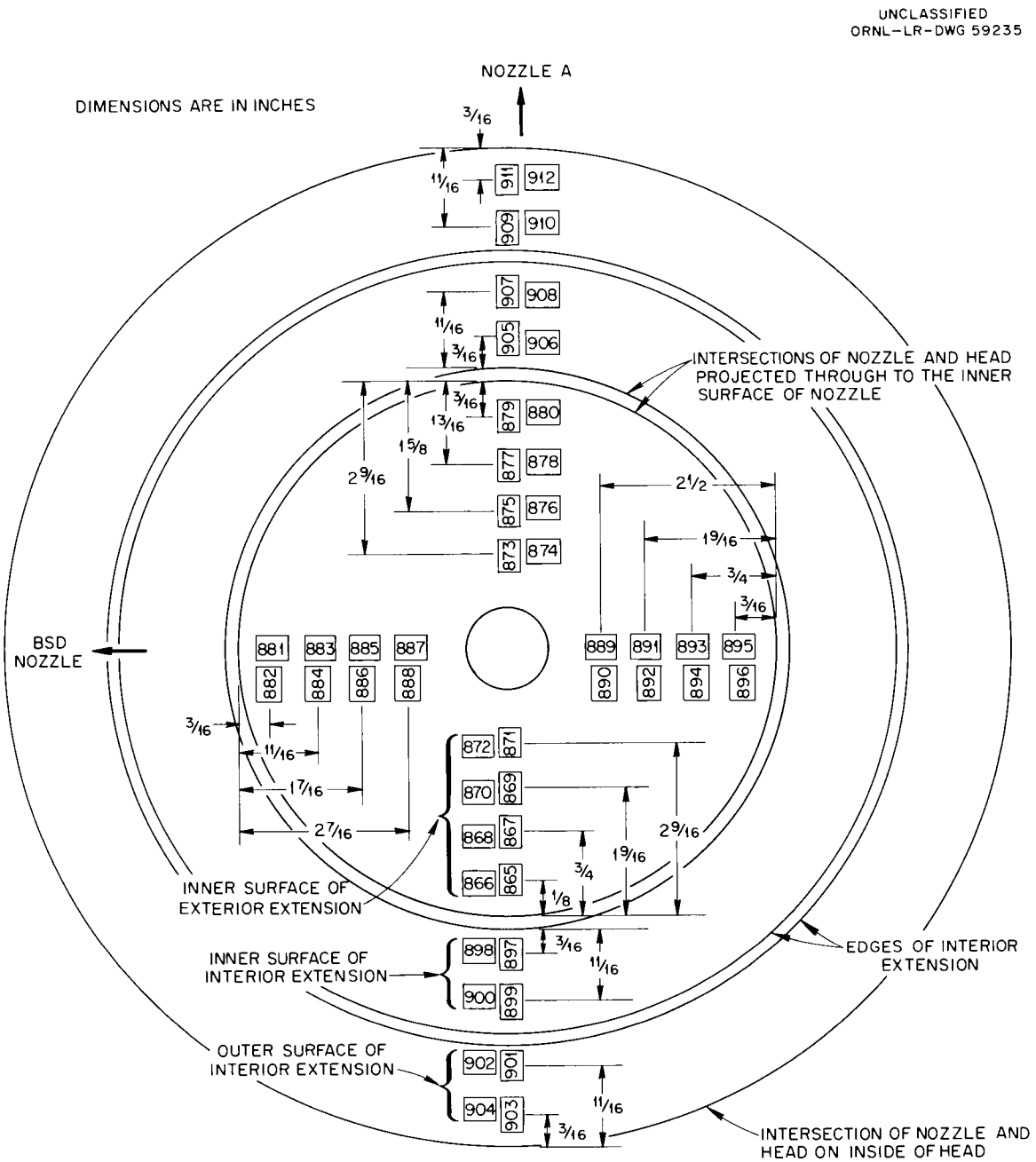

Fig. 12. Gage Locations on Inner Surface of Gas Outlet Nozzle and Its Extension Inside the Head.

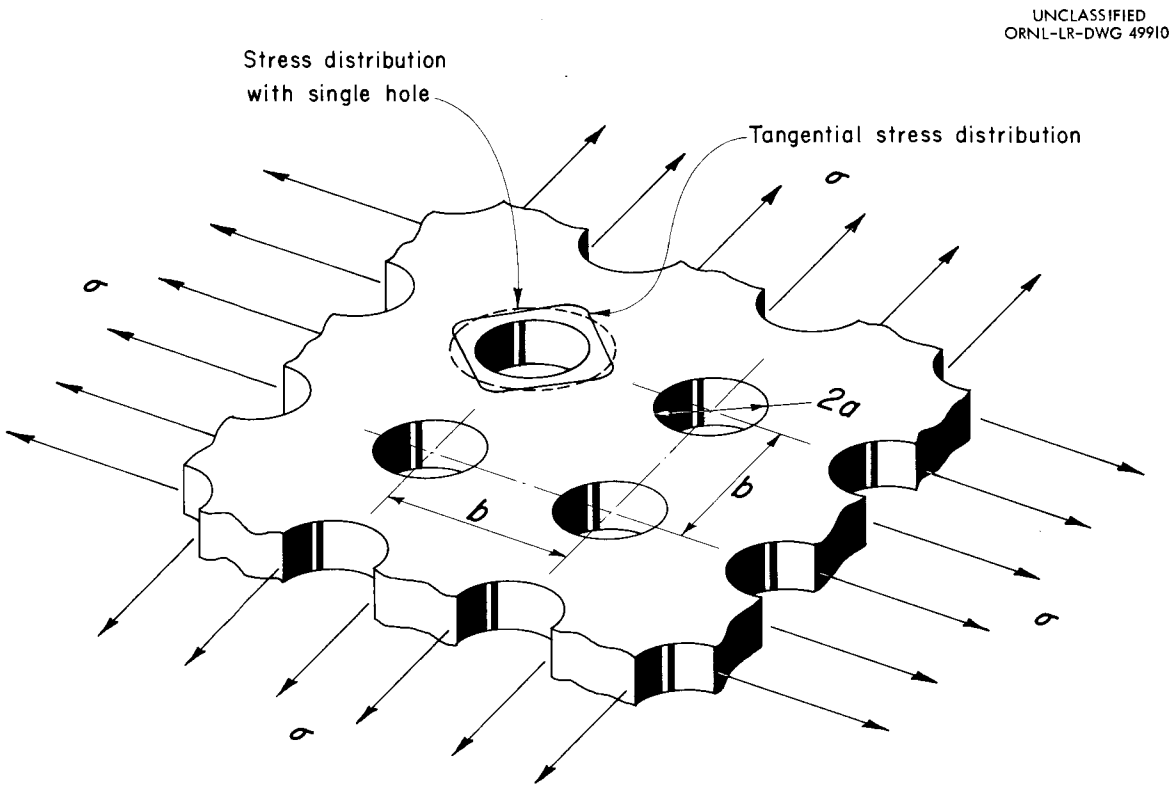

Fig. 13. Tangential Stress Distribution Around Hole in Perforated Plate for a/b = 0.27.

UNCLASSIFIED
PHOTO 54270

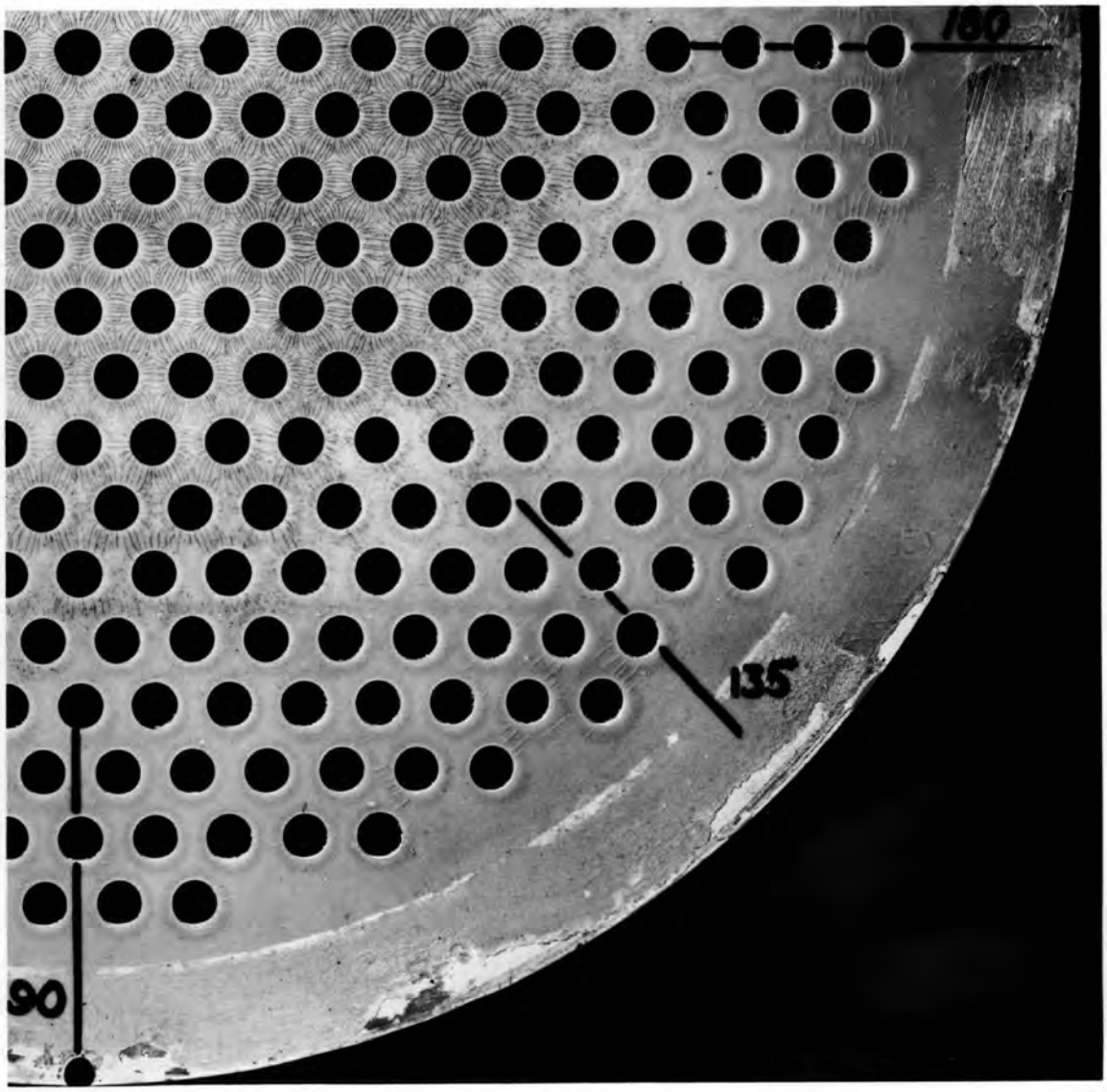

Fig. 14. Stresscoat Crack Pattern on Perforated Plate in Bending.

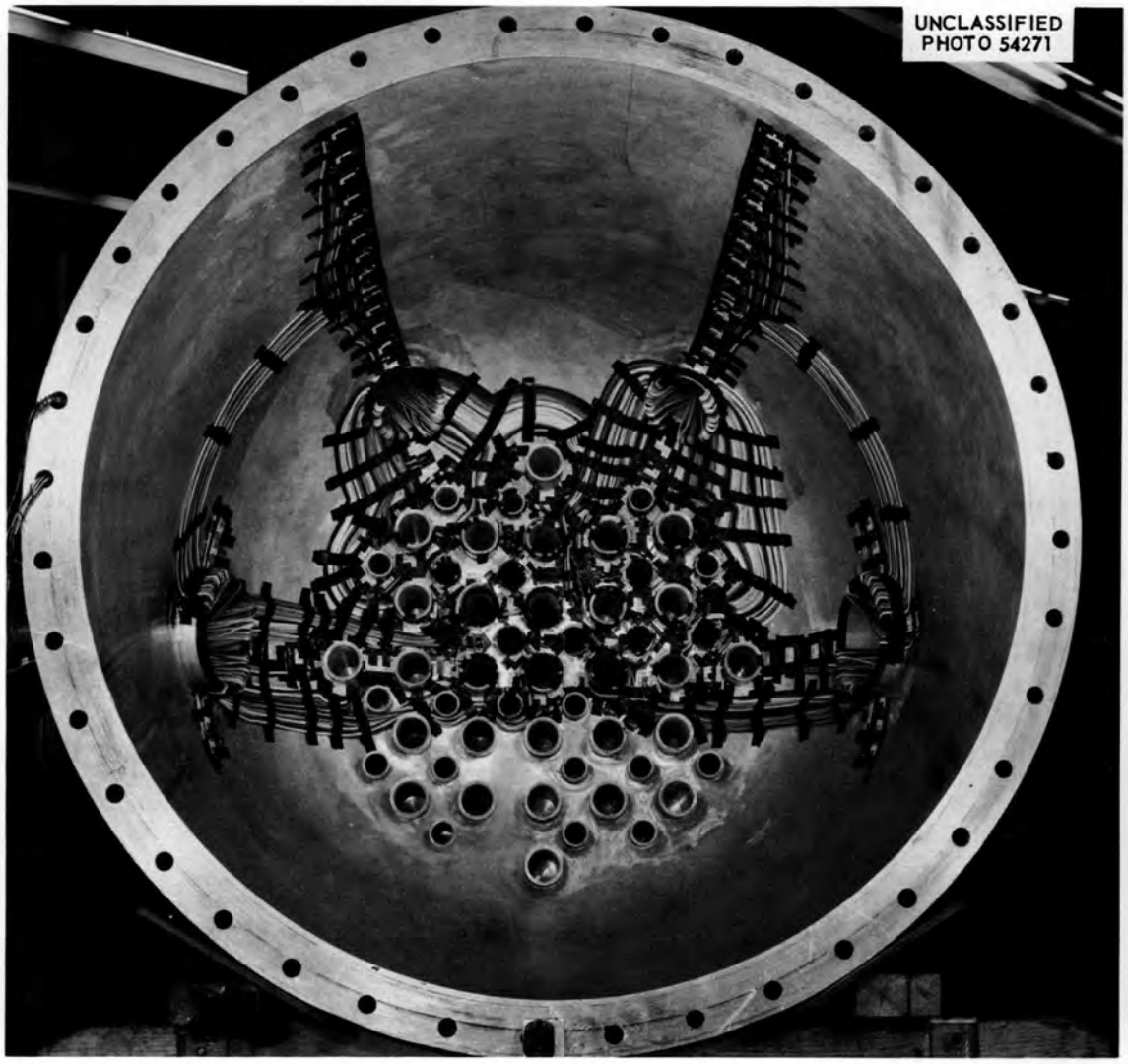

Fig. 15. Photograph of Gages in Place Inside Dome.

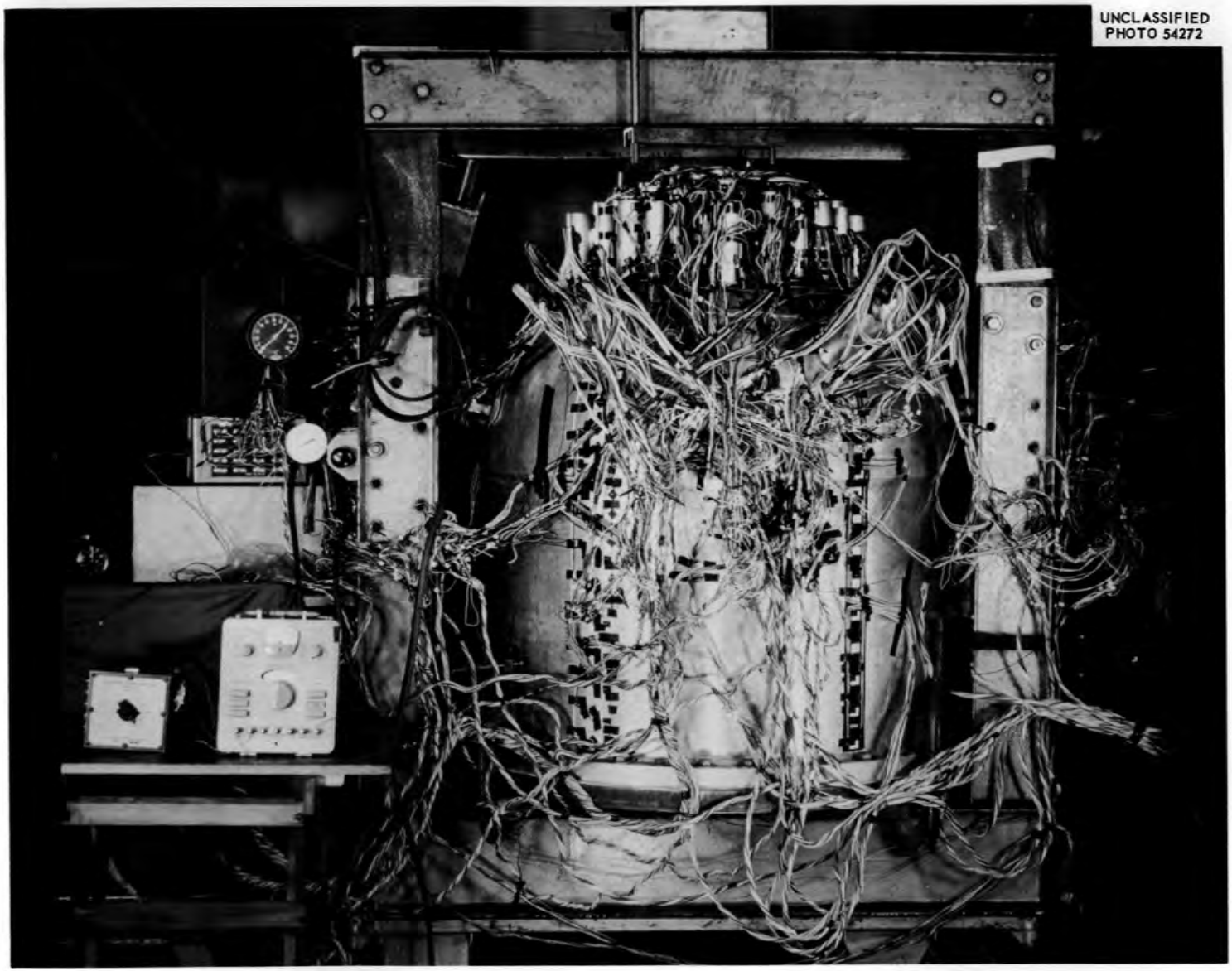

Fig. 16. Photograph of Gages in Place Outside Dome with Shell in Frame Ready for Testing.

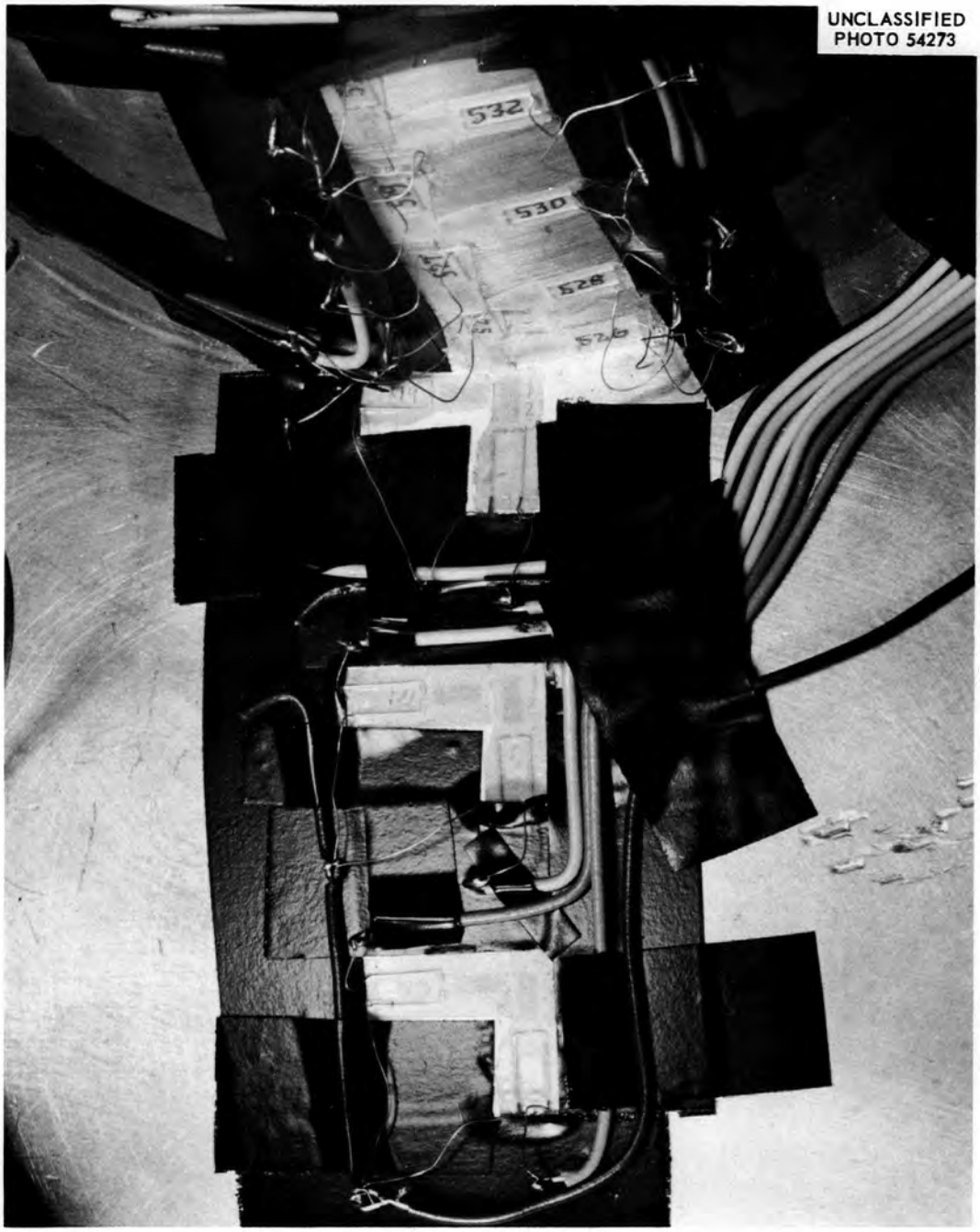

Fig. 17. Photograph of Gage Installation on and Near Nozzle A.

PART II. INTERPRETATION OF EXPERIMENTAL RESULTS AND EXAMINATION FOR STRUCTURAL INTEGRITY

F. J. Witt B. L. Greenstreet
L. R. Shobe M. E. LaVerne
R. L. Maxwell

NOMENCLATURE

a radius of cylinder, in.

E Young's modulus of elasticity of the material, psi

h thickness of cylinder, in.

M bending moment, in.-lb/in.

N normal force, lb/in.

N_i total number of safe stress cycles for stress state denoted by subscript i

n_i number of stress cycles given by design criteria for stress state denoted by subscript i

p uniform internal pressure, psig

S stress intensity (maximum algebraic stress difference = 2 times maximum shearing stress)

S_a allowable amplitude of alternating stress intensity

S_b stress intensity at limit of elastic behavior

S_p allowable primary-plus-secondary stress intensity

S_r calculated range of alternating stress intensity

S_{ij} stress difference $\sigma_i - \sigma_j$

S_{alt} calculated amplitude of alternating stress intensity = 0.5 S_r

S_{mean} adjusted value of the mean stress intensity

S'_{mean} basic value of the calculated mean stress intensity

U cumulative usage factor

μ Poisson's ratio of the material

β inverse of characteristic length for cylinders = $[3(1 - \mu)^2/a^2h^2]^{1/4}$

σ stress, psi

σ_i principal stress in the direction denoted by subscript i, i = 1, 2, 3

Subscripts

c circumferential designation for nozzles

r radial designation for nozzles or head

x axial designation for nozzles

ϕ meridional designation for head

θ circumferential designation for head

—i designates inner surface

—o designates outer surface

INTRODUCTION

The second phase of the pressure vessel design evaluation in which the experimental data were translated into quantities applicable to the full-scale vessel and the pressure vessel design was evaluated is summarized in this section. The experimental results were used to obtain the stress profiles along the nozzles based on the assumption that the distributions were correctly given by existing theoretical models. This assumption was made despite discrepancies in predicted and measured magnitudes. The profiles along the nozzles were obtained for each separate loading so that the total stresses could be determined for any combination of loads given by the design specifications. Experimental stresses in the spherical head were compared with nozzle stresses, and it was concluded that for a particular type of loading the maximum stress always occurs in the nozzles. For certain combinations of localized loads, the maximum stress may occur in the head; however, for critical design loadings this is not true.

It was found that the stresses determined analytically for a single nozzle radially attached to a spherical segment were in approximate agreement with the experimental results for a nozzle loaded by an axial force. For the cluster nozzles, much less agreement was found to exist for pressure stresses. From these observations, the simplified model appeared to be valid for localized loadings, and the thermal stresses were calculated on this basis. The results from these calculations are also included in this report.

The structural evaluations of the upper head of the vessel, including all nozzles except the burst-slug-detection and gas outlet nozzles were made using procedures outlined in "Tentative Structural Design Basis for Reactor Pressure Vessels and Directly Associated Components," PB 151987, 1 December Revision, Department of Commerce, Office of Technical Services. The primary and primary-plus-secondary stress intensities for the burst-slug-detection and gas outlet nozzles were examined, but the complete design evaluations of these units cannot be made until the temperature distributions are known.

DIMENSIONAL ANALYSIS

Since the experimental analysis was made using a 1/5.533-scale aluminum model, both scaling factors and materials properties had to be considered in applying the results to the pressure vessel. With the exception of thermal stresses, the stresses are independent of the modulus of elasticity. Although the stresses are not independent of Poisson's ratio and a difference exists between this quantity for the material of the prototype and that of the model, this difference was neglected in the analysis. The errors introduced because Poisson's ratio was 0.33 in the model and 0.3 in the prototype were usually insignificant. Also, it is often standard practice to ignore differences in Poisson's ratio that are of this order when the analyses involve ductile metals.

The pressure test for the model was conducted using an internal pressure of 60 psi, whereas the design pressure for the prototype is 350 psi. The stresses in the prototype will be the same as those in the model for a particular pressure loading. Taking σ_p as the prototype stress corresponding to a given model stress, σ_m, the relationship required for obtaining design pressure stresses in the reactor vessel, is therefore

$$\sigma_p = \frac{350}{60}\,\sigma_m = 5.833\,\sigma_m \quad . \tag{1}$$

A stress in the prototype produced by a concentrated load varies directly as the product of the ratio of the load on the prototype to the

load on the model and the square of the model dimensional scaling factor. If f_m and l_m are the concentrated load and characteristic dimension of the model, respectively, and if f_p and l_p are the corresponding values for the prototype, then

$$\sigma_p = \left(\frac{f_p}{f_m}\right)\left(\frac{l_m}{l_p}\right)^2 \sigma_m \tag{2}$$

or

$$\sigma_p = 3.266 \times 10^{-2} \left(\frac{f_p}{f_m}\right) \sigma_m \quad . \tag{3}$$

Similarly, if M_m and M_p are applied moments on the model and prototype, respectively, then

$$\sigma_p = \left(\frac{M_p}{M_m}\right)\left(\frac{l_m}{l_p}\right)^3 \sigma_m \tag{4}$$

or

$$\sigma_p = 5.904 \times 10^{-3} \left(\frac{M_p}{M_m}\right) \sigma_m \quad . \tag{5}$$

The stresses obtained from the experimental analysis of the model were translated, through the use of the above relationships, into quantities applicable to the full-scale vessel. The resulting stress values are tabulated in Appendix B.

ANALYSIS OF THE PRESSURE VESSEL

This section is devoted primarily to describing the methods used in obtaining stress profiles and maximum stresses from the experimental data. Since torsional loads on the nozzles and thermal stresses are involved in making a design evaluation of the pressure vessel, they are discussed.

Thermal stress analyses were made for the nozzles and the results are included.

Internal Pressure and Nozzle Loads

Nozzle Analysis

The mathematical model used in describing the behavior of a single nozzle radially attached to a spherical shell[3] is not a valid one for use in examining the nozzles in the cluster region of the EGCR top head; that is, the theoretical curves do not match the experimental data. However, for loadings of local character (axial and thermal loadings on a nozzle), the theoretical curves do approximate the experimental curves (see Appendix C). The theoretical pressure stresses for the burst-slug-detection nozzle agree favorably with the experimental data. Less agreement is found for the gas outlet nozzles, but the influence of the nonsymmetrical edge load is a large factor. A further discussion of this is found in Appendix C.

On the basis of these observations, the nozzles are considered as individual structural units. Since stresses along axial elements were determined experimentally, stress distributions could be plotted if the loadings were symmetrical. Asymmetries arise because of the presence of adjacent nozzles and the nonradial attachment to the shell. Although an assumption of symmetrical loading for any nozzle, except perhaps nozzle A and the burst-slug-detection nozzles, is unrealistic, it is reasonable to assume that in the neighborhood of a particular axial element the cylinder behaves the same as one with an axisymmetrical edge load and may be analyzed using this premise. Thus, the distributions may be determined using existing theory for a symmetrically loaded cylinder.

Assuming each nozzle to be an infinitely long, symmetrically loaded cylindrical shell, the following procedure was used to analyze an axial

---

[3]M. E. LaVerne and F. J. Witt, Analysis of Symmetrically Loaded, Radially-Joined Cylinder-to-Sphere Attachments, ORNL CF-61-5-26 (to be published).

element. From ref. 4 the principal stresses on the outside surface are given by

$$\sigma_x = \frac{N_x}{h} + \frac{6M_x}{h^2} \tag{6}$$

and

$$\sigma_c = \frac{N_c}{h} + \frac{6M_c}{h^2} \quad , \tag{7}$$

where M_x, M_c, and N_c are expressed as summations involving two unknown integration constants, C_1 and C_2. That is

$$M_x = \frac{1}{4a\beta^2} (C_1M_1 + C_2M_2) \quad , \tag{8}$$

$$M_c = \mu M_x \quad , \tag{9}$$

and

$$N_c = -(C_1N_1 + C_2N_2) + ap \quad , \tag{10}$$

where M_1, M_2, N_1, and N_2 are functions of the distance along the cylinder.

The axial membrane stresses, N_x/h, as determined by axial and pressure loadings, are known either from the gage readings or the magnitudes of the applied loads. In this case preference is given to the gage readings. Once the axial membrane stress is determined, the two integration

---

[4]F. J. Witt, Thermal Stress Analysis of Cylindrical Shells, ORNL CF-59-1-33 rev. (March 26, 1959). Subscript c is used here in place of the subscript θ used in the referenced report to designate the circumferential direction.

constants, C_1 and C_2, are evaluated by using two of the experimentally determined stresses in the region where bending occurs and Eqs. (6) and (7). After these evaluations are made, the stress distributions are completely determined. This entire procedure will be referred to as "stress-fitting."

Stress-fit analyses were carried out for axial elements on both the uphill and downhill sides of all gaged nozzles, except the A and burst-slug-detection nozzles,[5] which were assumed to be symmetrically loaded in all cases. (Uphill designates the side nearest the apex of the sphere, while the downhill side is farthest away.) Also, the sides 90 deg from the uphill side of the gas outlet nozzle were assumed to be alike. The experimental data used in the analyses are given in Tables B.1 and B.2 of Appendix B. Experimental stresses on the inner surface of the gas outlet nozzle are given in Table B.3, while Table B.4 contains the data for the nozzle extension on the inside of the head. The data for nozzle B (uphill side) were not acceptable and are omitted from Table B.2. The stress profiles obtained by the above method are shown in Figs. 18 through 79, in which the experimentally determined axial and circumferential stresses are also shown. These profiles are independent of nozzle subscript designations, except for nozzle L; in particular, nozzle L_4 is the one analyzed in Figs. 50 through 57 and all other figures pertaining to L. In most cases the curves were obtained by using the experimental axial and circumferential stress values (which may be the averages from several tests) corresponding to the point nearest the junction. These were chosen because, in general, much more accurate readings were obtained in the high strain regions. In cases where the data were questionable or an acceptable fit through the experimental points could not be obtained, the stresses from the second set of gages were used. In Figs. 60, 61, 64, and 65, for instance, the axial stresses at the first and second gages from the junction were used in the analyses. The experimental stresses at the inner surface

[5]The references in this report pertaining to specific nozzles are in accordance with Fig. 3.

of the gas outlet nozzle are plotted on Figs. 69, 71, 73, 75, 77, and 79. The maximum stresses in the nozzles for 350-psig internal pressure loading are given in Table B.5, while Table B.6 gives the maximum stresses for axial loadings of 1 lb/in. along the mean circumference of the cylinder.

In all cases the profiles were calculated using experimental stress values for the outer surface only. Hence, the accuracy of the method may be examined by comparing the calculated stresses for the inner surface with the experimental values. Since the inner surface of the gas outlet nozzle was instrumented, the comparisons may be made for this unit. The experimental points and stress profile for the outer surface of an axial element located on the side nearest the apex of the sphere (uphill side) are shown in Fig. 68. It may be seen that an excellent fit of the experimental points with the profile was obtained. Similar data for the inner surface are shown in Fig. 69. The agreement is good, with the fit being better for the axial than for the circumferential stress distribution. This comparison demonstrates that the method is sufficiently accurate for use in finding the peak stresses along the nozzle.

For transverse loadings (side loads acting normal to a nozzle), a theoretical analysis, considering the nozzle as a cantilever beam, shows fairly close agreement between the theoretical and experimental stress values, except in the nozzle-to-shell attachment regions. Some bending occurs in the head, so the experimental stresses near the junction also include discontinuity stresses. If the theoretical stress values are subtracted from the experimental stresses, the stress-fit analysis described above may be used to obtain the profiles of the stresses resulting from the discontinuity forces at the junction. In this case the membrane stress is zero. This method is probably less accurate than that used for pressure and axial loadings because the experimental errors are magnified, percentagewise, by the subtraction.

For transverse loadings only the B, K, and gas outlet nozzles need to be considered, since such loads probably will not be applied to the remaining nozzles. The experimental data for transverse loads of 1 lb exerted on these nozzles at various distances from the apex of the shell are given in Table B.7, in which the distances above the apex correspond

to the locations of the external piping attachment points. In obtaining the stress profiles, moment arms were measured along the axial elements being analyzed. The lines of action for transverse forces on the B and K nozzles were directed toward nozzle A. Positive directions for the forces and moments acting on the gas outlet nozzle are defined in Fig. 80.

The stress profiles along the outer surfaces of the nozzles for a transverse load of 1 lb applied at various distances along the nozzles are given in Figs. 81 through 89. Only the principal outer surface stresses are shown, since they are always larger than those on the inner surface. The maximum principal outer surface stresses are listed in Table B.8. On a given nozzle the peak stresses should be proportional to the moment arm. The discrepancies between this observation and the results in Table B.8 may be attributed to the percentagewise magnification of the error in the data used in the stress-fit analyses.

For applied moments the analysis was identical to that for transverse loadings, except that the nozzle was considered as a cantilever beam subjected to a pure moment loading. Hence, the "beam" stresses were constant with length. Only the gas outlet nozzle will be subjected to applied moments, and the experimental data for these loads are given in Table B.9. The applied moments on the gas outlet nozzle are, as indicated in Fig. 80, M_y and M_z. The stress profiles along the outside surface of the nozzle are shown in Figs. 90 through 92, and the maximum principal outer surface stresses are given in Table B.10.

Head Analysis

There was no technique similar to that used for the nozzle analyses available for obtaining stress profiles for the spherical head. The method of analysis described in ref. 3 yields stress distributions for single nozzle-to-shell attachments for axial and pressure loadings, and these distributions were calculated for single nozzles with the dimensions of those in the cluster. These stress profiles are given in Appendix C. The proximity of adjacent nozzles leads to interaction of the discontinuity forces and the resulting change in stress with distance from the nozzle is probably less than that given by the curves in the figures of Appendix C.

On this basis, maximum stresses could be approximated using theoretical analyses in combination with the experimental data; however, such an attempt was not made. Reasonable agreement between the analytical and experimental results was found to exist for the burst-slug-detection and gas outlet nozzles.

The experimental stresses at the gage locations around each nozzle are given in Tables B.11, B.12, and B.13 for axial loads and for the design pressure. The stresses in the head adjacent to nozzle B corresponding to a transverse load on this nozzle are given in Table B.14. These are the only stresses due to transverse loads tabulated for the head because the remainder were relatively small; those resulting from applied moments were also neglected for this reason.

A comparison of the stresses in the head with the peak values in the nozzles shows that the maximum pressure stresses occur in the nozzles, with one exception. This exception applies to the regions of the shell near the B nozzles, where the maximum stresses are approximately equal to the maximum nozzle stresses. For other types of loadings, the B nozzles are more highly stressed than the head. However, this exception is not of major significance, since the highest stresses for critical design loadings in the cluster region are not in the B nozzles or the head regions in their vicinities.

The experimental stress values around each nozzle were studied to determine the influence of adjacent nozzles on the stress distribution. No trend was found and no conclusions could be drawn from this study.

Discussion of Results

The principal of superposition holds for the pressure vessel. Thus, the results for individual loads may be used to obtain total stress values for combined loads. The maximum total stresses, including membrane stresses, in the various nozzles for a 350-psig loading in combination with axial compressive and tensile loadings are given in Figs. 93 through 108.

The pressure stresses are plotted as a function of the vessel profile in Figs. 109 through 114. These figures are paired to show the distributions on the inner and outer surfaces of the shell and those nozzles

which are bisected by the cutting-planes along three diametral sections. The sections are described in the figure titles. Curves were merely drawn through the experimental points for the shell, but the profiles for the nozzles are those obtained from the stress-fit analyses described earlier.

The effects of the structural discontinuity at the junction between the hemispherical head and the cylindrical body may be seen. The changes in the profiles in the junction region may be partially attributed to the discontinuity in the mean surface of the shell resulting from the change in thickness of the vessel. The plots were not carried into the region immediately adjacent to the flange because these stresses were highly dependent upon the characteristics of the flanged joint and seal. Hence, the stresses differed in tests using the same pressure loading.

The mean axial stresses for some locations along the cylindrical portion of the shell are less than the theoretical value of 7720 psi for the axial membrane stress. These discrepancies were observed for both axial elements along which gages were mounted. The elements were 180 deg apart. However, the discrepancies are of academic interest only and have no real bearing upon the structural integrity of the vessel. The differences in the axial stresses on the two surfaces of the cylindrical portion between the head and flange may be attributed to axial bending in the shell.

Torsional Loads on the Nozzles

Torsional loads will be imposed on the experimental loop and gas outlet nozzles. Since the strain gages on the model were not oriented in the directions of the principal stresses for this case, torsional loads for the nozzles in the cluster were not included in the test program. From the torsional load test on the gas outlet nozzle, it appears that the nozzle stresses can be determined adequately using analytical techniques, and the stresses in the head may be neglected. The values given for the pipe reactions yield negligible shear stresses in the nozzles with the result that the directions of the principal stresses are unchanged.

Thermal Stresses in the Nozzles and Head

Temperature gradients will exist along the external portions of the nozzles in the cluster. The temperature distributions were determined for both sizes of nozzles,[6] and they are given by functions of the form

$$T = T_0 e^{-bx} - T_0 \quad , \tag{11}$$

where T_0 is the temperature excess above the reference temperature, b is a constant, and x is the distance in inches along the cylinder. For the large nozzles, b is 0.255 in.$^{-1}$, and the value for the small nozzles is 0.260.

The thermal stresses in the head and nozzles were calculated neglecting the gradients in the head, since a thermal stress analysis of spherical shells was not available. A single nozzle-to-shell attachment configuration was assumed because the thermal stresses are localized.

The thermal stresses for a T_0 of unity are given in Figs. 115 through 120. The term "exterior nozzles" refers to the nozzles exterior to the spherical head, while the term "interior cylinders" refers to the nozzle extensions on the interior of the sphere. In order to determine the thermal stress for a particular nozzle, it is only necessary to multiply the stresses by the appropriate value of T_0. The maximum principal stresses in the nozzles for the designated T_0's[7] are given in Table B.16.

The temperature distributions along the burst-slug-detection and gas-outlet nozzles were not known. Therefore, thermal stress values for these nozzles could not be determined.

---

[6]Letter from L. G. Epel, dated June 7, 1960, Subject: "Thermal Stresses in Top Head Nozzles for EGCR Pressure Vessel."

[7]R. L. Miller, Experimental Gas-Cooled Reactor, Calculation No. MA-1.1, Reactor Vessel, Steady-State Thermal Analysis, Kaiser Engineers, August 12, 1960 (unpublished).

EXAMINATION FOR STRUCTURAL INTEGRITY

The criteria used for determining the adequacy of the design are given by the Navy Code.[8] The design basis prepared by Kaiser Engineers[9] permits higher allowable stress intensities in some cases. Therefore, a design that is adequate under the former also meets the requirements of the latter. The design data, except those for the experimental loops, were furnished by Kaiser Engineers.[10] The loads on the nozzles are summarized in Table 4. Values for the pipe reactions on the experimental loop nozzles were taken from ref. 11.

Stresses and Stress Concentrations

The stresses due to pressure and to mechanical loads were based on experimental data obtained from tests on the model. The method of analysis is such that stress concentration factors are reflected in the results. This gives conservative values for membrane and primary-plus-secondary stresses and adequate values for the fatigue analysis.

The method used for converting from model stresses to prototype stresses was discussed above in the "Dimensional Analysis" section. The pressure and mechanical stresses for the nozzles in the prototype are listed in Tables 5 through 16; those for the hemispherical head in the region of nozzle B are listed in Table 17.

The thermal stresses in the nozzles of the prototype were established through the use of refs. 3 and 6. Inasmuch as this was a theoretical

---

[8]Tentative Structural Design Basis for Reactor Pressure Vessels and Directly Associated Components, PB 151987, 1 December 1958 Revision, Department of Commerce, Office of Technical Services.

[9]R. L. Miller, E. Esztergar, G. Vitez, and E. O. Bergman, Experimental Gas-Cooled Reactor, Calculations No. MA-1.9, Reactor Vessel Design Basis, Kaiser Engineers, August 29, 1960 (unpublished).

[10]Letter from P. D. Bush to L. H. Jackson, dated September 16, 1960, Subject: Reactor Vessel Design Data (unpublished).

[11]Letter from W. S. Chmielewski to B. L. Greenstreet, Dated February 2, 1961, Subject: EGCR Experimental Loop Upper Nozzle Loads (unpublished).

Table 4. Loads Applied to Pressure Vessel Nozzles

Nozzle	Type of Load[a]	Magnitude of Load[b]	Source of Load
Control	Axial	−2 500 lb	Shield plug and control rod drive
		−42 000 lb	Service machine
Special plug	Axial	−2 000 lb	Shield plug and apparatus
		−25 000 lb	Service machine
Small experimental loop	Axial	−3 000 lb[c]	Shield plug and tube weight
		−25 000 lb	Service machine
	Axial	0	Experimental loop pipe reactions with loop cold and reactor cold
	Moment	0	
	Torque	0	
	Axial	−1 250 lb	Experimental loop pipe reactions with loop cold and reactor hot
	Moment	202 300 in.-lb	
	Torque	10 800 in.-lb	
	Axial	100 lb	Experimental loop pipe reactions with loop hot and reactor hot
	Moment	17 300 in.-lb	
	Torque	3 500 in.-lb	
Large experimental loop	Axial	−4 000 lb[d]	Shield plug and tube weight
		−42 000 lb	Service machine
	Axial	0	Experimental loop pipe reactions with loop cold and reactor cold
	Moment	0	
	Torque	0	
	Axial	−1 500 lb	Experimental loop pipe reactions with loop cold and reactor hot
	Moment	298 000 in.-lb	
	Torque	66 600 in.-lb	
	Axial	300 lb	Experimental loop pipe reactions with loop hot and reactor hot
	Moment	55 100 in.-lb	
	Torque	16 400 in.-lb	
Gas outlet nozzle	Axial	30 000 lb	Reactor and gas outlet pipe cold
	Moment	360 000 in.-lb	
	Axial	3 000 lb[e]	Reactor and gas outlet pipe hot
		36 000 in.-lb[e]	

[a]There is an internal pressure load of 350 psi on all nozzles.

[b]A positive axial load produces an axial tensile stress in the nozzles.

[c]Reference 10 lists 2000 lb; reference 11 lists 4000 lb; an average value of 3000 lb has been used.

[d]Reference 10 lists 3000 lb; reference 11 lists 5000 lb; an average value of 4000 lb has been used.

[e]Private communication, G. Meikel, Kaiser Engineers, January 12, 1961. Since the loadings may be either negative or positive, a positive loading was assumed in each case. This gave conservative stress values.

Table 5. Steady-State and Transient Stresses on Nozzle A

Source of Load	Load	Stress (psi)			
		Outer Surface		Inner Surface	
		σ_x	σ_c	σ_x	σ_c
Shield plug and drive	−2500 lb	−237	−122	157	−4
Shield plug and tube on each of the four small experimental loop nozzles	−3000 lb[a]	−265	−260	265	−101
Internal pressure	350 psig	21 586	16 322	−20 102	3815
Thermal gradient	50°F[b]	8 972	1 211	−8 972	−1814
Total stress at end of startup		30 056	17 151	−28 652	1896
Service machine load	−42 000 lb	−3 982	−2 054	2 629	−71

[a]See footnote c, Table 4.

[b]Temperature difference.

Table 6. Steady-State and Transient Stresses on Nozzle B (Uphill Side)

Source of Load	Load	Stress (psi)			
		Outer Surface		Inner Surface	
		σ_x	σ_c	σ_x	σ_c
Shield plug, tee, experimental apparatus, etc. on each of four B nozzles	−3000 lb	−1029	−207	574	360
Internal pressure	350 psig	6162	10 049	−4390	6884
Thermal gradient	34°F[a]	4893	807	−4893	−1028
Experimental loop piping: reactor hot and loop cold					
Thrust	−1250 lb	−429	−86	239	150
Moment	202 300 in.-lb[b]	−9834	−3 245		
Torque	10 800 in.-lb[c]				
Experimental loop piping: reactor hot and loop hot					
Thrust	100 lb	34	7	−19	−12
Moment	17 300 in.-lb[d]	−841	−277		
Torque	3500 in.-lb[c]				
Service machine	−25 000 lb	−4548	−1 820	2518	300

[a]Temperature difference.

[b]Assumed equivalent to a force of 1442 lb acting 139.7 in. above apex (actual length 140.3 in.).

[c]Stresses resulting from torque are zero where σ_x and σ_c are maximum.

[d]Assumed equivalent to a force of 123.3 lb acting 139.7 in. above apex (actual length 140.3 in.).

Table 7. Steady-State and Transient Stresses on Nozzle B (Downhill Side)

Source of Load	Load	Stress (psi)			
		Outer Surface		Inner Surface	
		σ_x	σ_c	σ_x	σ_c
Shield plug, tee, experimental apparatus, etc. on each of four B nozzles	−3000 lb	−986	−353	474	85
Internal pressure	350 psig	10 665	13 338	−9511	7285
Thermal gradient	34°F[a]	4 893	807	−4893	−1028
Experimental loop piping: reactor hot and loop cold					
Thrust	−1250 lb	−411	−148	198	35
Moment	202 300 in.-lb[b]	10 687	5 700		
Torque	10 800 lb-in.[c]				
Experimental loop piping: reactor hot and loop hot					
Thrust	100 lb	33	12	−16	−3
Moment	17 300 lb-in.[d]	914	487		
Torque	3500 in.-lb[c]				
Service machine	−25 000 lb	−4 548	−1 820	2518	300

[a]Temperature difference.

[b]Assumed equivalent to a force of 1442 lb acting 139.7 in. above apex (actual length 141.6 in.).

[c]Stresses resulting from torque are zero where σ_x and σ_c are maximum.

[d]Assumed equivalent to a force of 123.3 lb acting 139.7 in. above apex (actual length 141.6 in.).

Table 8. Steady-State and Transient Stresses on Nozzle J (Uphill Side)

Source of Load	Load	Stress (psi)			
		Outer Surface		Inner Surface	
		σ_x	σ_c	σ_x	σ_c
Shield plug and drive	−2 000 lb	−286	−111	121	11
Internal pressure	350 psig	8 715	6 878	−7 047	2 150
Thermal gradient	8°F[a]	1 152	190	−1 152	−242
Total stress at end of startup		9 581	6 957	−8 078	1 919
Service machine load	−25 000 lb	−3 580	−1 387	1 515	140

[a]Temperature difference.

Table 9. Steady-State and Transient Stresses on Nozzle J (Downhill Side)

Source of Load	Load	Stress (psi)			
		Outer Surface		Inner Surface	
		σ_x	σ_c	σ_x	σ_c
Shield plug and drive	−2 000 lb	−517	−183	367	82
Internal pressure	350 psig	21 054	16 174	−19 002	4 158
Thermal gradient	8°F[a]	1 152	190	−1 152	−242
Total stress at end of startup		21 689	16 181	−19 787	3 998
Service machine load	−25 000 lb	−6 465	−2 285	4 583	1 030

[a]Temperature difference.

Table 10. Steady-State and Transient Stresses on Nozzle K (Uphill Side)

Source of Load	Load	Stress (psi)			
		Outer Surface		Inner Surface	
		σ_x	σ_c	σ_x	σ_c
Shield plug, tee, experimental apparatus, etc.	−4000 lb	−348	−121	209	46
Internal pressure	350 psig	6585	6231	−5827	2508
Thermal gradient	6°F[a]	1076	145	−1076	−218
Experimental loop piping: reactor hot and loop cold					
Thrust	−1500 lb	−130	−45	78	17
Moment	298 200 in.-lb[b]	−7620	−2018		
Torque	66 600 in.-lb[c]				
Experimental loop piping: reactor hot and loop hot					
Thrust	300 lb	26	9	−16	−4
Moment	55 100 in.-lb[d]	−1408	−373		
Torque	16 400 in.-lb[c]				
Service machine	−42 000 lb	−3646	−1268	2188	483

[a]Temperature difference.

[b]Assumed equivalent to a force of 1959 lb acting 135.9 in. above apex (actual length 152.2 in.).

[c]Stresses resulting from torque are zero where σ_x and σ_c are maximum.

[d]Assumed equivalent to a force of 362 lb acting 135.9 in. above apex (actual length 152.2 in.).

Table 11. Steady-State and Transient Stresses on Nozzle K (Downhill Side)

Source of Load	Load	Stress (psi)			
		Outer Surface		Inner Surface	
		σ_x	σ_c	σ_x	σ_c
Shield plug, tee, experimental apparatus, etc.	−4000 lb	−504	−184	328	67
Internal pressure	350 psig	18 756	12 710	−16 896	2014
Thermal gradient	6°F[a]	1 076	145	−1 076	−218
Experimental loop piping: reactor hot and loop cold					
Thrust	−1500 lb	−189	−69	123	25
Moment	298 200 in.-lb[b]	5 054	2 277		
Torque	66 600 in.-lb[c]				
Experimental loop piping: reactor hot and loop hot					
Thrust	300 lb	38	14	−25	−5
Moment	55 100 in.-lb[d]	934	421		
Torque	16 400 in.-lb[c]				
Service machine	42 000 lb	−5 284	−1 915	3 436	697

[a]Temperature difference.

[b]Assumed equivalent to a force of 1959 lb acting 135.9 in. above apex (actual length 161.1 in.).

[c]Stresses due to torque are zero where σ_x and σ_c are maximum.

[d]Assumed equivalent to a force of 362 lb acting 135.9 in. above apex (actual length 161.1 in.).

Table 12. Steady-State and Transient Stresses on Nozzle L_4 (Uphill Side)

Source of Load	Load	Stress (psi)			
		Outer Surface		Inner Surface	
		σ_x	σ_c	σ_x	σ_c
Shield plug and drive	−2 000 lb	−278	−47	118	72
Internal pressure	350 psig	9 052	5 121	−6 848	350
Thermal gradient	5°F[a]	720	119	−720	−151
Total stress at end of startup		9 494	5 193	−7 450	271
Service machine load	−25 000 lb	−3 480	−585	1 470	903

[a]Temperature difference.

Table 13. Steady-State and Transient Stresses on Nozzle L_4 (Downhill Side)

Source of Load	Load	Stress (psi)			
		Outer Surface		Inner Surface	
		σ_x	σ_c	σ_x	σ_c
Shield plug and drive	−2 000 lb	−413	−120	249	79
Internal pressure	350 psig	16 293	11 799	−14 789	2 474
Thermal gradient	5°F[a]	720	119	−720	−151
Total stress at end of startup		16 600	11 798	−15 260	2 402
Service machine load	−25 000 lb	−5 160	−1 495	3 113	988

[a]Temperature difference.

Table 14. Steady-State and Transient Stresses on Nozzle M (Uphill Side)

Source of Load	Load	Stress (psi)			
		Outer Surface		Inner Surface	
		σ_x	σ_c	σ_x	σ_c
Shield plug and drive	−2 500 lb	−211	−103	81	−15
Internal pressure	350 psig	6 470	5 809	−4 070	2 647
Thermal gradient	5°F[a]	897	121	−897	−181
Total stress at end of startup		7 156	5 827	−4 886	2 451
Service machine load	−42 000 lb	−3 536	−1 726	1 365	−256

[a]Temperature difference.

Table 15. Steady-State and Transient Stresses on Nozzle M (Downhill Side)

Source of Load	Load	Stress (psi)			
		Outer Surface		Inner Surface	
		σ_x	σ_c	σ_x	σ_c
Shield plug and drive	−2 500 lb	−334	−178	221	−11
Internal pressure	350 psig	19 018	17 261	−16 696	6 547
Thermal gradient	5°F[a]	897	121	−897	−181
Total stress at end of startup		19 581	17 204	−17 372	6 355
Service machine load	−42 000 lb	−5 615	−2 986	3 712	189

[a]Temperature difference.

Table 16. Steady-State and Transient Stresses on Gas Outlet Nozzle

Source of Load	Load	Stress (psi)			
		Outer Surface		Inner Surface	
		σ_x	σ_c	σ_x	σ_c
Coolant piping: reactor and pipe cold					
Thrust	30 000 lb[a]	920	450	−650	50
Moment	360 000 in.-lb[a]	820	420	−580[b]	50
Internal pressure	350 psig[a]	14 958	12 714	−13 958	5381
Coolant piping: reactor and pipe hot					
Thrust	3000 lb[a,c]	92	45	−65	5
Moment	36 000 in.-lb[a,c]	82	42	−58[d]	5[e]
Thermal gradient	No data available				

[a]Tables B.5, B.6, and B.8 indicate considerable variation with location in some of the stresses. The maximum values have been used here.

[b]No data available; assumed to be in same ratio to −650 as 820/920.

[c]Private communication, G. Meikel, Kaiser Engineers, January 12, 1961. Since the loadings may be either negative or positive, a positive loading was assumed in each case. This gave conservative stress values.

[d]No data available; assumed to be in same ratio to −65 as 82/92.

[e]Assumed.

Table 17. Steady-State and Transient Stresses in Hemispherical Head Around Nozzle B

Source of Load	Load	Stress (psi)			
		Outer Surface		Inner Surface	
		σ_ϕ	σ_θ	σ_ϕ	σ_θ
Shield plug, tee, experimental apparatus, etc. on each of four B nozzles	−3000 lb[a]	−179	−182	161	121
Internal pressure	350 psig[a]	8393	13 658	7782	10 070
Thermal gradient	34°F[b]	580	−685	−211	158
Experimental loop pipe on nozzle B: reactor hot and loop cold					
Thrust	−1250 lb[a]	−75	−76	+67	+50
Moment[c]	202 300 in.-lb[a]	1608	1 392	−1658	1 518
Torque	10 800 in.-lb				
Experimental loop pipe on nozzle B: reactor hot and loop hot					
Thrust	100 lb[a]	6	6	−5	−4
Moment[c]	17 300 in.-lb[a]	137	119	−142	130
Torque	3500 in.-lb				
Service machine on nozzle B	−25 000 lb[a]	−1500	−1 520	1340	1 000

[a]Tables B.11, B.12, and B.14 indicate considerable variation with location in some of the stresses. The maximum values have been tabulated here.

[b]Temperature difference.

[c]Taken from Table B.14 assuming a lever arm of 139.7 in. above apex (actual length: 140.3 in. on uphill side, 141.6 in. on downhill side). See notes b and d, Tables 6 and 7.

development, stress concentration factors as suggested by paragraph A.8.11.5 of the Navy Code were applied in converting to the actual thermal stresses in the prototype.

The radius of the fillet in the nozzle-to-head connection of the model is 0.0625 in. The geometrically similar radius in the prototype would be 0.3458 in., and it has been assumed that the fillet radius of the prototype will be this large or larger.

For the control rod and large experimental loop nozzles the ratio of the fillet radius to cylinder thickness is 0.29. From Fig. A.7-1, page 92, of the Navy Code, the stress concentration factor is found to be ~1.78. Similarly, for the special plug and small experimental tube

nozzles the ratio of the fillet radius to the cylinder thickness is 0.395, and the stress concentration factor is ~1.6. Likewise, for the hemispherical head this ratio is 0.0865, and the stress concentration factor is 3.1.

Examination of the Design

As was pointed out earlier, the stress conditions in the nozzles are more severe than those in the hemispherical shell except for σ_θ on the outer surface of the shell adjacent to nozzle B at 90 deg from a meridional plane through the axes of nozzles A and B. Examination of Tables 5 through 16 indicates that nozzle A is the most critical of the nozzles. This investigation was confined to nozzles A, B, and K in the top head nozzle cluster, the gas outlet nozzle, and the aforementioned area in the head adjacent to nozzle B. The stresses in the hemispherical head away from the nozzles and in the cylindrical portion of the vessel are well within the allowable limits.

Nozzle A

Steady-State Conditions. In examining the steady-state conditions, the following loads and stresses were taken from Tables 4 and 5:

1. Loads

   350-psig internal pressure

   Shield plug and drive load on nozzle A = 2500-lb thrust

   Shield plug and experimental tube weight load on each of the four B nozzles = 3000-lb thrust

2. Membrane stresses (see Navy Code, 5.1.1)

$$\sigma_x = \frac{\sigma_{xo} + \sigma_{xi}}{2}$$

$$\sigma_c = \frac{\sigma_{co} + \sigma_{ci}}{2}$$

$$\sigma_r = \frac{\sigma_{ro} + \sigma_{ri}}{2}$$

Effect of pressure

$$\sigma_x = \frac{21\ 586 - 20\ 102}{2} = 742 \text{ psi}$$

$$\sigma_c = \frac{16\ 322 + 3815}{2} = 10\ 068 \text{ psi}$$

$$\sigma_r = \frac{0 - 350}{2} = -175 \text{ psi}$$

Effect of shield plug and drive on nozzle A

$$\sigma_x = \frac{-237 + 157}{2} = -40 \text{ psi}$$

$$\sigma_c = \frac{-122 - 4}{2} = -63 \text{ psi}$$

$$\sigma_r = 0$$

Effect of shield plug, etc. on B nozzles

$$\sigma_x = \frac{-265 + 265}{2} = 0$$

$$\sigma_c = \frac{-260 - 101}{2} = -180 \text{ psi}$$

$$\sigma_r = 0$$

In summary, the membrane stresses are:

Load	Principal Stresses (psi) σ_x	σ_c	σ_r
Internal pressure	742	10 068	−175
Shield plug, etc. on nozzle A	−40	−63	0
Shield plug, etc. on B nozzles	0	−180	0
Total	702	9 825	−175

and the stress intensity is 10 000 psi. From Table 5-1, page 25, of the Navy Code, it is found by interpolation that for a temperature of 650°F the permissible value for S_m is 17 000 psi. The membrane stress intensity given above is well under this limit and is therefore satisfactory. The primary plus secondary stresses are (see Navy Code, 5.1.3):

	Principal Stresses (psi)					
	Outer Surface			Inner Surface		
Load	σ_x	σ_c	σ_r	σ_x	σ_c	σ_r
Pressure	21 586	16 322	0	−20 102	3815	−350
Shield plug, etc. on nozzle A	−237	−122	0	157	−4	0
Shield plug, etc. on B nozzles	−265	−260	0	265	−101	0
Total	21 084	15 940	0	−19 680	3710	−350

and the stress intensities are 21 084 and 23 390 psi. From Table 5-1, page 25, of the Navy Code, it is found that for 650°C the permissible value for S_p is 24 000 psi. The total primary plus secondary stress intensities are therefore acceptable.

Combinations of Steady-State and Transient Conditions. Arbitrary time designations were assigned to changes in stress conditions for the vessel. The stresses at times I-V and VIII-X shown below were obtained from Table 5. The stresses at times VI and VII were obtained by assuming

a ±15% change in the temperature stresses shown in Table 5. The condition, stress, and stress difference summary is presented below:

Time	Condition	Principal Stresses (psi)			Stress Differences (psi)		
		σ_1	σ_2	σ_3	$S_{12}=\sigma_1-\sigma_2$	$S_{23}=\sigma_2-\sigma_3$	$S_{31}=\sigma_3-\sigma_1$
I	Shield plugs not in	0	0	0	0	0	0
II	Initial condition with shield plugs in	−502	−382	0	−120	−382	502
III	Pressurized 350 psig	21 084	15 940	0	5 144	15 940	−21 084
IV	End of startup	30 056	17 151	0	12 905	17 151	−30 056
V	Service machine on nozzle A	26 074	15 097	0	10 977	15 097	−26 074
VI	115% design temperature	31 402	17 332	0	14 070	17 332	−31 402
VII	85% design temperature	28 710	16 970	0	11 740	16 970	−28 710
VIII	Beginning of shutdown	30 056	17 151	0	12 905	17 151	−30 056
IX	End of shutdown	−502	−382	0	−120	−382	502
X	Shield plugs removed	0	0	0	0	0	0

Outer Surface Examination. The stress variations with time are sketched in Fig. 121 for the outer surface. The stress differences are plotted in Fig. 122. By inspection of these figures it is apparent that there are three classes of cycles to be investigated. These classes and the number of cycles are:

Class X. ±15% temperature fluctuations, 100 000 cycles

Class Y. Service machine loading, 500 cycles

Class Z. Initial condition to 100% power to shutdown, 500 cycles

In accordance with paragraph B.2.4.2 of the Navy Code, usage factors of 0.2, 0.3, and 0.3 for these three classes are arbitrarily assigned and the applicable values of allowable amplitude of alternating stress intensity, S_a, determined. For these usage factors the following values of S_a are obtained:

Class	Cycles	Assigned Usage Factor	Cycles for Determining S_a	Applicable Value of S_a (psi)
X	100 000	0.2	500 000	25 000
Y	500	0.3	1 670	62 000
Z	500	0.3	1 670	62 000

These are the values of S_a to be used in constructing the Fatigue Diagram (Fig. 123) discussed in paragraph 5.2.5 of the Navy Code. The three classes of combined steady-state and transient conditions are analyzed below (see Navy Code, 5.2 through 5.2.8).

Class X. ±15% Temperature Fluctuations

The principal stresses, in psi, are:

	σ_1	σ_2	σ_3
Design power	30 056	17 151	0
115% design temperature	31 402	17 332	0
85% design temperature	28 710	16 970	0
Design power	30 056	17 151	0

The maximum and minimum stress differences, $S_{ij} = \sigma_i - \sigma_j$, the stress difference ranges, S_{rij}, the alternating stress differences, $S_{alt\ ij} = S_{rij}/2$, and the basic mean stress differences, $S'_{mean\ ij}$, are:

	S_{12}	S_{23}	S_{31}
S_{ij} (115% design temperature)	14 070	17 332	−31 402
S_{ij} (85% design temperature)	11 740	16 970	−28 710
S_{rij}	2 330	362	2 692
$S_{alt\ ij}$	1 165	181	1 346
$S'_{mean\ ij}$	12 905	17 151	30 056

$$S_{alt\ ij} + S'_{mean\ ij} < 42\ 000 \text{ psi} = S_b \quad ;$$

therefore

$$S'_{mean\ ij} = S_{mean\ ij} \quad .$$

Rounding to the next hundred gives:

	S_{12}	S_{23}	S_{31}
$S_{alt\ ij}$	1 200	200	1 400
$S_{mean\ ij}$	13 000	17 200	30 100

These points all fall in the appropriate safe zone of the fatigue diagram; hence, the design is satisfactory for this cycle (see Fig. 123).

Class Y. Service Machine Loading

The principal stresses in psi are:

	σ_1	σ_2	σ_3
Design power	30 056	17 151	0
Plus service machine load	26 074	15 097	0
Design power	30 056	17 151	0

The stress differences needed are:

	S_{12}	S_{23}	S_{31}
S_{ij} (design power)	12 905	17 151	−30 056
S_{ij} (design power plus service machine)	10 977	15 097	−26 074
S_{rij}	1 928	2 054	3 982
$S_{alt\ ij}$	964	1 027	1 991
$S'_{mean\ ij}$	11 941	16 124	28 065

$$S_{alt\ ij} + S'_{mean\ ij} < 42\ 000 \text{ psi} = S_b \quad ;$$

therefore

$$S'_{mean\ ij} = S_{mean\ ij} \quad .$$

Rounded to the next hundred, the significant stress quantities are:

	S_{12}	S_{23}	S_{31}
$S_{alt\ ij}$	1 000	1 100	2 000
$S_{mean\ ij}$	12 000	16 200	28 100

Again, these points fall within the appropriate safe zone of the fatigue diagram (Fig. 123); hence, the design is adequate for this cycle.

Class Z. Initial Condition to 100% Power to Shutdown

The principal stresses in psi are:

	σ_1	σ_2	σ_3
Initial condition	−502	−382	0
Design power	30 056	17 151	0
Shutdown	−502	−382	0

The stress differences needed are:

	S_{12}	S_{23}	S_{31}
S_{ij} (design power)	12 905	17 151	−30 056
S_{ij} (shutdown)	−120	−382	502
S_{rij}	13 025	17 533	30 558
$S_{alt\ ij}$	6 513	8 767	15 279
$S'_{mean\ ij}$	6 393	8 385	14 777

$$S_{alt\ ij} + S'_{mean\ ij} < 42\ 000 \text{ psi} = S_b \quad ;$$

therefore

$$S'_{mean\ ij} = S_{mean\ ij} \quad .$$

Rounded to the next hundred, the significant stress quantities become:

	S_{12}	S_{23}	S_{31}
$S_{alt\ ij}$	6600	8800	15 300
$S_{mean\ ij}$	6400	8400	14 800

Again, these points fall in the appropriate safe zone of the fatigue diagram (see Fig. 123), and the design is safe for this cycle.

Alternate Fatigue Evaluation. Instead of assigning a usage factor to each class of cycles, an alternate method may be used wherein the cumulative usage factor is determined directly as described in paragraph 5.2.8 of the Navy Code. Straight lines are drawn from the allowable mean stress intensity, S_s, on the abscissa of the fatigue diagram (shown in Fig. 123) through that point ($S_{mean\ ij}$, $S_{alt\ ij}$) of each class that gives the largest intercept on the alternating stress axis. In this case the value of S_s is 68 000 psi and S_{ax}, S_{ay}, and S_{az} are 2 400, 3 200, and 19 500 psi, respectively. Since an infinite number of cycles, N, is associated with each of these values, the usage factor (page 32, Navy Code),

$$U = \frac{n_1}{N_1} + \frac{n_2}{N_2} + \frac{n_3}{N_3} \quad ,$$

is equal to zero, and the design is again shown to be satisfactory.

Inner Surface Examination. The inner surface of nozzle A was examined for fatigue damage in the same manner as the outer surface was analyzed. The three classes of cycles gave stress intensities which were found to fall well within the appropriate safe zones of the fatigue diagram. The design of nozzle A is therefore satisfactory.

Nozzle B

Examination of Tables 6 and 7 reveals that the outer surface on the downhill side is the area of greatest stress severity in nozzle B. An investigation similar to that made for nozzle A was made of this area with the loads exerted by the experimental loop piping also being considered. The location of the point and the sign of the maximum stress from these latter loads were assumed to be the same as for the pressure stress. Although this assumption is probably not true, it is conservative.

Steady-State Conditions. The following loads were taken from Table 4, and the stress values were derived from Table 7:

1. Loads

   350-psig internal pressure

   Shield plug, tee, and experimental loop on four B nozzles, 3000-lb thrust of each

2. Membrane stress evaluation [$\sigma_x = (\sigma_{xi} + \sigma_{xo})/2$, etc.]

Load	Principal Stresses (psi)		
	σ_x	σ_c	σ_r
Pressure	577	10 312	−175
Shield plug, etc.	−256	−134	0
Total	321	10 178	−175

The stress intensity is thus 10 353 psi, which is less than the allowable 17 000 psi and is therefore satisfactory.

3. Primary plus secondary stress evaluation

Load	Principal Stresses (psi)					
	Outer Surface			Inner Surface		
	σ_x	σ_c	σ_r	σ_x	σ_c	σ_r
Pressure	10 665	13 338	0	−9511	7285	−350
Shield plug, etc.	−986	−353	0	474	85	0
Pipe reactions – loop cold, reactor hot						
Thrust	−411	−148	0			0
Moment	10 687	5 700	0			0
Total	19 955	18 537	0			−350

The stress intensity is thus 19 955 psi, which is less than the allowable 24 000 psi and is therefore satisfactory.

Combinations of Steady-State and Transient Conditions. The stresses at times I-VII and X-XII shown below were obtained from Table 7; the stresses at times VIII and IX were obtained by assuming a ±15% change in the temperature stresses shown in the same table:

Time and Condition	Principal Stresses (psi)			Stress Differences (psi)		
	σ_1	σ_2	σ_3	$S_{12}=\sigma_1-\sigma_2$	$S_{23}=\sigma_2-\sigma_3$	$S_{31}=\sigma_3-\sigma_1$
I. Shield plugs, loops, etc. not in	0	0	0	0	0	0
II. Initial condition with shield plugs, etc. in	−986	−353	0	−633	−353	986
III. Pressurized	9 679	12 985	0	−3306	12 985	−9 679
IV. Vessel temperature increased to design temperature	14 572	13 792	0	780	13 792	−14 572
V. Cold pipe reaction at end of startup	24 848	19 344	0	5504	19 334	−24 848
VI. Hot pipe reaction	15 519	14 291	0	1228	14 291	−15 519
VII. Service machine load on B nozzles	20 300	17 524	0	2776	17 524	−20 300
VIII. 115% design temperature	25 582	19 466	0	6116	19 466	−25 582
IX. 85% design temperature	24 114	19 222	0	4892	19 222	−24 114
X. Beginning of shutdown	24 848	19 344	0	5504	19 344	−24 848
XI. End of shutdown	−986	−353	0	−633	−353	986
XII. Shield plugs, etc. removed	0	0	0	0	0	0

Outer Surface (Downhill Side) Examination. The variations of the stresses are sketched in Fig. 124. The stress differences are plotted in Fig. 125.

The stresses indicate that there are four classes of cycles to be investigated. These four classes and the number of cycles for each are:

Class W. ±15% temperature fluctuations, 100 000 cycles

Class X. Service machine loading, 500 cycles

Class Y. Experimental loop pipe loads, 500 cycles

Class Z. Initial condition to 100% power to shutdown, 500 cycles

In accordance with paragraph B.2.4.2 of the Navy Code, a usage factor of 0.2 was arbitrarily assigned to each, and the applicable values of S_a were determined:

Class	Cycles	Assigned Usage Factor	Cycles for Determining S_a	Applicable Value of S_a (psi)
W	100 000	0.2	500 000	25 000
X	500	0.2	2 500	56 000
Y	500	0.2	2 500	56 000
Z	500	0.2	2 500	56 000

These values of S_a were used in constructing the Fatigue Diagram (Fig. 126) discussed in paragraph 5.2.5 of the Navy Code. The four classes of combined steady-state and transient conditions were then analyzed (see Navy Code, 5.2 through 5.2.8).

Class W. ±15% Temperature Fluctuations

The principal stresses, in psi, are:

	σ_1	σ_2	σ_3
Design power	24 848	19 344	0
115% design temperature	25 582	19 466	0
85% design temperature	24 114	19 222	0
Design power	24 848	19 344	0

The stress differences needed are:

	S_{12}	S_{23}	S_{31}
S_{ij} (115% design temperature)	6116	19 466	−25 582
S_{ij} (85% design temperature)	4892	19 222	−24 114
S_{rij}	1224	244	1 468
$S_{alt\ ij}$	612	122	734
$S'_{mean\ ij}$	5504	19 344	24 848

$$S_{alt\ ij} + S'_{mean\ ij} < 42\ 000 \text{ psi} = S_b \quad ;$$

therefore

$$S'_{mean\ ij} = S_{mean\ ij} \quad .$$

Rounding to the next hundred gives:

	S_{12}	S_{23}	S_{31}
$S_{alt\ ij}$	700	200	800
$S_{mean\ ij}$	5600	19 400	24 900

Class X. Service Machine Loading

The principal stresses, in psi, are:

	σ_1	σ_2	σ_3
Design power	24 848	19 344	0
Plus service machine load	20 300	17 524	0
Design power	24 848	19 344	0

The stress differences are:

	S_{12}	S_{23}	S_{31}
S_{ij} (design power)	5504	19 344	−24 848
S_{ij} (design power plus service machine)	2776	17 524	−20 300
S_{rij}	2728	1 820	4 548
$S_{alt\ ij}$	1364	910	2 274
$S'_{mean\ ij}$	4140	18 434	22 574

$$S_{alt\ ij} + S'_{mean\ ij} < 42\ 000 \text{ psi} = S_b \ ;$$

therefore

$$S'_{mean\ ij} = S_{mean\ ij} \ .$$

Rounding to the next hundred, the significant stress quantities are:

	S_{12}	S_{23}	S_{31}
$S_{alt\ ij}$	1400	1 000	2 300
$S_{mean\ ij}$	4200	18 500	22 600

Class Y. Experimental Loop Pipe Loads

The principal stresses, in psi, are:

	σ_1	σ_2	σ_3
Design power, loop cold	24 848	19 344	0
Design power, loop hot	15 519	14 291	0
Design power, loop cold	24 848	19 344	0

The corresponding stress differences are:

	S_{12}	S_{23}	S_{31}
S_{ij} (loop cold)	5504	19 344	−24 848
S_{ij} (loop hot)	1228	14 291	−15 519
S_{rij}	4276	5 053	9 329
$S_{alt\ ij}$	2138	2 527	4 665
$S'_{mean\ ij}$	3366	16 818	20 184

$$S_{alt\ ij} + S'_{mean\ ij} < 42\ 000 \text{ psi} = S_b \quad ;$$

therefore

$$S'_{mean\ ij} = S_{mean\ ij} \quad .$$

Rounding to the next hundred, $S_{alt\ ij}$ and $S_{mean\ ij}$ become:

	S_{12}	S_{23}	S_{31}
$S_{alt\ ij}$	2200	2 600	4 700
$S_{mean\ ij}$	3400	16 900	20 200

Class Z. Initial Condition to 100% Power to Shutdown

The principal stresses, in psi, are:

	σ_1	σ_2	σ_3
Initial condition	−986	−353	0
Design power	24 848	19 344	0
Shutdown	−986	−353	0

The necessary stress differences are:

	S_{12}	S_{23}	S_{31}
S_{ij} (design power, loop cold)	5504	19 344	−24 848
S_{ij} (shutdown)	−633	−353	986
S_{rij}	6137	19 697	25 834
$S_{alt\ ij}$	3069	9 849	12 917
$S'_{mean\ ij}$	2436	9 496	11 931

$$S_{alt\ ij} + S'_{mean\ ij} < 42\ 000 \text{ psi} = S_b \quad ;$$

therefore

$$S'_{mean} = S_{mean\ ij} \quad .$$

Rounding to the next hundred, the significant stress quantities are:

	S_{12}	S_{23}	S_{31}
$S_{alt\ ij}$	3100	9900	13 000
$S_{mean\ ij}$	2500	9500	12 000

Fatigue Diagram. The fatigue diagram (Fig. 126) for the outer surface of nozzle B on the downhill side was constructed utilizing the derived values of S_{aW}, S_{aX}, S_{aY}, and S_{aZ}, and the values of S_b and S_u listed on page 25 of the Navy Code. The points $(S_{mean\ ij}, S_{alt\ ij})_{W,X,Y,Z}$ were plotted and found to fall well within the appropriate safe zones of the diagram. Application of a modification of Miner's hypothesis (Navy Code, 5.2.8) gives a usage factor well below the 0.8 allowable.

With respect to stress criteria, the design of nozzle B is adequate. It is to be noted, however, that the distortion limits necessitated by operational considerations (Navy Code, 1.5) were also examined and found to be greater than the calculated limits.[12]

[12]Private communication, W. S. Chmielewski, on assignment from Internuclear Co., Clayton, Missouri to Reactor Division.

Nozzle K

Examination of Tables 10 and 11 reveals that the outer surface on the downhill side is the area of greatest stress severity in nozzle K. An investigation similar to that made for nozzle B was made of this area with the stresses being combined in the same conservative way.

Steady-State Conditions. The following loads and stresses were taken from Tables 4 and 11, respectively.

1. Loads

   350-psig internal pressure

   Shield plug, tee, and experimental loop on four B nozzles, 2500-lb thrust on each

2. Membrane stress evaluation [$\sigma_x = (\sigma_{xi} + \sigma_{xo})/2$, etc.]

Load	Principal Stresses (psi)		
	σ_x	σ_c	σ_r
Pressure	930	7362	−175
Shield plug, etc.	−88	−58	0
Total	842	7304	−175

The stress intensity is thus 7479 psi, which is less than the allowable 17 000 psi and is therefore satisfactory.

3. Primary plus secondary stress evaluation

Load	Principal Stresses (psi)					
	Outer Surface			Inner Surface		
	σ_x	σ_c	σ_r	σ_x	σ_c	σ_r
Pressure	18 756	12 710	0	−16 896	2014	−350
Shield plugs, etc.	−504	−184	0	328	67	0
Pipe reactions – loop cold, reactor hot						
Thrust	−189	−69	0			0
Moment	5 054	2 277	0			0
Total	23 117	14 734	0			−350

The stress intensity is thus 23 117 psi, which is less than the allowable 24 000 psi and is therefore satisfactory.

Combinations of Steady-State and Transient Conditions. The stresses at times I-VII and X-XII shown below were obtained from Table 11; the stresses at times VIII and IX were obtained by assuming a ±15% change in the temperature stresses shown in the same table:

Time and Condition	Principal Stresses (psi)			Stress Differences (psi)		
	σ_1	σ_2	σ_3	S_{12}	S_{23}	S_{31}
I. Shield plugs, loop, etc. not in	0	0	0	0	0	0
II. Initial condition with shield plugs, etc. in	−504	−184	0	−320	−184	504
III. Pressurized	18 252	12 526	0	4 726	12 526	−18 252
IV. Vessel temperature increased to design temperature	19 328	12 671	0	6 657	12 671	−19 328
V. Cold pipe reaction at end of startup	24 193	14 879	0	9 314	14 879	−24 193
VI. Hot pipe reaction	20 111	13 037	0	7 074	13 037	−20 111
VII. Service machine load on nozzle K	18 909	12 964	0	5 945	12 964	−18 909
VIII. 115% design temperature	25 355	14 901	0	10 454	14 901	−25 355
IX. 85% design temperature	24 031	14 857	0	9 174	14 857	−24 031
X. Beginning of shutdown	24 193	14 879	0	9 314	14 879	−24 193
XI. End of shutdown	−504	−184	0	−320	−184	504
XII. Shield plugs, etc. removed	0	0	0	0	0	0

Outer Surface (Downhill Side) Examination. The variations of the stresses and of the stress differences given below with time have not been sketched, but four classes of cycles need to be investigated. The four classes, the number of cycles for each, the arbitrarily assigned usage

factors, and the respective values of S_a are the same as those listed for nozzle B, and the analyses which follow parallel those for nozzle B.

Class W. ±15% Temperature Fluctuations

The principal stresses, in psi, are:

	σ_1	σ_2	σ_3
Design power	24 193	14 879	0
115% design temperature	25 355	14 901	0
85% design temperature	24 031	14 859	0
Design power	24 193	14 879	0

The stress differences needed are:

	S_{12}	S_{23}	S_{31}
S_{ij} (115% design temperature)	10 454	14 901	−25 355
S_{ij} (85% design temperature)	9 174	14 857	−24 031
S_{rij}	1 280	44	1 324
$S_{alt\ ij}$	640	22	662
$S'_{mean\ ij}$	9 814	14 879	24 693

$$S_{alt\ ij} + S'_{mean\ ij} < 42\ 000 \text{ psi} = S_b \quad ;$$

therefore

$$S'_{mean\ ij} = S_{mean\ ij} \quad .$$

Rounding to the next hundred, $S_{alt\ ij}$ and $S_{mean\ ij}$ become:

	S_{12}	S_{23}	S_{31}
$S_{alt\ ij}$	700	100	700
$S_{mean\ ij}$	9 900	14 900	24 700

Class X. Service Machine Loading

The principal stresses in psi are as follow:

	σ_1	σ_2	σ_3
Design power	24 193	14 879	0
Plus service machine load	18 909	12 964	0
Design power	24 193	14 879	0

The stress differences are

	S_{12}	S_{23}	S_{31}
S_{ij} (design power)	9314	14 879	−24 193
S_{ij} (design power plus service machine)	5945	12 964	−18 909
S_{rij}	3369	1 915	5 284
$S_{alt\ ij}$	1685	958	2 642
$S'_{mean\ ij}$	7630	13 922	21 551

$$S_{alt\ ij} + S'_{mean\ ij} < 42\ 000 \text{ psi} = S_b \quad ;$$

therefore

$$S'_{mean\ ij} = S_{mean\ ij} \quad .$$

Rounding to the next hundred gives

	S_{12}	S_{23}	S_{31}
$S_{alt\ ij}$	1700	1 000	2 700
$S_{mean\ ij}$	7700	14 000	21 600

Class Y. Experimental Loop Pipe Loads

The principal stresses, in psi, to be considered are:

	σ_1	σ_2	σ_3
Design power, loop cold	24 193	14 879	0
Design power, loop hot	20 111	13 037	0
Design power, loop cold	24 193	14 879	0

The stress differences are:

	S_{12}	S_{23}	S_{31}
S_{ij} (loop cold)	9314	14 879	−24 193
S_{ij} (loop hot)	7074	13 037	−20 111
S_{rij}	2240	1 842	4 082
$S_{alt\ ij}$	1120	921	2 041
$S'_{mean\ ij}$	8194	13 958	22 152

$$S_{alt\ ij} + S'_{mean\ ij} < 42\ 000 \text{ psi} = S_b \quad ;$$

therefore

$$S'_{mean\ ij} = S_{mean\ ij} \quad .$$

Rounding to the next hundred, $S_{alt\ ij}$ and $S_{mean\ ij}$ become:

	S_{12}	S_{23}	S_{31}
$S_{alt\ ij}$	1200	1 000	2 100
$S_{mean\ ij}$	8200	14 000	22 200

Class Z. Initial Condition to 100% Power to Shutdown

The principal stresses, in psi, are:

	σ_1	σ_2	σ_3
Initial condition	−504	−184	0
Design power	24 193	14 879	0
Shutdown	−504	−184	0

The corresponding stress differences are:

	S_{12}	S_{23}	S_{31}
S_{ij} (initial)	−320	−184	504
S_{ij} (design power, loop cold)	9314	14 879	−24 193
S_{rij}	9634	15 063	24 697
$S_{alt\ ij}$	4817	7 532	12 349
$S'_{mean\ ij}$	4497	7 348	11 845

$$S_{alt\ ij} + S'_{mean\ ij} < 42\ 000 \text{ psi} = S_b \quad ;$$

therefore

$$S'_{mean\ ij} = S_{mean\ ij} \quad .$$

Rounding to the next hundred, $S_{alt\ ij}$ and $S_{mean\ ij}$ become:

	S_{12}	S_{23}	S_{31}
$S_{alt\ ij}$	4900	7600	12 400
$S_{mean\ ij}$	4500	7400	11 900

Fatigue Diagram. A fatigue diagram for the outer surface of nozzle K on the downhill side was not constructed, but the one for the outer surface on the downhill side of nozzle B is appropriate for nozzle K, since usage factors of the same magnitude were arbitrarily assigned the respective

classes of cycles. All the points $(S_{mean\ ij}, S_{alt\ ij})_{W,X,Y,Z}$ fall well within the appropriate safe zones of this diagram. Application of a modification of Miner's hypothesis (Navy Code, 5.2.8) results in a usage factor well below the 0.8 allowable.

With respect to stress criteria, the design of nozzle K is adequate. It is to be noted, however, that the distortion limits necessitated by operational considerations (Navy Code, 1.5) were also greater in this case than the calculated limits.[12]

Gas Outlet Nozzle

Examination of Tables B.5, B.6, and B.8 reveals that the points of maximum axial stress for pressure, pipe thrust, and moment are usually different. The same is true for radial and circumferential stresses. The maximum values are listed in Table 16. The stresses for pressure were obtained from Table B.5, and the stresses for pipe thrust and for pipe moment were derived from Tables B.6 and B.8, respectively.

In analyzing the gas outlet nozzle, the location and the sign of the maximum stress from the pipe loads were assumed to be the same as for the maximum pressure stress. This was done because of the variation in maximum stress location mentioned above and because the direction of the moment is unknown. The following analysis utilizes the steady-state and transient stress conditions of Table 16.

Steady-State Conditions. The steady-state examination is summarized below in the membrane stress and primary-plus-secondary stress evaluation tabulations:

1. Membrane stress evaluation $[\sigma_x = (\sigma_{xi} + \sigma_{xo})/2$, etc.$]$

Load	Principal Stresses (psi)		
	σ_x	σ_c	σ_r
Pressure	500	9048	−175

The stress intensity is thus 9223 psi, which is less than the 17 000 psi allowed and is therefore satisfactory.

2. Primary plus secondary stress evaluation

Load	Principal Stresses (psi)					
	Outer Surface			Inner Surface		
	σ_x	σ_c	σ_r	σ_x	σ_c	σ_r
Pressure	14 958	12 714	0	−13 958	5 381	−350
Pipe thrust	920	450	0	−650	50	0
Pipe moment	820	420	0	−580	50	0
Total	16 698	13 584	0	−15 188	5 481	−350
Stress intensity	16 698			20 669		

These stress intensities are for the cold condition which is more severe than the hot condition. They are well under the 24 000 psi allowed for the hot condition and are therefore acceptable.

Combinations of Steady-State and Transient Stress Conditions. The stresses tabulated below were obtained from Table 16.

Time and Condition	Principal Stresses (psi)					
	Outer Surface			Inner Surface		
	σ_x	σ_c	σ_r	σ_x	σ_c	σ_r
I. Initial	1 740	870	0	−1 230	100	0
II. Pressurized (350 psi)	16 698	13 584	0	−15 188	5 481	−350
III. End of startup	15 132	12 801	0	−14 081	5 391	−350
IV. Shutdown	1 740	870	0	−1 230	100	0

These data permitted the consideration of only one cycle, which passes from time and load conditions I through IV. The cycle was designated class X and an arbitrary usage factor of 0.2 was assigned to it. This leaves a usage factor of 0.6 for cycles which may subsequently need to be investigated. For a usage factor of 0.2 the following data were obtained:

Class	Cycles	Assigned Usage Factor	Cycles for Determining S_a	Applicable Value of S_a
X	500	0.2	2500	56 000

For this cycle the stress differences, in psi, are:

	Outer Surface			Inner Surface		
	S_{12}	S_{23}	S_{31}	S_{12}	S_{23}	S_{31}
S_{ij} initial	870	870	−1 740	−1 330	100	1 230
S_{ij} cold	3 114	13 584	−16 698	−20 669	5 831	14 838
S_{rij}	2 244	12 714	14 958	19 339	5 731	13 608
$S_{alt\ ij}$	1 122	6 357	7 479	9 670	2 866	6 804
$S'_{mean\ ij}$	1 992	7 227	9 219	11 000	2 966	8 034

$$S_{alt\ ij} + S'_{mean\ ij} < 42\ 000 \text{ psi} = S_b \quad ;$$

therefore

$$S'_{mean\ ij} = S_{mean\ ij} \quad .$$

Rounding to the next hundred, these stress quantities are:

	Outer Surface			Inner Surface		
	S_{12}	S_{23}	S_{31}	S_{12}	S_{23}	S_{31}
$S_{alt\ ij}$	1200	6400	7500	9 700	2900	6900
$S_{mean\ ij}$	2000	7300	9300	11 000	3000	8100

Fatigue Diagram. The fatigue diagram for the gas outlet nozzle is shown in Fig. 127. The points ($S_{mean\ ij}$, $S_{alt\ ij}$) for the outer and the inner surfaces fall well within the safe zone; the design is therefore adequate for this cycle. The value of S_{aX} is 11 500 psi, which gives a usage factor of zero.

Head Around Nozzle B

Examination of Tables B.11 and B.12 reveals that some of the stresses vary considerably with angular location around a nozzle. Therefore the maximum values associated with nozzle B were tabulated in Table 17. In

analyzing this region the stresses from the pipe loads on nozzle B were conservatively assumed to have the same sign as the pressure stresses, since for certain locations this would actually be true.

Steady-State Conditions. The steady-state examination is summarized below:

1. Membrane stress evaluation [$\sigma_\phi = (\sigma_{\phi i} + \sigma_{\phi o})/2$ etc.]

Load	Principal Stresses (psi)		
	σ_ϕ	σ_θ	σ_r
Pressure	8088	11 864	−175
Shield plug, etc.	9	−31	0
Total	8079	11 833	−175

The stress intensity is thus 12 008 psi, which is less than the allowable 17 000 psi and is therefore satisfactory.

2. Primary plus secondary stress evaluation

Load	Principal Stresses (psi)					
	Outer Surface			Inner Surface		
	σ_ϕ	σ_θ	σ_r	σ_ϕ	σ_θ	σ_r
Pressure	8 393	13 658	0	7782	10 070	−350
Shield plug, etc.	−179	−182	0	161	121	0
Pipe reactions – loop cold, reactor hot						
Thrust	75	76	0	67	50	0
Moment	1 608	1 392	0	1658	1 518	0
Total	10 076	14 944	0	9668	11 759	−350

The outer surface stress intensity of 14 944 psi and the inner surface value of 12 109 are below the allowable 24 000 psi and are therefore satisfactory.

Combinations of Steady-State and Transient Stress Conditions. The stresses at times I-VII and X-XII shown below have been obtained from

Table 17 by assuming the same sign for the stresses from pipe loads as for the corresponding pressure stresses; the stresses at times VIII and IX were obtained by assuming a ±15% change in the temperature stresses shown in the same table:

Time and Condition	Principal Stresses (psi)					
	Outer Surface			Inner Surface		
	σ_1	σ_2	σ_3	σ_1	σ_2	σ_3
I. Shield plugs, loops, etc. not in	0	0	0	0	0	0
II. Initial condition with shield plugs, etc. in	−179	−182	0	161	121	0
III. Pressurized	8 214	13 476	0	7 943	10 191	−350
IV. Vessel temperature increased to design temperature	8 794	12 791	0	7 732	10 349	−350
V. Cold pipe reaction at end of startup	10 477	14 259	0	9 457	11 917	−350
VI. Hot pipe reaction	8 937	12 916	0	7 879	10 483	−350
VII. Service machine load on nozzle B	8 977	12 739	0	10 797	12 917	−350
VIII. 115% design temperature	10 564	14 156	0	9 425	11 941	−350
IX. 85% design temperature	10 390	14 362	0	9 489	11 893	−350
X. Beginning of shutdown	10 477	14 259	0	9 457	11 917	−350
XI. End of shutdown	−179	−182	0	161	121	0
XII. Shield plugs, etc. removed	0	0	0	0	0	0

The stress differences corresponding to these times and stresses, in psi, are:

Time	Outer Surface S_{12}	Outer Surface S_{23}	Outer Surface S_{31}	Inner Surface S_{12}	Inner Surface S_{23}	Inner Surface S_{31}
I	0	0	0	0	0	0
II	3	−182	179	40	121	−161
III	−5262	13 476	−8 214	−2248	10 541	−8 293
IV	−3997	12 791	−8 794	−2617	10 699	−8 082
V	−3782	14 259	−10 477	−2460	12 267	−9 807
VI	−3979	12 916	−8 937	−2604	10 833	−8 229
VII	−3762	12 739	−8 977	−2120	13 267	−11 147
VIII	−3592	14 156	−10 564	−2516	12 291	−9 775
IX	−3972	14 362	−10 390	−2404	12 243	−9 839
X	−3782	14 259	−10 477	−2460	12 267	−9 807
XI	3	−182	179	40	121	−161
XII	0	0	0	0	0	0

The four classes, the number of cycles for each, the arbitrarily assigned usage factors, and the respective values of S_a are the same as those listed for nozzle B, and the analyses parallel those of nozzle B except that both the outer and the inner surfaces have been examined.

Class W. ±15% Temperature Fluctuations

The stress differences, in psi, are:

	Outer Surface S_{12}	Outer Surface S_{23}	Outer Surface S_{31}	Inner Surface S_{12}	Inner Surface S_{23}	Inner Surface S_{31}
S_{ij} (115% design temperature)	−3592	14 156	−10 564	−2516	12 291	−9775
S_{ij} (85% design temperature)	−3972	14 362	−10 390	−2404	12 243	−9839
S_{rij}	380	206	174	112	48	64
$S_{alt\ ij}$	190	103	87	56	24	32
$S'_{mean\ ij}$	3782	14 259	10 477	2460	12 267	9807

$$S_{alt\ ij} + S'_{mean\ ij} < 42\ 000 \text{ psi} \quad ;$$

therefore

$$S'_{mean\ ij} = S_{mean\ ij} \quad .$$

Class X. Service Machine Loading

The stress differences, in psi, are:

	Outer Surface			Inner Surface		
	S_{12}	S_{23}	S_{31}	S_{12}	S_{23}	S_{31}
S_{ij} (design power)	−3782	14 259	−10 477	−2460	12 267	−9 807
S_{ij} (design power plus service machine)	−3762	12 739	−8 977	−2120	13 267	−11 147
S_{rij}	20	1 520	1 500	340	1 000	1 340
$S_{alt\ ij}$	10	760	750	170	500	670
$S'_{mean\ ij}$	3772	13 499	9 727	2290	12 767	10 477

$$S_{alt\ ij} + S'_{mean\ ij} < 42\ 000 \text{ psi} \quad ;$$

therefore

$$S'_{mean\ ij} = S_{mean\ ij} \quad .$$

Class Y. Experimental Loop Pipe Loads

The stress differences, in psi, are:

	Outer Surface			Inner Surface		
	S_{12}	S_{23}	S_{31}	S_{12}	S_{23}	S_{31}
S_{ij} (loop cold)	−3782	14 259	−10 477	−2460	12 267	−9807
S_{ij} (loop hot)	−3979	12 916	−8 937	−2604	10 833	−8229
S_{rij}	197	1 343	1 540	144	1 434	1578
$S_{alt\ ij}$	99	672	770	72	717	789
$S'_{mean\ ij}$	3881	13 588	9 707	2532	11 550	9018

$$S_{alt\ ij} + S'_{mean\ ij} < 42\ 000 \text{ psi} \quad ;$$

therefore

$$S'_{mean\ ij} = S_{mean\ ij} \quad .$$

Class Z. Initial Condition to 100% Power to Shutdown

The stress differences, in psi, are:

	Outer Surface			Inner Surface		
	S_{12}	S_{23}	S_{31}	S_{12}	S_{23}	S_{31}
S_{ij} (initial)	3	−182	179	40	121	−161
S_{ij} (design power, loop cold)	−3782	14 259	−10 477	−2460	12 267	−9807
S_{rij}	3785	14 441	10 656	2500	12 146	9646
$S_{alt\ ij}$	1893	7 221	5 328	1250	6 073	4823
$S'_{mean\ ij}$	1890	7 039	5 149	1210	6 194	4984

$$S_{alt\ ij} + S'_{mean\ ij} < 42\ 000 \text{ psi} \quad ;$$

therefore

$$S'_{mean\ ij} = S_{mean\ ij} \quad .$$

Rounding to the next hundred, $S_{alt\ ij}$ and $S_{mean\ ij}$ for the four classes are:

		Outer Surface			Inner Surface		
Class		S_{12}	S_{23}	S_{31}	S_{12}	S_{23}	S_{31}
W	$S_{alt\ ij}$	200	200	100	100	100	100
	$S_{mean\ ij}$	3800	14 300	10 500	2500	12 300	9 900
X	$S_{alt\ ij}$	100	800	800	200	500	700
	$S_{mean\ ij}$	3800	13 500	9 800	2300	12 800	10 500
Y	$S_{alt\ ij}$	100	700	800	100	800	800
	$S_{mean\ ij}$	3900	13 600	9 800	2600	11 600	9 100
Z	$S_{alt\ ij}$	1900	7 300	5 400	1300	6 100	4 900
	$S_{mean\ ij}$	1900	7 100	5 200	1300	6 200	5 000

Fatigue Diagram. A fatigue diagram has not been constructed for the hemispherical shell in the region of nozzle B, but the one constructed for the outer surface on the downhill side of nozzle B is appropriate since usage factors of the same magnitude were arbitrarily assigned the respective classes of cycles. All the points $(S_{mean\ ij}, S_{alt\ ij})_{W,X,Y,Z}$ fall well within the appropriate safe zones of this diagram, and comparison of these points with the corresponding ones of the outer surface of nozzle B bears out the earlier statement to the effect that the critical stress condition is always more severe in the nozzles than in the head. Application of a modification of Miner's hypothesis (Navy Code, 5.2.8) would result in a usage factor of negligible magnitude.

CONCLUSIONS

The most significant conclusion reached is that the design of the upper head of the pressure vessel is adequate for the design loading conditions. For the nozzles in the cluster region, thermal stresses were included in the design evaluations, but for the burst-slug detection and gas outlet nozzles they were not taken into account. The axial thrusts exerted by the service machine and the primary coolant pipe reactions may be safely increased, within limits. The highest stresses are in the nozzles, rather than the head itself, with the peaks being on the downhill sides of all nozzles that are not radially attached. The pressure stresses are higher than from other loads, and the stresses induced by the service machine tend to nullify the pressure discontinuity stresses for a given nozzle. Finally, no trend in stress magnitudes for the spherical shell as a function of the angular coordinate around each nozzle could be found. Thus, the effects of adjacent nozzles on the stress pattern around any given nozzle were not apparent from the experimental data.

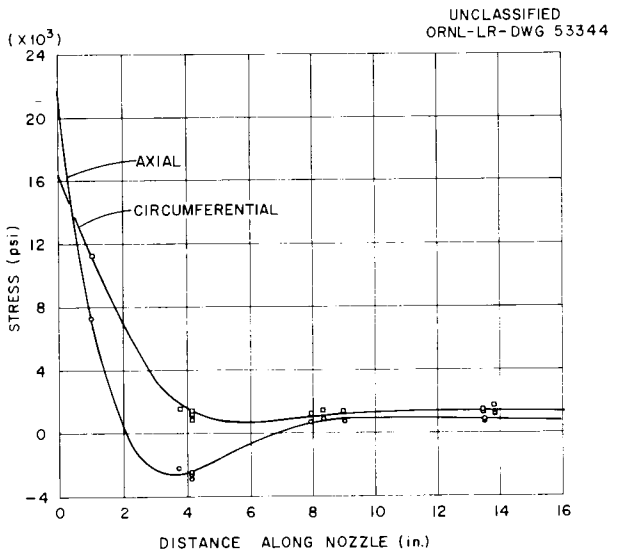

Fig. 18. Stress Distributions on Outer Surface of Nozzle A from 350-psig Pressure Loading.

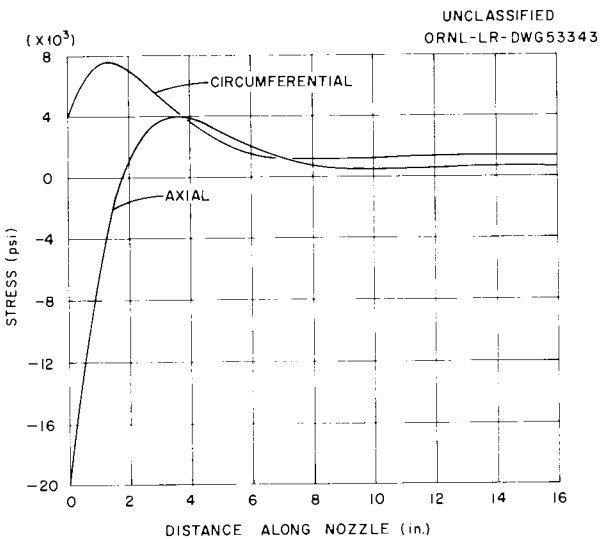

Fig. 19. Stress Distributions on Inner Surface of Nozzle A from 350-psig Pressure Loading.

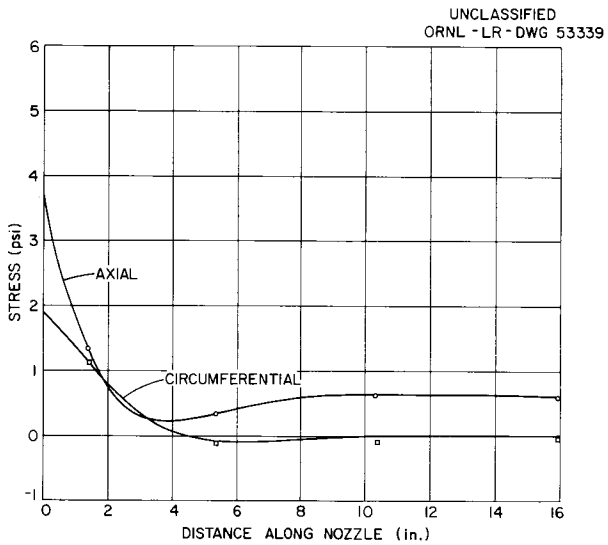

Fig. 20. Stress Distributions on Outer Surface of Nozzle A from Axial Tensile Loading of 1 lb/in. Along Mean Circumference.

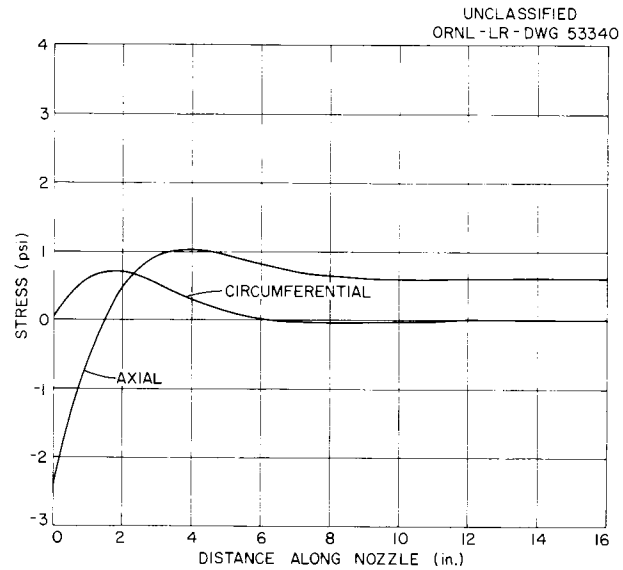

Fig. 21. Stress Distributions on Inner Surface of Nozzle A from Axial Tensile Loading of 1 lb/in. Along Mean Circumference.

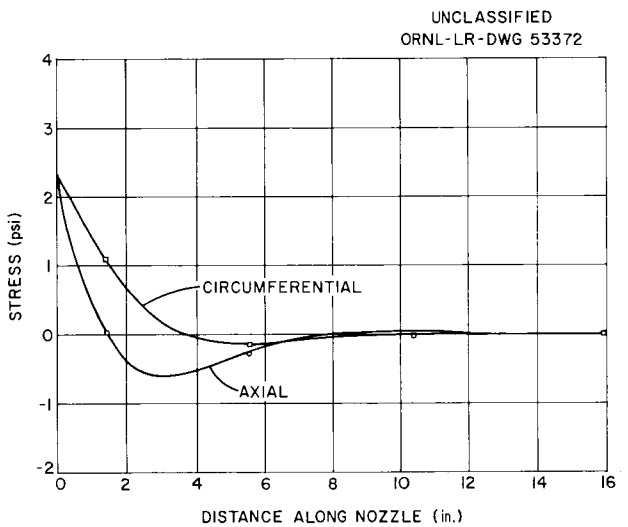

Fig. 22. Stress Distributions on Outer Surface of Nozzle A from Simultaneous Axial Tensile Loadings of 1 lb/in. Along Mean Circumference on Each of the B Nozzles.

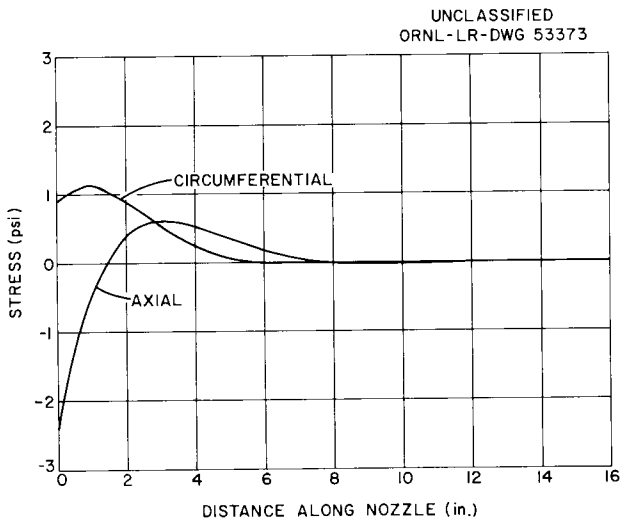

Fig. 23. Stress Distributions on Inner Surface of Nozzle A from Simultaneous Axial Tensile Loadings of 1 lb/in. Along Mean Circumference on Each of the B Nozzles.

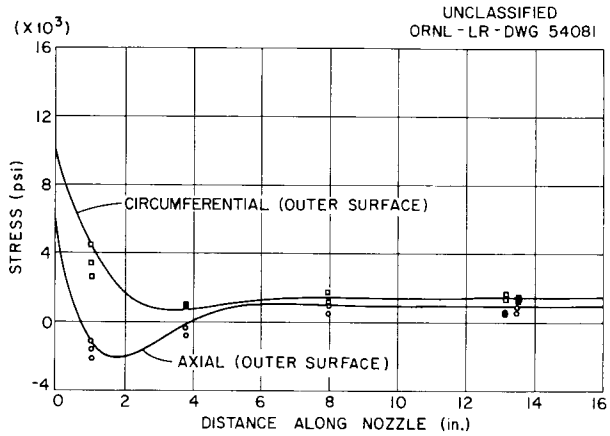

Fig. 24. Stress Distributions on Outer Surface of Nozzle B from 350-psig Pressure Loading (Uphill Side).

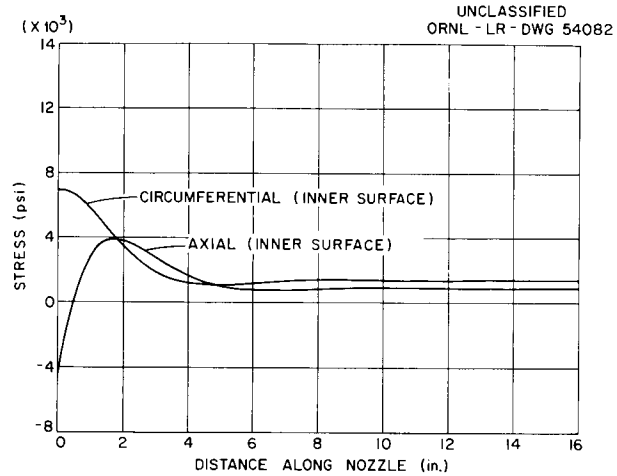

Fig. 25. Stress Distributions on Inner Surface of Nozzle B from 350-psig Pressure Loading (Uphill Side).

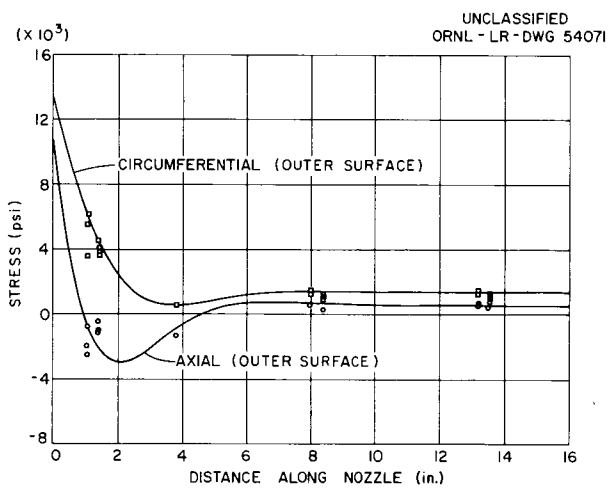

Fig. 26. Stress Distributions on Outer Surface of Nozzle B from 350-psig Pressure Loading (Downhill Side).

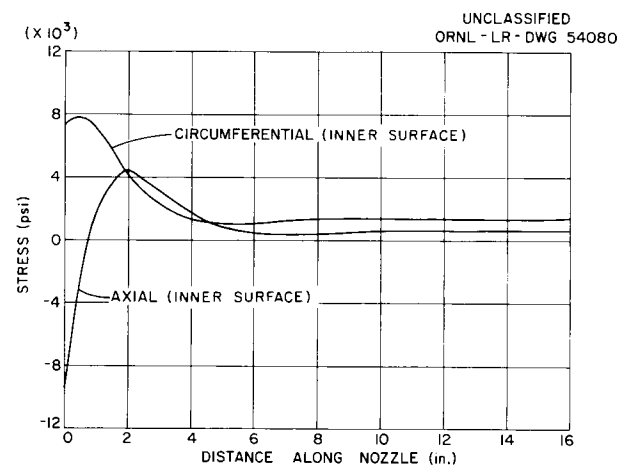

Fig. 27. Stress Distributions on Inner Surface of Nozzle B from 350-psig Pressure Loading (Downhill Side).

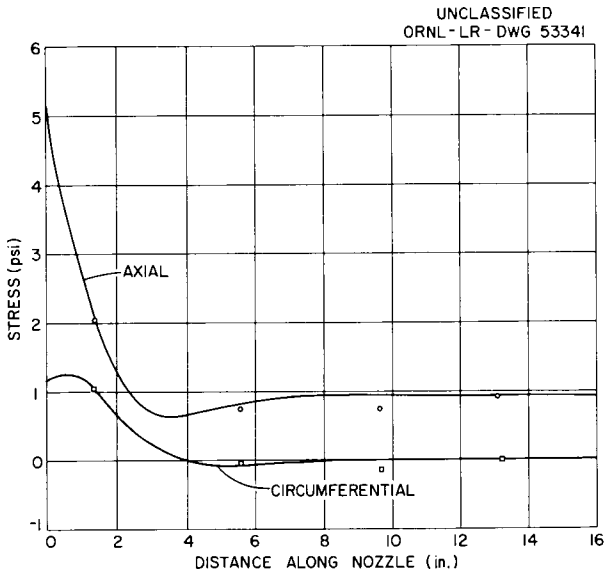

Fig. 28. Stress Distributions on Outer Surface on Nozzle B from Axial Tensile Loading of 1 lb/in. Along Mean Circumference (Uphill Side).

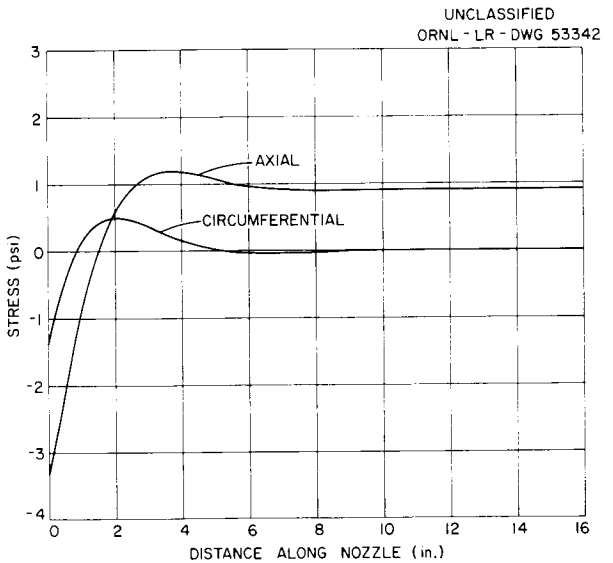

Fig. 29. Stress Distributions on Inner Surface of Nozzle B from Axial Tensile Loading of 1 lb/in. Along Mean Circumference (Uphill Side).

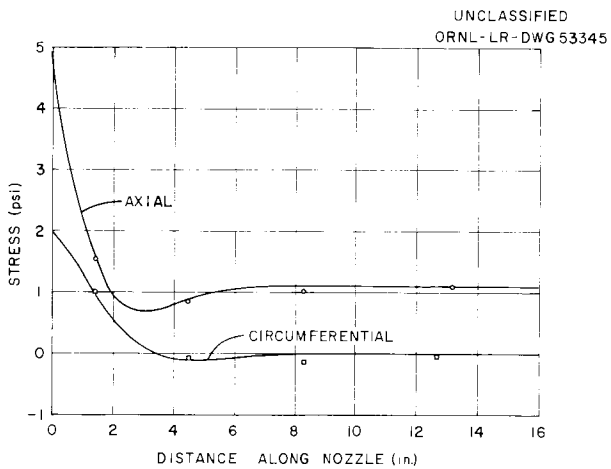

Fig. 30. Stress Distributions on Outer Surface of Nozzle B from Axial Tensile Loading of 1 lb/in. Along Mean Circumference (Downhill Side)

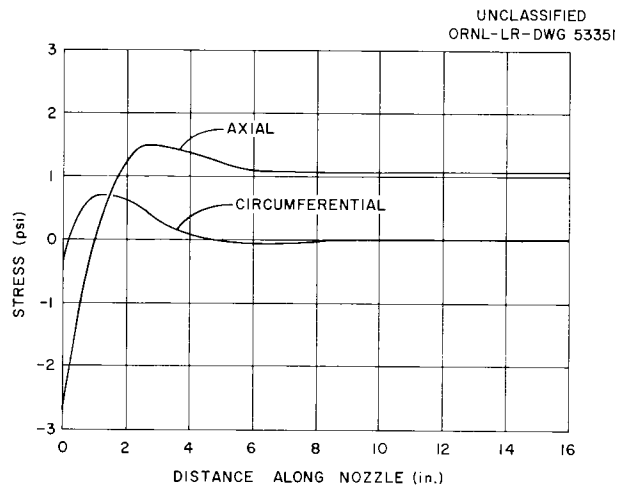

Fig. 31. Stress Distributions on Inner Surface of Nozzle B from Axial Tensile Loading of 1 lb/in. Along Mean Circumference (Downhill Side).

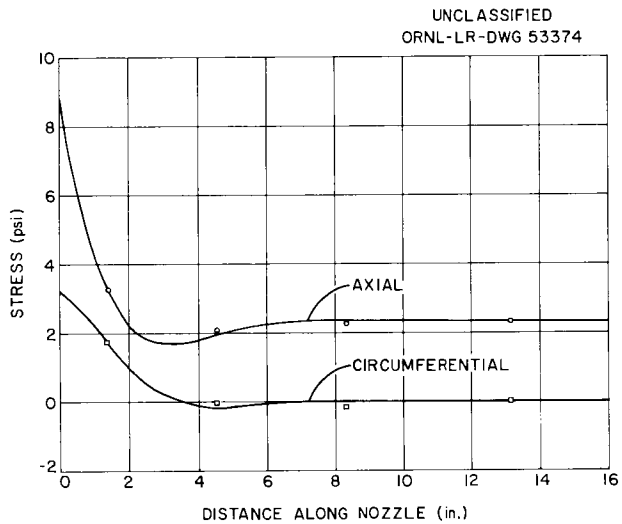

Fig. 32. Stress Distributions on Outer Surface of Nozzle B from Simultaneous Axial Tensile Loadings of 1 lb/in. Along Mean Circumference on Each of the B Nozzles (Downhill Side).

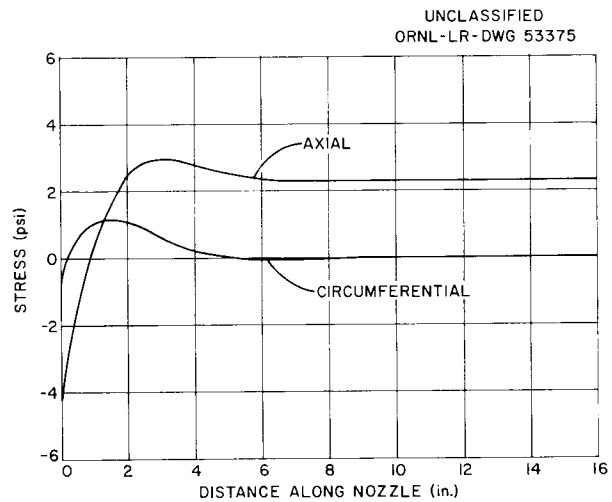

Fig. 33. Stress Distributions on Inner Surface of Nozzle B from Simultaneous Axial Tensile Loadings of 1 lb/in. Along Mean Circumference on Each of the B Nozzles (Downhill Side).

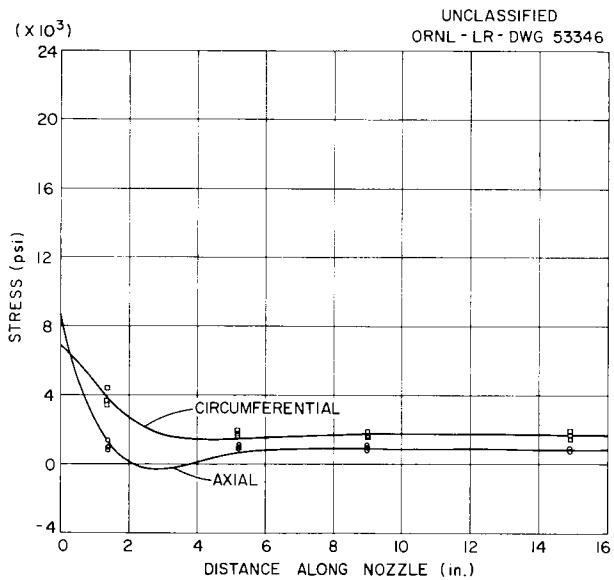

Fig. 34. Stress Distributions on Outer Surface of Nozzle J from 350-psig Pressure Loading (Uphill Side).

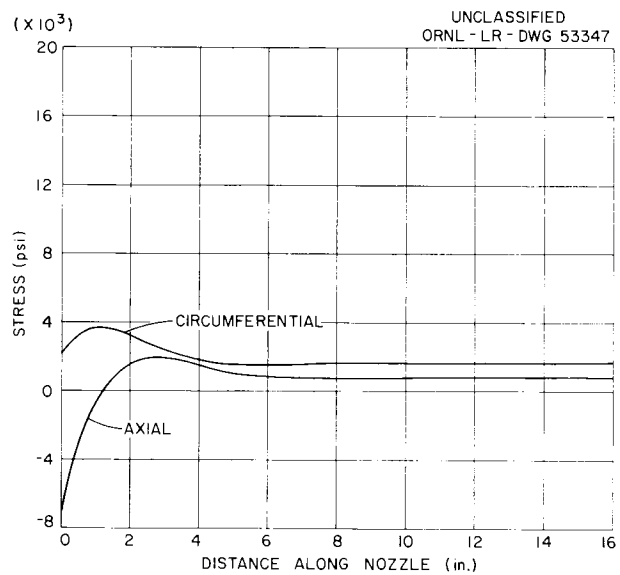

Fig. 35. Stress Distributions on Inner Surface of Nozzle J from 350-psig Pressure Loading (Uphill Side).

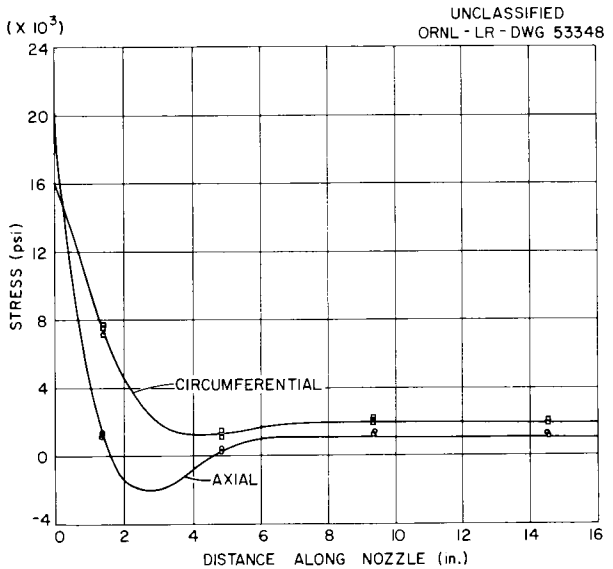

Fig. 36. Stress Distributions on Outer Surface of Nozzle J from 350-psig Pressure Loading (Downhill Side).

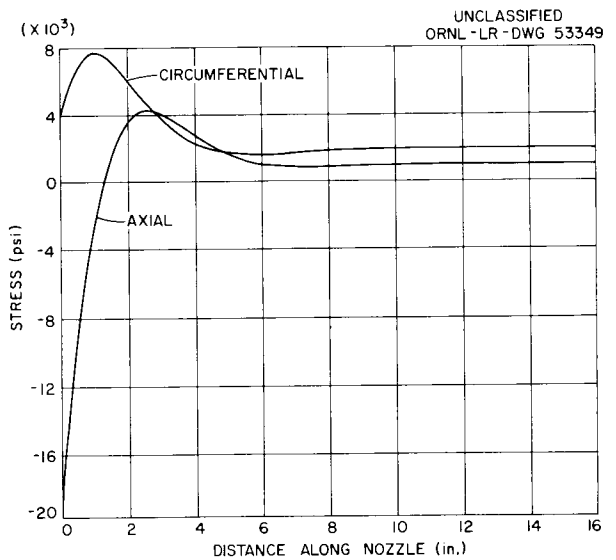

Fig. 37. Stress Distributions on Inner Surface of Nozzle J from 350-psig Pressure Loading (Downhill Side).

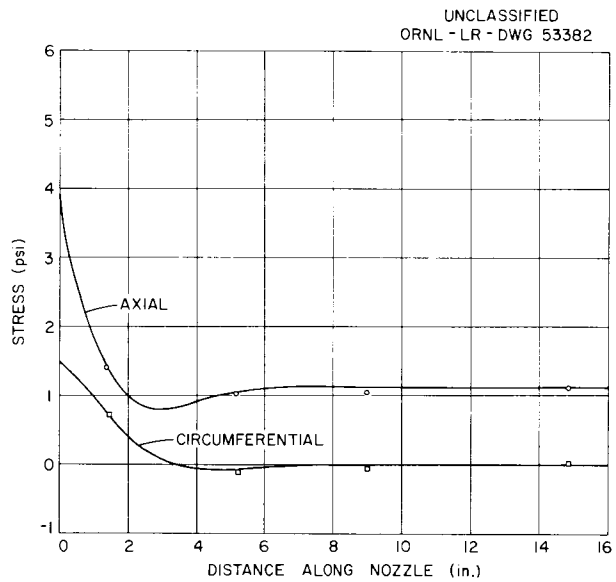

Fig. 38. Stress Distributions on Outer Surface of Nozzle J from Axial Tensile Loading of 1 lb/in. Along Mean Circumference (Uphill Side).

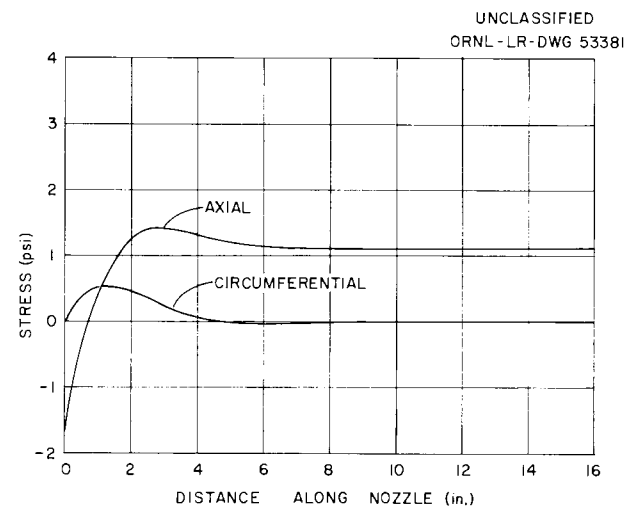

Fig. 39. Stress Distributions on Inner Surface of Nozzle J from Axial Tensile Loading of 1 lb/in. Along Mean Circumference (Uphill Side).

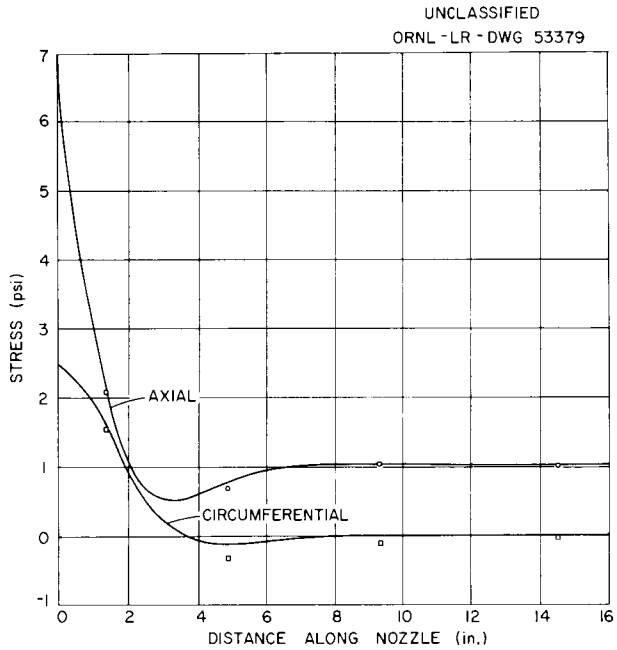

Fig. 40. Stress Distributions on Outer Surface of Nozzle J from Axial Tensile Loading of 1 lb/in. Along Mean Circumference (Downhill Side).

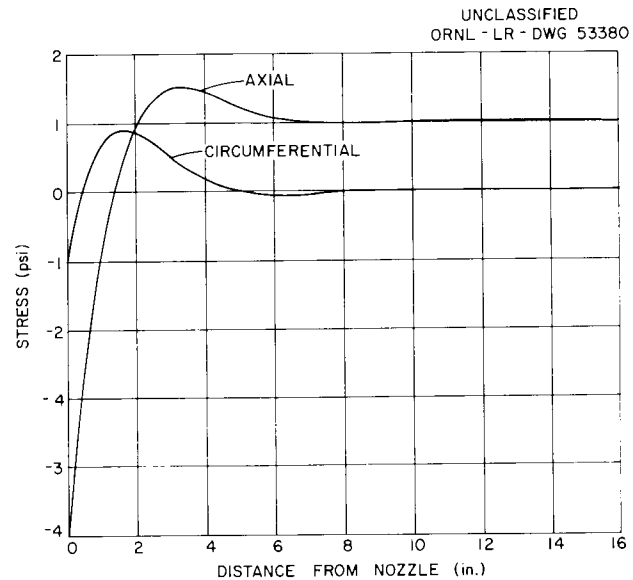

Fig. 41. Stress Distributions on Inner Surface of Nozzle J from Axial Tensile Loading of 1 lb/in. Along Mean Circumference (Downhill Side).

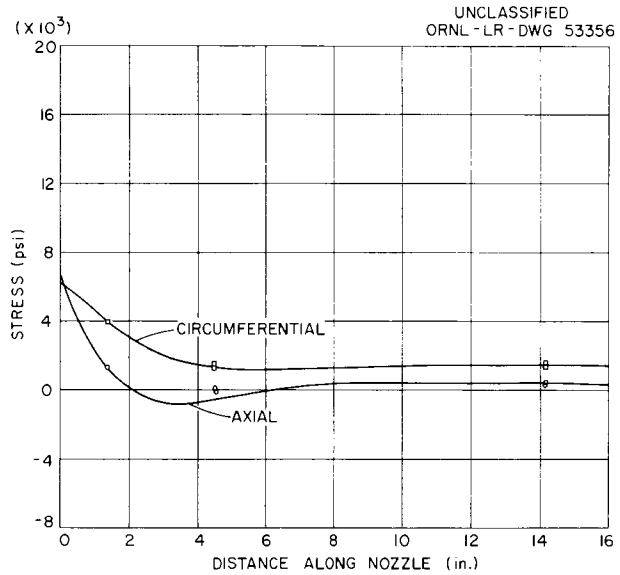

Fig. 42. Stress Distributions on Outer Surface of Nozzle K from 350-psig Pressure Loading (Uphill Side).

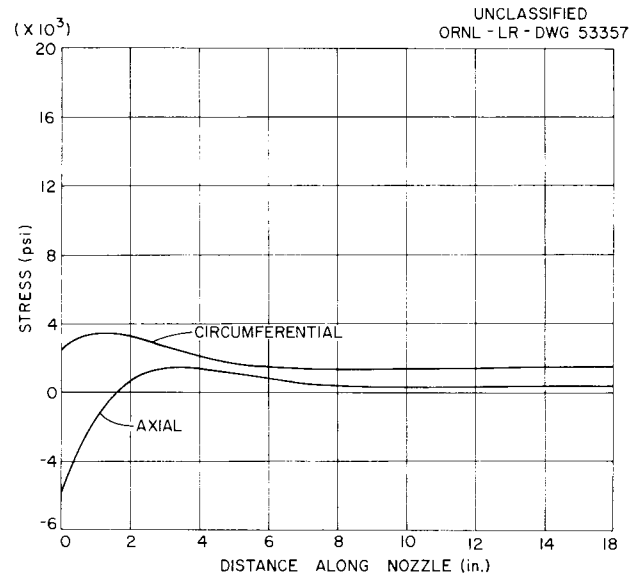

Fig. 43. Stress Distributions on Inner Surface of Nozzle K from 350-psig Pressure Loading (Uphill Side).

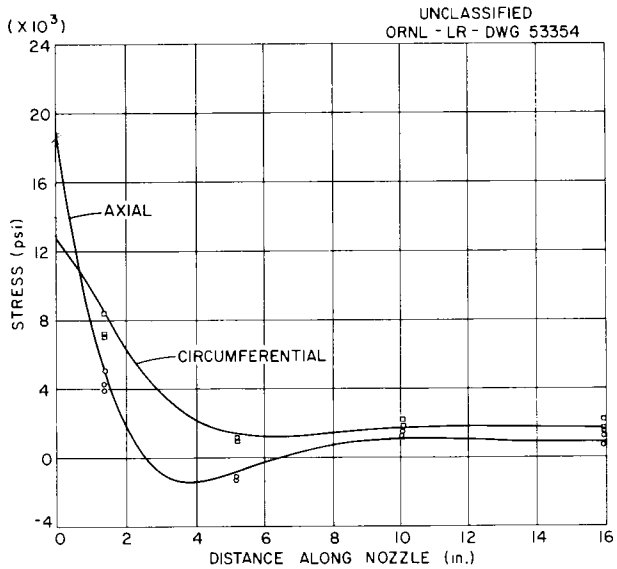

Fig. 44. Stress Distributions on Outer Surface of Nozzle K from 350-psig Pressure Loading (Downhill Side).

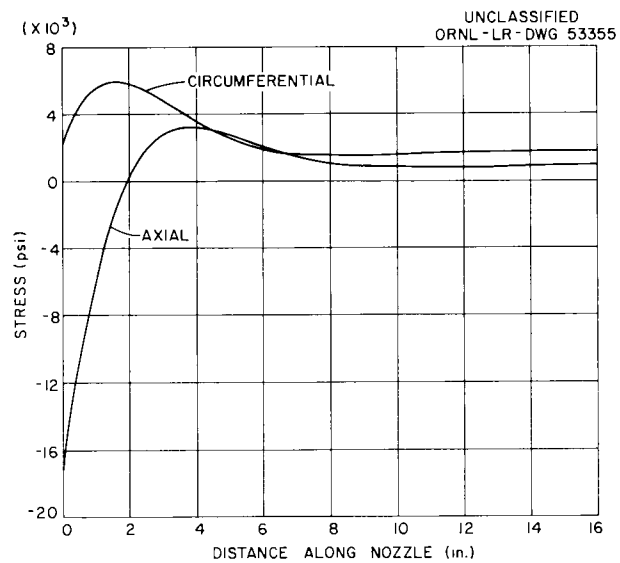

Fig. 45. Stress Distributions on Inner Surface of Nozzle K from 350-psig Pressure Loading (Downhill Side).

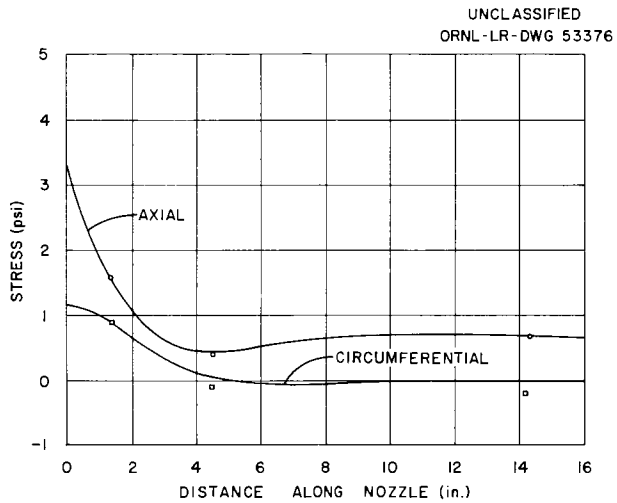

Fig. 46. Stress Distributions on Outer Surface of Nozzle K from Axial Tensile Loading of 1 lb/in. Along Mean Circumference (Uphill Side).

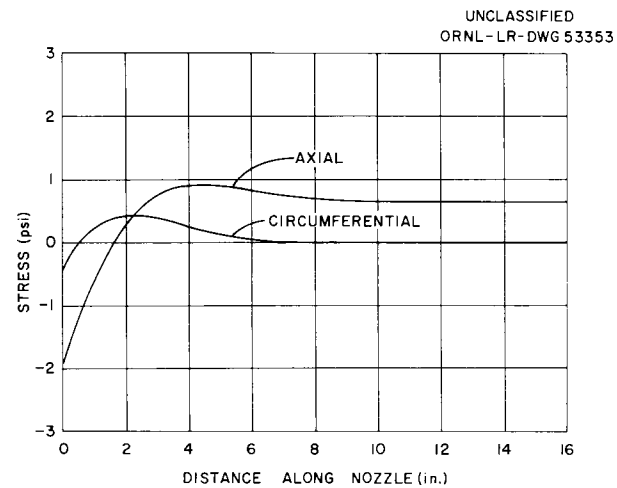

Fig. 47. Stress Distributions on Inner Surface of Nozzle K from Axial Tensile Loading of 1 lb/in. Along Mean Circumference (Uphill Side).

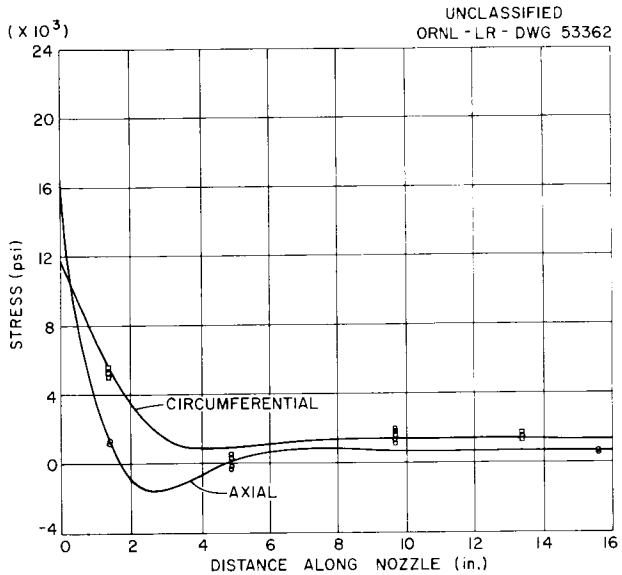

Fig. 52. Stress Distributions on Outer Surface of Nozzle L from 350-psig Pressure Loading (Downhill Side).

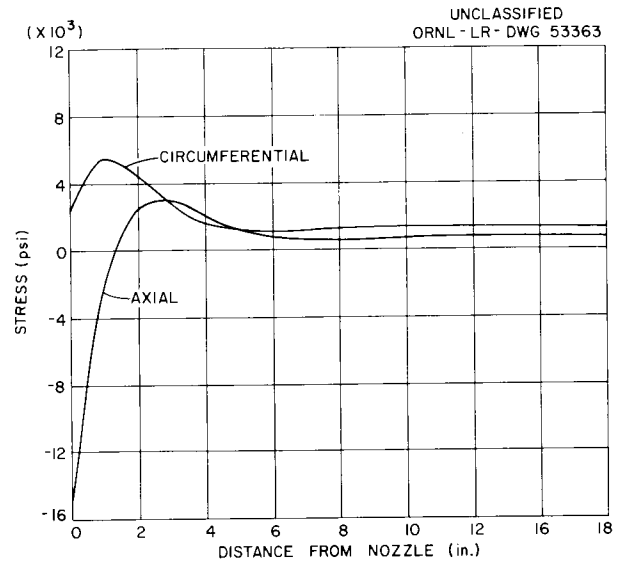

Fig. 53. Stress Distributions on Inner Surface of Nozzle L from 350-psig Pressure Loading (Downhill Side).

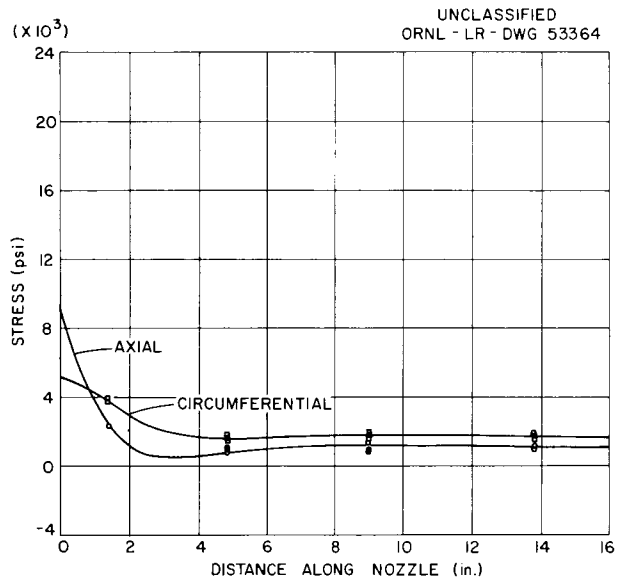

Fig. 50. Stress Distributions on Outer Surface of Nozzle L from 350-psig Pressure Loading (Uphill Side).

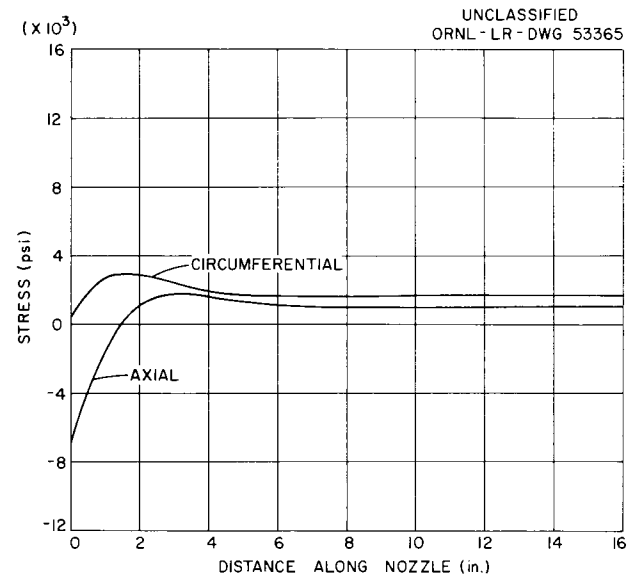

Fig. 51. Stress Distributions on Inner Surface of Nozzle L from 350-psig Pressure Loading (Uphill Side).

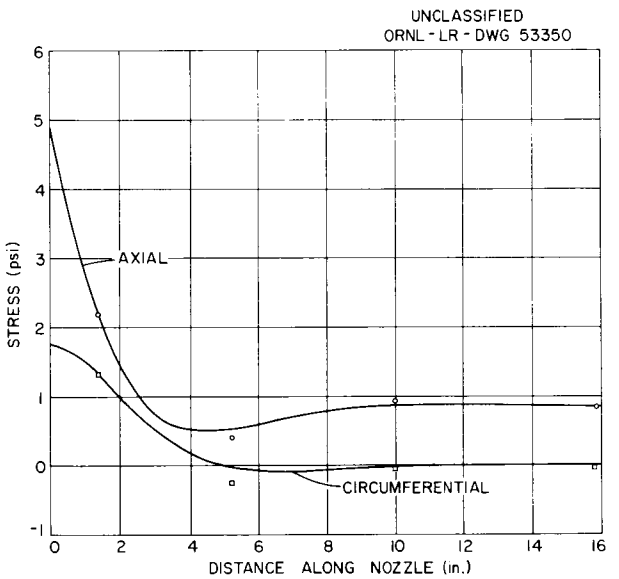

Fig. 48. Stress Distributions on Outer Surface of Nozzle K from Axial Tensile Loading of 1 lb/in. Along Mean Circumference (Downhill Side).

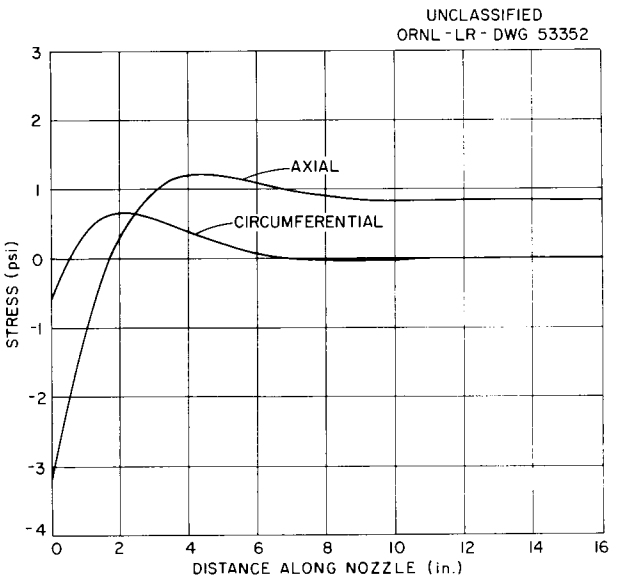

Fig. 49. Stress Distributions on Inner Surface of Nozzle K from Axial Tensile Loading of 1 lb/in. Along Mean Circumference (Downhill Side).

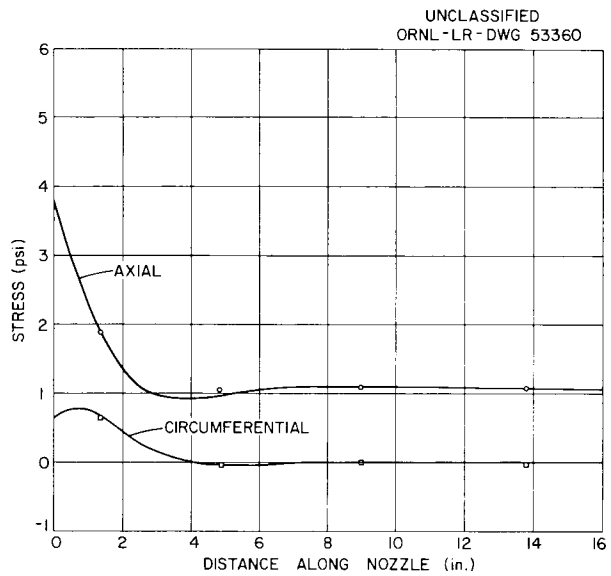

Fig. 54. Stress Distributions on Outer Surface of Nozzle L from Axial Tensile Loading of 1 lb/in. Along Mean Circumference (Uphill Side).

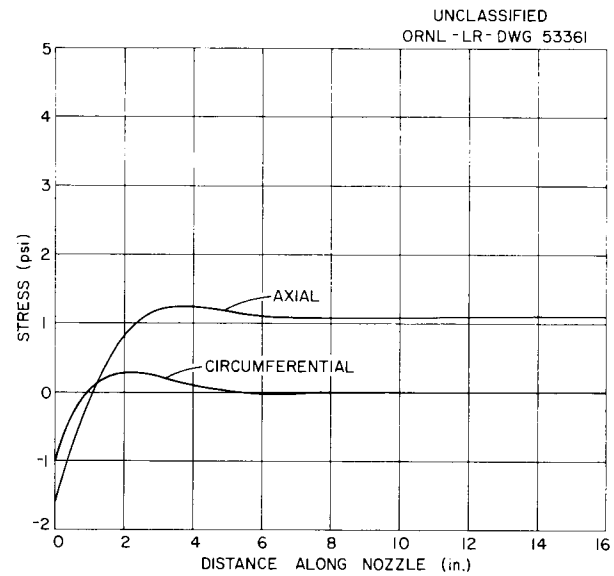

Fig. 55. Stress Distributions on Inner Surface of Nozzle L from Axial Tensile Loading of 1 lb/in. Along Mean Circumference (Uphill Side).

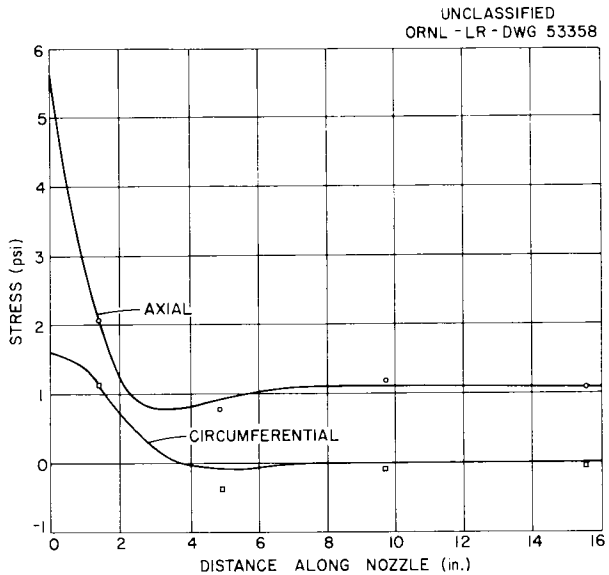

Fig. 56. Stress Distributions on Outer Surface of Nozzle L from Axial Tensile Loading of 1 lb/in. Along Mean Circumference (Downhill Side).

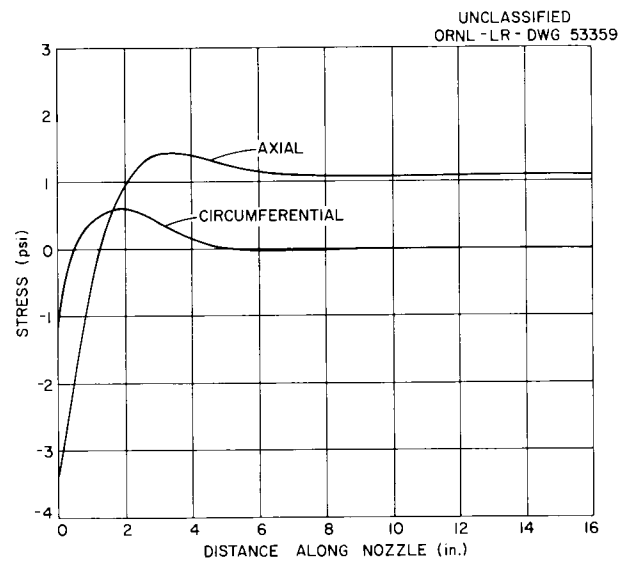

Fig. 57. Stress Distributions on Inner Surface of Nozzle L from Axial Tensile Loading of 1 lb/in. Along Mean Circumference (Downhill Side).

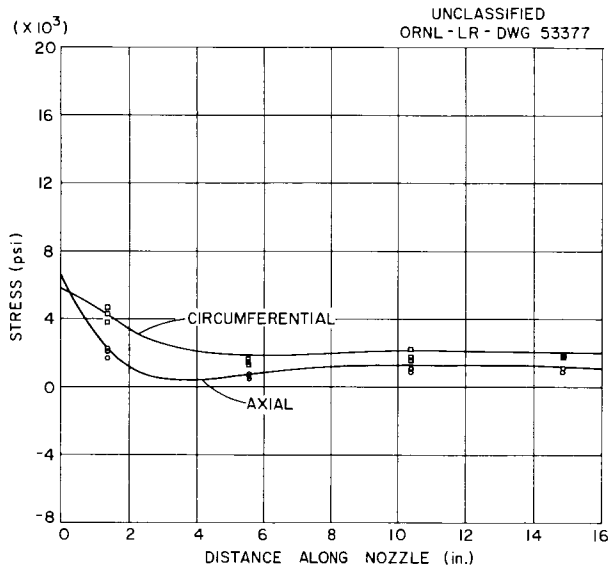

Fig. 58. Stress Distributions on Outer Surface of Nozzle M from 350-psig Pressure Loading (Uphill Side).

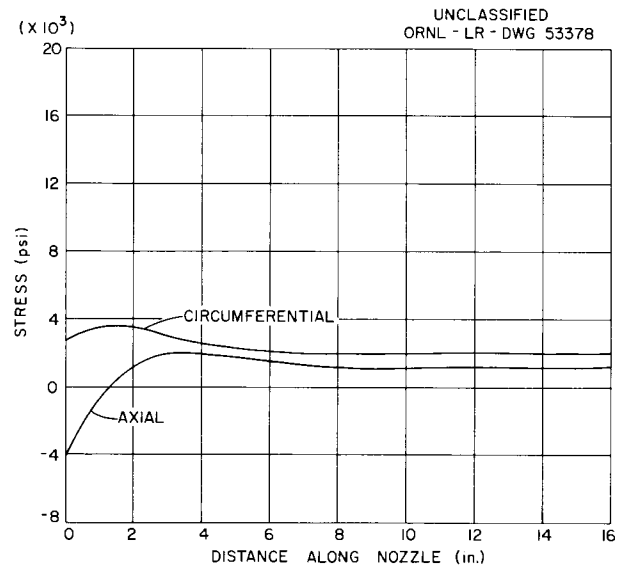

Fig. 59. Stress Distributions on Inner Surface of Nozzle M from 350-psig Pressure Loading (Uphill Side).

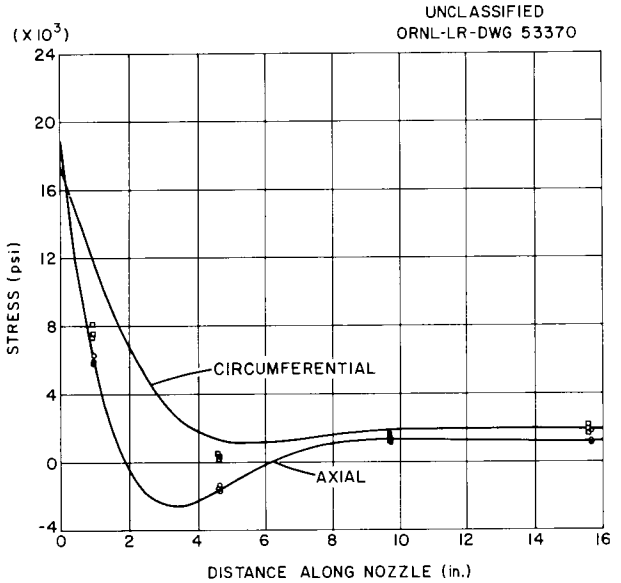

Fig. 60. Stress Distributions on Outer Surface of Nozzle M from 350-psig Pressure Loading (Downhill Side).

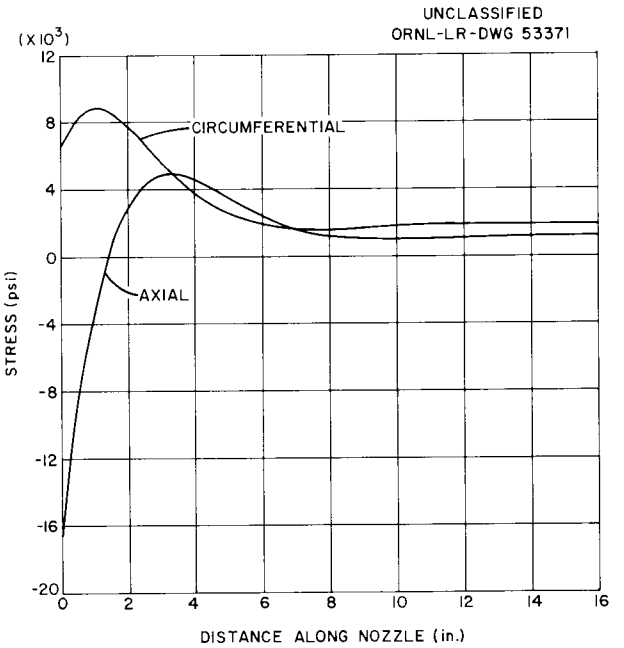

Fig. 61. Stress Distributions on Inner Surface of Nozzle M from 350-psig Pressure Loading (Downhill Side).

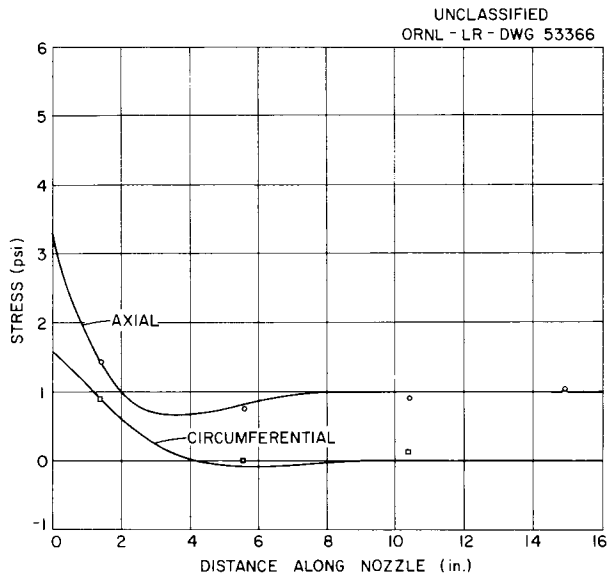

Fig. 62. Stress Distributions on Outer Surface of Nozzle M from Axial Tensile Loading of 1 lb/in. Along Mean Circumference (Uphill Side).

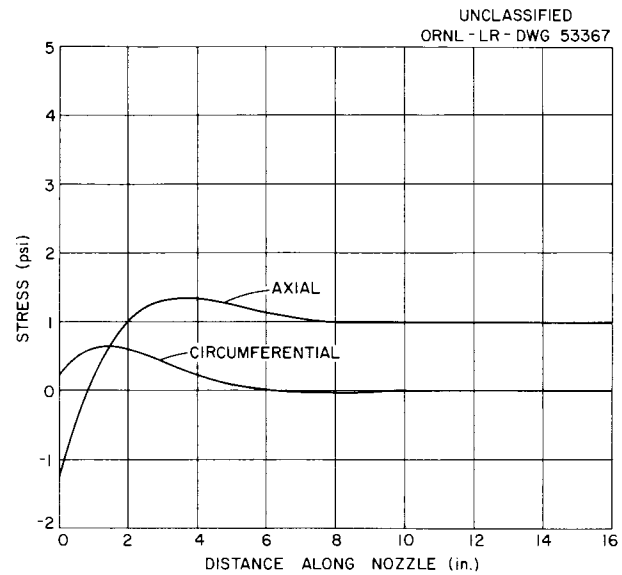

Fig. 63. Stress Distributions on Inner Surface of Nozzle M from Axial Tensile Loading of 1 lb/in. Along Mean Circumference (Uphill Side).

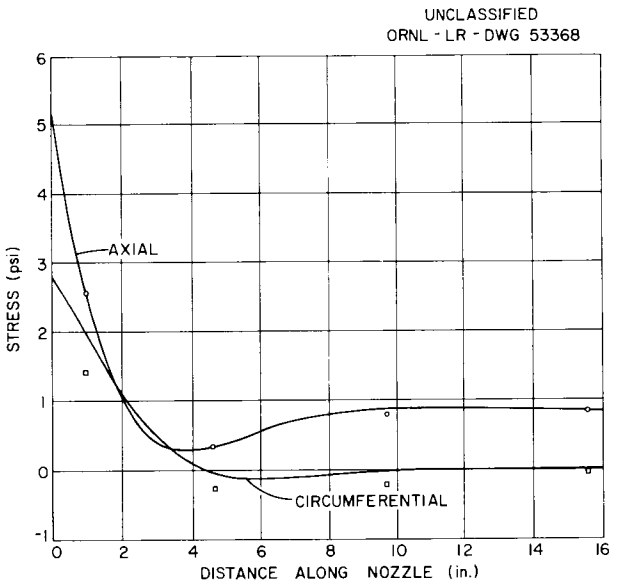

Fig. 64. Stress Distributions on Outer Surface of Nozzle M from Axial Tensile Loading of 1 lb/in. Along Mean Circumference (Downhill Side).

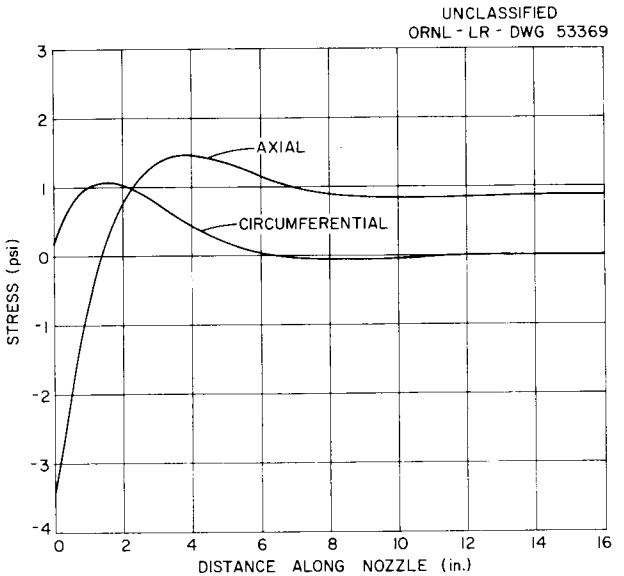

Fig. 65. Stress Distributions on Inner Surface of Nozzle M from Axial Tensile Loading of 1 lb/in. Along Mean Circumference (Downhill Side).

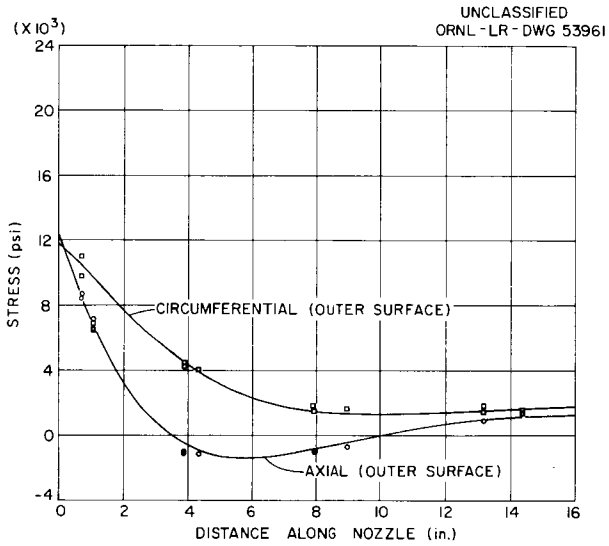

Fig. 66. Stress Distributions on Outer Surface of Burst-Slug-Detection Nozzle from 350-psig Pressure Loading.

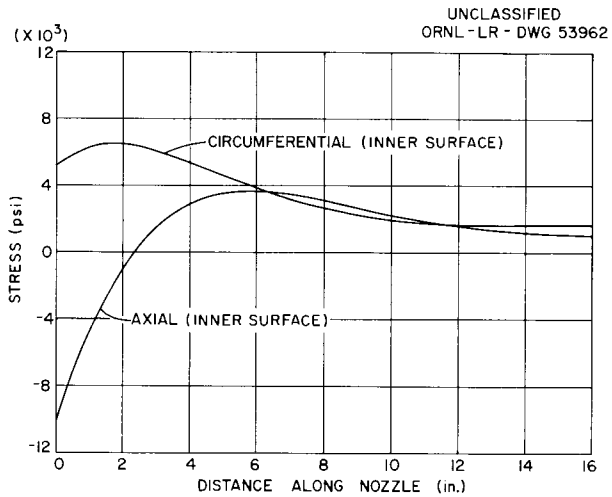

Fig. 67. Stress Distributions on Inner Surface of Burst-Slug-Detection Nozzle from 350-psig Pressure Loading.

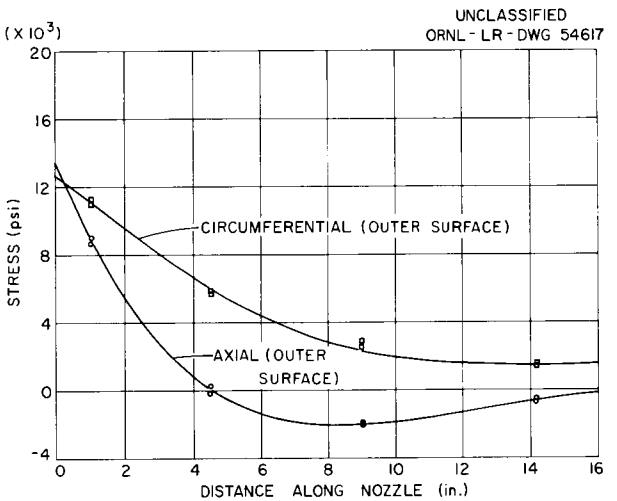

Fig. 68. Stress Distributions on Outer Surface of Gas Outlet Nozzle from 350-psig Pressure Loading (Uphill Side).

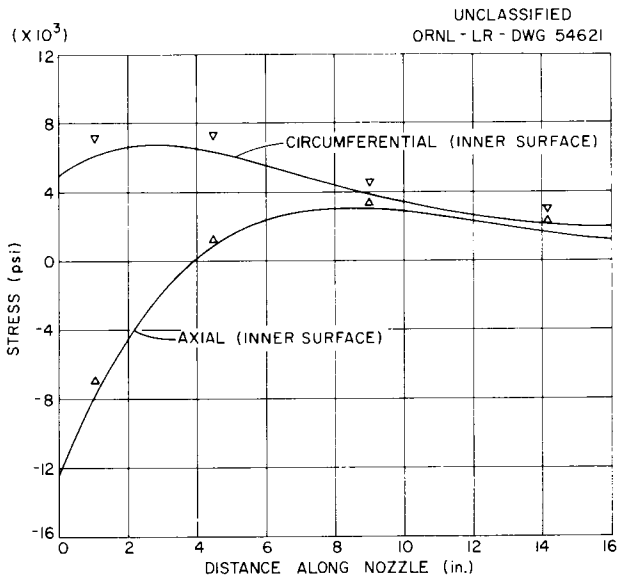

Fig. 69. Stress Distributions on Inner Surface of Gas Outlet Nozzle from 350-psig Pressure Loading (Uphill Side).

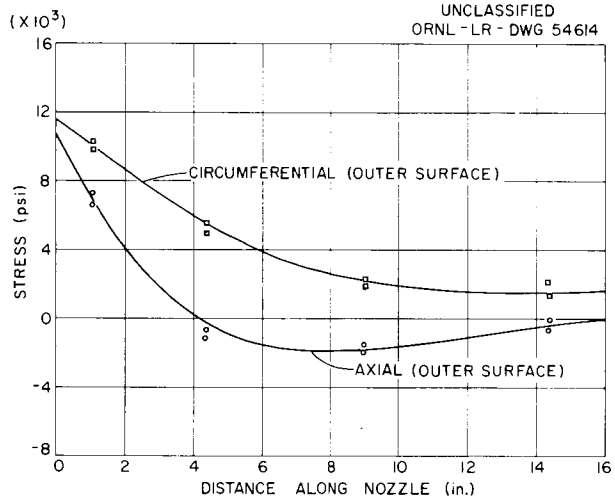

Fig. 70. Stress Distributions on Outer Surface of Gas Outlet Nozzle from 350-psig Pressure Loading (Downhill Side).

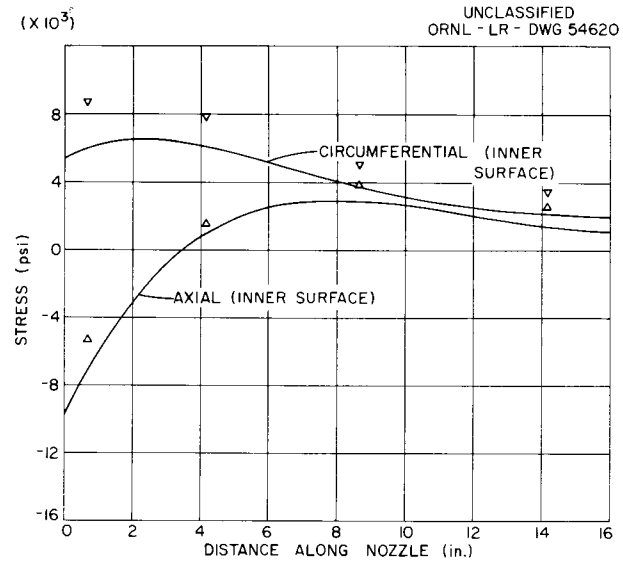

Fig. 71. Stress Distributions on Inner Surface of Gas Outlet Nozzle from 350-psig Pressure Loading (Downhill Side).

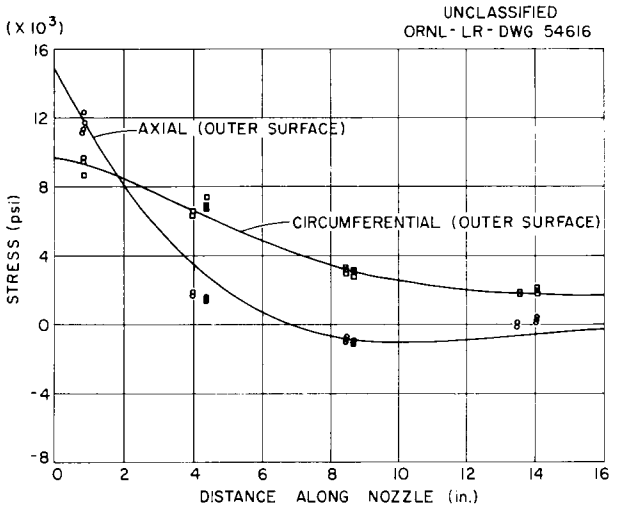

Fig. 72. Stress Distributions on Outer Surface of Gas Outlet Nozzle from 350-psig Pressure Loading (Side 90 deg from Uphill Side).

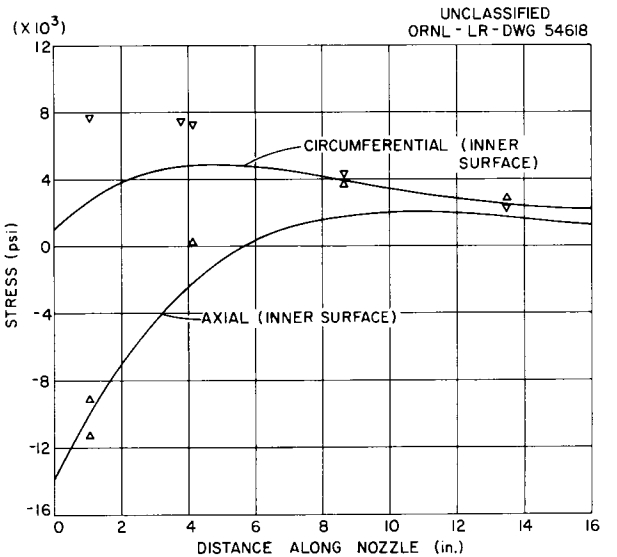

Fig. 73. Stress Distributions on Inner Surface of Gas Outlet Nozzle from 350-psig Pressure Loading (Side 90 deg from Uphill Side).

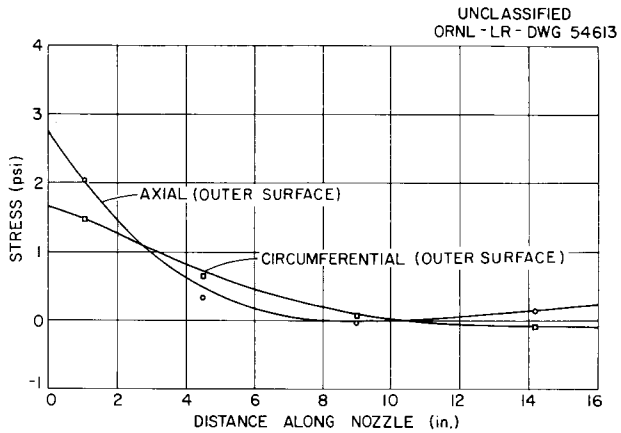

Fig. 74. Stress Distributions on Outer Surface of Gas Outlet Nozzle from Axial Tensile Loading of 1 lb/in. Along Mean Circumference (Uphill Side).

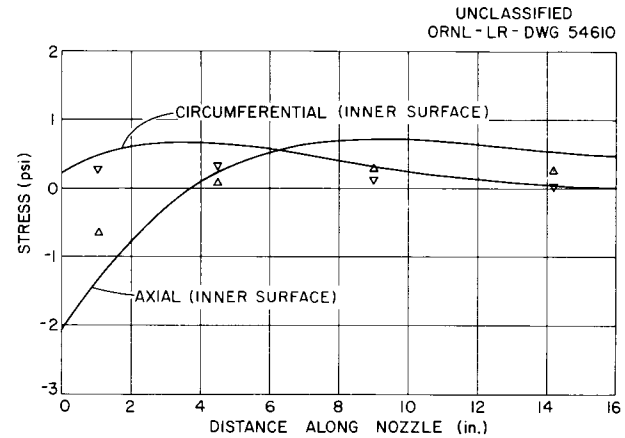

Fig. 75. Stress Distributions on Inner Surface of Gas Outlet Nozzle from Axial Tensile Loading of 1 lb/in. Along Mean Circumference (Uphill Side).

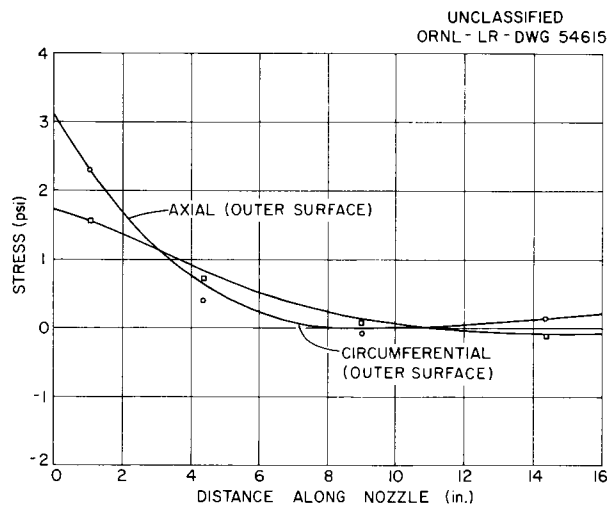

Fig. 76. Stress Distributions on Outer Surface of Gas Outlet Nozzle from Axial Tensile Loading of 1 lb/in. Along Mean Circumference (Downhill Side).

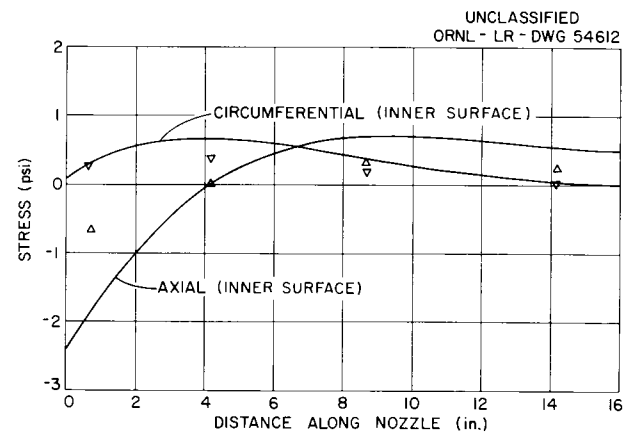

Fig. 77. Stress Distributions on Inner Surface of Gas Outlet Nozzle from Axial Tensile Loading of 1 lb/in. Along Mean Circumference (Downhill Side).

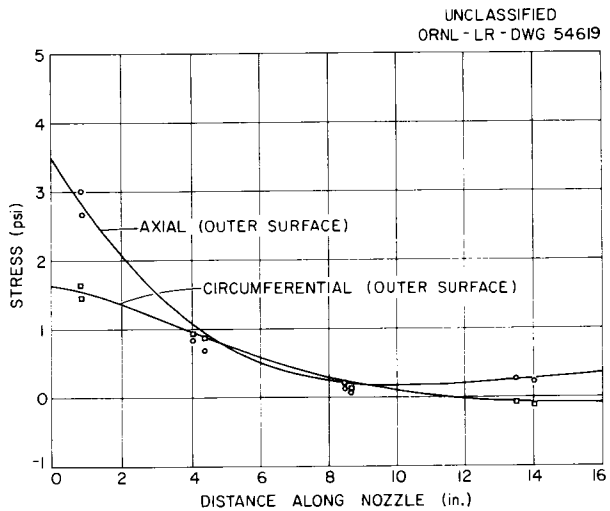

Fig. 78. Stress Distributions on Outer Surface of Gas Outlet Nozzle from Axial Tensile Loading of 1 lb/in. Along Mean Circumference (Side 90 deg from Uphill Side).

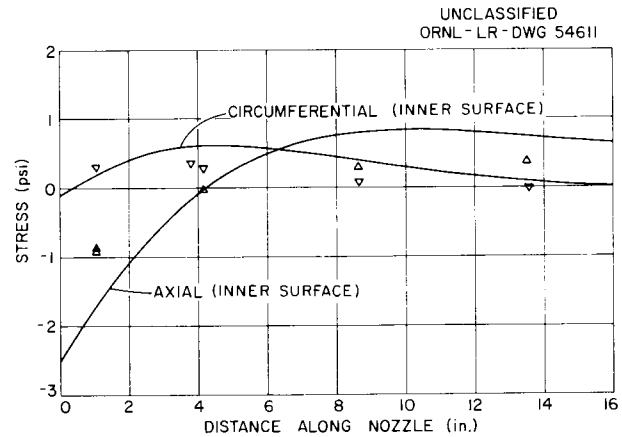

Fig. 79. Stress Distributions on Inner Surface of Gas Outlet Nozzle from Axial Tensile Loading of 1 lb/in. Along Mean Circumference (Side 90 deg from Uphill Side).

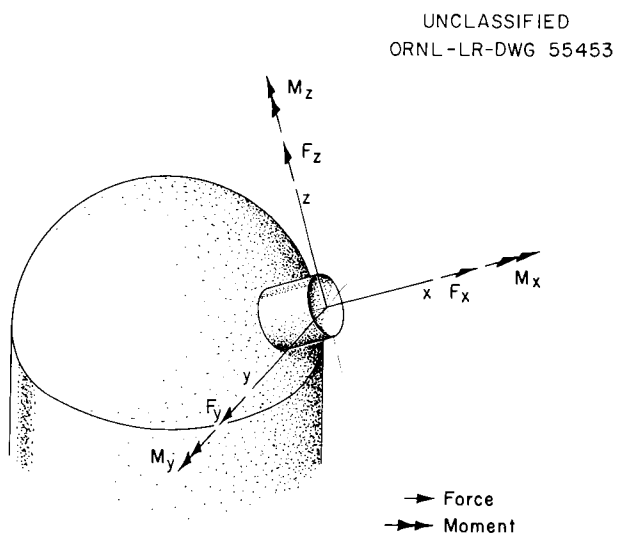

Fig. 80. Sign Convention for Transverse Loadings and Applied Moments on Gas Outlet Nozzle.

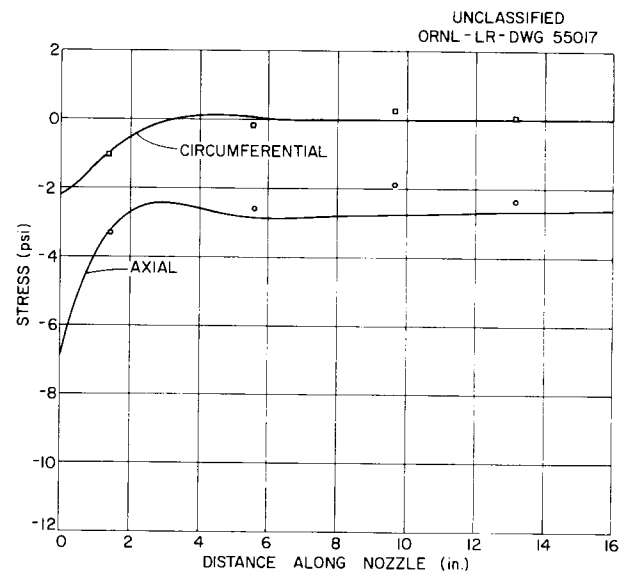

Fig. 81. Stress Distributions on Outer Surface of Nozzle B from Transverse Load of 1 lb Directed Toward Nozzle A at a Distance of 139.7 in. Above the Apex (Uphill Side).

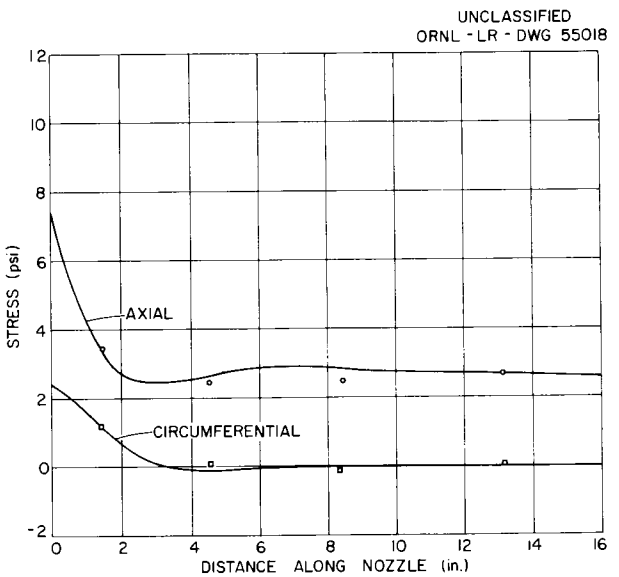

Fig. 82. Stress Distributions on Outer Surface of Nozzle B from Transverse Load of 1 lb Directed Toward Nozzle A at a Distance of 139.7 in. Above the Apex (Downhill Side).

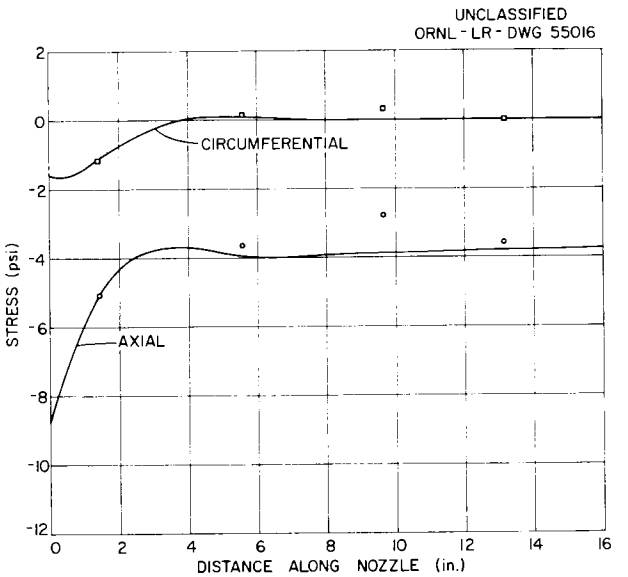

Fig. 83. Stress Distributions on Outer Surface of Nozzle B from Transverse Load of 1 lb Directed Toward Nozzle A at a Distance of 192.3 in. Above the Apex (Uphill Side).

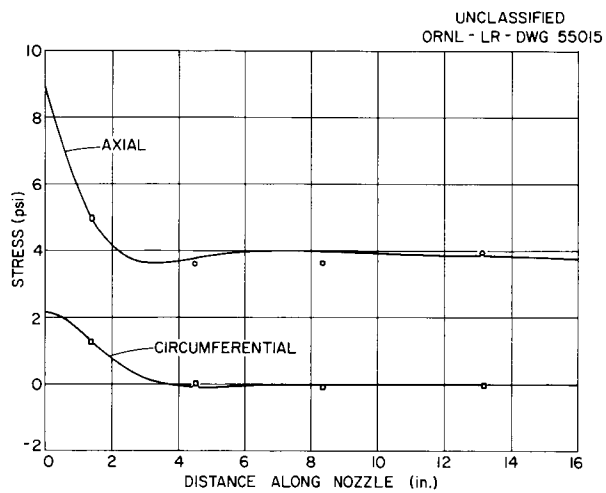

Fig. 84. Stress Distributions on Outer Surface of Nozzle B from Transverse Load of 1 lb Directed Toward Nozzle A at a Distance of 192.3 in. Above the Apex (Downhill Side).

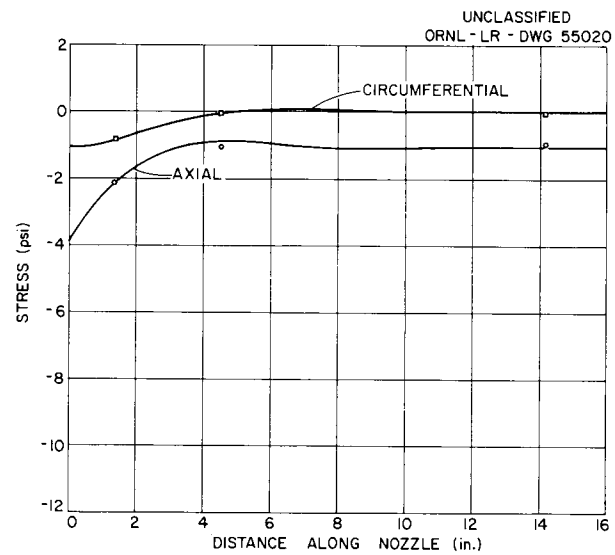

Fig. 85. Stress Distributions on Outer Surface of Nozzle K from Transverse Load of 1 lb Directed Toward Nozzle A at a Distance of 135.9 in. Above the Apex (Uphill Side).

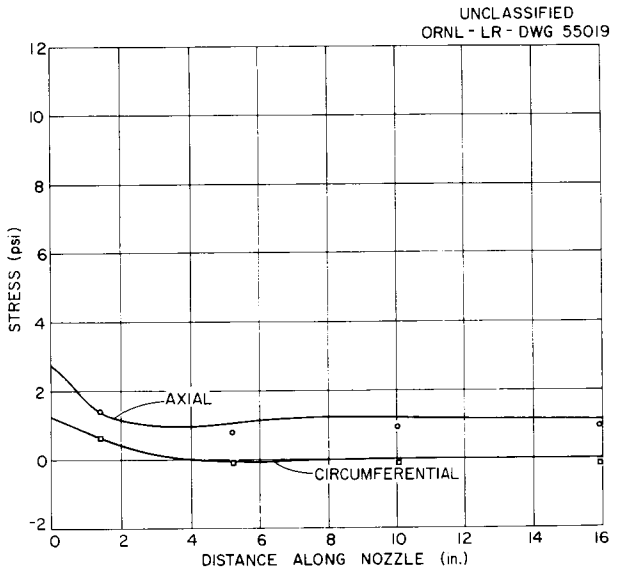

Fig. 86. Stress Distributions on Outer Surface of Nozzle K from Transverse Load of 1 lb Directed Toward Nozzle A at a Distance of 135.9 in. Above the Apex (Downhill Side).

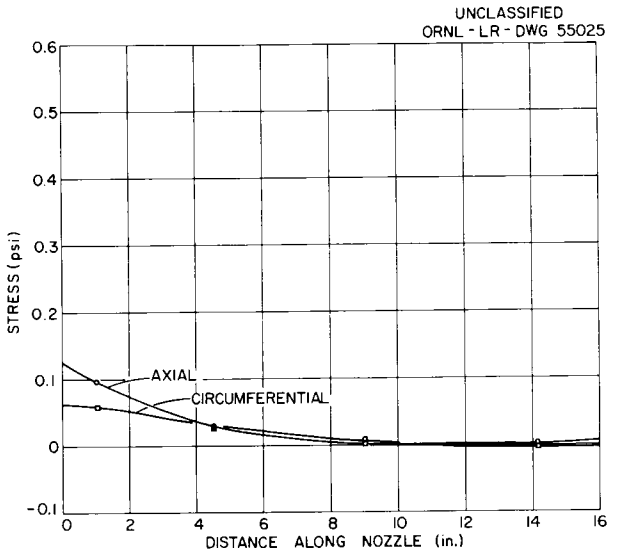

Fig. 87. Stress Distributions on Outer Surface of Gas Outlet Nozzle from Transverse Load of 1 lb Directed in $-F_z$ Direction at a Distance of 47.0 in. from the Junction (Uphill Side).

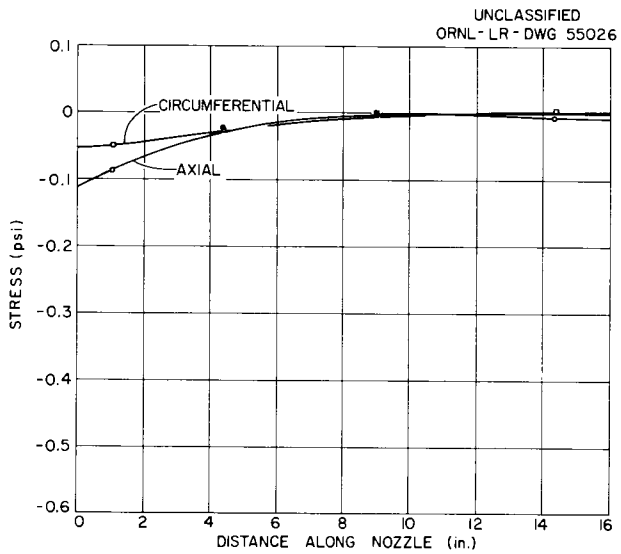

Fig. 88. Stress Distributions on Outer Surface of Gas Outlet Nozzle from Transverse Load of 1 lb Directed in $-F_z$ Direction at a Distance of 47.0 in. from the Junction (Downhill Side).

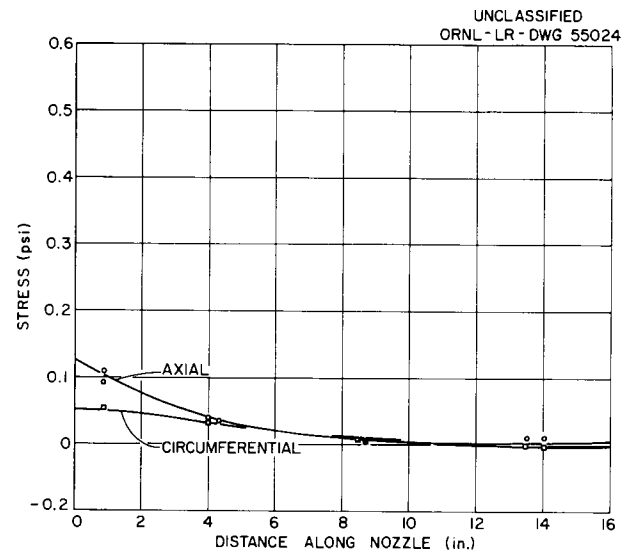

Fig. 89. Stress Distributions on Outer Surface of Gas Outlet Nozzle from Transverse Load of 1 lb Directed in F_y Direction at a Distance of 47.0 in. from the Junction (Side 90 deg from Uphill Side).

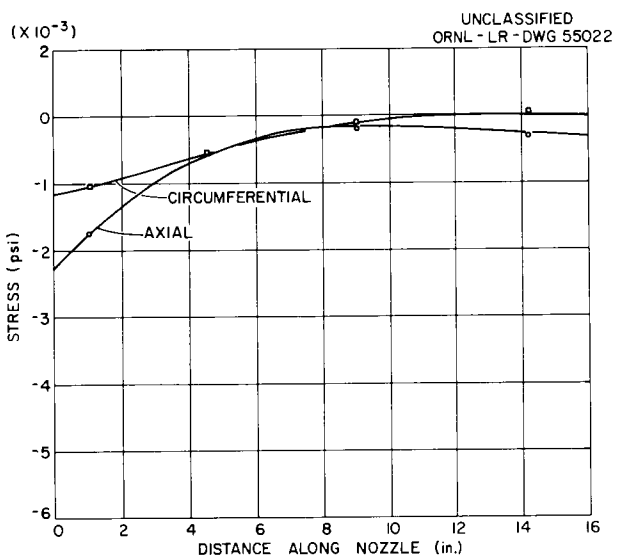

Fig. 90. Stress Distributions on Outer Surface of Gas Outlet Nozzle from an Applied Moment of 1 in.-lb Directed in M_z Direction (Uphill Side).

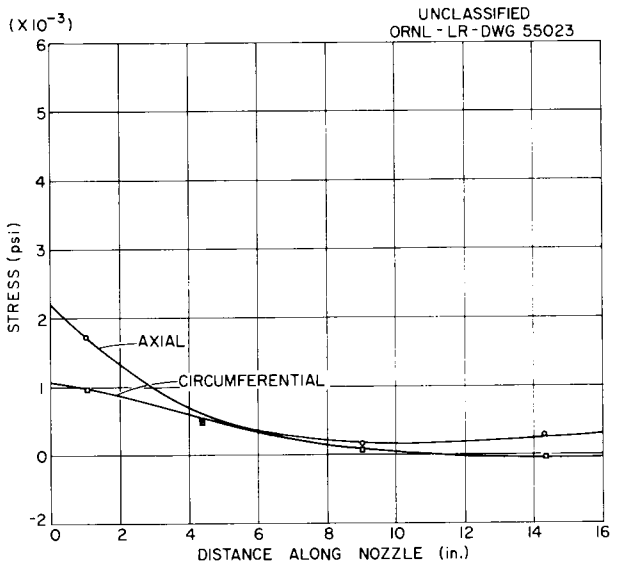

Fig. 91. Stress Distributions on Outer Surface of Gas Outlet Nozzle from an Applied Moment of 1 in.-lb Directed in M_z Direction (Downhill Side).

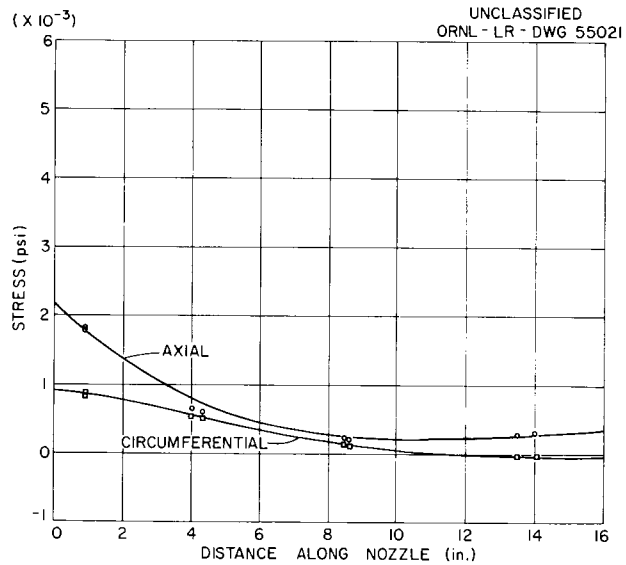

Fig. 92. Stress Distributions on Outer Surface of Gas Outlet Nozzle from an Applied Moment of 1 in.-lb Directed in M_y Direction (Side 90 deg from Uphill Side).

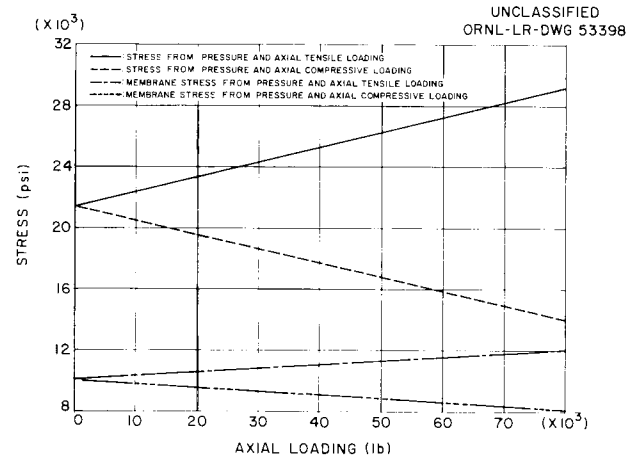

Fig. 93. Maximum Stresses (Absolute) for Nozzle A as a Function of Axial Load While Vessel Is Subjected to 350-psig Pressure Loading.

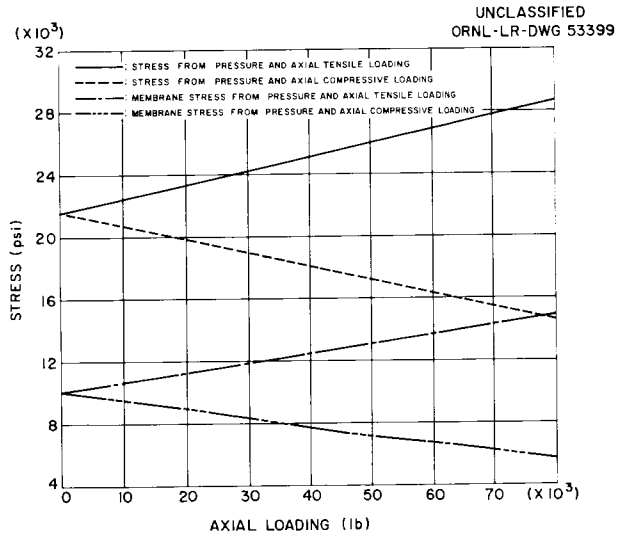

Fig. 94. Maximum Stresses (Absolute) for Nozzle A as a Function of Axial Loads Simultaneously Applied to Four B Nozzles While Vessel Is Subjected to 350-psig Pressure Loading.

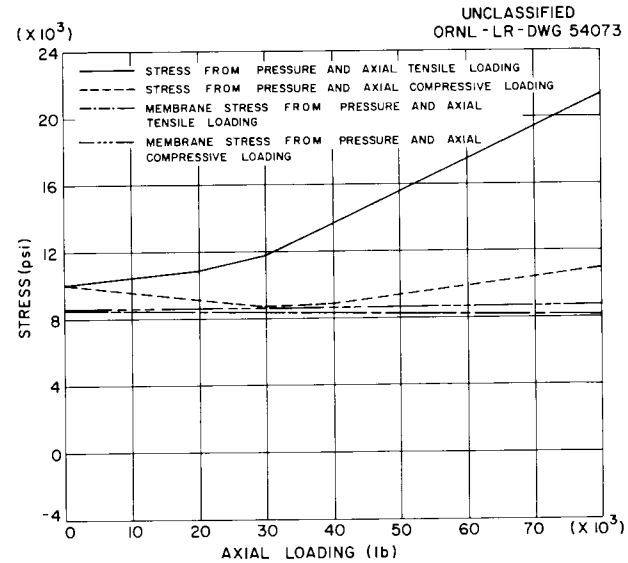

Fig. 95. Maximum Stresses (Absolute) for Nozzle B as a Function of Axial Load While Vessel Is Subjected to 350-psig Pressure Loading (Downhill Side).

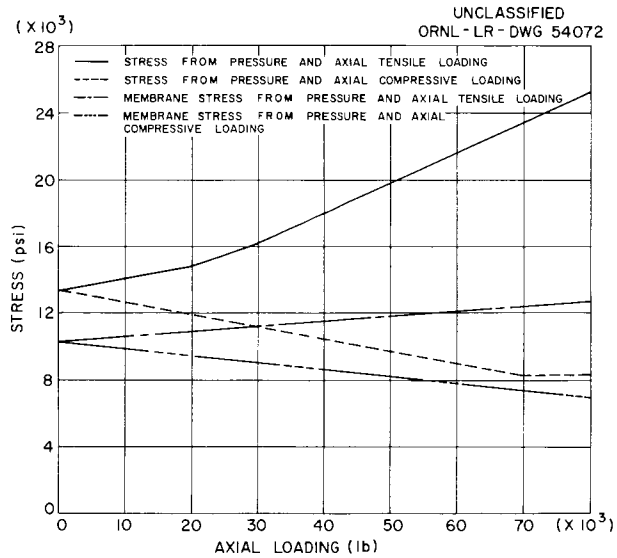

Fig. 96. Maximum Stresses (Absolute) for Nozzle B as a Function of Axial Load While Vessel Is Subjected to 350-psig Pressure Loading (Downhill Side).

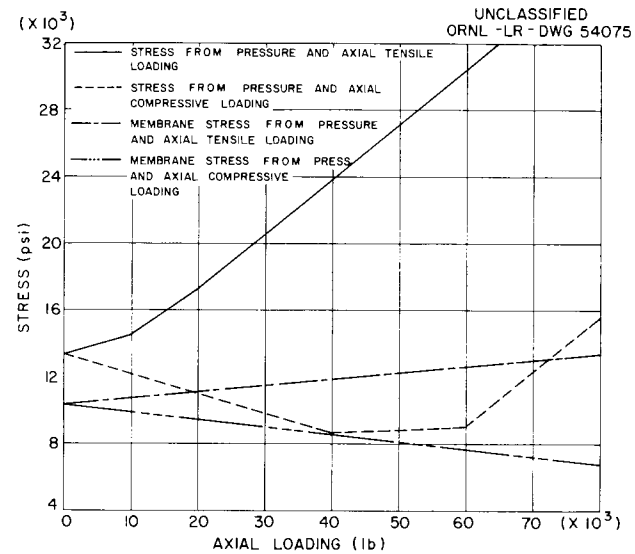

Fig. 97. Maximum Stresses (Absolute) for Nozzle B as a Function of Axial Loads Simultaneously Applied to Four B Nozzles While Vessel Is Subjected to 350-psig Pressure Loading (Downhill Side).

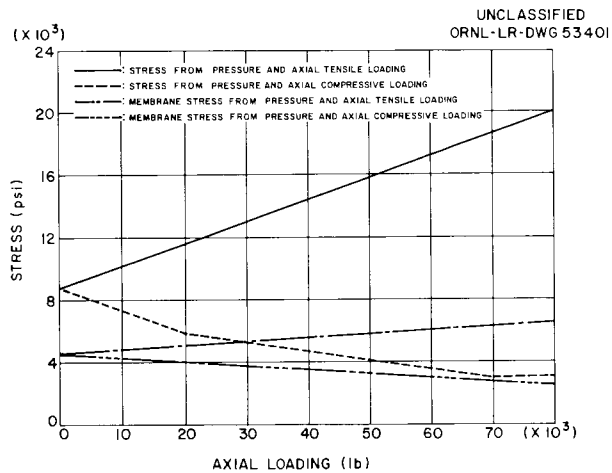

Fig. 98. Maximum Stresses (Absolute) for Nozzle J as a Function of Axial Load While Vessel Is Subjected to 350-psig Pressure Loading (Uphill Side).

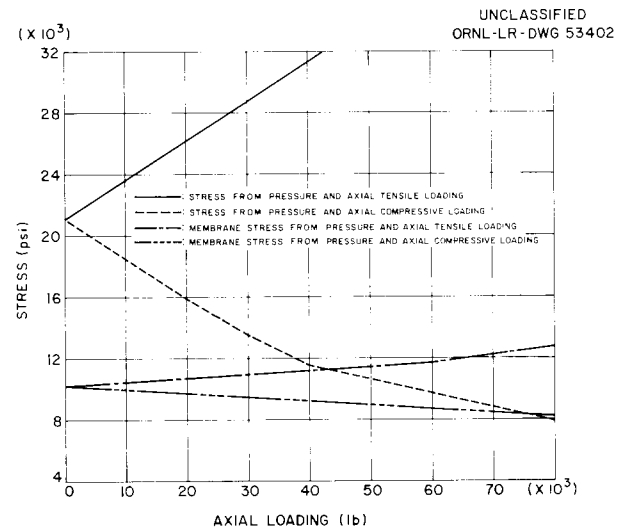

Fig. 99. Maximum Stresses (Absolute) for Nozzle J as a Function of Axial Load While Vessel Is Subjected to 350-psig Pressure Loading (Downhill Side).

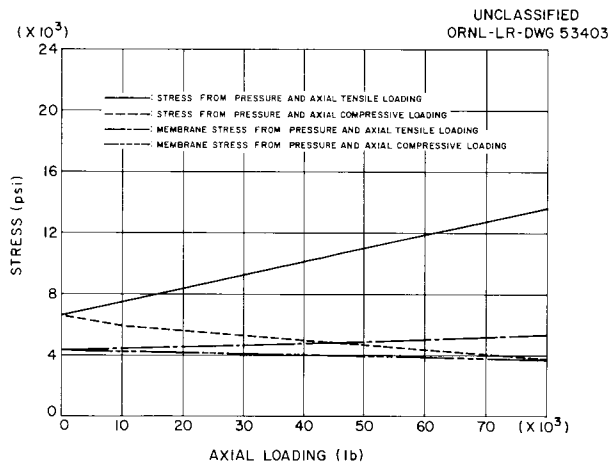

Fig. 100. Maximum Stresses (Absolute) for Nozzle K as a Function of Axial Load While Vessel Is Subjected to 350-psig Pressure Loading (Uphill Side).

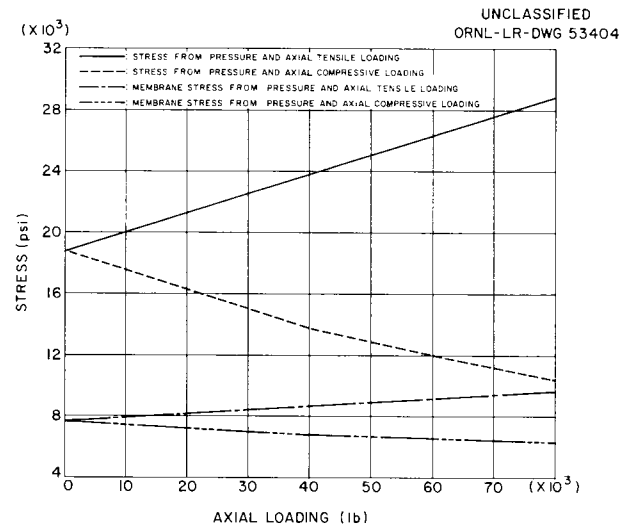

Fig. 101. Maximum Stresses (Absolute) for Nozzle K as a Function of Axial Load While Vessel Is Subjected to 350-psig Pressure Loading (Downhill Side).

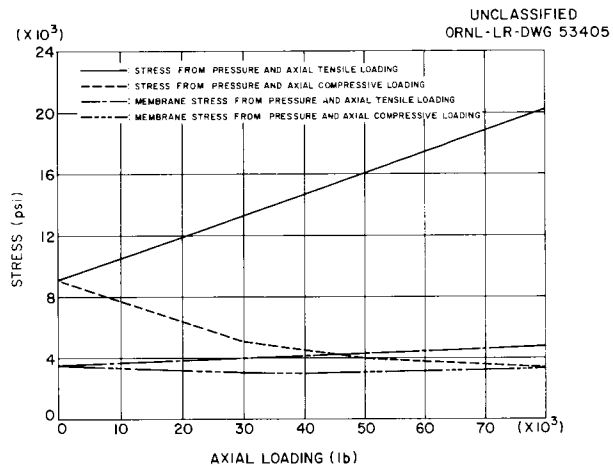

Fig. 102. Maximum Stresses (Absolute) for Nozzle L as a Function of Axial Load While Vessel Is Subjected to 350-psig Pressure Loading (Uphill Side).

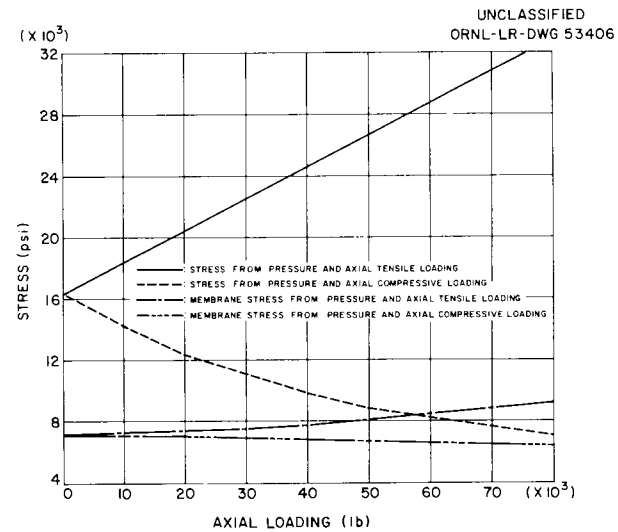

Fig. 103. Maximum Stresses (Absolute) for Nozzle L as a Function of Axial Load While Vessel Is Subjected to 350-psig Pressure Loading (Downhill Side).

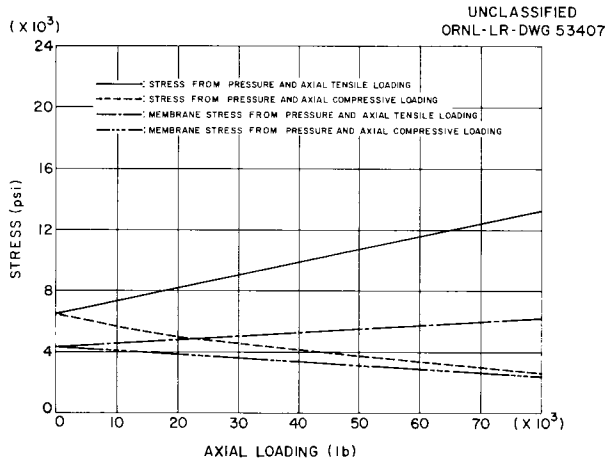

Fig. 104. Maximum Stresses (Absolute) for Nozzle M as a Function of Axial Load While Vessel Is Subjected to 350-psig Pressure Loading (Uphill Side).

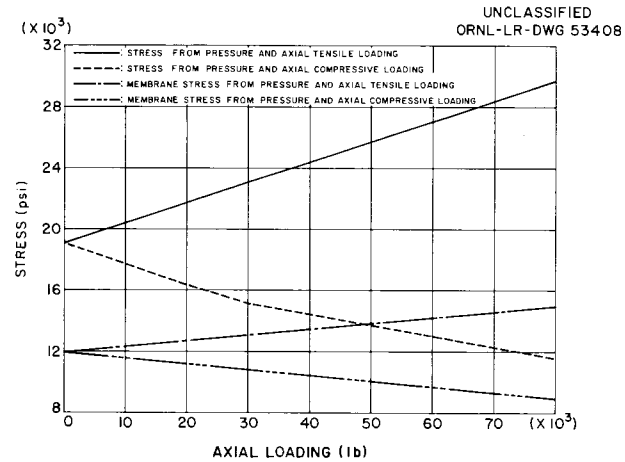

Fig. 105. Maximum Stresses (Absolute) for Nozzle M as a Function of Axial Load While Vessel Is Subjected to 350-psig Pressure Loading (Downhill Side).

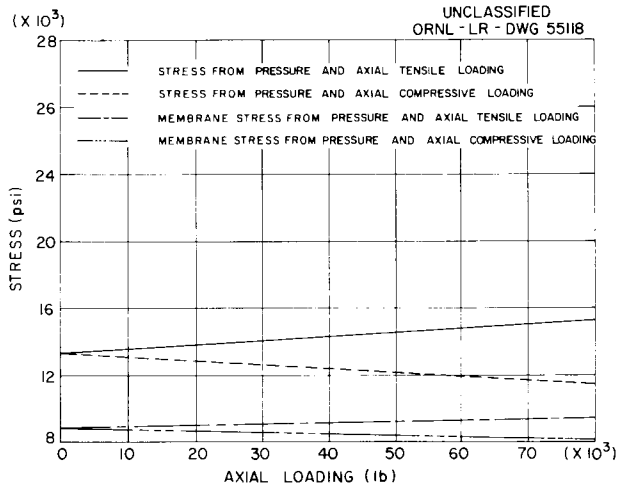

Fig. 106. Maximum Stresses (Absolute) for Gas Outlet Nozzle as a Function of Axial Load While Vessel Is Subjected to 350-psig Pressure Loading (Uphill Side).

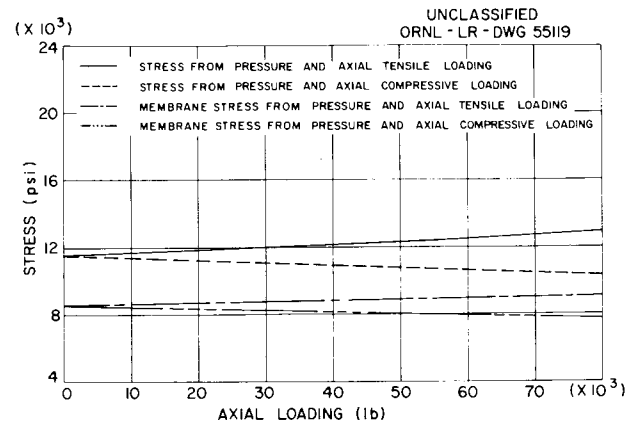

Fig. 107. Maximum Stresses (Absolute) for Gas Outlet Nozzle as a Function of Axial Load While Vessel Is Subjected to 350-psig Pressure Loading (Downhill Side).

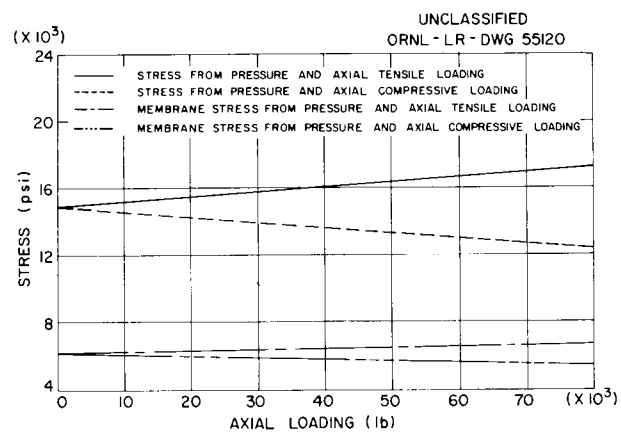

Fig. 108. Maximum Stresses (Absolute) for Gas Outlet Nozzle as a Function of Axial Load While Vessel Is Subjected to 350-psig Pressure Loading (Side 90 deg from Uphill Side).

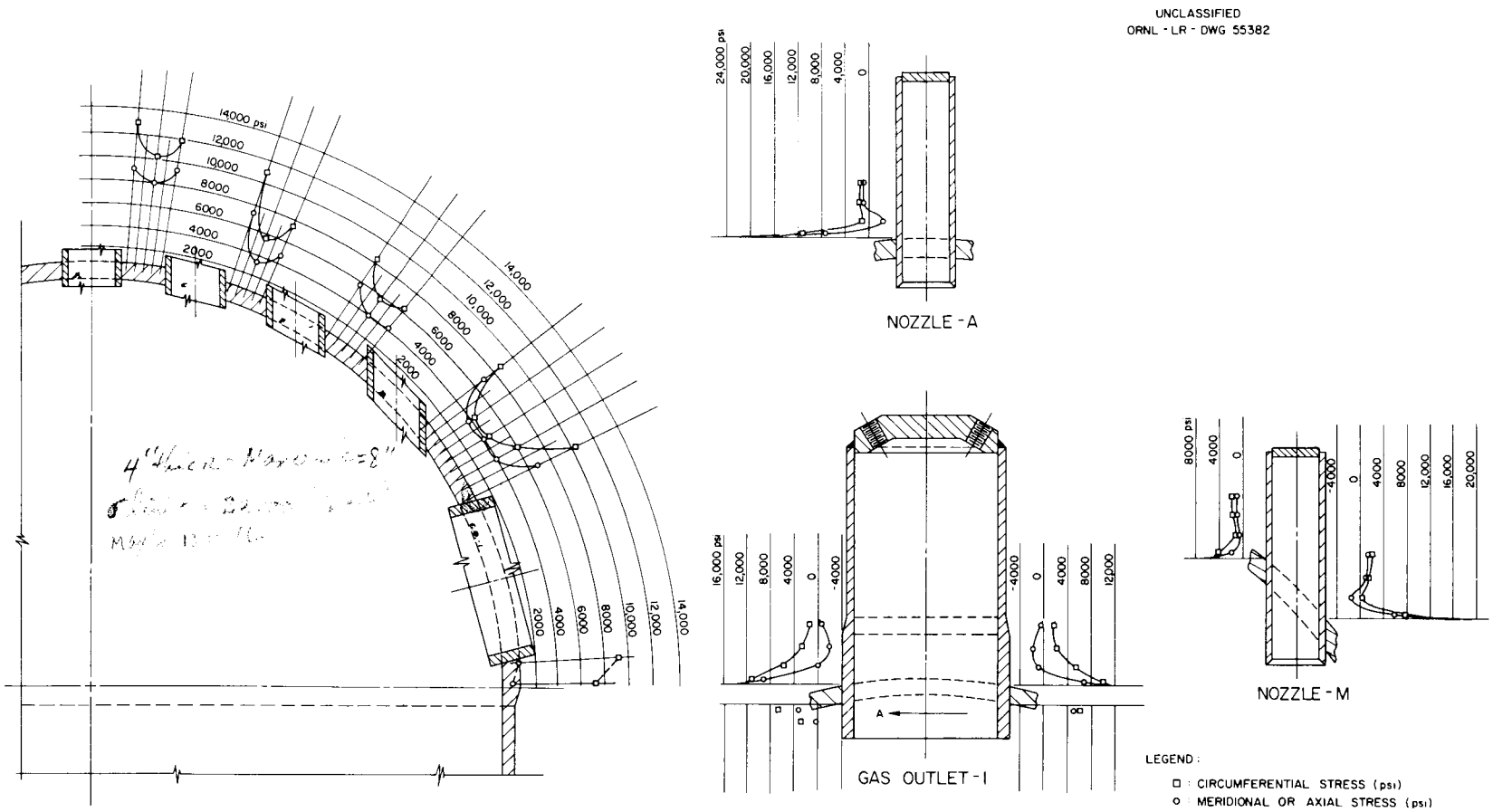

Fig. 109. Circumferential and Meridional or Axial Stresses on Outer Surface of Head, Gas Outlet Nozzle, and Nozzles A and M on a Diametral Section Through Gas Outlet Nozzle.

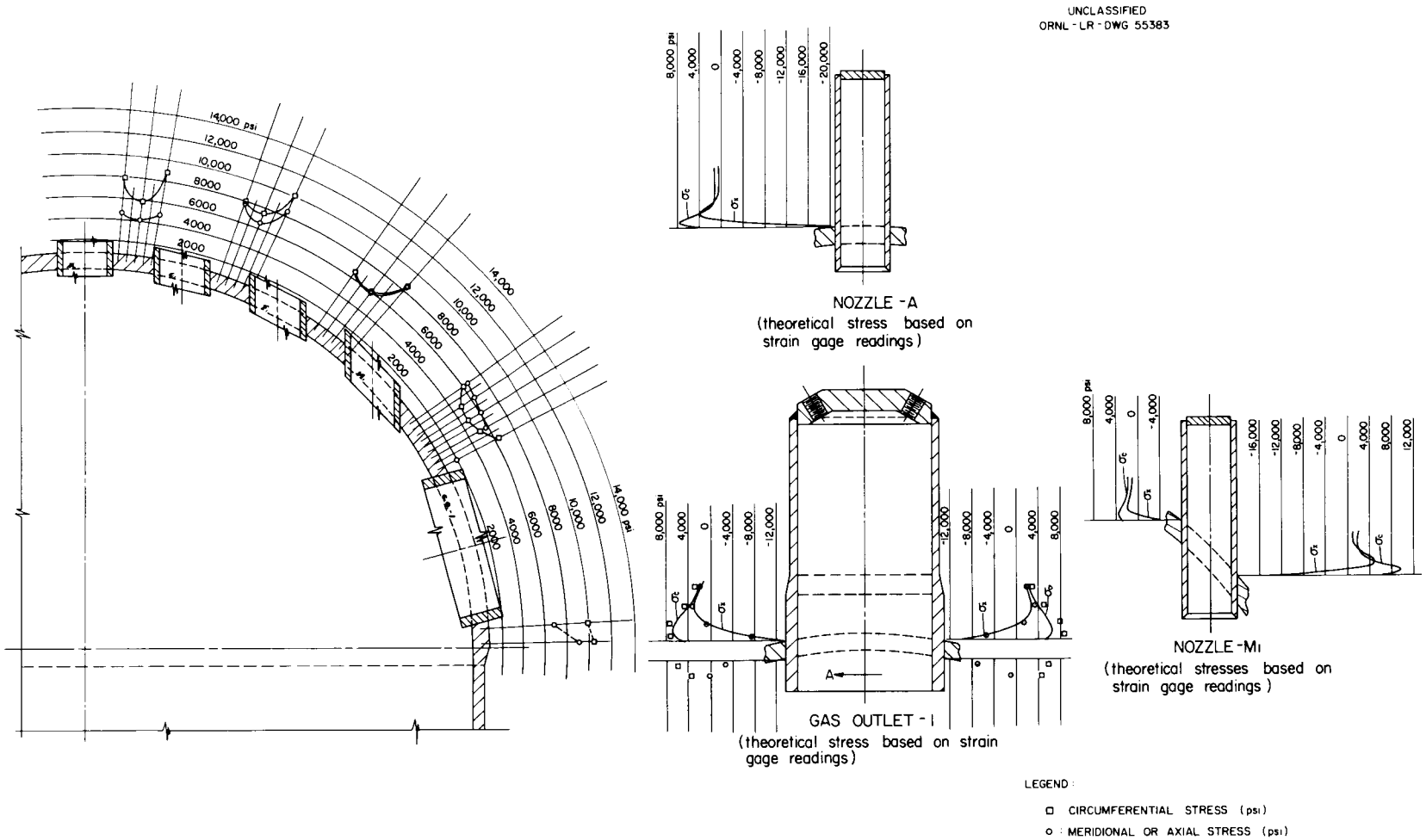

Fig. 110. Circumferential and Meridional or Axial Stresses on Inner Surface of Head, Gas Outlet Nozzle, and Nozzles A and M on a Diametral Section Through Gas Outlet Nozzle.

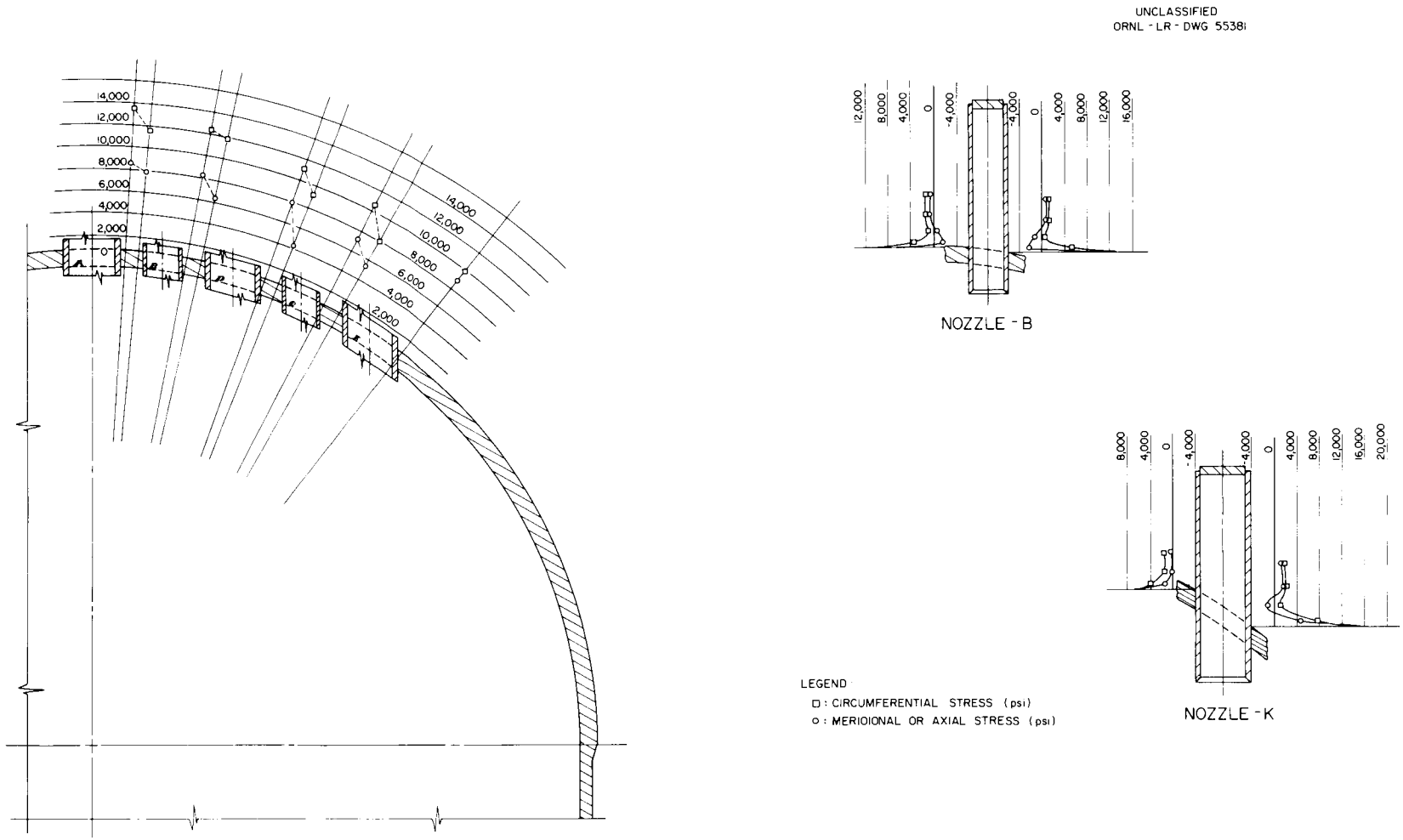

Fig. 111. Circumferential and Meridional or Axial Stresses on Outer Surface of Head and Nozzles B and K on a Diametral Section Through Nozzles A, B, D, G, and K.

UNCLASSIFIED
ORNL - LR - DWG 55384

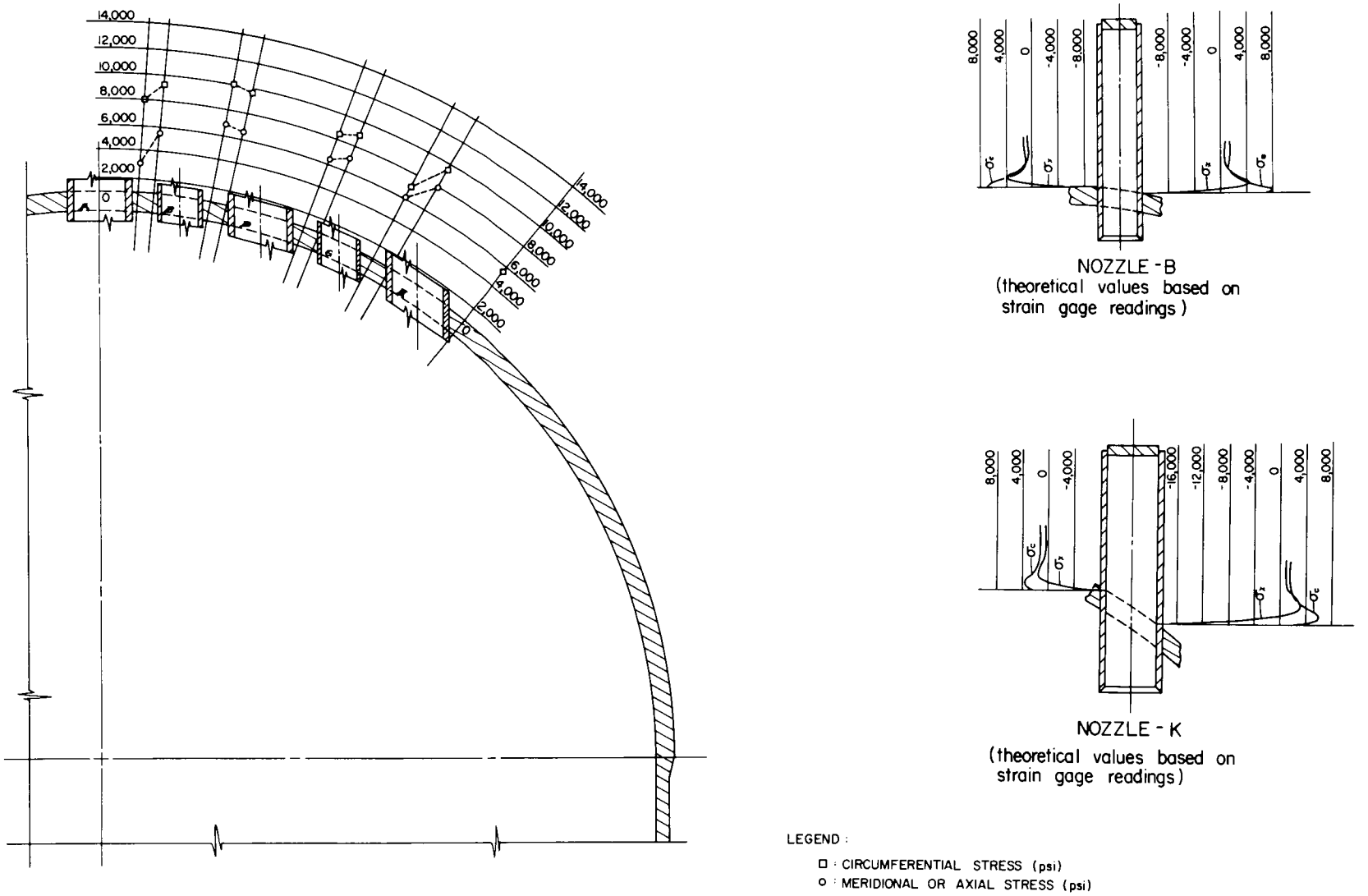

Fig. 112. Circumferential and Meridional or Axial Stresses on Inner Surface of Head and Nozzles B and K on a Diametral Section Through Nozzles A, B, D, G, and K.

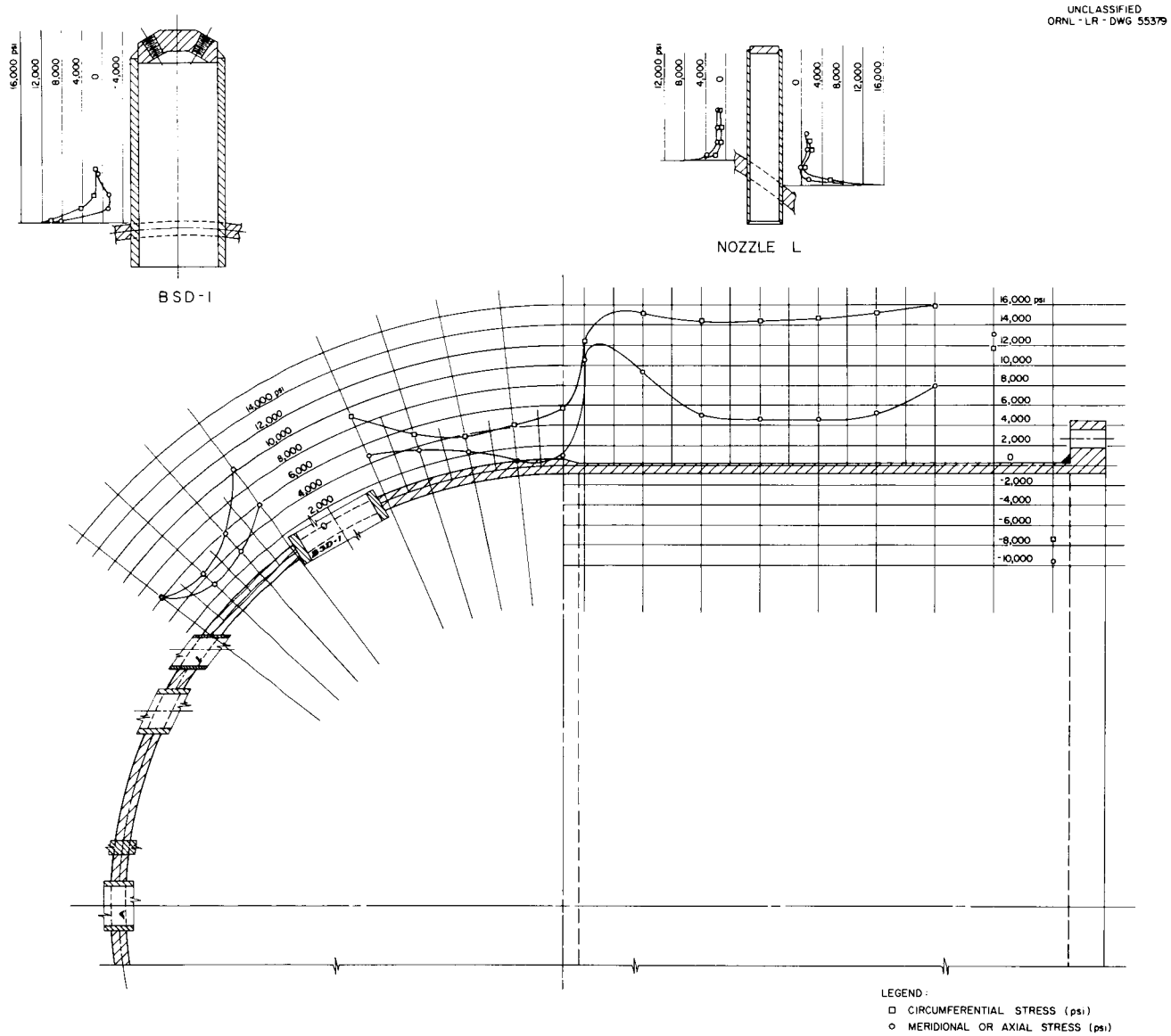

Fig. 113. Circumferential and Meridional or Axial Stresses on Outer Surface of Head, BSD Nozzle, and Nozzle L on a Diametral Section Through BSD Nozzle.

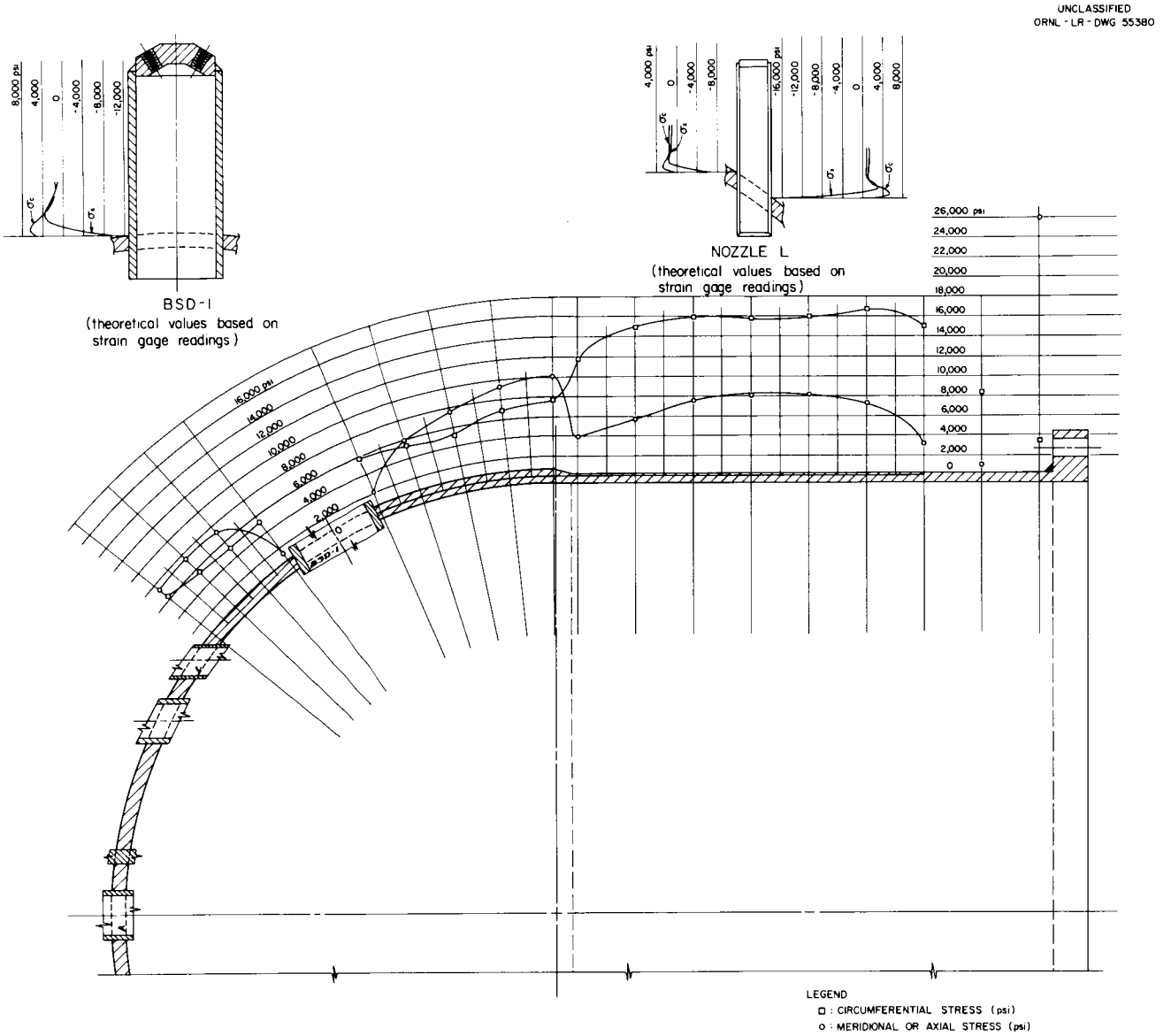

Fig. 114. Circumferential and Meridional or Axial Stresses on Inner Surface of Head, BSD Nozzle, and Nozzle L Along a Diametral Section Through BSD Nozzle.

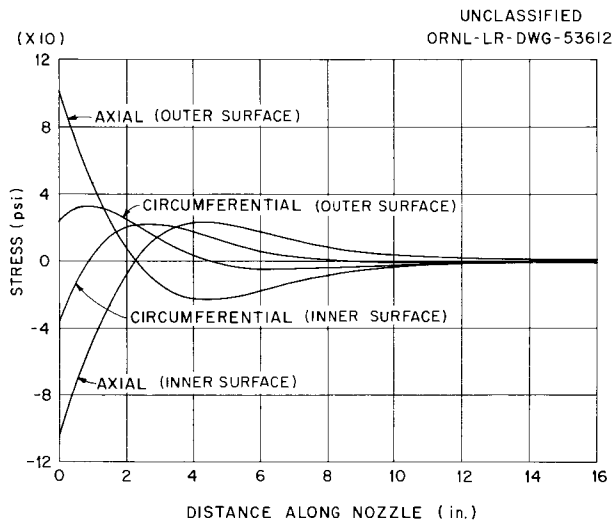

Fig. 115. Thermal Stresses (Theoretical) in Exterior Control Rod or Large Experimental Loop Nozzle Assuming a Single Nozzle-to-Shell Attachment.

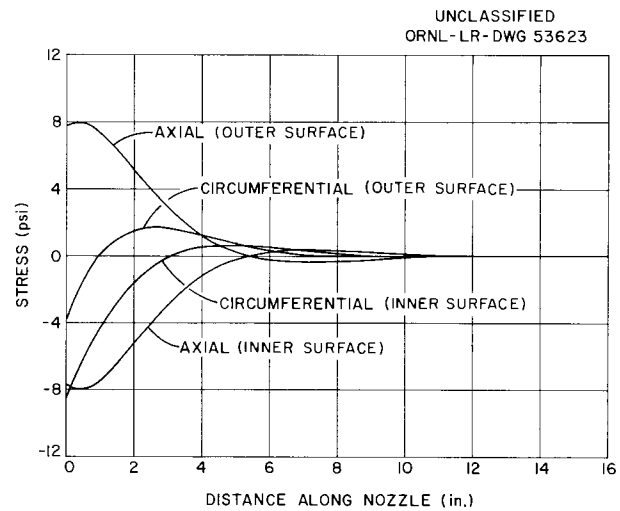

Fig. 116. Thermal Stresses (Theoretical) in Interior Control Rod or Large Experimental Loop Nozzle Assuming a Single Nozzle-to-Shell Attachment.

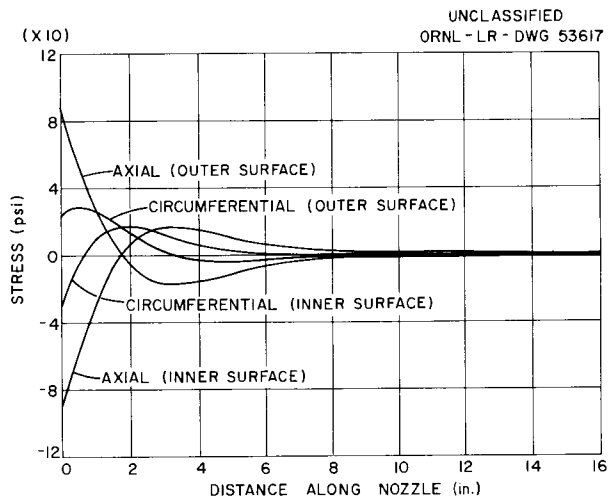

Fig. 117. Thermal Stresses (Theoretical) in Exterior Special Plug or Small Experimental Loop Nozzle Assuming a Single Nozzle-to-Shell Attachment.

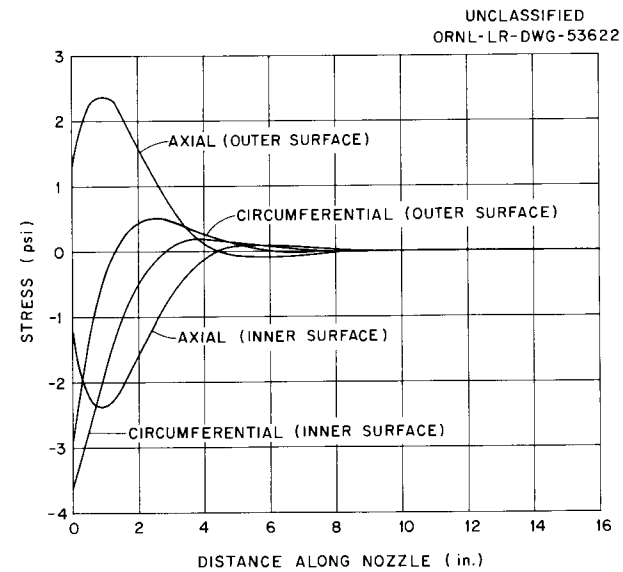

Fig. 118. Thermal Stresses (Theoretical) in the Interior Special Plug or Small Experimental Loop Nozzle Assuming a Single Nozzle-to-Shell Attachment.

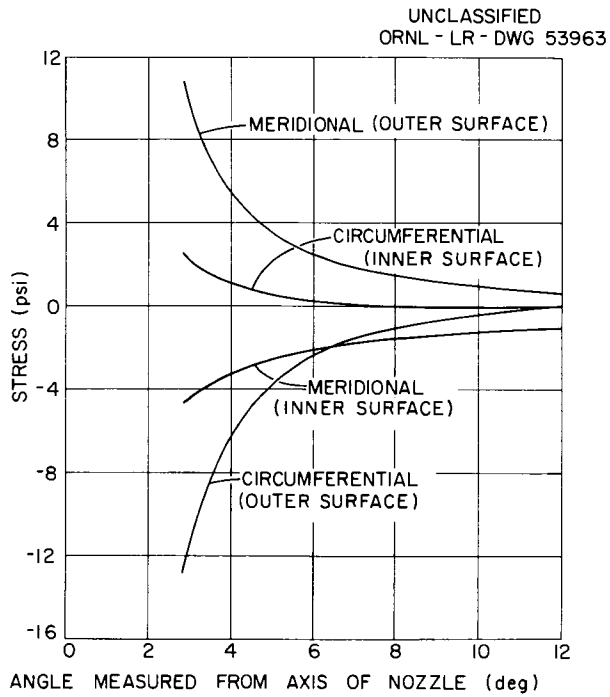

Fig. 119. Theoretical Stresses in the Spherical Head from Axial Temperature Gradient Along Control Rod Nozzle.

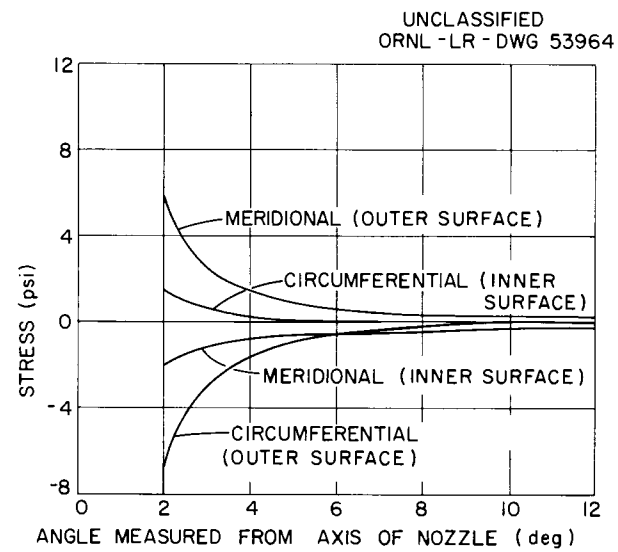

Fig. 120. Theoretical Stresses in the Spherical Head from Axial Temperature Gradient Along Special Plug Nozzle.

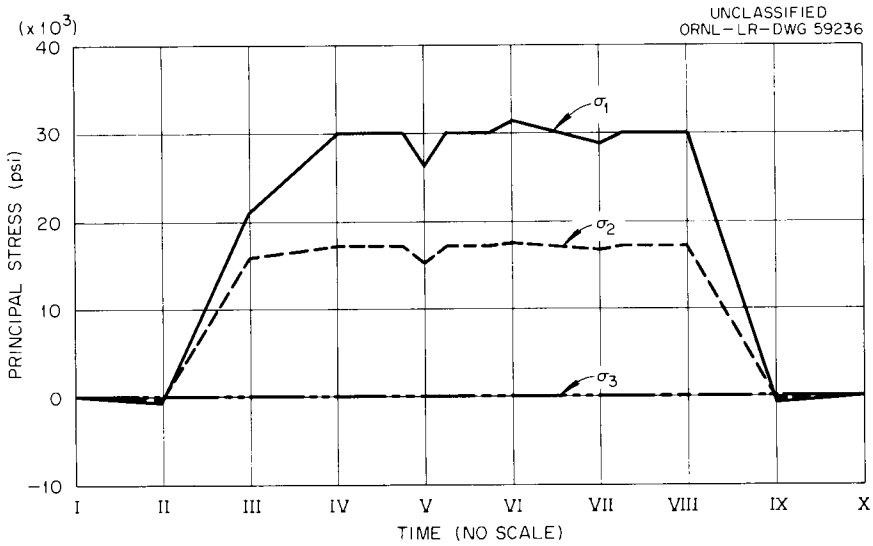

Fig. 121. Principal Stresses Versus Time for the Outer Surface of Nozzle A.

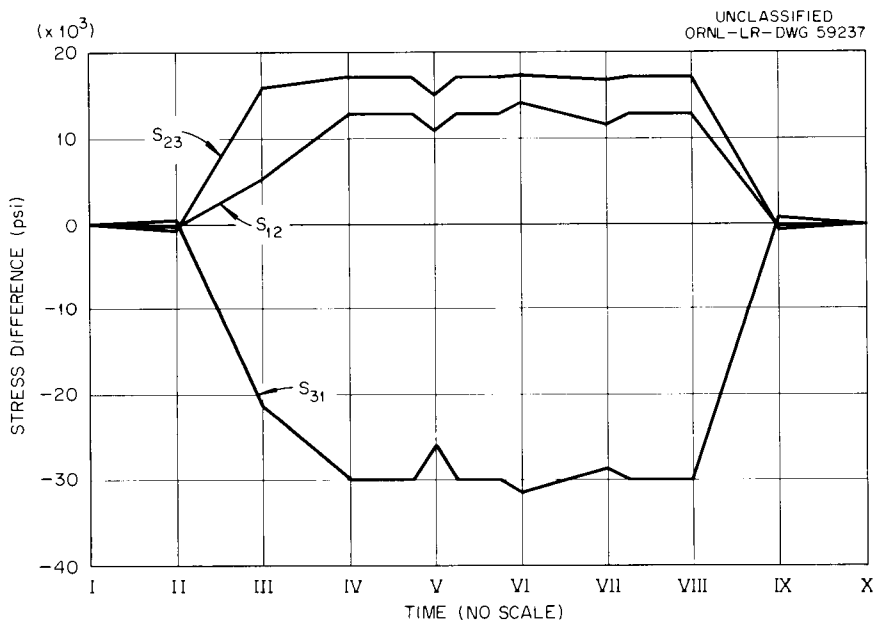

Fig. 122. Principal Stress Differences Versus Time for the Outer Surface of Nozzle A.

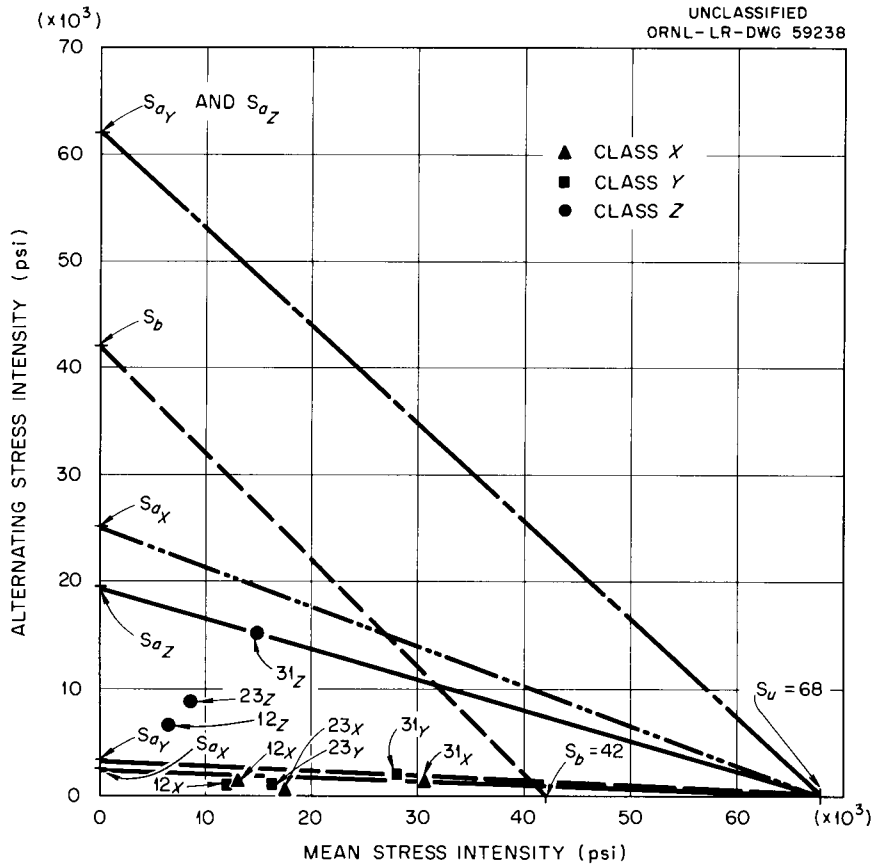

Fig. 123. Fatigue Diagram for the Outer Surface of Nozzle A.

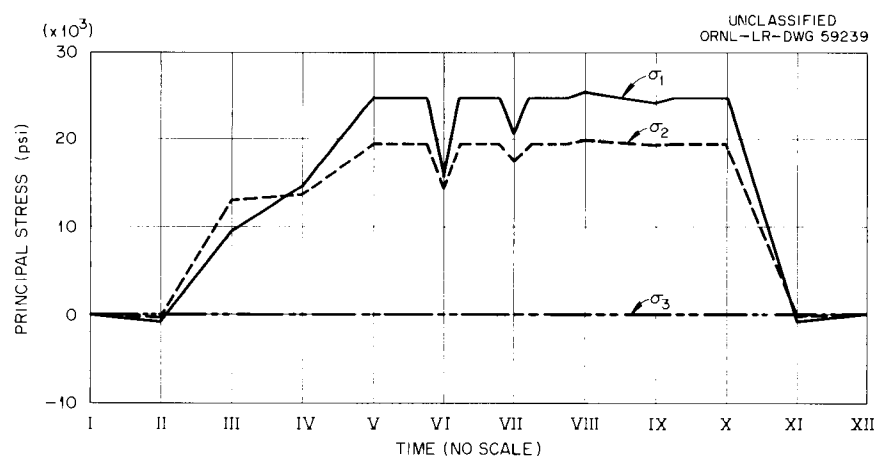

Fig. 124. Principal Stresses Versus Time for the Outer Surface of Nozzle B on the Downhill Side.

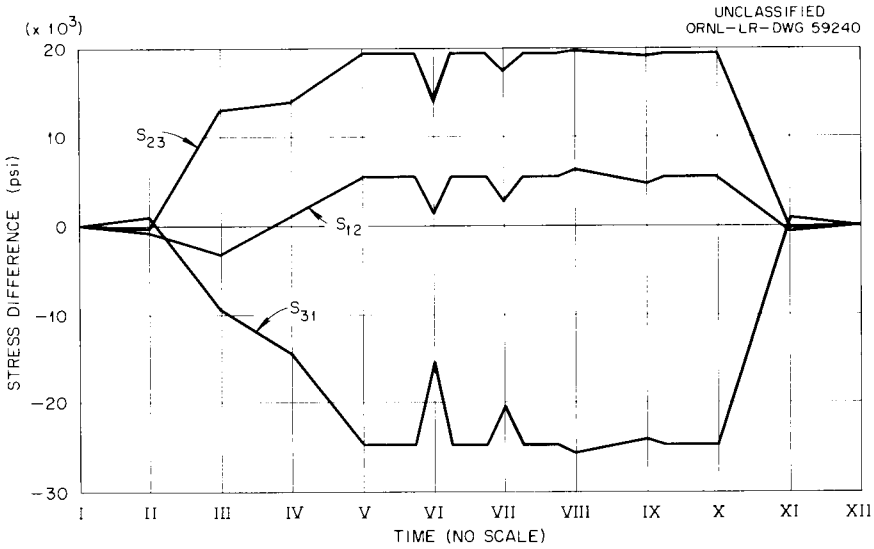

Fig. 125. Principal Stress Differences Versus Time for the Outer Surface of Nozzle B on the Downhill Side.

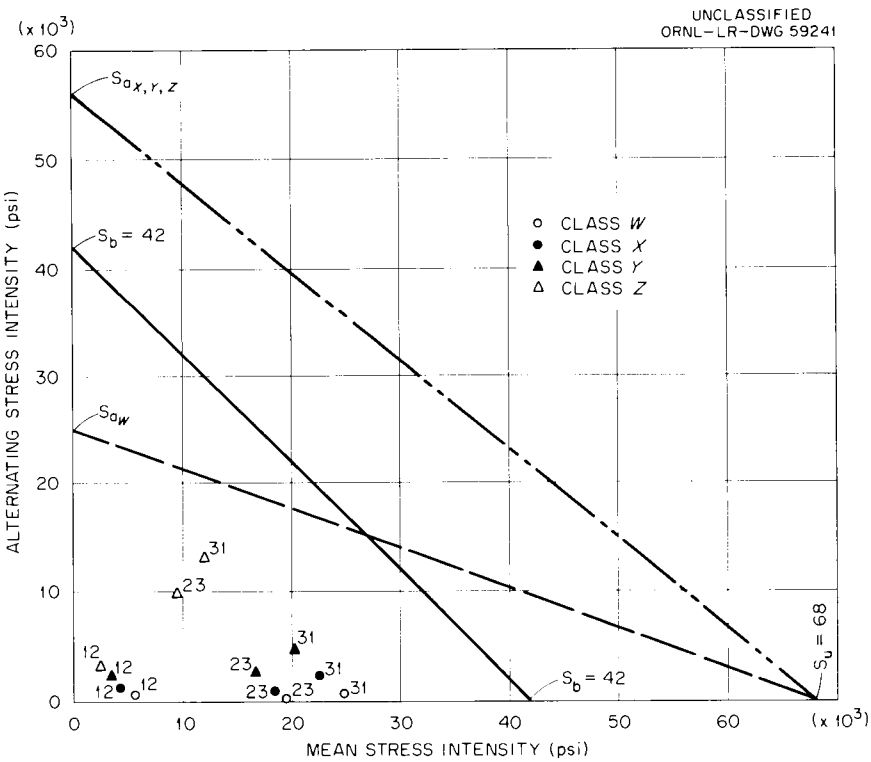

Fig. 126. Fatigue Diagram for the Outer Surface of Nozzle B on the Downhill Side.

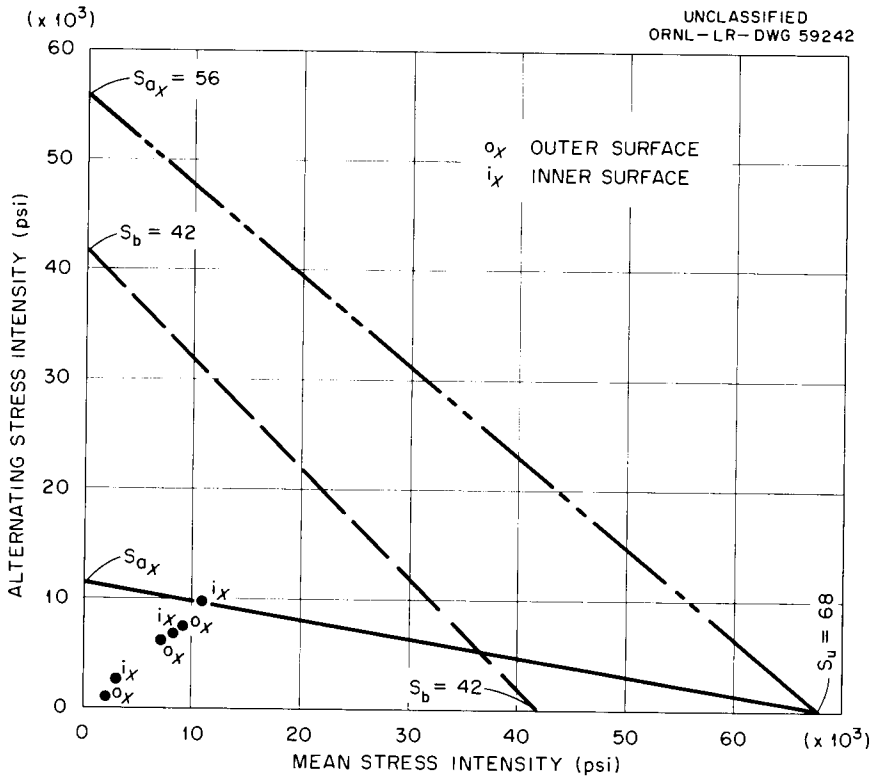

Fig. 127. Fatigue Diagram for the Gas Outlet Nozzle.

Appendix A

EXPERIMENTAL RESULTS

The experimental strain data and the stress values calculated from the data are listed in this appendix. The stresses were computed through the use of the following relationships in which the subscript θ always indicates the stress in the direction of the even-numbered gages, the subscript ϕ always indicates the stress in the direction of the odd-numbered gages, the superscript T indicates the total stress, the superscript m indicates the membrane stress, and the supercript b indicates the bending stress. The sign for the bending stress is that on the outer surface of the dome. In these expressions, ϵ is strain in microinches per inch.

1. Total stresses on inside and outside surfaces

$$\sigma_\theta^T = \frac{E}{1 - \mu^2} (\epsilon_\theta + \mu\epsilon_\phi)$$

$$\sigma_\phi^T = \frac{E}{1 - \mu^2} (\epsilon_\phi + \mu\epsilon_\theta)$$

2. Membrane stresses

$$\sigma_\theta^m = \frac{(\sigma_\theta^T)_o + (\sigma_\theta^T)_i}{2}$$

$$\sigma_\phi^m = \frac{(\sigma_\phi^T)_o + (\sigma_\phi^T)_i}{2}$$

3. Bending stresses

$$\sigma_\theta^b = \sigma_\theta^T - \sigma_\theta^m$$

$$\sigma_{\phi}^{b} = \sigma_{\phi}^{T} - \sigma_{\phi}^{m}$$

The experimental strain data are listed in Tables A.1 through A.26 and the calculated stress values are listed in Tables A.27 through A.52.

List of Tables

		Page
Table A.1	Strain at Each Gage Position Caused by Internal Pressure Loading of 60 psig	145
Table A.2	Strain at Each Gage Position Caused by an Axial Load of 2000 lb Downward on Nozzle A	153
Table A.3	Strain at Each Gage Position Caused by an Axial Load of 1500 lb Downward on Nozzle B_2	154
Table A.4	Strain at Each Gage Position Caused by an Axial Load of 2000 lb Downward on Nozzle M_3	156
Table A.5	Strain at Each Gage Position Caused by an Axial Load of 1500 lb Downward on Nozzle J_2	157
Table A.6	Strain at Each Gage Position Caused by an Axial Load of 1500 lb Downward on Nozzle L_4	158
Table A.7	Strain at Each Gage Position Caused by an Axial Load of 2000 lb Downward on Nozzle K_2	159
Table A.8	Strain at Each Gage Position Caused by a Combined Load of 60 psig Internal Pressure and an Axial Load of 2000 lb on Nozzle A	160
Table A.9	Strain at Each Gage Position Caused by a Normal Load of 50 lb on Nozzle A at a Distance of 34 3/4 in. Above the Apex of the Dome	161
Table A.10	Strain at Each Gage Position Caused by a Normal Load of 150 lb on Nozzle A at a Distance of 13 3/16 in. from the Apex of the Dome	162
Table A.11	Strain at Each Gage Position Caused by a Normal Load of 30 lb on Nozzle B_2 at a Distance of 34 3/4 in. from the Apex of the Dome	163
Table A.12	Strain at Each Gage Position Caused by a Normal Load of 40 lb on Nozzle B_2 at a Distance of 25 1/4 in. from the Apex of the Dome	165
Table A.13	Strain at Each Gage Position Caused by a Normal Load of 50 lb on Nozzle M_3 at a Distance of 34 3/4 in. Above the Apex of the Dome	167
Table A.14	Strain at Each Gage Position Caused by a Normal Load of 150 lb on Nozzle M_3 at a Distance of 13 3/16 in. from the Apex of the Dome	168
Table A.15	Strain at Each Gage Position Caused by a Normal Load of 30 lb on Nozzle J_2 at a Distance of 34 3/4 in. from the Apex of the Dome	169

		Page
Table A.16	Strain at Each Gage Position Caused by a Normal Load of 80 lb on Nozzle J_2 at a Distance of 13 3/16 in. from the Apex of the Dome	170
Table A.17	Strain at Each Gage Position Caused by a Normal Load of 30 lb on Nozzle L_4 at a Distance of 34 3/4 in. from the Apex of the Dome	171
Table A.18	Strain at Each Gage Position Caused by a Normal Load of 80 lb on Nozzle L_4 at a Distance of 13 3/16 in. from the Apex of the Dome	172
Table A.19	Strain at Each Gage Position Caused by a Normal Load of 75 lb on Nozzle K_2 at a Distance of 24 9/16 in. from the Apex of the Dome	173
Table A.20	Strain at Each Gage Position Caused by Axial Loads of 1500 lb Applied Simultaneously to Four Small Experimental Loop Nozzles	174
Table A.21	Strain at Each Gage Position Caused by an Axial Load of 5000 lb on Gas Outlet	176
Table A.22	Strain at Each Gage Position Caused by a Normal Load of 2000 lb on Gas Outlet in Transverse Plane at a Distance of 8 1/2 in. from Dome Surface	178
Table A.23	Strain at Each Gage Position Caused by a Normal Load of 2000 lb on Gas Outlet in Axial Plane at a Distance of 8 1/2 in. from Dome Surface	179
Table A.24	Strain at Each Gage Position Caused by a Pure Moment of 19 200 in.-lb on Gas Outlet in Transverse Plane	180
Table A.25	Strain at Each Gage Position Caused by a Pure Moment of 19 200 in.-lb on Gas Outlet in Axial Plane	181
Table A.26	Strain at Each Gage Position Caused by a Torsional Load of 32 000 in.-lb on Gas Outlet	182
Table A.27	Stress at Each Gage Position Caused by an Internal Pressure Loading of 60 psig	183
Table A.28	Stress at Each Gage Position Caused by an Axial Load of 2000 lb Downward on Nozzle A	191
Table A.29	Stress at Each Gage Position Caused by an Axial Load of 1500 lb Downward on Nozzle B_2	192
Table A.30	Stress at Each Gage Position Caused by an Axial Load of 2000 lb Downward on Nozzle M_3	194
Table A.31	Stress at Each Gage Position Caused by an Axial Load of 1500 lb Downward on Nozzle J_2	195

Page

Table A.32	Stress at Each Gage Position Caused by an Axial Load of 1500 lb Downward on Nozzle L_4	196
Table A.33	Stress at Each Gage Position Caused by an Axial Load of 2000 lb Downward on Nozzle K_2	197
Table A.34	Stress at Each Gage Position Caused by a Combined Load of 60 psig Internal Pressure and an Axial Load of 2000 lb on Nozzle A	198
Table A.35	Stress at Each Gage Position Caused by a Normal Load of 50 lb on Nozzle A at a Distance of 34 3/4 in. Above the Apex of the Dome	199
Table A.36	Stress at Each Gage Position Caused by a Normal Load of 150 lb on Nozzle A at a Distance of 13 3/16 in. from the Apex of the Dome	200
Table A.37	Stress at Each Gage Position Caused by a Normal Load of 30 lb on Nozzle B_2 at a Distance of 34 3/4 in. from the Apex of the Dome	201
Table A.38	Stress at Each Gage Position Caused by a Normal Load of 40 lb on Nozzle B_2 at a Distance of 25 1/4 in. from the Apex of the Dome	203
Table A.39	Stress at Each Gage Position Caused by a Normal Load of 50 lb on Nozzle M_3 at a Distance of 34 3/4 in. Above the Apex of the Dome	205
Table A.40	Stress at Each Gage Position Caused by a Normal Load of 150 lb on Nozzle M_3 at a Distance of 13 3/16 in. from the Apex of the Dome	206
Table A.41	Stress at Each Gage Position Caused by a Normal Load of 30 lb on Nozzle J_2 at a Distance of 34 3/4 in. from the Apex of the Dome	207
Table A.42	Stress at Each Gage Position Caused by a Normal Load of 80 lb on Nozzle J_2 at a Distance of 13 3/16 in. from the Apex of the Dome	208
Table A.43	Stress at Each Gage Position Caused by a Normal Load of 30 lb on Nozzle L_4 at a Distance of 34 3/4 in. from the Apex of the Dome	209
Table A.44	Stress at Each Gage Position Caused by a Normal Load of 80 lb on Nozzle L_4 at a Distance of 13 3/16 in. from the Apex of the Dome	210
Table A.45	Stress at Each Gage Position Caused by a Normal Load of 75 lb on Nozzle K_2 at a Distance of 24 9/16 in. from the Apex of the Dome	211

		Page
Table A.46	Stress at Each Gage Position Caused by Axial Loads of 1500 lb Applied Simultaneously to Four Small Experimental Loop Nozzles	212
Table A.47	Stress at Each Gage Position Caused by an Axial Load of 5000 lb on Gas Outlet	215
Table A.48	Stress at Each Gage Position Caused by a Normal Load of 2000 lb on Gas Outlet in Transverse Plane at a Distance of 8 1/2 in. from Dome Surface	217
Table A.49	Stress at Each Gage Position Caused by a Normal Load of 2000 lb on Gas Outlet in Axial Plane at a Distance of 8 1/2 in. from Dome Surface	218
Table A.50	Stress at Each Gage Position Caused by a Pure Moment of 19 200 in.-lb on Gas Outlet in Transverse Plane	219
Table A.51	Stress at Each Gage Position Caused by a Pure Moment of 19 200 in.-lb. on Gas Outlet in Axial Plane	220
Table A.52	Stress at Each Gage Position Caused by a Torsional Load of 32 000 in.-lb on Gas Outlet	221

Table A.1. Strain at Each Gage Position Caused by Internal Pressure Loading of 60 psig

Gage Position	Strain (μin./in.) Outer Surface	Strain (μin./in.) Inner Surface	Gage Position	Strain (μin./in.) Outer Surface	Strain (μin./in.) Inner Surface
1	-44	102	43	13	68
2	162	125	44	116	124
3	-34	61	45	34	117
4	158	126	46	103	142
5	150	82	47	26	82
6	98	-17	48	96	108
7	102	83	49	59	82
8	29	65	50	144	105
9	69	76	51	84	82
10	29	84	52	165	115
11	159	110	53	62	42
12	90	-2	54	171	147
13	103	84	55	105	43
14	27	73	56	148	132
15	71	73	57	83	44
16	26	80	58	135	88
17	67	-8	59	89	38
18	143	99	60	169	116
19	36	75	61	77	13
20	81	65	62	189	136
21	43	77	63	102	
22	54	51	64	167	
23	40	80	65	98	61
24	54	52	66	160	120
25	68	79	67	80	38
26	115	4	68	181	130
27	59	18	69	91	43
28	101	75	70	177	119
29	26	66	71	85	44
30	131	104	72	134	87
31	32	27	73	92	38
32	119	88	74	160	137
33	47	92	75	92	38
34	91	103	76	160	137
35	39	75	77	36	25
36	80	81	78	189	139
37	61	90	79	85	52
38	122	77	80	159	152
39	61	45	81	67	82
40	144	100	82	147	116
41	45	74	83	9	89
42	110	159	84	56	100

Table A.1 (continued)

Gage Position	Strain (μin./in.) Outer Surface	Strain (μin./in.) Inner Surface	Gage Position	Strain (μin./in.) Outer Surface	Strain (μin./in.) Inner Surface
85	47	92	128	143	110
86	96	138	129		103
87	5	59	130	61	120
88	123	127	131	33	76
89	45	88	132	128	125
90	99	92	133	28	69
91	30	83	134	140	101
92	67	88	135	33	33
93	31	120	136	163	121
94	72	122	137	37	50
95	15	25	138	138	160
96	117	90	139	38	109
97	17	23	140	166	76
98	100	87	141	56	59
99	73	80	142	176	144
100	105	77	143	105	100
101	44	86	144	71	55
102	57	49	145	76	83
103	44	88	146	168	132
104	53	48	147	68	38
105	39	72	148	162	165
106	89	61	149	76	43
107	57	-1	150	185	139
108	142	111	151	81	38
109	156	115	152	168	150
110	87	-8	153	113	25
111	102	86	154	189	149
112	28	62	155	83	25
113	69	72	156	172	123
114	29	86	157	68	24
115	-40	72	158	164	151
116	154	144	159	83	52
117	-46	102	160	133	140
118	157	139	161	84	59
119	159	122	162	137	74
120	92	-11	163	53	51
121	99	90	164	163	135
122	28	63	165	42	100
123	70	76	166	130	129
124	24	80	167	85	48
125	49	98	168	164	119
126	147	70	169	50	74
127	36	53	170	103	98

Table A.1 (continued)

Gage Position	Strain (μin./in.) Outer Surface	Strain (μin./in.) Inner Surface	Gage Position	Strain (μin./in.) Outer Surface	Strain (μin./in.) Inner Surface
171	75	72	214	112	119
172	160	113	215	80	60
173	112	63	216	133	65
174	137	120	217	38	11
175		78	218	149	114
176	143	112	219	13	49
177	47	79	220	128	89
178	178	136	221	41	34
179	41	44	222	136	100
180	140	191	223	82	34
181	87	66	224	149	87
182	162	143	225	49	
183	86	79	226	133	158
184	165	117	227	29	89
185	84	47	228	133	136
186	162	141	229	42	32
187		22	230	176	124
188	157		231	-25	21
189	347	72	232	146	169
190	182	119	233	75	58
191	68	31	234	126	120
192	178	157	235	55	42
193	77	49	236	55	189
194	118	102	237	26	70
195	84	36	238	177	110
196	153	170	239	108	87
197	86	50	240	17	86
198	149	103	241	87	18
199	109	44	242	163	134
200	145	120	243	60	69
201	82	49	244	144	94
202	149	137	245	38	38
203	58	53	246	122	174
204	179	143	247	32	87
205	47	88	248	139	136
206	104	148	249	45	17
207	61	49	250	157	85
208	127	181	251	72	71
209	116	59	252	133	96
210	145	90	253	38	49
211	71	67	254	114	125
212	147	99	255	14	61
213	16		256	106	111

Table A.1 (continued)

Gage Position	Strain (μin./in.) Outer Surface	Strain (μin./in.) Inner Surface	Gage Position	Strain (μin./in.) Outer Surface	Strain (μin./in.) Inner Surface
257	102	68	300	155	96
258	127	72	301	69	58
259	46	19	302	119	79
260	154	135	303	36	90
261	83	75	304	100	122
262	125	118	305	65	98
263	70	60	306	84	73
264	123	140	307	20	28
265	58		308	87	129
266	160	110	309	18	66
267	75	70	310	86	142
268	149	110	311	22	26
269	68	95	312	129	109
270	128	98	313	31	65
271	26	80	314	141	94
272	133	115	315	-146	93
273	48	76	316	119	65
274	108	148	317	39	49
275	41	77	318	156	128
276	136	160	319	84	93
277	25	70	320	60	131
278	140	120	321	27	31
279	72	101	322	128	113
280	134	100	323	40	34
281	16	60	324	120	114
282		89	325	72	103
283	31	63	326	125	72
284	116	176	327	28	77
285		109	328	143	128
286	113	147	329	37	70
287	59	51	330	115	95
288	167	129	331	40	23
289	119	76	332	123	91
290	136	61	333	80	86
291	42	63	334	122	65
292	169	150	335	53	22
293	24	113	336	102	78
294	142	129	337	30	65
295	53	29	338	127	109
296	163	124	339	50	72
297	106	71	340	83	139
298	129	62	341	-104	465
299	29	19	342	-67	-84

Table A.1 (continued)

Gage Position	Strain (μin./in.) Outer Surface	Strain (μin./in.) Inner Surface	Gage Position	Strain (μin./in.) Outer Surface	Strain (μin./in.) Inner Surface
343	171	-24	386	53	55
344	121	131	387	-12	129
345	597	-20	388	68	75
346	217	237	389	-26	111
347	50	34	390	123	132
348	223	240	391	111	13
349	43	52	392	147	170
350	214	234	393	77	12
351	42	51	394	196	227
352	212	230	395	42	40
353	46	41	396	206	233
354	201	232	397	40	47
355	81	10	398	198	225
356	208	228	399	33	51
357	115	12	400	203	229
358	155	173	401	39	30
359	-20	111	402	208	260
360	118	123	403	88	-21
361	-10	133	404	202	234
362	63	77	405	152	-32
363	21	114	406	119	111
364	50	53	407	-118	414
365	25	78	408	-59	-90
366	69	55	409	67	60
367	40	9	410	60	56
368	129	100	411	66	63
369	52	-14	412	55	60
370	145	91	413	50	68
371	30	89	414	64	63
372	80	58	415	48	61
373	27	95	416	55	60
374	57	11	417		183
375	29	100	418		-156
376	60	58	419		163
377	33	80	420		-143
378	82	52	421		197
379	42	0	422		-153
380	139	89	423		195
381	30	10	424		-160
382	128	93	501	72	
383	42	74	502	138	
384	69	58	503	-40	
385	20	106	504	98	

Table A.1 (continued)

Gage Position	Strain (μin./in.) Outer Surface	Strain (μin./in.) Inner Surface	Gage Position	Strain (μin./in.) Outer Surface	Strain (μin./in.) Inner Surface
505	-37		548	22	
506	46		549	95	
507	-11		550	62	
508	35		551	-25	
509	97		552	12	
510	148		553	14	
511	-26		554	20	
512	101		555	18	
513	-48		556	28	
514	61		557	16	
515	-17		558	63	
516	30		559	5	
517	159		560	24	
518	107		561	10	
519	0		562	32	
520	103		563	4	
521	-29		564	28	
522	58		565	-16	
523	-4		566	123	
524	30		567	8	
525	151		568	23	
526	75		569	11	
527	-13		570	30	
528	111		571	5	
529	-34		572	26	
530	53		573	-2	
531	-2		574	58	
532	29		575	9	
533	-29		576	23	
534	132		577	7	
535	-26		578	24	
536	-22		579	6	
537	3		580	24	
538	21		581	-29	
539	10		582	72	
540	24		583	1	
541	-40		584	-7	
542	138		585	6	
543	-27		586	16	
544	18		587	9	
545	3		588	21	
546	20		589	-60	
547	0		590	74	

Table A.1 (continued)

Gage Position	Strain (μin./in.) Outer Surface	Strain (μin./in.) Inner Surface	Gage Position	Strain (μin./in.) Outer Surface	Strain (μin./in.) Inner Surface
591	-22		634	31	
592	-29		635	6	
593	-38		636	28	
594	23		637	92	
595	2		638	145	
596	24		639	-39	
597	-4		640	79	
598	83		641	-27	
599	-5		642	38	
600	8		643	2	
601	14		644	15	
602	25		865		-135
603	3		866		177
604	20		867		-15
605	20		868		128
606	55		869		40
607	7		870		68
608	23		871		26
609	7		872		46
610	23		873		25
611	2		874		40
612	23		875		35
613	32		876		62
614	100		877		-15
615	-29		878		120
616	17		879		-172
617	8		880		165
618	25		881		-196
619	2		882		180
620	24		883		-55
621	1		884		133
622	62		887		37
623	-8		888		26
624	27		889		39
625			890		170
626	24		891		41
627	-1		892		55
628	23		893		-33
629	87		894		124
630	81		895		-185
631	-33		896		29
632	69		897		-152
633	-18		898		137

Table A.1 (continued)

Gage Position	Strain (μin./in.) Outer Surface	Strain (μin./in.) Inner Surface	Gage Position	Strain (μin./in.) Outer Surface	Strain (μin./in.) Inner Surface
899		-40	906		116
900		80	907		-15
901	1		908		62
902	132		909	-8	
903	58		910	46	
904	75		911	20	
905		-75	912	97	

Table A.2. Strain at Each Gage Position Caused by an Axial Load of 2000 lb Downward on Nozzle A

Gage Position	Strain (μin./in.) Outer Surface	Strain (μin./in.) Inner Surface	Gage Position	Strain (μin./in.) Outer Surface	Strain (μin./in.) Inner Surface
51	-9	-80	146	-69	-20
52	-9	-15	147	-83	60
53	-78	30	148	-39	-75
54	-65	-50	149	-81	42
55	-40	-20	150	-202	95
56	-115	46	153	-111	52
57	-80	23	154	-62	-77
58	-155	85	155	-13	-13
59	-183	151	156	-59	18
60	-213	109	157	-75	48
61	-175	150	158	-52	-89
62	-217	110	159	-89	32
63	-209	139	160	3	82
64	-205	110	181	-56	20
65	-171	118	182	-24	-84
66	-199	92	183	23	-50
67	-195	174	184	-9	12
68	-174	98	185	6	9
69	-192	168	186	-8	-54
70	-202	101	189	2	-21
71	-176	115	190	-120	46
72	-194	90	191	-81	33
73	-77	10	192	-70	-19
74	-139	73	533	-202	
75	-31	-20	534	-93	
76	-100	42	535	-77	
77	-48	30	536	35	
78	-67	-10	537	-49	
79	-57	19	538	45	
80	-23	-83	541	-103	
81	24	-50	542	-143	
82	-10	19	543	-49	
83	35	-56	544	37	
84	-9	16	545	-104	
143	-5	-35	546	43	
144	-36	4	547	-100	
145	-14	-29	548	35	

Table A.3. Strain at Each Gage Position Caused by an Axial Load of 1500 lb Downward on Nozzle B_2

Gage Position	Strain (μin./in.) Outer Surface	Strain (μin./in.) Inner Surface	Gage Position	Strain (μin./in.) Outer Surface	Strain (μin./in.) Inner Surface
47	17	-47	145	-190	149
48	-19	2	146	-197	115
49	-11	-37	147	-147	191
50	-19	-17	148	-197	111
51	-85	-7	149	-117	145
52	-38	-36	150	-219	124
53	-71	29	153	-62	24
54	-140	71	154	-46	0
55	-112	73	155	-1	-20
56	-77	3	156	-26	-26
57	-113	97	157	-3	0
58	-47	-8	158	-12	-48
59	-108	100	159	-44	22
60	-61	-3	160	-24	-8
61	-80	60	169	19	-32
62	-144	63	170	-17	-11
65	-59	31	171	10	-44
66	-42	-38	172	-19	13
67	-15	-19	173	-22	-27
68	-19	-16	174	-57	16
69	-65	20	177	-70	9
70	-28	-8	178	-131	62
71	-12	-30	179	-42	37
72	-26	-21	180	-60	-28
73	4	-25	181	-97	79
74	-21	3	182	-78	-10
75	11	-17	183	-20	-14
76	-19	4	184	-54	19
77	7	-26	185	10	-29
78	-16	14	186	96	13
79	-21	4	191	-73	22
80	-8	-41	192	-148	68
135	8	-19	193	3	-19
136	-7	18	194	-21	-6
137	-27	9	581	-214	
138	-33	-20	582	-92	
139	-40	-31	583	-148	
140	-44	0	584	54	
141	2	-23	585	-178	
142	-50	15	586	75	
143	-46	-28	587	-191	
144	-118	73	588	65	

Table A.3 (continued)

Gage Position	Strain (μin./in.) Outer Surface	Strain (μin./in.) Inner Surface	Gage Position	Strain (μin./in.) Outer Surface	Strain (μin./in.) Inner Surface
589	-290		593	-131	
590	-74		594	58	
591	-126		595	-156	
592	44		596	48	

Table A.4. Strain at Each Gage Position Caused by an Axial Load of 2000 lb Downward on Nozzle M_3

Gage Position	Strain (μin./in.) Outer Surface	Strain (μin./in.) Inner Surface	Gage Position	Strain (μin./in.) Outer Surface	Strain (μin./in.) Inner Surface
17	-1	-7	45	16	-17
18	15	18	46	1	3
19	-8	-24	125	-60	52
20	12	20	126	-66	-30
21	5	-50	127	5	-19
22	14	29	128	-30	21
23	0	-76	129	-131	-15
24	-23	39	130	-18	-31
25	-152	2	131	-42	17
26	-133	72	132	-54	-24
27	-131	50	133	-36	40
28	-136	29	134	-126	46
29	-134	78	549	-99	
30	-195	44	550	-344	
31	-90	-37	551	-68	
32	-139	40	552	58	
33	-102	93	553	-138	
34	-133	70	554	70	
35	-21	9	555	-140	
36	-100	50	556	46	
37	-5	-25	557	-180	
38	-59	23	558	-74	
39	-33	26	559	-116	
40	-39	-32	560	34	
41	7	-31	561	-139	
42	1	-11	562	26	
43	-20	10	563	-160	
44	-17	-32	564	25	

Table A.5. Strain at Each Gage Position Caused by an Axial Load of 1500 lb Downward on Nozzle J_2

Gage Position	Strain (μin./in.) Outer Surface	Strain (μin./in.) Inner Surface	Gage Position	Strain (μin./in.) Outer Surface	Strain (μin./in.) Inner Surface
25	-12	-43	136	-39	-1
26	-24	33	137	6	-12
27	-77	39	138	-15	11
28	-37	-38	139	5	-38
29	-36	-36	140	-20	24
30	-110	43	141	-24	16
31	-8	-14	142	-9	-5
32	-34	-32	161	-69	59
33	-97	11	162	-51	-35
34	-50	-14	163	12	-28
35	-90	57	164	-17	13
36	-28	-34	165	-54	14
37	-61	75	166	-52	-16
38	-49	-17	167	-47	33
39	-28	31	168	-115	53
40	-105	40	565	-277	
41	-54	9	566	-154	
42	-19	-23	567	-139	
43	-1	-14	568	94	
44	-28	19	569	-185	
45	-11	-19	570	72	
46	-5	-25	571	-175	
125	-146	19	572	59	
126	-214	90	573	-201	
127	-89	95	574	-53	
128	-182	76	575	-179	
131	-67	108	576	70	
132	-180	59	577	-179	
133	-99	74	578	62	
134	-160	55	579	-190	
135	-18	9	580	55	

Table A.6. Strain at Each Gage Position Caused by an Axial Load of 1500 lb Downward on Nozzle L_4

Gage Position	Strain (μin./in.)		Gage Position	Strain (μin./in.)	
	Outer Surface	Inner Surface		Outer Surface	Inner Surface
161	-38	37	260	-12	3
162	-76	32	261	-16	0
163	-33	11	262	-14	-32
164	-38	-17	597	-290	
165	19	-20	598	-88	
166	-12	-4	599	-152	
167	-48	30	600	104	
168	-34	-30	601	-208	
215	-172	0	602	76	
216	-164	79	603	-191	
217	-69	68	604	65	
218	-196	50	605	-280	
219	-39	69	606	-17	
220	-175	85	607	-182	
221	-76	35	608	62	
222	-179	49	609	-188	
257	-54	5	610	57	
258	-28	-33	611	-185	
259	14	-20	612	58	

Table A.7. Strain at Each Gage Position Caused by an Axial Load of 2000 lb Downward on Nozzle K_2

Gage Position	Strain (μin./in.) Outer Surface	Strain (μin./in.) Inner Surface	Gage Position	Strain (μin./in.) Outer Surface	Strain (μin./in.) Inner Surface
161	-55	33	260	-154	29
162	-24	-54	261	-156	82
163	-51	22	262	-185	50
164	-30	-59	267	1	-27
165	6	-28	268	-72	29
166	3	-33	269	-47	45
167	3	-2	270	-37	-38
168	-19	10	271	20	-28
169	-16	3	272	0	10
170	-5	-32	273	-35	5
171	17	-29	274	-4	-47
172	-18	12	275	-43	-1
173	-11	-2	276	-38	-17
174	-7	-10	305	-45	-14
177	20	-19	306	-12	-35
178	12	5	307	7	-35
179	-7	-6	308	-41	9
180	-4	-50	309	-71	11
215	-49	1	310	-21	-92
216	-61	-9	311	-38	0
217	-50	12	312	-110	32
218	-136	45	613	-282	
219	-57	19	614	-107	
220	-28	-61	615	-75	
221	0	-36	616	59	
222	-35	24	617	-151	
223	-45	21	618	51	
224	-126	66	619	-133	
227	6	-12	620	41	
228	-40	1	621	-206	
229	-36	30	622	-66	
230	-47	-32	623	-106	
257	-260	10	624	48	
258	-154	66	627	-116	
259	-112	66	628	65	

Table A.8. Strain at Each Gage Position Caused by a Combined Load of 60 psig Internal Pressure and an Axial Load of 2000 lb on Nozzle A

Gage Position	Strain (μin./in.)		Gage Position	Strain (μin./in.)	
	Outer Surface	Inner Surface		Outer Surface	Inner Surface
51	80	-9	145	65	15
52	162	100	146	101	102
53	-2	56	149	-24	45
54	108	82	150	-19	200
55	63	31	153	1	40
56	38	169	154	132	24
57	7	66	155	75	38
58	-20	161	156	121	176
59	-99	201	157	1	53
60	-31	232	158	123	21
61	-100	169	159	-4	52
62	-29	249	160	141	173
65	-71	127	181	5	95
66	9	214	182	137	67
67	-92	205	183	110	74
68	-10	190	184	155	165
69	-110	195	185	98	51
70	-15	222	186	162	105
71	-70	146	191	-7	103
72	4	188	192	107	139
73	30	71	533	-225	
74	13	147	534	-13	
75	83	15	535	-110	
76	70	153	536	15	
77	4	51	537	-138	
78	130	132	538	77	
79	42	101	541	-110	
80	148	57	542	4	
81	102	6	543	-58	
82	157	117	544	48	
83	60	15	545	-75	
84	60	93	546	55	
143	109	38	547	-83	
144	38	21	548	53	

Table A.9. Strain at Each Gage Position Caused by a Normal Load of 50 lb on Nozzle A at a Distance of 34 3/4 in. Above the Apex of the Dome

Gage Position	Strain (μin./in.) Outer Surface	Strain (μin./in.) Inner Surface	Gage Position	Strain (μin./in.) Outer Surface	Strain (μin./in.) Inner Surface
51	15	8	146	12	7
52	13	6	147	12	4
53	42	-27	148	10	1
54	30	-8	149	37	-27
55	34	-15	150	59	-48
56	50	-27	153	-10	-1
57	55	-41	154	-12	-6
58	60	-53	155	-20	13
59	95	-117	156	-22	20
60	84	-90	157	-42	31
61	78	-97	158	-30	14
62	100	-25	159	-50	31
65	-79	79	160	2	51
66	-98	92	181	10	-6
67	-5	15	182	6	6
68	-34	51	183	0	4
69	87	-70	184	3	-11
70	21	-60	185	-13	18
71	-105	111	186	-6	-27
72	-95	93	191	-7	18
73	-56	40	192	15	-27
74	-62	51	533	280	
75	-38	17	534	24	
76	-47	30	535	183	
77	-29	32	536	-51	
78	-28	5	537	195	
79	-20	-18	538	-77	
80	-12	-7	541	-261	
81	-5	-1	542	-60	
82	-19	12	543	-160	
83	5	-1	544	61	
84	-8	-3	545	-205	
143	17	-6	546	72	
144	12	-4	547	-192	
145	18	-5	548	68	

Table A.10. Strain at Each Gage Position Caused by a Normal Load of 150 lb on Nozzle A at a Distance of 13 3/16 in. from the Apex of the Dome

Gage Position	Strain (μin./in.)		Gage Position	Strain (μin./in.)	
	Outer Surface	Inner Surface		Outer Surface	Inner Surface
51	16	6	146	13	11
52	10	2	147	9	6
53	43	-33	148	10	7
54	35	-8	149	44	-29
55	41	-11	150	60	-50
56	57	-28	153	-9	2
57	58	-40	154	-18	-5
58	70	-52	155	-21	11
59	111	-121	156	-27	21
60	94	-91	157	-58	35
61	82	-109	158	-35	11
62	108	-89	159	-56	37
65	-93	95	160	8	52
66	-110	110	181	11	-20
67	0	12	182	3	-5
68	-39	58	183	-1	-3
69	99	-82	184	2	-13
70	25	-67	185	-15	10
71	-120	127	186	-3	-26
72	-104	107	191	-10	20
73	-67	47	192	21	-27
74	-68	60	533	333	
75	-41	19	534	39	
76	-53	32	535	203	
77	-32	33	536	-59	
78	-32	4	537	217	
79	-23	14	538	-78	
80	-17	-8	541	-290	
81	-8	-4	542	-70	
82	-18	3	543	-169	
83	4	-12	544	63	
84	-6	3	545	-210	
143	13	0	546	73	
144	10	0	547	-183	
145	17	-5	548	60	

Table A.11. Strain at Each Gage Position Caused by a Normal Load of 30 lb on Nozzle B_2 at a Distance of 34 3/4 in. from the Apex of the Dome

Gage Position	Strain (μin./in.) Outer Surface	Strain (μin./in.) Inner Surface	Gage Position	Strain (μin./in.) Outer Surface	Strain (μin./in.) Inner Surface
47	5	-6	143	13	-1
48	1	5	144	27	-28
49	-3	-5	145	105	-107
50	-1	7	146	85	-78
51	19	-25	147	-8	-3
52	8	5	148	53	-80
53	0	8	149	-50	95
54	-18	-4	150	-94	92
55	0	0	153	-26	17
56	-27	17	154	-4	-14
57	-29	31	155	0	-1
58	-16	8	156	-6	6
59	-43	42	157	-5	3
60	-22	5	158	-2	-11
61	-41	34	159	-7	3
62	-61	40	160	9	12
65	-19	11	169	2	0
66	-15	8	170	8	-4
67	-13	8	171	14	-1
68	-11	0	172	14	0
69	-21	5	177	46	-22
70	-13	11	178	50	-38
71	-10	5	179	10	-13
72	-11	2	180	26	-21
73	-5	0	181	-2	1
74	-10	1	182	19	-30
75	0	-5	183	13	-10
76	-10	0	184	10	4
77	-11	0	185	0	8
78	-6	-2	186	2	-18
79	-3	2	191	-6	-6
80	0	-6	192	6	-8
135	2	4	193	-9	6
136	-7	3	194	0	-5
137	0	-2	581	409	
138	20	-14	582	20	
139	20	-17	583	330	
140	9	15	584	-91	
141	5	5	585	344	
142	-20	-4	586	-123	

Table A.11 (continued)

Gage Position	Strain (μin./in.) Outer Surface	Strain (μin./in.) Inner Surface	Gage Position	Strain (μin./in.) Outer Surface	Strain (μin./in.) Inner Surface
587	368		592	87	
588	-118		593	-266	
589	-425		594	114	
590	-2		595	-329	
591	-333		596	101	

Table A.12. Strain at Each Gage Position Caused by a Normal Load of 40 lb on Nozzle B_2 at a Distance of 25 1/4 in. from the Apex of the Dome

Gage Position	Strain (μin./in.)		Gage Position	Strain (μin./in.)	
	Outer Surface	Inner Surface		Outer Surface	Inner Surface
47	10	-2	143	14	-2
48	3	8	144	28	-29
49	10	-3	145	102	-106
50	2	8	146	78	-76
51	20	-27	147	-17	7
52	10	8	148	50	-71
53	4	4	149	-40	98
54	-15	-6	150	-93	88
55	5	-2	153	-24	17
56	-21	20	154	-9	-13
57	-25	33	155	0	-4
58	-14	10	156	-7	3
59	-45	46	157	-8	7
60	-19	8	158	-3	-10
61	-40	37	159	-12	4
62	-54	39	160	11	11
65	-17	9	169	6	-1
66	-16	6	170	6	-5
67	-10	3	171	11	-7
68	-9	2	172	11	-1
69	-22	5	173	15	-3
70	-10	15	174	18	-8
71	-10	5	177	39	-21
72	-12	4	178	46	-34
73	-4	1	179	13	-12
74	-6	3	180	26	-14
75	-1	-2	181	-9	3
76	-7	2	182	20	-29
77	-2	-1	183	11	-7
78	-9	-1	184	7	1
79	-8	5	185	0	9
80	-4	-7	186	6	-18
135	4	1	191	-9	-1
136	6	2	192	7	0
137	8	-1	193	-6	6
138	17	-12	194	0	-2
139	20	-19	581	379	
140	8	11	582	17	
141	2	-1	583	300	
142	-19	-9	584	-83	

Table A.12 (continued)

Gage Position	Strain (μin./in.) Outer Surface	Strain (μin./in.) Inner Surface	Gage Position	Strain (μin./in.) Outer Surface	Strain (μin./in.) Inner Surface
585	309		591	-302	
586	-107		592	69	
587	322		593	-241	
588	-93		594	99	
589	-362		595	-291	
590	-6		596	92	

Table A.13. Strain at Each Gage Position Caused by a Normal Load of 50 lb on Nozzle M_3 at a Distance of 34 3/4 in. Above the Apex of the Dome

Gage Position	Strain (μin./in.)		Gage Position	Strain (μin./in.)	
	Outer Surface	Inner Surface		Outer Surface	Inner Surface
17	-1	2	44	-14	4
18	-2	-2	45	0	-6
19	-3	9	46	-8	-5
20	0	-2	125	-32	20
21	2	16	126	-29	-30
22	5	-7	127	-4	1
23	14	-4	128	-18	-11
24	24	-9	131	-38	33
25	86	-64	132	-34	-2
26	68	-40	133	-36	65
27	-17	5	134	-59	-4
28	-25	-70	549	47	
29	-134	57	550	278	
30	-74	-35	551	158	
31	-12	0	552	-54	
32	-30	-79	553	200	
33	-87	70	554	-90	
34	-88	85	555	208	
35	-32	46	556	-94	
36	-58	42	557	-400	
37	-12	21	558	-58	
38	-40	18	559	-230	
39	-24	33	560	48	
40	-22	-2	561	-231	
41	-5	-6	562	50	
42	-5	0	563	-197	
43	-12	6	564	47	

Table A.14. Strain at Each Gage Position Caused by a Normal Load of 150 lb on Nozzle M_3 at a Distance of 13 3/16 in. from the Apex of the Dome

Gage Position	Strain (μin./in.)		Gage Position	Strain (μin./in.)	
	Outer Surface	Inner Surface		Outer Surface	Inner Surface
17	-3	4	44	-19	0
18	-2	-4	45	5	-11
19	-1	11	46	-9	-4
20	-2	-6	125	-43	24
21	-4	15	126	-41	-37
22	9	-6	127	-10	3
23	15	7	128	-30	-13
24	31	-12	131	-55	36
25	127	-83	132	-50	-4
26	87	-50	133	-52	81
27	-38	13	134	-90	-2
28	-41	-86	549	60	
29	-200	81	550	384	
30	-120	-40	551	225	
31	-19	-3	552	-71	
32	-48	-101	553	275	
33	-138	89	554	-128	
34	-169	103	555	188	
35	-57	63	556	-128	
36	-89	57	557	-562	
37	-21	26	558	-92	
38	-58	22	559	-310	
39	-38	41	560	53	
40	-41	-4	561	-291	
41	-7	-12	562	56	
42	-2	-8	563	-250	
43	-16	7	564	78	

Table A.15. Strain at Each Gage Position Caused by a Normal Load of 30 lb on Nozzle J_2 at a Distance of 34 3/4 in. from the Apex of the Dome

Gage Position	Strain (μin./in.)		Gage Position	Strain (μin./in.)	
	Outer Surface	Inner Surface		Outer Surface	Inner Surface
25	10	-8	136	-14	-3
26	13	-1	137	2	-1
27	12	-12	138	-12	6
28	11	-11	139	-4	-3
29	40	-1	140	-12	2
30	13	-16	141	-16	12
31	-8	5	142	1	9
32	0	-16	161	0	-22
33	30	-28	162	-23	24
34	-9	15	163	-4	0
35	-18	-6	164	-3	-14
36	-9	1	165	-31	18
37	-39	47	166	-12	-4
38	-11	-5	167	-10	53
39	-24	41	168	-30	-18
40	-49	12	565	432	
41	-25	14	566	51	
42	-8	7	567	277	
43	0	-2	568	-149	
44	-8	10	569	339	
45	-13	6	570	-160	
46	-6	-6	571	364	
125	69	-63	572	-162	
126	84	-59	573	-544	
127	-42	30	574	-27	
128	-36	-89	575	-360	
131	-31	78	576	87	
132	-87	1	577	-321	
133	42	-48	578	75	
134	42	-79	579	-323	
135	-12	12	580	48	

Table A.16. Strain at Each Gage Position Caused by a Normal Load of 80 lb on Nozzle J_2 at a Distance of 13 3/16 in. from the Apex of the Dome

Gage Position	Strain (μin./in.)		Gage Position	Strain (μin./in.)	
	Outer Surface	Inner Surface		Outer Surface	Inner Surface
25	16	-6	136	-24	1
26	16	-2	137	-1	-1
27	21	-14	138	-14	7
28	21	-12	139	-8	-2
29	52	-1	140	-20	8
30	19	-23	141	-24	24
31	-4	5	142	1	9
32	2	-15	161	-2	-23
33	41	-35	162	-30	29
34	-3	16	163	-7	0
35	-15	-15	164	-4	-17
36	-9	1	165	-40	19
37	-43	48	166	-18	-7
38	-18	-8	167	-17	64
39	-26	50	168	-42	-14
40	-55	11	565	571	
41	-39	18	566	65	
42	-14	2	567	368	
43	0	-5	568	-188	
44	-12	11	569	429	
45	-22	5	570	-199	
46	-10	-9	571	444	
125	82	-64	572	-188	
126	99	-51	573	-686	
127	-64	53	574	-50	
128	-56	-78	575	-441	
131	-52	81	576	107	
132	-97	-19	577	-381	
133	56	-66	578	97	
134	63	-78	579	-360	
135	-13	14	580	66	

Table A.17. Strain at Each Gage Position Caused by a Normal Load of 30 lb on Nozzle L_4 at a Distance of 34 3/4 in. from the Apex of the Dome

Gage Position	Strain (μin./in.)		Gage Position	Strain (μin./in.)	
	Outer Surface	Inner Surface		Outer Surface	Inner Surface
161	-37	74	261	-18	9
162	-32	-1	262	-10	-19
163	-22	14	597	339	
164	-20	13	598	28	
165	-2	1	599	290	
166	-12	-3	600	-120	
167	-17	10	601	351	
168	-18	22	602	-151	
215	91	-35	603	378	
216	68	-44	604	-150	
217	-58	24	605	-674	
218	-18	-81	606	-12	
221	-8	-30	607	-365	
222	9	-82	608	82	
257	7	-24	609	-342	
258	1	7	610	85	
259	-3	-5	611	-325	
260	-7	-6	612	78	

Table A.18. Strain at Each Gage Position Caused by a Normal Load of 80 lb on Nozzle L_4 at a Distance of 13 3/16 in. from the Apex of the Dome

Gage Position	Strain (μin./in.)		Gage Position	Strain (μin./in.)	
	Outer Surface	Inner Surface		Outer Surface	Inner Surface
161	-51	85	260	-11	-10
162	-40	-3	261	-27	10
163	-28	16	262	-12	-20
164	-27	13	597	423	
165	-6	-1	598	32	
166	-13	-4	599	356	
167	-22	12	600	-152	
168	-25	26	601	419	
215	112	-40	602	-181	
216	81	-50	603	440	
217	-82	28	604	-168	
218	-27	-91	605	-822	
219	-24	58	606	-26	
220	-93	29	607	-431	
221	-8	-31	608	92	
222	12	-92	609	-394	
257	6	-22	610	84	
258	1	4	611	-351	
259	-3	-5	612	61	

Table A.19. Strain at Each Gage Position Caused by a Normal Load of 75 lb on Nozzle K_2 at a Distance of 24 9/16 in. from the Apex of the Dome

Gage Position	Strain (μin./in.) Outer Surface	Strain (μin./in.) Inner Surface	Gage Position	Strain (μin./in.) Outer Surface	Strain (μin./in.) Inner Surface
161	-20	5	261	-142	88
162	-6	-17	262	-96	-30
163	-26	8	267	-13	22
164	-25	18	268	-45	11
165	-13	-4	269	-39	34
166	-5	-16	270	-18	-20
167	3	-9	271	1	-8
168	-7	13	272	-8	-10
169	-17	13	273	-30	11
170	-7	-13	274	-7	-6
171	-7	-2	275	-23	2
172	-22	2	276	-27	23
173	-15	2	305	15	-47
174	-10	-5	306	-2	20
177	7	-7	307	-2	-4
178	-1	0	308	-22	2
179	-8	4	309	-42	24
180	-4	-15	310	-12	-3
215	17	-24	311	11	17
216	3	30	312	-10	-19
217	20	20	613	278	
218	-5	-34	614	49	
221	-6	-15	615	180	
222	-8	-21	616	-70	
223	-43	49	617	227	
224	-87	56	618	-93	
227	-14	11	619	221	
228	-32	6	620	-103	
229	-22	20	621	-431	
230	-37	35	622	-49	
257	173	-62	623	-235	
258	84	-52	624	57	
259	-29	14	627	-220	
260	-27	-69	628	56	

Table A.20. Strain at Each Gage Position Caused by Axial Loads of 1500 lb Applied Simultaneously to Four Small Experimental Loop Nozzles

Gage Position	Strain (μin./in.)		Gage Position	Strain (μin./in.)	
	Outer Surface	Inner Surface		Outer Surface	Inner Surface
41	38	-85	88	-12	-130
42	26	-77	135	25	-51
43	-9	-10	136	13	53
44	-8	-128	137	-33	0
45	115	-118	138	-32	-106
46	22	30	139	-3	-135
47	69	-122	140	-55	65
48	-42	29	141	11	-49
49	-4	-94	142	-260	-32
50	-73	11	143	-64	-67
53	-199	35	144	-161	65
54	-250	7	145	-285	153
55	-269	95	146	-329	150
56	-162	-23	147	-200	158
57	-229	129	148	-306	58
58	-176	-23	149	-161	99
59	-219	106	150	-307	41
60	-225	-26	153	-308	131
65	-184	85	154	-325	62
66	-269	-3	155	-282	80
67	-248	136	156	-311	136
68	-166	-48	157	-218	111
69	-185	93	158	-315	69
70	-273	-23	159	-223	123
71	-223	116	160	-16	57
72	-234	-32	161	46	-63
73	-241	146	162	66	54
74	-177	-23	163	-2	-15
75	-256	108	164	-11	-101
76	-179	-16	165	90	-72
77	-110	50	166	32	41
78	-262	18	167	14	-62
79	-180	71	168	-34	-79
80	-135	-138	169	53	-66
81	-12	-101	170	-6	-41
82	-69	24	171	75	-111
83	61	-145	172	20	46
84	-37	49	173	9	-72
85	88	-111	174	-68	37
86	15	42	177	-52	-51
87	-10	-20	178	-197	100

Table A.20 (continued)

Gage Position	Strain (μin./in.) Outer Surface	Strain (μin./in.) Inner Surface	Gage Position	Strain (μin./in.) Outer Surface	Strain (μin./in.) Inner Surface
179	-65	43	237	8	-50
180	-90	-135	238	-52	13
181	-116	51	239	-7	0
182	-136	-129	240	40	-87
183	-10	-90	241	10	-5
184	-65	1	242	5	-120
185	-70	15	243	34	-66
186	-69	-105	244	41	23
191	-131	38	245	4	-17
192	-230	-15	246	29	-112
193	-161	82	247	86	-89
194	-57	-79	248	21	26
195	-96	29	533	1	
196	-93	-134	534	-109	
197	66	-101	535	70	
198	17	44	536	6	
199	8	-21	537	6	
200	-66	-34	538	8	
201	-160	37	541	48	
202	-96	-60	542	-184	
203	-68	-40	543	42	
204	-208	86	544	8	
205	74	-89	545	3	
206	32	-20	546	8	
207	1	-22	547	2	
208	16	-105	548	2	
209	5	-46	581	-460	
210	-11	-52	582	-128	
211	38	-43	583	-354	
212	64	26	584	106	
223	43	-44	585	-394	
224	43	21	586	147	
227	90	-82	587	-392	
228	-77	43	588	119	
229	8	-9	589	-59	
230	1	-128	590	-120	
231	16	13	591	61	
232	-10	-95	592	12	
233	25	-90	593	3	
234	12	-30	594	19	
235	-29	-27	595	-21	
236	-6	-160	596	14	

Table A.21. Strain at Each Gage Position Caused by an Axial Load of 5000 lb on Gas Outlet

Gage Position	Strain (μin./in.) Outer Surface	Strain (μin./in.) Inner Surface	Gage Position	Strain (μin./in.) Outer Surface	Strain (μin./in.) Inner Surface
91	-6	2	508	25	
92	9	10	509	-235	
93	0	1	510	-128	
94	16	29	511	-23	
95	4	5	512	-80	
96	-20	-25	513	10	
97	0	2	514	-12	
98	-19	-22	515	-28	
99	-3	-24	516	20	
100	27	34	517	-373	
101	-7	-53	518	-109	
102	28	40	519	-82	
103	9	-97	520	-103	
104	16	49	521	-9	
105	7	-98	522	-28	
106	-46	41	523	-43	
107	-164	118	524	24	
108	-120	-17	525	-331	
109	-150	-19	526	-94	
110	-248	172	527	-60	
111	-96	22	528	-100	
112	-42	-59	529	-8	
113	-37	42	530	-13	
114	10	-116	531	-40	
115	-95	82	532	28	
116	-137	-9	865		220
117	-4	-103	866		-144
118	-107	63	867		26
119	-142	-24	868		-112
120	-225	142	869		-78
121	-89	26	870		-32
122	-35	-64	871		-70
123	-34	42	872		16
124	12	-112	873		-78
501	-273		874		18
502	-129		875		-72
503	-28		876		-16
504	-88		877		4
505	15		878		-88
506	-15		879		216
507	-29		880		-136

Table A.21 (continued)

Gage Position	Strain (μin./in.) Outer Surface	Strain (μin./in.) Inner Surface	Gage Position	Strain (μin./in.) Outer Surface	Strain (μin./in.) Inner Surface
881		278	898		-2
882		-162	899		-42
883		70	900		36
884		-118	901	28	
887		-114	902	-30	
888		36	903	60	
889		-88	904	-4	
890		-146	905		-82
891		-82	906		-10
892		0	907		-56
893		40	908		16
894		-94	909	20	
895		236	910	10	
896		40	911	82	
897		-60	912	-8	

Table A.22. Strain at Each Gage Position Caused by a Normal Load of 2000 lb on Gas Outlet in Transverse Plane at a Distance of 8 1/2 in. from Dome Surface

Gage Position	Strain (μin./in.)		Gage Position	Strain (μin./in.)	
	Outer Surface	Inner Surface		Outer Surface	Inner Surface
91	-1	0	501	-18	
92	-3	0	502	10	
93	0	0	503	-7	
94	-7	-5	504	8	
95	-1	-3	505	-5	
96	5	4	506	5	
97	2	4	507	-6	
98	-5	0	508	-6	
99	1	-1	509	19	
100	2	3	510	-1	
103	-2	-9	511	0	
104	-1	0	512	1	
105	-2	-9	513	-1	
106	4	10	514	2	
107	2	-21	515	-2	
108	24	10	516	10	
109	181	-9	517	588	
110	372	-327	518	124	
111	144	-18	519	174	
112	98	-10	520	131	
113	76	-17	521	49	
114	7	79	522	32	
115	4	2	523	70	
116	-1	-7	524	-40	
117	1	20	525	-492	
118	2	-20	526	-105	
119	-164	13	527	-131	
120	-341	300	528	-118	
121	-141	16	529	-41	
122	-90	21	530	-20	
123	-75	16	531	-67	
124	-8	-60	532	31	

Table A.23. Strain at Each Gage Position Caused by a Normal Load of 2000 lb on Gas Outlet in Axial Plane at a Distance of 8 1/2 in. from Dome Surface

Gage Position	Strain (μin./in.)		Gage Position	Strain (μin./in.)	
	Outer Surface	Inner Surface		Outer Surface	Inner Surface
91	0	0	501	-444	
92	-7	-2	502	-141	
93	-1	-2	503	-101	
94	-11	-14	504	-107	
95	-5	3	505	-20	
96	10	18	506	-22	
97	-1	-4	507	-51	
98	7	16	508	27	
99	-1	25	509	476	
100	-22	-19	510	178	
103	-21	79	511	129	
104	11	-26	512	114	
105	18	47	513	48	
106	97	-21	514	11	
107	340	-296	515	72	
108	180	-4	516	-41	
109	-4	-32	517	-57	
110	-26	3	518	-20	
111	-3	-33	519	-20	
112	0	15	520	-12	
113	-2	-19	521	-16	
114	5	8	522	1	
115	-191	200	523	-10	
116	-168	16	524	11	
117	-38	-41	525	-58	
118	-150	55	526	-18	
119	-19	-13	527	-20	
120	-29	1	528	-16	
121	-2	-7	529	-12	
122	-2	3	530	3	
123	-1	-2	531	-11	
124	2	-10	532	5	

Table A.24. Strain at Each Gage Position Caused by a Pure Moment of 19 200 in.-lb on Gas Outlet in Transverse Plane

Gage Position	Strain (μin./in.) Outer Surface	Strain (μin./in.) Inner Surface	Gage Position	Strain (μin./in.) Outer Surface	Strain (μin./in.) Inner Surface
91	2	0	501	-18	
92	-1	-1	502	13	
93	2	0	503	1	
94	-2	-4	504	3	
95	0	0	505	0	
96	6	0	506	-2	
97	2	-5	507	0	
98	-8	-5	508	-6	
99	1	-5	509	-2	
100	2	10	510	-14	
101	2	-10	511	-2	
102	-4	3	512	-14	
103	1	-13	513	-1	
104	0	3	514	1	
105	-1	27	515	-6	
106	1	4	516	4	
107	-9	-21	517	501	
108	10	3	518	110	
109	165	-16	519	161	
110	338	-311	520	110	
111	142	-18	521	63	
112	89	-33	522	23	
113	79	-19	523	93	
114	1	47	524	-36	
115	2	-6	525	-496	
116	0	-23	526	-102	
117	-1	2	527	-141	
118	8	-30	528	-116	
119	-170	8	529	-61	
120	-346	297	530	-12	
121	-150	6	531	-102	
122	-86	-3	532	36	
123	-87	-1			
124	-2	12			

Table A.25. Strain at Each Gage Position Caused by a Pure Moment of 19 200 in.-lb on Gas Outlet in Axial Plane

Gage Position	Strain (μin./in.) Outer Surface	Strain (μin./in.) Inner Surface	Gage Position	Strain (μin./in.) Outer Surface	Strain (μin./in.) Inner Surface
91	0	1	502	148	
92	9	6	503	118	
93	2	0	504	108	
94	11	14	505	46	
95	5	-1	506	11	
96	-8	-15	507	97	
97	4	0	508	-41	
98	-4	-14	509	-466	
99	7	-30	510	-170	
100	21	19	511	-135	
101	9	-52	512	-110	
102	12	23	513	-62	
103	24	-80	514	-6	
104	-16	25	515	-107	
105	-10	-40	516	45	
106	-106	21	517	47	
107	665	335	518	22	
108	-184	13	519	16	
109	0	38	520	15	
110	21	-1	521	6	
111	-2	36	522	3	
112	0	-18	523	15	
113	1	16	524	-10	
114	-6	-5	525	49	
115	196	-234	526	13	
116	188	-13	527	15	
117	35	32	528	22	
118	168	-53	529	11	
119	7	16	530	-1	
120	30	1	531	16	
501	466		532	-10	

Table A.26. Strain at Each Gage Position Caused by a Torsional Load of 32 000 in.-lb on Gas Outlet

Gage Position	Strain (μin./in.)		Gage Position	Strain (μin./in.)	
	Outer Surface	Inner Surface		Outer Surface	Inner Surface
91	1	1	501	7	
92	-1	-2	502	-13	
93	0	1	503	-9	
94	-2	-2	504	4	
95	-1	0	505	-5	
96	1	0	506	9	
97	1	2	507	-4	
98	-2	-2	508	-8	
99	-1	0	509	25	
100	1	-1	510	10	
101	0	0	511	6	
102	0	3	512	-15	
103	-1	0	513	10	
104	0	2	514	9	
105	2	-1	515	10	
106	-2	3	516	-10	
107	13	-8	517	4	
108	-13	1	518	10	
109	16	6	519	-8	
110	10	-14	520	2	
111	3	-2	521	-16	
112	1	-1	522	4	
113	2	-4	523	9	
114	4	5	524	-1	
115	1	-2	525	8	
116	-10	4	526	13	
117	0	-1	527	15	
118	-5	6	528	-9	
119	15	-2	529	7	
120	-22	-1	530	7	
121	-3	5	531	-2	
122	1	-2	532	16	
123	0	6			
124	-1	-5			

Table A.27. Stress at Each Gage Position Caused by an Internal Pressure Loading of 60 psig

Gage Position	Stress (psi)							
	Outer Surface		Inner Surface		Membrane		Bending	
	σ_θ^T	σ_ϕ^T	σ_θ^T	σ_ϕ^T	σ_θ^m	σ_ϕ^m	σ_θ^b	σ_ϕ^b
1-2	1635	51	1710	1533	1672	792	-37	-741
3-4	1624	147	1586	1086	1605	616	19	-469
5-6	1571	1971	84	845	827	1408	744	563
7-8	655	1216	988	1126	821	1171	-166	45
9-10	546	854	1174	1112	860	983	-314	-129
11-12	1513	2044	341	1202	927	1623	586	421
13-14	636	1221	1080	1170	858	1195	-222	26
15-16	520	866	1120	1066	820	966	-300	-100
17-18	1792	1208	1062	238	1427	723	365	485
19-20	1009	663	962	1038	985	850	24	-187
21-22	735	651	814	1014	774	832	-39	-181
23-24	725	618	835	1051	780	834	-55	-216
25-26	1488	1126	304	881	896	1003	592	123
27-28	1304	901	884	445	1094	713	210	268
29-30	1525	718	1360	1068	1442	893	83	-175
31-32	1413	744	1056	587	1234	665	179	79
33-34	1155	816	1435	1351	1295	1083	-140	-267
35-36	1008	692	1137	1091	1072	891	-64	-199
37-38	1542	1073	1143	1243	1342	1158	200	-85
39-40	1784	1145	1247	824	1515	984	269	161
41-42	1357	857	1991	1337	1674	1097	-317	-240
43-44	1318	525	1587	1156	1452	840	-134	-315
45-46	1244	713	1946	1754	1595	1233	-351	-520
47-48	1141	602	1457	1257	1299	929	-158	-327
49-50	1777	1123	1424	1247	1600	1185	177	-62
51-52	2090	1467	1534	1280	1812	1373	278	94
53-54	2080	1250	1754	946	1917	1098	163	152
55-56	1973	1642	1592	908	1782	1275	191	367
57-58	1757	1357	1112	774	1434	1065	323	292
59-60	2151	1535	1400	800	1775	1167	376	368
61-62	2331	1469	1537	591	1934	1030	397	439
63-64								
65-66	2301	1470	1520	566	1910	1018	391	452
67-68	2081	1604	1520	1066	1800	1335	281	269
69-70	2253	1476	1554	846	1903	1161	350	315
71-72	2245	1584	1449	865	1847	1224	398	360
73-74	1753	1376	1101	770	1427	1073	326	303
75-76	2062	1538	1631	869	1846	1203	216	335
77-78	2196	1019	1610	733	1903	876	293	143

Table A.27 (Continued)

Gage Position	Stress (psi)							
	Outer Surface		Inner Surface		Membrane		Bending	
	σ_θ^T	σ_ϕ^T	σ_θ^T	σ_ϕ^T	σ_θ^m	σ_ϕ^m	σ_θ^b	σ_ϕ^b
79-80	2027	1458	1842	1073	1934	1265	93	193
81-82	1836	1221	1545	1284	1690	1252	146	-31
83-84	645	284	1392	1308	1018	796	-373	-512
85-86	1210	833	1820	1466	1515	1149	-305	-316
87-88	1368	460	1590	1067	1479	763	-111	-303
89-90	1236	821	1301	1270	1268	1045	-32	-224
91-92	835	551	1241	1202	1038	876	-203	-325
93-94	893	578	1736	1721	1314	1149	-421	-571
95-96	1335	551	1071	571	1203	561	132	-10
97-98	1155	516	1032	540	1093	528	62	-12
99-100	1395	1148	1110	1133	1252	1140	143	8
101-102	771	671	822	1107	796	889	-25	-218
103-104	727	658	818	1125	772	891	-45	-233
105-106	1107	722	908	992	1007	857	100	-135
107-108	1748	1095	1216	355	1482	725	266	370
109-110	1470	2001	291	1237	880	1619	590	382
111-112	644	1213	965	1149	804	1181	-160	32
113-114	546	854	1182	1075	864	964	-318	-110
115-116	1560	68	1820	1266	1690	667	-130	-599
117-118	1574	12	1864	1579	1719	795	-145	-783
119-120	1535	2051	281	1304	908	1677	627	374
121-122	634	1180	989	1197	811	1188	-177	-8
123-124	495	848	1130	1099	812	973	-317	-125
125-126	1777	1023	1092	1308	1434	1165	343	-142
127-128	1690	867	1384	945	1537	906	153	-39
129-130								
131-132	1515	785	1624	1247	1569	1016	-54	-231
133-134	1631	769	1337	1091	1484	930	147	-161
135-136	1900	900	1438	762	1669	831	231	69
137-138	1638	862	1923	1077	1780	969	-142	-107
139-140	1949	965	1195	1448	1572	1206	377	-241
141-142	2119	1196	1777	1123	1948	1159	171	37
143-144	1126	1388	934	1280	1030	1334	96	54
145-146	2097	1389	1724	1347	1910	1368	187	21
147-148	2004	1281	1938	962	1971	1121	33	160
149-150	2284	1445	1669	931	1976	1188	308	257
151-152	2113	1444	1774	912	1943	1178	170	266
153-154	2449	1865	1720	766	2084	1315	365	550
155-156	2164	1479	1434	680	1799	1079	365	400
157-158	2026	1288	1738	762	1882	1025	144	263

Table A.27 (Continued)

Gage Position	Stress (psi)							
	Outer Surface		Inner Surface		Membrane		Bending	
	σ_θ^T	σ_ϕ^T	σ_θ^T	σ_ϕ^T	σ_θ^m	σ_ϕ^m	σ_θ^b	σ_ϕ^b
159-160	1735	1351	1710	1033	1722	1192	13	159
161-162	1782	1375	1008	892	1395	1133	387	242
163-164	1966	1120	1652	1005	1809	1062	157	58
165-166	1567	890	1747	1524	1657	1207	-90	-317
167-168	2082	1475	1466	920	1774	1197	308	278
169-170	1297	889	1321	1136	1309	1012	-12	-123
171-172	2005	1352	1479	1164	1742	1258	263	94
173-174	1875	1682	1526	1088	1700	1385	175	297
175-176								
177-178	2111	1103	1755	1316	1933	1209	178	-106
179-180	1674	912	2244	1113	1959	1012	-285	-100
181-182	2067	1490	1789	1197	1928	1343	139	147
183-184	2097	1489	1546	1254	1821	1371	276	118
185-186	2057	1457	1704	981	1880	1219	177	238
187-188								
189-190	3144	4413	1545	1184	2344	2798	800	1615
191-192	2180	1334	1827	858	2003	1096	177	238
193-194	1551	1235	1282	875	1416	1055	135	180
195-196	1958	1427	1987	956	1972	1191	-14	236
197-198	1921	1436	1297	889	1609	1162	312	274
199-200	1953	1676	1464	879	1708	1277	245	399
201-202	1908	1392	1667	990	1787	1191	121	201
203-204	2158	1227	1746	1054	1952	1140	206	87
205-206	1298	859	1916	1455	1607	1157	-309	-298
207-208	1597	1089	2151	1135	1874	1112	-277	-23
209-210	1976	1753	1184	945	1580	1349	396	404
211-212	1849	1265	1309	1063	1579	1164	270	101
213-214								
215-216	1725	1318	912	874	1318	1096	407	222
217-218	1763	909	1289	497	1526	703	237	206
219-220	1449	565	1140	832	1294	698	155	-133
221-222	1630	899	1211	703	1420	801	210	98
223-224	1908	1392	1068	660	1488	1026	420	366
225-226								
227-228	1557	757	1788	1426	1672	1091	-115	-334
229-230	2073	1042	1468	760	1770	901	303	141
231-232	1522	207	1926	788	1724	497	-202	-290
233-234	1632	1240	1510	1033	1571	1136	61	104
235-236	786	786	2215	1085	1500	935	-714	-149
237-238	2031	869	1440	1132	1735	1000	296	-131

Table A.27 (Continued)

Gage Position	Stress (psi)							
	Outer Surface		Inner Surface		Membrane		Bending	
	σ_θ^T	σ_ϕ^T	σ_θ^T	σ_ϕ^T	σ_θ^m	σ_ϕ^m	σ_θ^b	σ_ϕ^b
239-240	543	1246	1233	1240	888	1243	355	3
241-242	2078	1493	1532	640	1805	1066	273	427
243-244	1780	1134	1260	1068	1520	1101	260	33
245-246	1466	820	2037	991	1751	905	-285	-85
247-248	1633	810	1781	1404	1707	1107	-74	-297
249-250	1874	1012	990	467	1432	739	442	273
251-252	1699	1230	1289	1097	1494	1163	205	67
253-254	1378	793	1535	951	1456	872	-78	-79
255-256	1211	503	1421	1036	1316	769	-105	-266
257-258	1732	1540	1015	985	1373	1262	359	278
259-260	1844	1013	1546	654	1695	833	149	180
261-262	1647	1324	1544	1213	1595	1268	52	56
263-264	1582	1175	1736	1121	1659	1148	-77	27
265-266								
267-268	1885	1315	1440	1132	1662	1223	223	92
269-270	1589	1097	1390	1367	1489	1232	100	-135
271-272	1547	724	1527	1258	1537	991	10	-267
273-274	1345	884	1877	1323	1611	1103	-266	-219
275-276	1630	899	2012	1374	1821	1136	-191	-237
277-278	1621	736	1549	1165	1585	950	36	-214
279-280	1710	1233	1432	1440	1571	1336	139	-103
281-282								
283-284	1377	723	2142	1273	1759	998	-382	-275
285-286								
287-288	2030	1199	1586	986	1808	1092	222	107
289-290	1887	1756	921	1036	1404	1396	483	360
291-292	1996	1019	1856	1187	1926	1103	70	-84
293-294	1640	732	1790	1667	1715	1199	-75	-467
295-296	1966	1120	1458	727	1712	923	254	197
297-298	1767	1590	915	985	1341	1287	426	303
299-300	1799	830	1118	525	1458	677	341	153
301-302	1535	1151	1059	898	1297	1024	238	127
303-304	1217	725	1636	1390	1426	1057	-209	-332
305-306	1137	991	1125	1318	1131	1154	6	-163
307-308	1022	507	1510	733	1266	620	-244	-113
309-310	1004	481	1778	1193	1391	837	-387	-356
311-312	1490	667	1284	645	1387	656	103	11
313-314	1652	805	1247	1024	1449	914	203	-109
315-316	826	-1212	1021	1236	923	12	-97	-1224
317-318	1843	943	1568	960	1705	951	138	-8

Table A.27 (Continued)

Gage Position	Stress (psi)							
	Outer Surface		Inner Surface		Membrane		Bending	
	σ_θ^T	σ_ϕ^T	σ_θ^T	σ_ϕ^T	σ_θ^m	σ_ϕ^m	σ_θ^b	σ_ϕ^b
319-320	936	1121	1746	1454	1341	1287	-405	-166
321-322	1496	719	1344	713	1420	716	76	3
323-324	1451	835	1365	749	1408	792	43	43
325-326	1611	1203	1131	1369	1371	1286	240	-83
327-328	1665	779	1660	1282	1662	1030	3	-251
329-330	1386	786	1275	1082	1330	934	56	-148
331-332	1484	845	1076	553	1280	699	204	146
333-334	1604	1281	998	1159	1301	1220	303	61
335-336	1296	919	930	499	1113	709	183	210
337-338	1495	748	1412	1074	1453	911	42	-163
339-340	1077	823	1765	1249	1421	1030	-344	-213
341-342	-1079	-1364	610	4833	-234	1734	-845	-3098
343-344	1893	2278	1360	168	1626	1223	267	1055
345-346	4353	7276	2538	562	3445	3919	908	3357
347-348	2615	1285	2749	1165	2682	1225	-67	60
349-350	2493	1178	2743	1343	2618	1260	-125	-82
351-352	2468	1160	2696	1319	2582	1239	-114	-79
353-354	2360	1168	2685	1215	2522	1191	-162	-23
355-356	2553	1576	2538	862	2545	1219	8	357
357-358	2082	1775	1941	702	2011	1238	71	537
359-360	1231	169	1718	1625	1474	897	-243	-728
361-362	659	98	1285	1715	972	906	-313	-808
363-364	619	396	958	1427	788	911	-169	-515
365-366	841	502	862	1038	851	770	-10	-268
367-368	1549	865	1129	429	1339	647	210	218
369-370	1765	1049	954	146	1359	597	406	452
371-372	978	593	931	1169	954	881	24	-288
373-374	715	485	434	1080	574	782	141	-297
375-376	755	516	967	1290	861	903	-106	-387
377-378	1010	633	835	1051	922	842	88	-209
379-380	1666	920	978	293	1322	606	344	314
381-382	1505	752	1055	416	1280	584	225	168
383-384	897	689	881	1004	889	846	8	-157
385-386	648	395	954	1346	801	870	-153	-475
387-388	708	92	1249	1665	978	878	-270	-786
389-390	1266	120	1816	1655	1541	887	-275	-767
391-392	1981	1704	1911	703	1946	1203	35	501
393-394	2408	1492	2534	880	2471	1186	-63	306
395-396	2402	1141	2692	1208	2547	1174	-145	-33
397-398	2308	1092	2627	1258	2467	1175	-159	-83

Table A.27 (Continued)

Gage Position	Stress (psi)							
	Outer Surface		Inner Surface		Membrane		Bending	
	σ_θ^T	σ_ϕ^T	σ_θ^T	σ_ϕ^T	σ_θ^m	σ_ϕ^m	σ_θ^b	σ_ϕ^b
399-400	2340	1032	2685	1315	2512	1173	-172	-141
401-402	2414	1114	2956	1187	2685	1150	-271	-36
403-404	2510	1633	2502	541	2506	1087	4	546
405-406	1809	2063	1114	14	1461	1038	348	1025
407-408	-1037	-1491	376	4253	-330	1381	-707	-2872
409-411	844	913	867	890	855	901	-11	12
412-414	815	885	868	890	841	887	-26	-2
417-418			-1111	1497				
419-420			-1034	1320				
421-422			-1032	1660				
423-424			-1115	1615				
501-502	1754	1246						
503-504	945	-116						
505-506	384	-255						
507-508	348	-5						
509-510	1946	1554						
511-512	1024	47						
513-514	512	-326						
515-516	274	-88						
517-518	1700	2100						
519-520	1132	340						
521-522	542	-127						
523-524	316	55						
525-526	1322	1907						
527-528	1177	223						
529-530	470	-199						
531-532	312	74						
533-534	1357	116						
535-536	-327	-358						
537-538	241	102						
539-540	297	189						
541-542	1385	15						
543-544	109	-237						
545-546	230	99						
547-548	242	73						
549-550	995	1248						
551-552	49	-235						
553-554	266	220						
555-556	367	290						
557-558	745	384						

Table A.27 (Continued)

Gage Position	Stress (psi)							
	Outer Surface		Inner Surface		Membrane		Bending	
	σ_θ^T	σ_ϕ^T	σ_θ^T	σ_ϕ^T	σ_θ^m	σ_ϕ^m	σ_θ^b	σ_ϕ^b
559-560	280	134						
561-562	385	215						
563-564	321	136						
565-566	1299	230						
567-568	279	164						
569-570	360	200						
571-572	302	141						
573-574	631	169						
575-576	282	175						
577-578	287	156						
579-580	284	145						
581-582	696	-81						
583-584	-74	-12						
585-586	196	119						
587-588	260	168						
589-590	615	-416						
591-592	-391	-337						
593-594	127	-342						
595-596	270	101						
597-598	899	230						
599-600	71	-29						
601-602	321	236						
603-604	230	99						
605-606	670	401						
607-608	276	153						
609-610	276	153						
611-612	259	98						
613-614	1204	681						
615-616	91	-263						
617-618	301	170						
619-620	270	101						
621-622	685	215						
623-624	270	1						
625-626								
627-628	249	65						
629-630	1177	1223						
631-632	649	-135						
633-634	281	-96						
635-636	327	158						
637-638	1897	1489						
639-640	740	-168						

Table A.27 (Continued)

Gage Position	Stress (psi)							
	Outer Surface		Inner Surface		Membrane		Bending	
	σ_θ^T	σ_ϕ^T	σ_θ^T	σ_ϕ^T	σ_θ^m	σ_ϕ^m	σ_θ^b	σ_ϕ^b
641-642	329	-171						
643-644	171	71						
865-866			1502	-901				
867-868			1359	257				
869-870			880	664				
871-872			592	438				
873-874			523	407				
875-876			798	590				
877-878			1271	231				
879-880			1247	-1348				
881-882			1333	-1562				
883-884			1282	-166				
887-888			408	493				
889-890			1999	990				
891-892			740	633				
893-894			1254	46				
895-896			-292	-1939				
897-898			1005	-1220				
899-900			748	-176				
901-902	1455	447						
903-904	1016	886						
905-906			1029	-442				
907-908			633	40				
909-910	480	64						
911-912	1133	539						

Table A.28. Stress at Each Gage Position Caused by an Axial Load of 2000 lb Downward on Nozzle A

Gage Position	Stress (psi)							
	Outer Surface		Inner Surface		Membrane		Bending	
	σ_θ^T	σ_ϕ^T	σ_θ^T	σ_ϕ^T	σ_θ^m	σ_ϕ^m	σ_θ^b	σ_ϕ^b
51-52	-129	-129	-429	-929	-279	-529	150	400
53-54	-971	-1071	-451	165	-711	-453	-260	-618
55-56	-1396	-819	440	-68	-478	-443	-918	-376
57-58	-1967	-1390	1010	533	-478	-428	-1489	-962
59-60	-2944	-2713	1696	2019	-624	-347	-2320	-2366
61-62	-2962	-2638	1703	2011	-629	-313	-2333	-2325
63-64	-2942	-2973	1667	1890	-637	-541	-2305	-2432
65-66	-2751	-2535	1400	1600	-675	-467	-2076	-2068
67-68	-2555	-2716	1651	2235	-452	-240	-2103	-2476
69-70	-2853	-2776	1664	2179	-594	-298	-2259	-2478
71-72	-2712	-2574	1368	1560	-672	-507	-2040	-2067
73-74	-1781	-1304	835	351	-473	-476	-1308	-828
75-76	-1201	-670	396	-81	-402	-375	-799	-295
77-78	-895	-748	-11	297	-453	-225	-442	-523
79-80	-441	-702	-849	-65	-645	-383	204	-319
81-82	-31	231	44	-487	6	-128	-37	359
83-84	16	355	-9	-563	3	-104	13	459
143-144	-412	-174	-71	-371	-241	-272	-171	98
145-146	-804	-381	124	-253	-340	-317	-464	-64
147-148	-702	-1041	-626	412	-664	-314	-38	-727
149-150	-2487	-1556	1182	775	-652	-390	-1835	-1166
153-154	-1047	-1424	-675	318	-861	-553	-186	-871
155-156	-691	-337	155	-84	-268	-210	-423	-127
157-158	-819	-996	-820	234	-819	-381		-615
159-160	-260	-968	1007	622	373	-173	-633	-795
181-182	-448	-695	-857	-57	-652	-376	204	-319
183-184	-23	223	-33	-510	-28	-143	5	366
185-186	-68	40	-564	-79	-316	-19	248	59
189-190	-1312	-374	436	-79	-438	-226	-874	-148
191-192	-1036	-1121	-100	300	-568	-410	-468	-711
533-534	-1688	-2526						
535-536	131	-731						
537-538	333	-390						
541-542	-1911	-1603						
543-544	245	-416						
545-546	130	-1001						
547-548	55	-984						

Table A.29. Stress at Each Gage Position Caused by an Axial Load of 1500 lb Downward on Nozzle B_2

Gage Position	Stress (psi)							
	Outer Surface		Inner Surface		Membrane		Bending	
	σ_θ^T	σ_ϕ^T	σ_θ^T	σ_ϕ^T	σ_θ^m	σ_ϕ^m	σ_θ^b	σ_ϕ^b
47-48	-153	124	-133	-510	-143	-193	-10	317
49-50	-245	-184	-309	-463	-277	-323	32	139
51-52	-698	-1059	-419	-196	-558	-627	-140	-432
53-54	-1773	-1242	876	553	-448	-344	-1325	-898
55-56	-1215	-1485	274	812	-470	-336	-745	-1149
57-58	-889	-1397	232	1040	-328	-178	-561	-1219
59-60	-1026	-1388	297	1089	-364	-149	-662	-1239
61-62	-1846	-1354	890	867	-478	-243	-1368	-1111
65-66	-656	-787	-315	215	-485	-286	-171	-501
67-68	-258	-227	-238	-262	-248	-244	-10	17
69-70	-522	-807	-22	193	-272	-307	-250	-500
71-72	-325	-218	-330	-399	-327	-308	2	90
73-74	-218	-25	-49	-265	-133	-145	-85	120
75-76	-173	58	-12	-174	-92	-58	-81	116
77-78	-153	24	68	-240	-42	-108	-111	132
79-80	-157	-257	-437	-91	-297	-174	140	-83
135-136	-51	65	135	-149	42	-42	-93	107
137-138	-452	-405	-190	33	-321	-186	-131	-219
139-140	-615	-585	-102	-341	-358	-463	-257	-122
141-142	-543	-143	89	-203	-227	-173	-316	30
143-144	-1448	-895	710	-67	-369	-481	-1079	-414
145-146	-2791	-2737	1755	2016	-518	-360	-2273	-2377
147-148	-2649	-2265	1849	2465	-400	100	-2249	-2365
149-150	-2792	-2008	1841	2002	-475	-3	-2317	-2005
153-154	-710	-833	79	264	-315	-284	-395	-549
155-156	-289	-97	-352	-305	-320	-201	31	104
157-158	-142	-73	-527	-158	-334	-115	192	42
159-160	-409	-563	-15	215	-212	-174	-197	-389
169-170	-124	153	-226	-388	-175	-117	51	270
171-172	-176	47	-2	-441	-89	-197	-87	244
173-174	-699	-430	87	-244	-306	-337	-393	-93
177-178	-1670	-1201	711	303	-479	-449	-1191	-752
179-180	-798	-659	-186	314	-492	-172	-306	-487
181-182	-1177	-1323	151	835	-513	-244	-664	-1079
183-184	-659	-398	163	-91	-248	-244	-411	-154
185-186	1088	426	47	-276	567	75	521	351
191-192	-1867	-1290	820	466	-523	-412	-1344	-878
193-194	-221	-36	-129	-229	-175	-132	-46	96

Table A.29 (Continued)

Gage Position	Stress (psi)							
	Outer Surface		Inner Surface		Membrane		Bending	
	σ_θ^T	σ_ϕ^T	σ_θ^T	σ_ϕ^T	σ_θ^m	σ_ϕ^m	σ_θ^b	σ_ϕ^b
581-582	-1716	-2655						
583-584	105	-1448						
585-586	237	-1709						
587-588	85	-1885						
589-590	-1769	-3431						
591-592	68	-1240						
593-594	205	-1248						
595-596	13	-1556						

Table A.30. Stress at Each Gage Position Caused by an Axial Load of 2000 lb Downward on Nozzle M_3

Gage Position	Stress (psi)							
	Outer Surface		Inner Surface		Membrane		Bending	
	σ_θ^T	σ_ϕ^T	σ_θ^T	σ_ϕ^T	σ_θ^m	σ_ϕ^m	σ_θ^b	σ_ϕ^b
17-18	162	38	175	-18	168	10	-6	28
19-20	105	-48	141	-198	123	-123	-18	75
21-22	170	101	154	-454	162	-176	8	277
23-24	-253	-76	178	-707	-37	-391	-216	315
25-26	-1963	-2109	798	259	-582	-925	-1381	-1184
27-28	-1926	-1888	484	645	-721	-621	-1205	-1267
29-30	-2585	-2115	741	1002	-922	-556	-1663	-1559
31-32	-1824	-1447	318	-275	-753	-861	-1071	-586
33-34	-1798	-1559	1076	1253	-361	-153	-1437	-1406
35-36	-1168	-560	579	264	-294	-148	-874	-412
37-38	-665	-249	170	-199	-247	-224	-418	-25
39-40	-537	-491	-266	180	-401	-155	-136	-336
41-42	34	80	-233	-377	-94	-148	128	228
43-44	-253	-276	-319	4	-286	-136	33	-140
45-46	64	179	-23	-177	20	1	44	178
125-126	-923	-877	-158	473	-540	-202	-383	-675
127-128	-313	-44	168	-140	-72	-92	-241	48
129-130	-630	-1499	-390	-267	-510	-883	-120	-616
131-132	-732	-640	-208	108	-470	-266	-262	-374
133-134	-1503	-811	637	591	-433	-110	-1070	-701
549-550	-4107	-2222						
551-552	413	-556						
553-554	314	-1286						
555-556	44	-1387						
557-558	-1407	-2222						
559-560	-9	-1163						
561-562	-173	-1442						
563-564	-253	-1676						

Table A.31. Stress at Each Gage Position Caused by an Axial Load of 1500 lb Downward on Nozzle J_2

Gage Position	Stress (psi)							
	Outer Surface		Inner Surface		Membrane		Bending	
	σ_θ^T	σ_ϕ^T	σ_θ^T	σ_ϕ^T	σ_θ^m	σ_ϕ^m	σ_θ^b	σ_ϕ^b
25-26	-303	-211	221	-364	-41	-287	-262	76
27-28	-660	-968	-289	303	-474	-332	-186	-636
29-30	-1327	-758	354	-254	-486	-506	-841	-252
31-32	-400	-200	-398	-259	-399	-229	-1	29
33-34	-869	-1231	-118	75	-493	-578	-376	-653
35-36	-604	-1081	-186	514	-395	-283	-209	-798
37-38	-704	-832	60	768	-340	-32	-400	-800
39-40	-1246	-654	542	473	-352	-90	-894	-564
41-42	-387	-656	-223	23	-305	-316	-82	-340
43-44	-311	-103	163	-91	-74	-97	-237	-6
45-46	-91	-137	-337	-291	-214	-214	123	77
125-126	-2833	-2310	1052	505	-890	-902	-1943	-1408
127-128	-2293	-1578	1148	1295	-572	-141	-1721	-1437
131-132	-2199	-1330	1004	1381	-597	25	-1602	-1355
133-134	-2085	-1615	848	995	-618	-310	-1467	-1305
135-136	-488	-326	19	96	-234	-115	-254	-211
137-138	-145	16	81	-96	-32	-40	-113	56
139-140	-203	-11	138	-338	-32	-174	-171	163
141-142	20	-234	-2	159	9	-37	11	-197
161-162	-788	-926	-190	533	-489	-196	-299	-730
163-164	-147	76	51	-265	-48	-94	-99	170
165-166	-749	-765	-130	101	-439	-332	-310	-433
167-168	-1419	-896	691	537	-364	-179	-1055	-717
565-566	-2605	-3552						
567-568	575	-1218						
569-570	181	-1796						
571-572	71	-1729						
573-574	-1245	-2384						
575-576	179	-1736						
577-578	91	-1763						
579-580	-22	-1907						

Table A.32. Stress at Each Gage Position Caused by an Axial Load of 1500 lb Downward on Nozzle L_4

Gage Position	Stress (psi)							
	Outer Surface		Inner Surface		Membrane		Bending	
	σ_θ^T	σ_ϕ^T	σ_θ^T	σ_ϕ^T	σ_θ^m	σ_ϕ^m	σ_θ^b	σ_ϕ^b
161-162	-960	-668	474	512	-243	-78	-717	-590
163-164	-526	-488	-151	65	-338	-211	-188	-277
165-166	-69	169	-110	-233	-89	-32	20	201
167-168	-532	-640	-231	231	-381	-204	-151	-436
215-216	-2369	-2431	868	260	-750	-1085	-1619	-1346
217-218	-2381	-1404	774	912	-803	-246	-1578	-1158
219-220	-2052	-1005	1162	1038	-445	16	-1607	-1021
221-222	-2218	-1425	654	546	-782	-439	-1436	-986
257-258	-486	-686	-346	-54	-416	-370	-70	-316
259-260	-86	114	-33	-210	-59	-48	-27	162
261-262	-207	-222	-352	-105	-279	-163	72	-59
597-598	-1923	-3477						
599-600	642	-1327						
601-602	149	-2035						
603-604	85	-1885						
605-606	-1110	-3133						
607-608	81	-1796						
609-610	7	-1878						
611-612	27	-1842						

Table A.33. Stress at Each Gage Position Caused by an Axial Load of 2000 lb Downward on Nozzle K_2

Gage Position	Stress (psi)							
	Outer Surface		Inner Surface		Membrane		Bending	
	σ_θ^T	σ_ϕ^T	σ_θ^T	σ_ϕ^T	σ_θ^m	σ_ϕ^m	σ_θ^b	σ_ϕ^b
161-162	-445	-684	-485	185	-465	-249	20	-435
163-164	-498	-659	-576	47	-537	-306	39	-353
165-166	53	76	-455	-416	-201	-170	254	246
167-168	-199	-30	103	11	-48	-9	-151	-21
169-170	-108	-192	-342	-73	-225	-132	117	-60
171-172	-142	127	36	-279	-53	-76	-89	203
173-174	-113	-144	-116	-55	-114	-99	1	-45
177-178	198	259	-8	-192	95	33	103	226
179-180	-67	-90	-569	-231	-318	-160	251	70
215-216	-832	-740	-96	-19	-464	-379	-368	-361
217-218	-1659	-998	534	280	-562	-359	-1097	-639
219-220	-496	-719	-608	8	-552	-355	56	-364
221-222	-385	-115	145	-316	-120	-215	-265	100
223-224	-1533	-910	795	448	-369	-231	-1164	-679
227-228	-420	-66	-29	-129	-224	-97	-196	31
229-230	-635	-551	-253	224	-444	-163	-191	-388
257-258	-2549	-3365	758	327	-895	-1519	-1654	-1846
259-260	-2062	-1738	536	821	-763	-458	-1299	-1280
261-262	-2547	-2324	820	1066	-863	-629	-1684	-1695
267-268	-788	-226	230	-201	-279	-213	-509	-13
269-270	-562	-638	-269	369	-415	-134	-147	-504
271-272	66	220	18	-275	42	-27	24	247
273-274	-159	-398	-500	-100	-329	-249	170	-149
275-276	-559	-598	-190	-67	-374	-332	-185	-266
305-306	-280	-534	-431	-269	-355	-401	75	-133
307-308	-427	-58	-16	-355	-221	-206	-206	148
309-310	-465	-849	-975	-182	-720	-515	255	-334
311-312	-1334	-780	352	105	-491	-337	-843	-443
613-614	-2105	-3452						
615-616	401	-630						
617-618	63	-1491						
619-620	12	-1326						
621-622	-1404	-2481						
623-624	178	-1007						
627-628	332	-1060						

Table A.34. Stress at Each Gage Position Caused by a Combined Load of 60 psig Internal Pressure and an Axial Load of 2000 lb on Nozzle A

Gage Position	Stress (psi)							
	Outer Surface		Inner Surface		Membrane		Bending	
	σ_θ^T	σ_ϕ^T	σ_θ^T	σ_ϕ^T	σ_θ^m	σ_ϕ^m	σ_θ^b	σ_ϕ^b
51-52	2044	1413	1069	231	1556	822	488	591
53-54	1180	334	1086	886	1133	610	47	-276
55-56	625	818	1959	898	1292	858	-667	-40
57-58	-197	11	1987	1256	895	633	-1092	-622
59-60	-667	-1190	3212	2974	1272	892	-1939	-2082
61-62	-648	-1195	3293	2678	1322	741	-1970	-1936
65-66	-135	-751	2770	2101	1317	675	-1452	-1426
67-68	-413	-1044	2764	2879	1175	917	-1588	-1961
69-70	-527	-1258	3082	2875	1277	808	-1804	-2066
71-72	-187	-756	2547	2224	1180	734	-1367	-1490
73-74	242	373	1849	1265	1045	819	-803	-446
75-76	1043	1143	1731	669	1387	906	-344	237
77-78	1442	473	1619	996	1530	734	-88	-261
79-80	1765	949	959	1298	1362	1123	403	-174
81-82	2062	1638	1305	452	1683	1045	379	593
83-84	857	857	1071	471	964	664	-107	193
143-144	777	1323	356	487	566	905	211	418
145-146	1324	1047	1170	501	1247	774	77	273
149-150	-288	-326	2346	1154	1029	414	-1317	-740
153-154	1454	446	396	519	925	482	529	-36
155-156	1577	1223	2059	998	1818	1110	-241	113
157-158	1355	416	405	652	880	534	475	-118
159-160	1536	421	2073	1142	1804	781	-268	-360
181-182	1522	507	1049	1265	1285	886	237	-379
183-184	2066	1720	2057	1357	2061	1538	5	182
185-185	2103	1611	1322	907	1712	1259	391	352
191-192	1153	276	1867	1590	1510	933	-357	-657
533-534	-885	-2515						
535-536	-198	-1159						
537-538	391	-1263						
541-542	-319	-1196						
543-544	336	-479						
545-546	357	-643						
547-548	309	-737						

Table A.35. Stress at Each Gage Position Caused by a Normal Load of 50 lb on Nozzle A at a Distance of 34 3/4 in. Above the Apex of the Dome

Gage Position	Stress (psi)							
	Outer Surface		Inner Surface		Membrane		Bending	
	σ_θ^T	σ_ϕ^T	σ_θ^T	σ_ϕ^T	σ_θ^m	σ_ϕ^m	σ_θ^b	σ_ϕ^b
51-52	192	208	92	108	142	158	50	50
53-54	468	560	-177	-323	145	118	323	442
55-56	662	538	-346	-254	158	142	504	396
57-58	841	802	-718	-625	61	88	780	714
59-60	1236	1321	-1375	-1582	-69	-130	1305	1451
61-62	1356	1187	-595	-1148	380	19	976	1168
65-66	-1337	-1191	1271	1171	-33	-10	-1304	-1181
67-68	-390	-167	610	333	110	83	-500	-250
69-70	518	1025	-890	-967	-186	29	704	996
71-72	-1390	-1467	1388	1526	-1	29	-1389	-1496
73-74	-866	-820	692	608	-87	-106	-779	-714
75-76	-642	-573	386	286	-128	-143	-514	-430
77-78	-403	-411	160	368	-121	-21	-282	-390
79-80	-198	-259	-136	-221	-167	-240	-31	-19
81-82	-225	-118	129	29	-48	-44	-177	-74
83-84	-71	29	-36	-21	-53	4	-18	25
143-144	188	226	-64	-79	62	73	126	153
145-146	191	237	60	-32	125	102	66	135
147-148	149	165	24	47	86	106	63	59
149-150	770	601	-616	-455	77	73	693	528
153-154	-165	-149	-69	-31	-117	-90	-48	-59
155-156	-308	-292	263	209	-22	-41	-286	-251
157-158	-468	-560	256	387	-106	-86	-362	-474
159-160	-143	-543	663	509	260	-17	-403	-526
181-182	99	130	46	-46	72	42	27	88
183-184	33	10	-108	8	-37	9	70	1
185-186	-109	-163	-237	109	-173	-27	64	-136
191-192	142	-27	-237	109	-47	41	189	-68
533-534	1187	3156						
535-536	43	1843						
537-538	-203	1889						
541-542	-1520	-3066						
543-544	143	-1557						
545-546	115	-2015						
547-548	114	-1886						

Table A.36. Stress at Each Gage Position Caused by a Normal Lead of 150 lb on Nozzle A at a Distance of 13 3/16 in. from the Apex of the Dome

Gage Position	Stress (psi)							
	Outer Surface		Inner Surface		Membrane		Bending	
	σ_θ^T	σ_ϕ^T	σ_θ^T	σ_ϕ^T	σ_θ^m	σ_ϕ^m	σ_θ^b	σ_ϕ^b
51-52	163	209	42	73	102	141	61	68
53-54	526	588	-197	-389	164	99	362	489
55-56	762	638	-344	-213	209	212	553	426
57-58	960	868	-703	-611	128	128	832	740
59-60	1399	1530	-1399	-1630	0	-50	1399	1580
61-62	1457	1257	-1337	-1491	60	-117	1397	1374
65-66	-1515	-1385	1522	1407	3	11	-1518	-1396
67-68	-429	-129	677	323	124	97	-553	-226
69-70	601	1170	-1007	-1122	-203	24	804	1146
71-72	-1538	-1662	1595	1748	28	43	-1566	-1705
73-74	-968	-960	814	714	-77	-123	-891	-837
75-76	-718	-625	414	314	-152	-155	-566	-470
77-78	-457	-457	153	376	-152	-40	-305	-417
79-80	-263	-309	-42	127	-152	-91	-111	-218
81-82	-224	-147	20	-34	-102	-90	-122	-57
83-84	-53	24	-7	-122	-30	-49	-23	73
143-144	153	176	0	0	76	88	77	88
145-146	199	230	104	-19	151	105	48	125
147-148	140	132	97	89	118	110	22	22
149-150	804	681	-645	-484	79	98	725	583
153-154	-227	-158	-48	5	-137	-76	-90	-82
155-156	-366	-320	267	190	-49	-65	-317	-255
157-158	-576	-753	236	421	-170	-166	-406	-587
159-160	-97	-589	693	578	298	-5	-395	-584
181-182	69	131	-121	-236	-26	-52	95	183
183-184	19	-4	-153	-76	-67	-40	86	36
185-186	-82	-175	-253	24	-167	-75	85	-100
191-192	198	-41	-231	131	-16	45	214	-86
533-534	1526	3788						
535-536	21	2036						
537-538	-142	2127						
541-542	-1725	-3418						
543-544	135	-1649						
545-546	110	-2067						
547-548	56	-1813						

Table A.37. Stress at Each Gage Position Caused by a Normal Load of 30 lb on Nozzle B_2 at a Distance of 34 3/4 in. from the Apex of the Dome

Gage Position	Stress (psi)							
	Outer Surface		Inner Surface		Membrane		Bending	
	σ_θ^T	σ_ϕ^T	σ_θ^T	σ_ϕ^T	σ_θ^m	σ_ϕ^m	σ_θ^b	σ_ϕ^b
47-48	27	58	35	-49	31	4	-4	54
49-50	-21	-36	60	-32	19	-34	-40	-2
51-52	151	235	-27	-258	62	-11	89	246
53-54	-198	-59	-18	75	-108	8	-90	-67
55-56	-297	-89	187	56	-55	-16	-242	-73
57-58	-271	-371	190	367	-40	-2	-231	-369
59-60	-384	-545	193	478	-95	-33	-289	-512
61-62	-805	-652	552	505	-126	-73	-679	-579
65-66	-227	-258	124	147	-51	-55	-176	-203
67-68	-164	-179	26	88	-69	-45	-95	-134
69-70	-212	-274	137	91	-37	-91	-175	-183
71-72	-154	-146	38	62	-58	-42	-96	-104
73-74	-126	-88	11	3	-57	-42	-69	-46
75-76	-110	-33	-16	-55	-63	-44	-47	11
77-78	-102	-141	-22	-7	-62	-74	-40	-67
79-80	-10	-33	-59	2	-34	-15	24	-18
135-136	-70	-1	46	54	-12	26	-58	-27
137-138	220	66	-160	-68	30	-1	190	67
139-140	165	249	109	-137	137	56	28	193
141-142	-203	-11	-27	42	-115	15	-88	-26
143-144	340	232	-311	-103	14	64	326	168
145-146	1280	1434	-1210	-1433	35	0	1245	1434
147-148	556	87	-889	-297	-166	-105	722	192
149-150	-1198	-859	1324	1347	63	244	-1261	-1103
153-154	-130	-299	-98	141	-114	-79	-16	-220
155-156	-66	-20	63	9	-1	-5	-65	-15
157-158	-38	-62	-111	-3	-74	-32	36	-30
159-160	76	-47	142	73	109	13	-33	-60
169-170	95	48	-44	-13	25	17	70	31
171-172	200	200	-3	-11	98	94	102	106
177-178	701	670	-490	-367	105	151	596	519
179-180	319	196	-274	-212	22	-8	297	204
181-182	202	41	-326	-88	-62	-23	264	64
183-184	153	176	11	-97	82	39	71	137
185-186	22	7	-171	29	-74	18	96	-11
191-192	46	-46	-108	-92	-31	-69	77	23
193-194	-30	-99	-35	49	-32	-25	2	-74
581-582	1568	4560						
583-584	88	3326						

Table A.37 (Continued)

Gage Position	Stress (psi)							
	Outer Surface		Inner Surface		Membrane		Bending	
	σ_θ^T	σ_ϕ^T	σ_θ^T	σ_ϕ^T	σ_θ^m	σ_ϕ^m	σ_θ^b	σ_ϕ^b
585-586	-218	3375						
587-588	-84	3655						
589-590	-1423	-4677						
591-592	-142	-3373						
593-594	376	-2547						
595-596	25	-3282						

Table A.38. Stress at Each Gage Position Caused by a Normal Load of 40 lb on Nozzle B_2 at a Distance of 25 1/4 in. from the Apex of the Dome

Gage Position	Stress (psi)							
	Outer Surface		Inner Surface		Membrane		Bending	
	σ_θ^T	σ_ϕ^T	σ_θ^T	σ_ϕ^T	σ_θ^m	σ_ϕ^m	σ_θ^b	σ_ϕ^b
47-48	66	120	81	4	73	62	-7	58
49-50	55	116	78	-7	66	54	-11	62
51-52	176	253	-1	-270	87	-8	89	261
53-54	-152	-5	-53	24	-102	9	-50	-14
55-56	-214	-14	213	44	0	15	-214	-29
57-58	-236	-321	219	396	-8	37	-228	-358
59-60	-357	-557	240	532	-58	-12	-299	-545
61-62	-725	-618	551	535	-87	-41	-638	-577
65-66	-232	-240	96	119	-68	-60	-164	-180
67-68	-132	-140	32	40	-50	-50	-82	-90
69-70	-182	-275	181	104	0	-85	-182	-190
71-72	-165	-149	60	68	-52	-40	-113	-109
73-74	-79	-64	36	21	-21	-21	-58	-43
75-76	-80	-34	15	-15	-32	-24	-48	-10
77-78	-105	-52	-14	-14	-59	-33	-46	-19
79-80	-70	-101	-60	32	-65	-34	-5	-67
135-136	79	64	25	18	52	41	27	23
137-138	213	144	-135	-51	39	46	174	98
139-140	154	246	58	-173	106	36	48	210
141-142	-202	-41	-102	-41	-152	-41	-50	0
143-144	354	246	-325	-118	14	64	340	182
145-146	1193	1378	-1185	-1415	4	-18	1189	1396
147-148	493	-22	-757	-157	-132	-89	625	67
149-150	-1154	-746	1290	1367	68	310	-1222	-1056
153-154	-178	-293	-87	144	-132	-74	-46	-219
155-156	-77	-23	20	-34	-28	-28	-49	5
157-158	-59	-98	-87	44	-73	-27	14	-71
159-160	81	-96	134	80	107	-8	-26	-88
169-170	86	86	-58	-27	14	29	72	57
171-172	157	157	-34	-80	61	38	96	119
173-174	247	224	-98	-59	74	82	173	142
177-178	634	580	-443	-343	95	118	539	462
179-180	329	229	-193	-178	68	25	261	204
181-182	190	-33	-309	-63	-59	-48	249	15
183-184	113	144	-12	-74	50	35	63	109
185-186	66	20	-168	40	-51	30	117	-10
191-192	47	-76	-3	-11	22	-43	25	-33
193-194	-20	-66	-2	59	-11	-3	-9	-63

Table A.38 (Continued)

Gage Position	Stress (psi)							
	Outer Surface		Inner Surface		Membrane		Bending	
	σ_θ^T	σ_ϕ^T	σ_θ^T	σ_ϕ^T	σ_θ^m	σ_ϕ^m	σ_θ^b	σ_ϕ^b
581-582	1436	4221						
583-584	77	3023						
585-586	-157	3043						
587-588	40	3232						
587-590	-1259	-3998						
591-592	-237	-3091						
593-594	293	-2322						
595-596	52	-2895						

Table A.39. Stress at Each Gage Position Caused by a Normal Load of 50 lb on Nozzle M_3 at a Distance of 34 3/4 in. Above the Apex of the Dome

Gage Position	Stress (psi)							
	Outer Surface		Inner Surface		Membrane		Bending	
	σ_θ^T	σ_ϕ^T	σ_θ^T	σ_ϕ^T	σ_θ^m	σ_ϕ^m	σ_θ^b	σ_ϕ^b
17-18	-25	-18	-15	15	-20	-1	-5	-17
19-20	-10	-33	8	92	-1	29	-9	-62
21-22	62	38	-24	153	19	95	43	-57
23-24	310	233	-112	-74	99	79	211	154
25-26	1031	1169	-651	-835	190	167	841	1002
27-28	-331	-269	-753	-176	-542	-222	211	-47
29-30	-1255	-1716	-197	511	-726	-602	-529	-1114
31-32	-369	-231	-868	-260	-618	-245	249	14
33-34	-1254	-1246	1165	1049	-44	-98	-1210	-1148
35-36	-743	-543	613	644	-65	50	-678	-593
37-38	-479	-264	267	290	-106	13	-373	-277
39-40	-321	-336	87	356	-117	10	-204	-346
41-42	-71	-71	-20	-66	-45	-68	-26	-3
43-44	-193	-178	64	79	-64	-49	-129	-129
45-46	-88	-26	-75	-82	-81	-54	-7	28
125-126	-424	-447	-264	121	-344	-163	-80	-284
127-128	-211	-103	-118	-25	-164	-64	-47	-39
131-132	-499	-530	87	356	-206	-87	-293	-443
133-134	-767	-590	170	701	-298	55	-469	-645
549-550	3210	1433						
551-552	-73	1558						
553-554	-330	1901						
555-556	-347	1976						
557-558	-1956	-4587						
559-560	-231	-2369						
561-562	-212	-2374						
563-564	-133	-2010						

Table A.40. Stress at Each Gage Position Caused by a Normal Load of 150 lb on Nozzle M_3 at a Distance of 13 3/16 in. from the Apex of the Dome

Gage Position	Stress (psi)							
	Outer Surface		Inner Surface		Membrane		Bending	
	σ_θ^T	σ_ϕ^T	σ_θ^T	σ_ϕ^T	σ_θ^m	σ_ϕ^m	σ_θ^b	σ_ϕ^b
17-18	-32	-40	-31	31	-31	-4	-1	-36
19-20	-25	-18	-30	101	-27	41	2	-59
21-22	86	-14	-16	145	35	65	51	-79
23-24	390	267	-109	37	140	152	250	115
25-26	1375	1682	-823	-1077	276	302	1099	1380
27-28	-576	-553	-902	-141	-739	-347	163	-206
29-30	-1978	-2593	-173	758	-1075	-917	-903	-1676
31-32	-590	-367	-1120	-366	-855	-366	265	-1
33-34	-2312	-2074	1425	1318	-443	-378	-1869	-1696
35-36	-1166	-920	834	880	-166	-20	-1000	-900
37-38	-707	-422	327	358	-190	-32	-517	-390
39-40	-576	-553	91	437	-242	-58	-334	-495
41-42	-45	-84	-127	-158	-86	-121	41	37
43-44	-262	-238	23	77	-119	-80	-143	-158
45-46	-82	25	-80	-134	-81	-54	-1	79
125-126	-592	-608	-327	142	-459	-233	-133	-375
127-128	-363	-209	-133	-10	-248	-109	-115	-100
131-132	-731	-769	75	382	-328	-193	-403	-576
133-134	-1160	-868	245	884	-457	8	-703	-876
540-550	4418	1925						
551-552	-38	2238						
553-554	-500	2600						
555-556	-787	1644						
557-558	-2864	-6479						
559-560	-440	-3232						
561-562	-344	-3013						
563-564	33	-2490						

Table A.41. Stress at Each Gage Position Caused by a Normal Load of 30 lb on Nozzle J_2 at a Distance of 34 3/4 in. from the Apex of the Dome

Gage Position	Stress (psi)							
	Outer Surface		Inner Surface		Membrane		Bending	
	σ_θ^T	σ_ϕ^T	σ_θ^T	σ_ϕ^T	σ_θ^m	σ_ϕ^m	σ_θ^b	σ_ϕ^b
25-26	176	153	-37	-91	69	31	107	122
27-28	160	168	-160	-168	0	0	160	168
29-30	275	482	-179	-64	48	209	227	273
31-32	-26	-88	-159	2	-92	-43	66	-45
33-34	0	300	73	-258	36	21	-36	279
35-36	-158	-227	-9	-63	-83	-145	-75	-82
37-38	-249	-465	100	500	-74	17	-175	-482
39-40	-618	-425	267	490	-175	32	-443	-457
41-42	-170	-301	123	177	-23	-62	-147	-239
43-44	-88	-26	103	11	7	-7	-95	-19
45-46	-109	-163	-46	46	-77	-58	-32	-105
125-126	1151	1035	-856	-887	147	74	1004	961
127-128	-534	-580	-879	36	-706	-272	172	-308
131-132	-1058	-627	268	860	-395	116	-663	-743
133-134	600	600	-1026	-788	-213	-94	813	694
135-136	-193	-178	7	122	-93	-28	-100	-150
137-138	-125	-18	63	9	-31	-4	-94	-14
139-140	-145	-84	12	-26	-66	-55	-79	-29
141-142	-42	-173	138	162	48	-5	-90	-168
161-162	-253	-76	191	-163	-31	-119	-222	43
163-164	-46	-54	-154	-46	-100	-50	54	-4
165-166	-234	-380	15	185	-109	-97	-125	-283
167-168	-363	-209	-23	523	-193	157	-170	-366
565-566	1985	4915						
567-568	-724	2553						
569-570	-641	3198						
571-572	-580	3466						
573-574	-2090	-6067						
575-576	-231	-3669						
577-578	-234	-3280						
579-580	-537	-3391						

Table A.42. Stress at Each Gage Position Caused by a Normal Load of 80 lb on Nozzle J_2 at a Distance of 13 3/16 in. from the Apex of the Dome

Gage Position	Stress (psi)							
	Outer Surface		Inner Surface		Membrane		Bending	
	σ_θ^T	σ_ϕ^T	σ_θ^T	σ_ϕ^T	σ_θ^m	σ_ϕ^m	σ_θ^b	σ_ϕ^b
25-26	228	228	-42	-73	93	78	135	150
27-28	300	300	-178	-193	61	53	239	247
29-30	380	634	-256	-87	62	273	318	361
31-32	9	-37	-148	5	-69	-16	78	-21
33-34	102	441	60	-332	81	54	21	387
35-36	-148	-195	-38	-162	-93	-178	-55	-17
37-38	-340	-532	70	501	-135	-15	-205	-517
39-40	-690	-467	286	586	-202	59	-488	-526
41-42	-282	-475	81	204	-100	-135	-182	-340
43-44	-132	-40	104	-19	-14	-29	-118	-11
45-46	-182	-275	-82	25	-132	-125	-50	-150
125-126	1358	1227	-771	-871	293	178	1065	1049
127-128	-826	-888	-682	325	-754	-281	-72	-607
131-132	-1237	-891	58	827	-589	-32	-648	-859
133-134	877	823	-1057	-982	-99	-79	976	902
135-136	-307	-222	57	157	-125	-32	-182	-190
137-138	-157	-57	74	12	-41	-22	-116	-35
139-140	-246	-154	81	4	-82	-75	-164	-79
141-142	-68	-260	178	293	55	16	-123	-276
161-162	-336	-121	243	-157	-46	-139	-290	18
163-164	-67	-90	-187	-56	-127	-73	60	-17
165-166	-330	-499	-14	186	-172	-156	-158	-343
167-168	-518	-325	57	657	-230	166	-288	-491
565-566	2597	6489						
567-568	-853	3424						
569-570	-773	4058						
571-572	-602	4259						
573-574	-2811	-7703						
575-576	-278	-4493						
577-578	-190	-3867						
579-580	-462	-3738						

Table A.43. Stress at Each Gage Position Caused by a Normal Load of 30 lb on Nozzle L_4 at a Distance of 34 3/4 in. from the Apex of the Dome

Gage Position	Stress (psi)							
	Outer Surface		Inner Surface		Membrane		Bending	
	σ_θ^T	σ_ϕ^T	σ_θ^T	σ_ϕ^T	σ_θ^m	σ_ϕ^m	σ_θ^b	σ_ϕ^b
161-162	-474	-512	233	810	-120	149	-354	-661
163-164	-292	-308	189	197	-51	-55	-241	-253
165-166	-138	-62	-30	1	-84	-30	-54	-32
167-168	-254	-246	275	182	10	-32	-264	-214
215-216	1047	1224	-599	-530	224	347	823	877
217-218	-389	-697	-811	-3	-600	-350	211	-347
221-222	73	-58	-1000	-600	-463	-329	536	271
257-258	34	80	-2	-241	16	-80	18	160
259-260	-87	-56	-82	-75	-84	-65	-3	9
261-262	-169	-231	-179	36	-174	-97	5	-134
597-598	1425	3818						
599-600	-363	2791						
601-602	-502	3359						
603-604	-402	3659						
605-606	-2354	-7446						
607-608	-302	-3741						
609-610	-193	-3478						
611-612	-214	-3314						

Table A.44. Stress at Each Gage Position Caused by a Normal Load of 80 lb on Nozzle L_4 at a Distance of 13 3/16 in. from the Apex of the Dome

Gage Position	Stress (psi)							
	Outer Surface		Inner Surface		Membrane		Bending	
	σ_θ^T	σ_ϕ^T	σ_θ^T	σ_ϕ^T	σ_θ^m	σ_ϕ^m	σ_θ^b	σ_ϕ^b
161-162	-608	-692	247	924	-180	116	-428	-808
163-164	-389	-397	196	219	-96	-89	-293	-308
165-166	-163	-109	-47	-24	-105	-66	-58	-43
167-168	-347	-324	325	218	-11	-53	-336	-271
215-216	1259	1498	-681	-604	289	447	970	1051
217-218	-567	-990	-908	8	-737	-491	170	-499
219-220	-1101	-570	510	733	-295	81	-806	-651
221-222	105	-48	-1113	-644	-504	-346	609	298
257-258	31	69	-29	-229	1	-80	30	149
259-260	-131	-69	-126	-88	-128	-78	-3	9
261-262	-221	-336	-187	44	-204	-146	-17	-190
597-598	1746	4754						
599-600	-497	3411						
601-602	-608	4008						
603-604	-396	4281						
605-606	-2996	-9119						
607-608	-410	-4433						
609-610	-376	-4053						
611-612	-487	-3656						

Table A.45. Stress at Each Gage Position Caused by a Normal Load of 75 lb on Nozzle K_2 at a Distance of 24 9/16 in. from the Apex of the Dome

Gage Position	Stress (psi)							
	Outer Surface		Inner Surface		Membrane		Bending	
	σ_θ^T	σ_ϕ^T	σ_θ^T	σ_ϕ^T	σ_θ^m	σ_ϕ^m	σ_θ^b	σ_ϕ^b
161-162	-132	-240	-170	-1	-151	-120	19	-120
163-164	-360	-368	224	147	-68	-110	-292	-258
165-166	-98	-159	-189	-97	-143	-128	45	-31
167-168	-67	10	113	-56	23	-23	-90	33
169-170	-133	-210	-100	100	-116	-55	-17	-155
171-172	-265	-149	15	-15	-125	-82	-140	-67
173-174	-159	-198	-48	5	-103	-96	-56	-102
177-178	12	74	-23	-77	-5	-1	17	75
179-180	-70	-101	-152	-5	-111	-53	41	-48
215-216	89	197	251	-165	170	16	-81	181
217-218	11	203	-308	108	-148	155	159	48
221-222	-108	-92	-280	-234	-194	-163	86	71
223-224	-1098	-759	777	723	-160	-18	-938	-741
227-228	-398	-259	102	141	-148	-59	-250	-200
229-230	-479	-364	451	335	-14	-14	-465	-350
257-258	1493	2178	-776	-853	358	662	1135	1516
259-260	-392	-408	-712	-74	-552	-241	160	-167
261-262	-1523	-1877	-40	868	-781	-504	-742	-1373
267-268	-537	-291	193	278	-172	-6	-365	-285
269-270	-326	-488	-108	308	-217	-90	-109	-398
271-272	-85	-15	-136	-121	-110	-68	25	53
273-274	-176	-353	-30	101	-103	-126	-73	-227
275-276	-373	-342	259	98	-57	-122	-316	-220
305-306	27	158	65	-451	46	-146	-19	304
307-308	-248	-95	9	-37	-119	-66	-129	-29
309-310	-270	-501	46	254	-112	-123	-158	-378
311-312	-74	88	-153	124	-113	106	39	-18
613-614	1455	3216						
615-616	-176	1747						
617-618	-274	2188						
619-620	-403	2089						
621-622	-1959	-4898						
623-624	-148	-2395						
627-628	-110	-2233						

Table A.46. Stress at Each Gage Position Caused by Axial Load of 1500 lb Applied Simultaneously to Four Small Experimental Loop Nozzles

Gage Position	Stress (psi)							
	Outer Surface		Inner Surface		Membrane		Bending	
	σ_θ^T	σ_ϕ^T	σ_θ^T	σ_ϕ^T	σ_θ^m	σ_ϕ^m	σ_θ^b	σ_ϕ^b
41-42	411	503	-1126	-1188	-357	-342	768	845
43-44	-118	-125	-1440	-532	-779	-328	661	203
45-46	621	1336	-59	-1198	281	69	340	1267
47-48	-234	620	-84	-1254	-159	-312	-75	932
49-50	-815	-285	-189	-997	-502	-641	-313	356
53-54	-3403	-3011	192	408	-1605	-1301	-1798	-1710
55-56	-2667	-3490	60	968	-1303	-1261	-1364	-2229
57-58	-2689	-3097	173	1342	-1258	-877	-1431	-2220
59-60	-3195	-3148	64	1079	-1565	-1034	-1630	-2114
65-66	-3563	-2909	247	924	-1658	-992	-1905	-1917
67-68	-2642	-3273	-79	1336	-1360	-968	-1282	-2305
69-70	-3610	-2933	54	946	-1778	-993	-1832	-1940
71-72	-3307	-3222	31	1169	-1638	-1026	-1669	-2196
73-74	-2740	-3232	229	1529	-1255	-851	-1485	-2381
75-76	-2811	-3403	180	1134	-1315	-1134	-1496	-2269
77-78	-3242	-2073	363	609	-1439	-732	-1803	-1341
79-80	-2077	-2423	-1282	325	-1679	-1049	-398	-1374
81-82	-798	-359	-69	-1031	-433	-695	-365	336
83-84	-205	548	60	-1432	-72	-442	-133	990
85-85	455	1016	96	-1081	275	-32	180	1048
87-88	-165	-149	-1495	-648	-830	-398	665	249
135-136	225	318	414	-386	319	-34	-94	352
137-138	-460	-468	-1165	-349	-812	-408	352	-60
139-140	-614	-214	269	-1269	-172	-741	-442	527
141-142	-2821	-736	-513	-644	-1667	-690	-1154	-46
143-144	-1980	-1234	493	-522	-743	-878	-1237	-356
145-146	-4555	-4216	2153	2176	-1201	-1020	-3354	-3196
147-148	-4022	-3207	1158	1927	-1432	-640	-2590	-2567
149-150	-3904	-2781	777	1223	-1563	-779	-2341	-2002
153-154	-4587	-4456	1113	1644	-1737	-1406	-2850	-3050
155-156	-4347	-4124	1758	1327	-1294	-1398	-3053	-2726
157-158	-4180	-3434	1124	1447	-1528	-993	-2652	-2441
159-160	-911	-2503	1032	1540	60	-481	-971	-2022
161-162	877	723	386	-514	631	104	246	619
163-164	-127	-58	-1159	-498	-643	-278	516	220
165-166	648	1095	213	-656	430	219	218	876
167-168	-327	42	-1073	-942	-700	-450	373	492

Table A.46 (Continued)

Gage Position	Stress (psi)							
	Outer Surface		Inner Surface		Membrane		Bending	
	σ_θ^T	σ_ϕ^T	σ_θ^T	σ_ϕ^T	σ_θ^m	σ_ϕ^m	σ_θ^b	σ_ϕ^b
169-170	109	563	-668	-860	-279	-148	388	711
171-172	467	890	140	-1068	303	-89	164	979
173-174	-718	-125	169	-669	-274	-397	-444	272
177-178	-2336	-1221	931	-231	-702	-726	-1634	-495
179-180	-1203	-1011	-1342	27	-1272	-492	69	-519
181-182	-1877	-1723	-1249	135	-1563	-794	-314	-929
183-184	-747	-324	-286	-986	-516	-655	-231	331
185-186	-989	-997	-1104	-181	-1046	-589	57	-408
191-192	-2959	-2198	-40	368	-1499	-915	-1460	-1283
193-194	-1157	-1957	-598	641	-877	-658	-280	-1299
195-196	-1338	-1362	-1377	-123	-1357	-742	19	-620
197-198	404	781	151	-965	277	-92	127	873
199-200	-699	-130	-443	-343	-571	-236	-128	106
201-202	-1582	-2075	-537	209	-1059	-933	-523	-1142
203-204	-2510	-1433	813	-156	-848	-794	-1662	-639
205-206	596	919	-513	-1044	41	-62	555	981
207-208	179	64	-1226	-588	-523	-262	702	326
209-210	-104	19	-723	-677	-413	-329	309	348
211-212	829	629	144	-387	486	121	343	508
223-224	614	614	86	-414	350	100	264	514
227-228	-549	735	202	-759	-173	-12	-376	747
229-230	37	91	-1436	-521	-699	-215	736	306
231-232	-57	143	-1001	-170	-529	-13	472	156
233-234	214	314	-626	-1088	-206	-387	420	701
235-236	-162	-338	-1847	-824	-1004	-581	842	243
237-238	-545	-84	-22	-507	-283	-295	-262	211
239-240	416	55	-956	-287	-270	-116	686	171
241-242	88	126	-1335	-451	-623	-162	711	288
243-244	563	509	35	-649	299	-70	264	579
245-246	332	140	-1287	-556	-477	-208	809	348
247-248	514	1014	-8	-892	253	61	261	953
533-534	-1195	-348						
535-536	297	789						
537-538	108	92						
541-542	-1864	-79						
543-544	226	488						
545-546	98	59						
547-548	29	29						
581-582	-2923	-5477						

Table A.46. (Continued)

Gage Position	Stress (psi)							
	Outer Surface		Inner Surface		Membrane		Bending	
	σ_θ^T	σ_ϕ^T	σ_θ^T	σ_ϕ^T	σ_θ^m	σ_ϕ^m	σ_θ^b	σ_ϕ^b
583-584	-2	-3541						
585-586	316	-3845						
587-588	15	-3915						
589-590	-1513	-1044						
591-592	333	710						
593-594	219	96						
595-596	85	-185						

Table A.47. Stress at Each Gage Position Caused by an Axial Load of 5000 lb on Gas Outlet

Gage Position	Stress (psi)							
	Outer Surface		Inner Surface		Membrane		Bending	
	σ_θ^T	σ_ϕ^T	σ_θ^T	σ_ϕ^T	σ_θ^m	σ_ϕ^m	σ_θ^b	σ_ϕ^b
91-92	79	-36	116	55	97	9	-18	-45
93-94	176	53	322	107	249	80	-73	-27
95-96	-207	-22	-258	-27	-232	-24	25	2
97-98	-209	-63	-235	-51	-222	-57	13	-6
99-100	287	56	295	-152	291	-48	-4	104
101-102	285	15	265	-451	275	-218	10	233
103-104	205	152	219	-904	212	-376	-7	528
105-106	-482	-75	127	-942	-177	-508	-305	433
107-108	-1859	-2198	202	1241	-828	-478	-1031	-1720
109-110	-3220	-2466	1827	358	-696	-1054	-2524	-1412
111-112	-778	-1193	-576	47	-677	-573	-101	-620
113-114	-12	-374	-1136	79	-574	-147	562	-227
115-116	-1819	-1496	171	871	-824	-312	-995	-1184
117-118	-1189	-397	353	-924	-418	-660	-771	263
119-120	-2941	-2302	1481	204	-730	-1049	-2211	-1253
121-122	-678	-1093	-618	75	-648	-509	-30	-584
123-124	20	-334	-1092	92	-536	-121	556	-213
501-502	-2318	-3425						
503-504	-1059	-598						
505-506	-115	115						
507-508	179	-236						
509-510	-2181	-3004						
511-512	-955	-516						
513-514	-99	70						
515-516	127	-242						
517-518	-2427	-4458						
519-520	-1402	-1241						
521-522	-337	-191						
523-524	122	-393						
525-526	-2124	-3947						
527-528	-1297	-989						
529-530	-169	-131						
531-532	176	-347						
865-866			-858	1944				
867-868			-1146	-84				
869-870			-610	-964				
871-872			-56	-718				
873-874			-60	-798				

Table A.47 (Continued)

Gage Position	Stress (psi)							
	Outer Surface		Inner Surface		Membrane		Bending	
	σ_θ^T	σ_ϕ^T	σ_θ^T	σ_ϕ^T	σ_θ^m	σ_ϕ^m	σ_θ^b	σ_ϕ^b
875-876			-407	-844				
877-878			-954	-246				
879-880			-784	1928				
881-882			-864	2524				
883-884			-1068	380				
887-888			20	-1136				
889-890			-1896	-1450				
891-892			-270	-902				
893-894			-902	130				
895-896			1218	2728				
897-898			-220	-666				
899-900			258	-344				
901-902	-238	205						
903-904	154	646						
905-906			-380	-936				
907-908			-8	-564				
909-910	176	258						
911-912	182	976						

Table A.48. Stress at Each Gage Position Caused by a Normal Load of 2000 lb on Gas Outlet in Transverse Plane at a Distance of 8 1/2 in. from Dome Surface

Gage Position	Stress (psi)							
	Outer Surface		Inner Surface		Membrane		Bending	
	σ_θ^T	σ_ϕ^T	σ_θ^T	σ_ϕ^T	σ_θ^m	σ_ϕ^m	σ_θ^b	σ_ϕ^b
91-92	-36	-21			-18	-10	-18	-11
93-94	-77	-23	-55	-16	-66	-19	-11	-4
95-96	52	5	34	-20	43	-7	9	12
97-98	-48	5	13	44	-17	24	-31	-19
99-100	25	18	30	-1	27	8	-2	10
103-104	-18	-25	-30	-99	-24	-62	6	37
105-106	37	-9	80	-66	58	-37	-21	28
107-108	270	101	41	-198	155	-48	115	149
109-110	4685	3215	-3623	-1177	531	1019	4154	2196
111-112	1552	1905	-169	-231	691	837	861	1068
113-114	327	858	812	74	569	466	-242	392
115-116	2	41	-70	-1	-34	20	36	21
117-118	25	18	-15	15	5	17	20	1
119-120	-4288	-2926	3340	1132	-474	-897	-3814	-2029
121-122	-1454	-1846	284	245	-585	-800	-869	-1046
123-124	-335	-851	-607	-22	-471	-436	136	-415
501-502	51	-165						
503-504	65	-51						
505-506	38	-38						
507-508	-86	-86						
509-510	52	205						
511-512	11	3						
513-514	19	-4						
515-516	103	11						
517-518	3301	6870						
519-520	2013	2344						
521-522	513	644						
523-524	-209	637						
525-526	-2776	-5753						
527-528	-1729	-1829						
529-530	-355	-516						
531-532	120	-634						

Table A.49. Stress at Each Gage Position Caused by a Normal Load of 2000 lb on Gas Outlet in Axial Plane at a Distance of 8 1/2 in. from Dome Surface

Gage Position	Stress (psi)							
	Outer Surface		Inner Surface		Membrane		Bending	
	σ_θ^T	σ_ϕ^T	σ_θ^T	σ_ϕ^T	σ_θ^m	σ_ϕ^m	σ_θ^b	σ_ϕ^b
91-92	-77	-23	-22	-7	-49	-15	-28	-8
93-94	-124	-47	-160	-68	-142	-57	18	10
95-96	93	-22	208	92	150	35	-57	-57
97-98	74	12	163	9	118	10	-44	2
99-100	-245	-84	-126	212	-185	64	-60	-148
103-104	52	-195	-25	782	13	293	39	-488
105-106	1125	518	-76	447	524	482	601	36
107-108	3099	4330	-1020	-3266	1039	532	2060	3798
109-110	-299	-130	-73	-342	-186	-236	-113	106
111-112	-10	-33	56	-313	23	-173	-33	140
113-114	48	-5	25	-182	36	-93	12	88
115-116	-2476	-2653	835	2251	-820	-201	-1656	-2452
117-118	-1774	-912	469	-269	-652	-590	-1122	-322
119-120	-381	-304	-32	-140	-206	-222	-175	-82
121-122	-29	-29	10	-67	-9	-48	-20	19
123-124	19	-4	-116	-55	-48	-29	67	25
501-502	-3013	-5344						
503-504	-1509	-1463						
505-506	-308	-292						
507-508	129	-471						
509-510	3525	5818						
511-512	1678	1793						
513-514	279	564						
515-516	-213	656						
517-518	-408	-692						
519-520	-198	-259						
521-522	-42	-173						
523-524	88	-74						
525-526	-389	-697						
527-528	-242	-273						
529-530	-7	-122						
531-532	19	-104						

Table A.50. Stress at Each Gage Position Caused by a Pure Moment of 19 200 in.-lb on Gas Outlet in Transverse Plane

Gage Position	Stress (psi)							
	Outer Surface		Inner Surface		Membrane		Bending	
	σ_θ^T	σ_ϕ^T	σ_θ^T	σ_ϕ^T	σ_θ^m	σ_ϕ^m	σ_θ^b	σ_ϕ^b
91-92	-4	19	-11	-3	-7	8	3	11
93-94	-15	15	-44	-13	-29	1	14	14
95-96	66	20	0	0	33	10	33	10
97-98	-81	-4	-71	-71	-76	-37	-5	33
99-100	25	18	93	-22	59	-2	-34	20
101-102	-37	9	0	-100	-18	-45	-19	54
103-104	3	11	-10	-133	-3	-61	6	72
105-106	8	-8	133	310	70	151	-62	-159
107-108	80	-66	-36	-221	22	-143	58	77
109-110	4258	2927	-3470	-1201	394	863	3864	2064
111-112	1446	1854	-422	-307	512	773	934	1081
113-114	271	871	454	-54	362	408	-91	463
115-116	7	22	-273	-142	-133	-60	140	82
117-118	85	15	-323	-77	-119	-31	204	46
119-120	-4363	-3009	3290	1067	-536	-971	-3827	-2038
121-122	-1440	-1932	-13	56	-726	-938	-714	-994
123-124	-309	-963	129	29	-90	-469	-219	-496
501-502	84	-155						
503-504	36	21						
505-506	-22	-7						
507-508	-66	-20						
509-510	-160	-68						
511-512	-160	-68						
513-514	8	-8						
515-516	24	-53						
517-518	2860	5868						
519-520	1740	2132						
521-522	460	768						
523-524	-89	903						
525-526	-2756	-5787						
527-528	-1740	-1932						
529-530	-333	-710						
531-532	59	-1002						

Table A.51. Stress at Each Gage Position Caused by a Pure Moment of 19 200 in.-lb on Gas Outlet in Axial Plane

Gage Position	Stress (psi)							
	Outer Surface		Inner Surface		Membrane		Bending	
	σ_θ^T	σ_ϕ^T	σ_θ^T	σ_ϕ^T	σ_θ^m	σ_ϕ^m	σ_θ^b	σ_ϕ^b
91-92	99	30	69	31	84	30	15	0
93-94	127	58	154	46	140	52	-13	6
95-96	-71	29	-168	-60	-119	-15	48	44
97-98	-31	31	-154	-46	-92	-7	61	38
99-100	254	146	110	-267	182	-60	72	206
101-102	162	138	81	-496	121	-179	41	317
103-104	-97	211	11	-797	-43	-293	-54	504
105-106	-1198	-459	99	-370	-549	-414	-649	-45
107-108	170	6701	1247	3724	708	5212	-538	1489
109-110	231	69	114	414	172	241	59	-172
111-112	-7	-22	-79	336	-43	157	36	-179
113-114	-63	-9	-2	159	-32	75	-31	-84
115-116	2712	2774	-914	-2614	899	80	1813	2694
117-118	1962	938	-477	177	742	557	1220	381
119-120	353	176	64	179	208	177	145	-1
501-502	3163	5609						
503-504	1576	1653						
505-506	273	542						
507-508	-131	931						
509-510	-3404	-5681						
511-512	-1654	-1846						
513-514	-270	-701						
515-516	142	-1027						
517-518	397	589						
519-520	218	225						
521-522	53	76						
523-524	-60	132						
525-526	304	581						
527-528	291	237						
529-530	25	118						
531-532	-57	143						

Table A.52. Stress at Each Gage Position Caused by a Torsional Load of 32 000 in.-lb on Gas Outlet

Gage Position	Stress (psi)							
	Outer Surface		Inner Surface		Membrane		Bending	
	σ_θ^T	σ_ϕ^T	σ_θ^T	σ_ϕ^T	σ_θ^m	σ_ϕ^m	σ_θ^b	σ_ϕ^b
91-92	-8	8	-19	4	-13	6	5	2
93-94	-22	-7	-19	4	-20	-1	-2	-6
95-96	8	-8	0	0	4	-4	4	-4
97-98	-19	4	-15	15	-17	9	-2	-5
99-100	8	-8	-11	-3	-1	-5	9	-3
101-102	0	0	33	10	16	5	-16	-5
103-104	-3	-11	22	7	9	-2	-12	-9
105-106	-15	15	30	-1	7	7	-22	8
107-108	-100	100	-15	-85	-57	7	-43	93
109-110	163	209	-134	20	14	114	149	95
111-112	21	36	-18	-25	1	5	20	31
113-114	51	35	42	-27	46	4	5	31
115-116	-107	-22	37	-9	-35	-15	-72	-7
117-118	-55	-16	63	9	4	-3	-59	-13
119-120	-192	92	-18	-25	-105	33	-87	59
121-122	1	-30	-5	48	-2	9	3	-39
123-124	-11	-3	-35	49	-23	23	12	-26
501-502	-120	34						
503-504	14	-86						
505-506	82	-25						
507-508	-101	-70						
509-510	192	308						
511-512	-145	16						
513-514	132	140						
515-516	-77	77						
517-518	123	77						
519-520	-4	-81						
521-522	-9	-163						
523-524	19	96						
525-526	169	131						
527-528	-49	135						
529-530	100	100						
531-532	169	31						

Appendix B

STRESSES IN FULL-SCALE PRESSURE VESSEL

This appendix presents stress values applicable to the EGCR pressure vessel. These values were obtained by applying the appropriate factors, discussed in Part II, to the data listed in Appendix A. Also included are tables of the maximum stresses in the nozzles obtained from the stress-fit analyses, since these were required in the structural evaluations. Finally, the thermal stresses in the cluster nozzle are listed.

List of Tables

		Page
Table B.1	Experimental Outer Surface Stresses (Scaled to Prototype) for Nozzles with 350-psig Pressure Loading and Axial Tensile Loading of 1 lb/in. Along Mean Circumference	226
Table B.2	Experimental Outer Surface Stresses (Scaled to Prototype) for Nozzles A and B with Each of the Four B Nozzles Under Axial Tensile Loading of 1 lb/in. Along Mean Circumference	229
Table B.3	Experimental Inner Surface Stresses (Scaled to Prototype) for the Gas Outlet Nozzle with 350-psig Pressure Loading and Axial Tensile Loading of 1 lb/in. Along Mean Circumference	229
Table B.4	Experimental Stresses (Scaled to Prototype) for Extension of the Gas Outlet Nozzle Inside the Spherical Head with 350-psig Pressure Loading and Axial Tensile Loading of 1 lb/in. Along Mean Circumference	230
Table B.5	Maximum Principal Stresses in the Nozzles for 350-psig Pressure Loading	231
Table B.6	Maximum Principal Stresses in the Nozzles for an Axial Tensile Load of 1 lb/in. Along Mean Circumference	232
Table B.7	Experimental Outer Surface Stresses (Scaled to Prototype) for B, K, and Gas Outlet Nozzles When Subjected to a Transverse Loading of 1 lb at Various Distances from Apex	233
Table B.8	Maximum Outer Surface Principal Stresses for B, K, and Gas Outlet Nozzles When Subjected to a Transverse Loading of 1 lb at Various Distances Above Apex	234
Table B.9	Experimental Outer Surface Stresses (Scaled to Prototype) for Gas Outlet Nozzle When Subjected to an Applied Moment of 1 in.-lb	235
Table B.10	Maximum Outer Surface Principal Stresses for Gas Outlet Nozzle When Subjected to an Applied Moment of 1 in.-lb	235
Table B.11	Stresses at Gage Locations (Scaled to Prototype) on Sphere Around Designated Nozzles for an Internal Pressure Loading of 350 psig	236

Page

Table B.12	Stresses at Gage Locations (Scaled to Prototype) on Sphere Around Designated Nozzles for an Axial Load Separately Applied on Each Nozzle of 1 lb/in. Along Their Mean Circumference	238
Table B.13	Stresses at Gage Locations (Scaled to Prototype) in the Sphere with the Four B Nozzles Subjected Simultaneously to an Axial Load of 1 lb/in. Along Their Mean Circumference	239
Table B.14	Stresses at Gage Locations (Scaled to Prototype) in the Sphere Around Nozzle B When Nozzle B Is Subjected to a Transverse Loading of 1 lb at 139.7 in. Above the Apex	239
Table B.15	Stresses in the Spherical Head Around the Burst-Slug-Detection and Gas Outlet Nozzles	240
Table B.16	Maximum Thermal Stresses in Nozzles	241

Table B.1. Experimental Outer Surface Stresses (Scaled to Prototype) for Nozzles with 350-psig Pressure Loading and Axial Tensile Loading of 1 lb/in. Along Mean Circumference

Nozzle Type	Reference Circle and/or Gage Location	Distance of Gage from Intersection[a] (in.)	Stress (psi)[b]							
			From Axial Load		From Pressure Load					
			σ_x	σ_c	σ_{x1}	σ_{x2}	σ_{x3}	σ_{c1}	σ_{c2}	σ_{c3}
Control rod	A	1.04			7 379			11 368		
		1.38	1.33	1.14						
		3.8			-2 193			1 441		
		4.15			-2 887	-2 596	- 2 619	887	1 260	1 370
		5.36	0.36	-0.12						
		7.95			712			1 207		
		8.30			922			1 324		
		8.99			706			1 377		
		10.37	0.63	-0.08						
		13.49			665	688		1 248	1 312	
		13.83			1 102			1 318	1 732	
		15.91	0.62	-0.04						
	M, uphill side	1.38	1.40	0.89	2 240	1 604	1 989	4 346	3 786	4 678
		5.53	0.74	0.01	782	449	659	1 633	1 219	1 423
		10.37	0.91	0.11	923	1 102		2 246	1 540	1 732
		14.87	1.06		1 114	951		1 872	1 989	1 802
	M, downhill side	0.95	2.60	1.40	5 804	5 838	6 335	7 280	7 472	8 085
		4.58	0.35	-0.26	-1 371	-1 604	-1 680	286	128	432
		9.68	0.81	-0.20	1 283	1 027	1 371	1 552	1 219	1 464
		15.56	0.88	-0.03	1 691	1 091	1 161	2 141	1 732	1 925
Large experimental loop	K, uphill side	1.38	1.57	0.89	1 254			3 996		
		4.50	0.64	-0.11	-64	6		1 318	1 575	
		9.34								
		14.18	0.67	-0.21	426	379		1 412	1 452	
	K, downhill side	1.38	2.18	1.33	3 972	4 235	5 028	7 023	7 058	8 388
		5.19	0.40	-0.25	-1 347	-1 102		939	1 184	
		10.03	0.94	-0.04	1 231	1 540		1 756	1 767	2 211
		15.91	0.84	-0.01	741	1 237		1 575	1 680	2 182
Special plug	J, uphill side	1.38	1.41	0.74	986	717	1 371	3 681	3 366	4 381
		5.19	1.02	-0.11	1 021	962	1 097	1 645	1 626	1 902
		8.99	1.04	-0.05	910	898	904	1 674	1 604	1 843
		14.87	1.12	0.01	846	834	817	1 657	1 412	1 937

Table B.1 (Continued)

Nozzle Type	Reference Circle and/or Gage Location	Distance of Gage from Intersection[a] (in.)	Stress (psi)[b]							
			From Axial Load		From Pressure Load					
			σ_x	σ_c	σ_{x1}	σ_{x2}	σ_{x3}	σ_{c1}	σ_{c2}	σ_{c3}
	J, downhill side	1.38	2.10	1.54	1 342	1 027	1 255	7 577	7 186	7 775
		4.84	0.72	-0.34	321	397		1 196	1 517	
		9.34	1.06	-0.11	1 283	1 242	1 347	2 135	2 007	2 152
		14.52	1.02	-0.04	1 050	1 219		1 948	2 117	
	L, uphill side	1.38	1.85	0.65	2 339			3 908	3 786	
		4.84	1.06	-0.05	892	682	1 056	1 610	1 487	1 773
		8.99	1.11	-0.01	892	822	1 289	1 610	1 767	1 960
		13.8	1.09	-0.02	834	1 009		1 511	1 592	1 995
	L, downhill side	1.38	2.05	1.13	1 342	1 091	1 219	5 244	4 993	5 617
		4.84	0.78	-0.38	-169	-362		414	87	362
		9.68	1.20	-0.09	1 377	1 044	1 400	1 872	1 540	1 937
		15.56	1.11	-0.05	642	735		1 342	1 353	1 680
Small experimental loop	B, uphill side	1.04			-2 082	-1 598	-1 178	2 584	3 433	4 433
		1.38	2.02	1.042						
		3.80			-314	-770		898	939	
		5.53	0.73	-0.04						
		7.95			986	456	974	1 129	1 692	
		9.68	0.735	-0.121				863	741	
		13.14	0.916	-0.008	513	426		1 318	1 575	1 412
		13.49			432	577	881	1 237	1 341	1 371
	B, downhill side	1.04			-1 826	-706	-2 427	5 576	6 211	3 593
		1.38	1.504	1.011	-472	-1 108		4 060	3 850	3 692
		1.38						4 486		
		3.80			-1 318			484		
		4.50	0.853	-0.062						
		7.95			595			1 318	1 464	
		8.30	1.006	-0.140	344			1 143	1 155	1 044
		13.14	1.110	-0.05	642	577		1 283	1 342	
		13.49			776	472		1 225	1 196	
Burst-slug detection		0.69			8 382	8 685		9 864	11 066	
		1.04			6 562	7 134		6 521	6 865	
		3.89			-1 027	-986		4 356	4 486	
		4.32			-1 102			4 101		
		7.96			-986	-997		1 569	1 919	
		8.99			-665			1 668		
		13.14			950			1 505	1 802	
		14.35						1 575	1 511	

Table B.1. (Continued)

Nozzle Type	Reference Circle and/or Gage Location	Distance of Gage from Intersection[a] (in.)	Stress (psi)[b]							
			From Axial Load		From Pressure Load					
			σ_x	σ_c	σ_{x1}	σ_{x2}	σ_{x3}	σ_{c1}	σ_{c2}	σ_{c3}
Gas outlet	Uphill side	1.04	2.03	1.47	9 064	8 668		11 351	11 001	
		4.50	0.35	0.64	274	-146		5 973	5 728	
		8.99	-0.05	0.07	-1 902	-1 867		2 986	2 532	
		14.18	0.16	-0.09	-513	-659		1 598	1 493	
	Downhill side	1.04	2.31	1.56	7 268	6 591		10 231	9 910	
		4.32	0.40	0.71	-677	-1 137		5 512	4 970	
		8.99	-0.08	0.08	-1 487	-1 995		2 240	1 907	
		14.35	0.16	-0.12	-30	-636		2 030	1 382	
	Sides 90 deg from uphill side, assumed to be alike	0.87	2.66	1.43	11 124	11 345	12 260	8 656	9 741	9 461
		0.87	3.00	1.64	11 707					
		3.98	0.84	0.95	1 983	1 604		6 603	6 311	
		4.32	0.67	0.87	1 301	1 412	1 517	6 865	6 842	7 396
		8.47	0.13	0.23	-741	-957	-922	3 161	3 039	3 342
		8.65	0.09	0.11	-1 161	-1 032	-1 027	2 742	2 782	3 191
		13.49	0.27	-0.08	-64	105		1 732	1 896	
		14.01	0.23	-0.12	432	204	268	1 820	2 047	2 065

[a]See Fig. 11.

[b]σ_{xi} and σ_{ci} designate data from more than one test.

Table B.2. Experimental Outer Surface Stresses (Scaled to Prototype) for Nozzles A and B with Each of the Four B Nozzles Under Axial Tensile Loading of 1 lb/in. Along Mean Circumference

Nozzle Type	Reference Circle and Gage Location	Distance of Gage From Intersection (in.)	Stress (psi)	
			σ_x	σ_c
Control rod	A, assumed symmetrical	1.38	0.05	1.10
		5.53	-0.29	-0.13
		10.37	-0.03	-0.06
		15.91	-0.02	-0.02
Small experimental loop	B, uphill side	1.38		
		5.53		
		9.68		
		13.1		
	B, downhill side	1.38	3.23	1.72
		4.50	2.09	-0.00
		8.3	2.27	-0.19
		13.1	2.31	-0.01

Table B.3. Experimental Inner Surface Stresses (Scaled to Prototype) for the Gas Outlet Nozzle with 350-psig Pressure Loading and Axial Tensile Loading of 1 lb/in. Along Mean Circumference

Nozzle Type	Gage Location	Distance of Gage from Intersection (in.)	Stress (psi)			
			From Axial Loading		From Pressure Loading	
			σ_x	σ_c	σ_x	σ_c
Gas outlet	Uphill side	1.04	-0.65	0.26	-7 863	7274
		4.50	0.08	0.32	1 347	7414
		8.99	0.28	0.14	3 441	4655
		14.18	0.27	0.02	2 374	3051
	Downhill side	0.69	-0.66	0.29	-5 256	8761
		4.15	0.03	0.39	1 499	7927
		8.65	0.33	0.21	3 873	5133
		14.18	0.24	0.02	2 555	3453
	Sides 90 deg from uphill side, assumed to be alike	1.04	-0.85	0.29	-9 111	7775
		1.04	-0.92		-11 310	
		3.80	-0.13	0.36	-968	7478
		4.15	-0.04	0.30	268	7314
		7.95				
		8.65	0.30	0.09	3 692	4316
		13.49	0.38	-0.01	2 876	2380
		13.83				

Table B.4. Experimental Stresses (Scaled to Prototype) for Extension of the Gas Outlet Nozzle Inside the Spherical Head with 350-psig Pressure Loading and Axial Tensile Loading of 1 lb/in. Along Mean Circumference

Nozzle Type	Gage Location	Distance of Gage from Intersection (in.)	Stress (psi)			
			From Axial Loading		From Pressure Loading	
			σ_x	σ_c	σ_x	σ_c
Gas outlet	Uphill side on outer surface	1.04	-0.30	-0.06	3144	6609
		3.80	-0.09	-0.06	373	2800
	Downhill side on outer surface	1.04	-0.22	-0.05	5168	5926
		3.80				
	Uphill side on inner surface	1.04	0.32	0.13	-2578	6002
		3.80	0.19	0.00	233	3692
	Downhill side on inner surface	1.04	0.22	0.07	-7116	5862
		3.80	0.12	-0.09	-1027	4363

Table B.5. Maximum Principal Stresses[a] in the Nozzles for 350-psig Pressure Loading

Nozzle Type	Reference Circle	Stress (psi)							
		Uphill Side				Downhill Side			
		Outer Surface		Inner Surface		Outer Surface		Inner Surface	
		σ_x	σ_c	σ_x	σ_c	σ_x	σ_c	σ_x	σ_c
Control rod	A	Assumed symmetrical				21 586	16 321	-20 102	3815 (7346:1)
	M	6 470	5 809	-4 070	2647 (3544:1)	19 018	17 261	-16 696	6547 (8825:1)
Large experimental loop	K	6 585	6 231	-5 827	2507 (3460:1)	18 756	12 710	-16 896	2014 (5852:2)
Special plug	J	8 715	6 878	-7 047	2150 (3732:1)	21 054	16 175	-19 002	4158 (7761:1)
	L	9 052	5 121	-6 848	351 (2913:2)	16 293	11 799	-14 789	2474 (5515:1)
Small experimental loop	B	6 162	10 049	-4 390	6884	10 665	13 338	-9 511	7285 (7816:5)
Burst-slug detection		Assumed symmetrical				12 380	11 887	-10 088	5147 (6444:2)
Gas outlet		13 375	12 714	-12 375	4989 (6748:2.5)	10 833	11 581	-9 833	5381 (6508:2.5)
		Sides 90 deg from uphill side, assumed to be alike				14 958	9 670	-13 958	995 (4888:4.5)

[a]All the maximum stresses are at the junction except as indicated by parentheses below the number. The number is the stress at the junction; the numbers in parentheses are of the form (a:b) where a is the maximum stress and b is its location measured in inches along nozzle from the junction.

Table B.6. Maximum Principal Stresses[a] in the Nozzles for an Axial Tensile Load of 1 lb/in. Along Mean Circumference

Nozzle Type	Reference Circle	Stress (psi)							
		Uphill Side				Downhill Side			
		Outer Surface		Inner Surface		Outer Surface		Inner Surface	
		σ_x	σ_c	σ_x	σ_c	σ_x	σ_c	σ_x	σ_c
Control rod	A	Assumed symmetrical				3.67	1.89	-2.42	0.067 (0.71:2)
	A, with four B nozzles loaded	Assumed symmetrical				2.39	2.34	-2.39	0.091 (1.13:1)
	M	3.26	1.59	-1.26	0.235 (0.625:1)	5.17	2.75	-3.42	0.174 (1.034:2)
Large experimental loop	K	3.36	1.17	-2.02	-0.443	4.87	1.76	-3.17	-0.644 (0.647:2)
Special plug	J	3.88	1.51	-1.64	-0.152 (0.537:1)	7.01	4.97	2.48	-1.12
	L	3.77	0.76	-1.59	-0.978	5.59	1.62	-3.37	-1.07
Small experimental loop	B	5.15	1.16	-3.31	-1.38	4.93	1.97	-2.73	-0.325 (0.679:1)
	B, with four B nozzles loaded					8.90	3.19	-4.28	0.769 (1.06:2)
Gas outlet		2.78	1.66	-2.07	0.20 (0.67:3.5)	3.12	1.73	-2.42	0.07 (0.67:4)
		Sides 90 deg from uphill side, assumed to be alike				3.50	1.63	-2.50	-0.17 (0.61:4.5)

[a]All the maximum stresses are at the junction except as indicated by parentheses below the number. The number is the stress at the junction; the numbers in parentheses are of the form (a:b) where a is the maximum stress and b is its location measured in inches along nozzle from junction.

Table B.7. Experimental Outer Surface Stresses (Scaled to Prototype) for B, K, and Gas Outlet Nozzles When Subjected to a Transverse Loading of 1 lb at Various Distances from Apex

Nozzle Type	Reference Circle and/or Gage Location	Distance of Applied Load Above Apex[a] (in.)	Direction of Applied Load	Distance of Gage from Intersection (in.)	Stress (psi)	
					σ_x	σ_c
Small experimental loop	B, uphill side	139.7	Toward nozzle A	1.38	-3.27	-1.03
				5.53	-2.52	-0.19
				9.68	-1.90	0.24
				13.14	-2.36	0.04
	B, downhill side	139.7	Toward nozzle A	1.38	3.45	1.17
				4.50	2.47	0.06
				8.3	2.48	-0.13
				13.14	2.64	0.03
	B, uphill side	192.3	Toward nozzle A	1.38	-5.09	-1.16
				5.53	-3.67	-0.12
				9.68	-2.77	0.31
				13.14	-3.57	0.02
	B, downhill side	192.3	Toward nozzle A	1.38	4.97	1.28
				4.50	3.62	0.07
				8.30	3.67	-0.18
				13.14	3.98	-0.07
Large experimental loop	K, uphill side	135.9	Toward nozzle A	1.38	-2.13	-0.85
				4.49	-1.04	-0.06
				9.34		
				14.18	-0.97	-0.05
	K, downhill side	135.9	Toward nozzle A	1.38	1.40	0.63
				5.19	0.76	-0.08
				10.03	0.95	-0.12
				15.91	0.91	-0.18
Gas outlet[b]	Uphill side	47.0	$-F_z$	1.04	0.0950	0.0576
				4.50	0.0293	0.0274
				8.99	0.0092	0.0046
				14.18	0.0107	-0.0035
	Downhill side	47.0	$-F_z$	1.04	-0.0873	-0.0492
				4.32	-0.0239	-0.0246
				8.99	-0.0048	-0.0050
				14.35	-0.0077	0.0021
	Sides 90 deg from uphill side, assumed to be alike[c]	47.0	F_y	0.87	0.1122	0.0539
				0.87	0.0939	0.0453
				3.98	0.0383	0.0329
				4.32	0.0298	0.0282
				8.47	0.0108	0.0084
				8.65	0.0084	0.0058
				13.49	0.0104	0.0034
				14.01	0.0104	0.0020

[a]For the gas outlet nozzle the distance is from the junction.

[b]The directions of the positive applied loads are defined in Fig. 80.

[c]Absolute stresses are given.

Table B.8. Maximum Outer Surface Principal Stresses for B, K, and Gas Outlet Nozzles When Subjected to a Transverse Loading of 1 lb at Various Distances Above Apex

Nozzle Type	Reference Circle and/or Gage Location	Distance of Applied Load Above Apex[a] (in.)	Direction of Applied Load	Stress (psi)	
				σ_x	σ_c
Small experimental loop	B, uphill side	139.7	Toward nozzle A	-6.82	-2.25
	B, downhill side	139.7	Toward nozzle A	7.46	2.41
	B, uphill side	192.3	Toward nozzle A	-8.71	-1.60 (-1.65:0.5)
	B, downhill side	192.3	Toward nozzle A	9.11	2.12
Large experimental loop	K, uphill side	135.9	Toward nozzle A	-3.89	-1.03 (-1.04:0.5)
	K, downhill side	135.9	Toward nozzle A	2.73	1.23
Gas outlet[b]	Uphill side	47.0	$-F_z$	0.126	0.063
	Downhill side	47.0	$-F_z$	-0.112	-0.053
	Sides 90 deg from uphill side, assumed to be alike[c]	47.0	F_y	0.127	0.051

[a]For the gas outlet nozzle the distance is from the junction.

[b]The directions of the positive applied loads are defined in Fig. 80.

[c]Absolute stresses are given.

Table B.9. Experimental Outer Surface Stresses (Scaled to Prototype) for Gas Outlet Nozzle When Subjected to an Applied Moment of 1 in.-lb

Nozzle Type	Gage Location	Direction of Positive Applied Moment	Distance of Gage from Intersection (in.)	Stress (psi)	
				σ_x	σ_c
				$\times 10^{-3}$	$\times 10^{-3}$
Gas Outlet	Uphill side	M_z	1.04	-1.75	-1.05
			4.50	-0.57	-0.51
			8.99	-0.22	-0.08
			14.18	-0.32	-0.04
	Downhill side	M_z	1.04	1.72	0.97
			4.32	0.51	0.48
			8.99	0.17	0.08
			14.35	0.29	-0.04
	Sides 90 deg from uphill side, assumed to be alike[b]	M_y	0.87	1.80	0.88
			0.87	1.78	0.85
			3.98	0.66	0.54
			4.32	0.59	0.54
			8.47	0.24	0.14
			8.65	0.22	0.10
			13.49	0.28	-0.03
			14.01	0.31	-0.02

[a]The directions of the positive applied moments are defined in Fig. 80.

[b]Absolute stresses are given.

Table B.10. Maximum Outer Surface Principal Stresses for Gas Outlet Nozzle When Subjected to an Applied Moment of 1 in.-lb

Nozzle Type	Gage Location	Direction of Positive Applied Moment[a]	Stress (psi)	
			σ_x	σ_c
			$\times 10^{-3}$	$\times 10^{-3}$
Gas outlet	Uphill side	M_z	-2.27	-1.16
	Downhill side	M_z	2.20	1.06
	Sides 90 deg from uphill side, assumed to be alike[b]	M_y	2.17	0.90

[a]The directions of the positive applied moments are defined in Fig. 80.

[b]Absolute stresses are given.

Table B.11. Stresses at Gage Locations (Scaled to Prototype) on Sphere Around Designated Nozzles for an Internal Pressure Loading of 350 psig

Nozzle Type	Reference Circle	Gage Location[a,b]	Stress (psi)			
			Outer Surface		Inner Surface	
			σ_ϕ	σ_θ	σ_ϕ	σ_θ
Control rod	A	In line with B nozzles	8 622	12 781	3 506	8 188
		In line with C nozzles	9 218	13 382	4 657	7 572
	C	0	9 287	11 754	5 301	8 756
		45	6 871	12 693	5 197	9 928
		90	7 885	11 655	6 870	10 548
		180	7 678	11 365	7 562	9 132
		225	8 594	12 215	6 650	9 578
		315	7 525	12 354	4 853	9 566
	D	0	6 533	11 906	6 560	9 711
		90	6 765	10 547	5 715	11 910
		180	8 072	11 270	6 296	8 495
		225	9 683	11 088	5 940	9 472
		315	7 846	10 792	6 164	9 530
	F	0	4 591	7 362	8 751	10 348
		90	3 445	8 471	6 261	8 665
		180	6 115	8 815	7 165	7 293
		225	6 641	10 310	5 263	7 821
		315	4 731	8 137	7 044	11 477
	H (1 and 3)	26° 34'	5 043	7 458	7 697	10 344
		71° 34'	5 252	9 189	6 596	11 488
		116° 34'	8 801	11 012	5 469	7 096
		161° 34'	6 813	9 875	7 093	7 553
		296° 34'	3 974	8 608	6 720	8 111
	H (2 and 4)	18° 26'	4 696	9 138	8 905	9 802
		108° 26'	8 113	12 263	5 235	8 702
		180°	8 870	10 462	5 399	5 749
		288° 26'	5 995	11 132	6 055	9 780
	M	0	4 439	6 154	8 190	8 989
		90	4 515	8 568	2 577	5 479
		180	7 302	9 113	6 210	6 088
		270	4 750	7 434	2 413	5 158
		315	4 492	9 036	5 966	7 638
Large experimental loop	K	0	5 542	8 167	7 970	9 697
		90	6 736	11 406	3 940	8 181
		180	9 033	10 178	5 600	5 631
		270	5 415	11 002	3 665	7 815
		315	7 280	9 432	5 888	7 279
Special plug	E	26° 34'	5 220	11 468	6 880	7 947
		116° 34'	6 872	10 368	5 967	10 219
		206° 34'	5 635	9 348	5 042	8 566
		296° 34'	4 902	9 567	5 249	9 857

Table B.11. (Continued)

Nozzle Type	Reference Circle	Gage Location[a,b]	Stress (psi)			
			Outer Surface		Inner Surface	
			σ_ϕ	σ_θ	σ_ϕ	σ_θ
	G	0	4 261	9 342	6 991	8 966
		90	7 597	12 488	3 832	7 918
		180	7 320	10 472	5 416	11 541
		270	5 100	9 036	6 763	7 089
	J	0	6 218	5 072	8 161	9 797
		33° 41'	4 129	8 559	5 476	8 336
		123° 41'	4 812	9 875	5 635	7 801
		180°	5 635	9 084	7 326	6 527
		303° 41'	5 088	10 060	6 135	8 594
	L (1 and 3)	75° 58'	4 967	9 847	3 208	6 856
		180°	6 838	9 052	6 570	6 681
		255° 58'	4 060	7 439	5 300	8 765
		345° 58'	3 152	6 764	6 625	9 542
	L (2 and 4)	14° 2'	4 488	8 508	5 465	7 328
		104° 2'	5 438	9 376	3 918	6 504
		180°	6 847	9 257	6 288	6 525
		284° 2'	5 429	10 383	4 712	8 122
Small experimental loop	B	0	7 933	11 715	5 568	9 370
		90	8 244	13 658	4 672	9 745
		180	8 393	12 450	4 555	10 070
		270	7 513	11 812	7 782	10 026
Burst-slug detection[b]		Assumed symmetrical	5 746 (4 719)	10 009 (8 907)	1 872	6 002
Gas outlet[b]		0	6 842	10 453	1 732	6 644
		90	8 913	11 718	1 452	6 690
		180	(630)	(9 286)	(6 860)	(9 934)

[a]Degrees clockwise from plane passing through designated nozzle and the nozzle at the apex.

[b]The stress values in parentheses were measured at a distance of about 2 in. (1 deg) from the junction; the others at 1 in. (0.5 deg).

Table B.12. Stresses at Gage Locations (Scaled to Prototype) on Sphere Around Designated Nozzles for an Axial Load Separately Applied on Each Nozzle of 1 lb/in. Along Mean Circumference

Nozzle Type	Reference Circle	Gage Location[a]	Stress (psi)			
			Outer Surface		Inner Surface	
			σ_ϕ	σ_θ	σ_ϕ	σ_θ
Control rod	A	In line with B nozzles	1.674	1.762	-1.219	-1.004
		In line with C nozzles	1.734	1.804	-1.217	-1.008
	M_3	0	0.985	1.136	-0.792	-0.680
		90	0.914	1.152		
		180	1.332	1.240	-0.164	-0.504
		270	1.193	1.217	-0.408	-0.306
		315	1.336	1.633	-0.633	-0.468
Large experimental loop	K_2	0			-0.733	-0.801
		90	1.146	1.492		
		180	2.126	1.610	-0.207	-0.479
		270	1.098	1.303	-0.519	-0.339
		315	1.468	1.609	-0.673	-0.518
Special plug	J_2	0			-1.012	-1.038
		33° 41'	0.785	1.297	-0.815	-0.592
		123° 41'	0.953	1.230	-0.587	-0.500
		180	1.363	1.671	-0.298	-0.621
		303° 41'	0.931	1.353	-0.764	-0.677
	L_4	14° 2'	0.593	1.211	-0.612	-0.686
		104° 2'	0.841	1.309	-0.322	-0.386
		180	1.434	1.398	-0.153	-0.512
		284° 2'	0.828	1.405	-0.538	-0.457
Small experimental loop	B_2	0	1.185	1.647	-1.181	-1.086
		90			-1.175	-1.058
		180	1.615	1.647	-1.189	-1.035
		270	1.336	1.563	-1.454	-1.091
Gas outlet[b]		0	1.482	1.253	-0.836	-0.136
		90	2.077	1.607	-1.115	-0.189
		180	(1.008)	(1.226)	(-0.587)	(-0.115)

[a]Degrees clockwise from plane passing through designated nozzle and the nozzle at the apex.

[b]The stress values in parentheses were measured at a distance of about 2 in. (1 deg) from the junction; the others at 1 in. (0.5 deg).

Table B.13. Stresses at Gage Locations (Scaled to Prototype) in the Sphere with the Four B Nozzles Subjected Simultaneously to an Axial Load 1 lb/in. Along Their Mean Circumference

Nozzle Type	Reference Circle	Gage Location[a]	Stresses at Gage Locations (psi)			
			Outer Surface		Inner Surface	
			σ_ϕ	σ_θ	σ_ϕ	σ_θ
Control rod	A	In line with C nozzles	1.928	1.783	-0.705	0
		In line with B nozzles	1.726	2.119	-0.569	-0.090
	C	0	2.038	1.616	-0.620	-0.071
		45	1.434	1.889	-0.273	-0.102
		90	1.223	1.166	-0.136	0.747
		180	0.189	0.465	0.593	0.106
		225	0.588	0.584	0.107	0.651
		315				
Small experimental loop	B	0	1.559	2.303	-0.815	-0.534
		90	2.261	2.540	-1.001	-0.673
		180	2.460	2.626	-1.034	-1.154
		270	2.026	2.466	-1.054	-0.670

[a]Degrees clockwise from plane passing through designated nozzle and the nozzle at the apex.

Table B.14. Stresses at Gage Locations (Scaled to Prototype) in the Sphere Around Nozzle B When Nozzle B is Subjected to a Transverse Loading of 1 lb at 139.7 in. Above the Apex

Gage Location[a,b]	Stress (psi)			
	Outer Surface		Inner Surface	
	σ_ϕ	σ_θ	σ_ϕ	σ_θ
0	-0.61	-0.94	1.12	1.05
90				
180	1.13	0.97	-1.16	-0.97
270	-0.02	0.40	-0.13	-0.62

[a]Degrees clockwise from plane passing through designated nozzle and the nozzle at the apex.

[b]The stress values were measured at a distance of about 1 in. (0.5 deg) from the junction.

Table B.15. Stresses in the Spherical Head Around the Burst-Slug-Detection and Gas Outlet Nozzles

Nozzle	Side Nearest Gages	Gage Location[a]	Stress (psi)							
			From Axial Load				From Pressure Loading			
			Outer Surface		Inner Surface		Outer Surface		Inner Surface	
			σ_ϕ	σ_θ	σ_ϕ	σ_θ	σ_ϕ	σ_θ	σ_ϕ	σ_θ
Burst-slug detection	Assumed symmetrical	6.2[b]					5746	10 009	1872	6002
		6.7[b]					4719	8 907		
		12.7					3739	5 687	6031	5186
Gas outlet	Uphill side	9.1[b]	1.482	1.253	-0.836	-0.136	6842	10 453	1731	6644
		12.8	0.051	0.325	0.635	-0.086	3710	5 751	5699	5676
		16.6	-0.102	-0.138	0.609	-0.148	3914	4 474	6224	4876

[a]Degrees from the axis of the nozzle along a meridian.

[b]The stresses at this location are those listed in Tables B.11 and B.12.

Table B.16. Maximum Thermal Stresses in Nozzles

Nozzle Type	Reference Circle	T_0[a] (°F)	Stress (psi)			
			Outer Surface		Inner Surface	
			σ_x	σ_c	σ_x	σ_c
Control rod	A	50	8972	1211	-8972	-1814
	M	5	897	121	-897	-181
Large experimental loop	K	6	1076	145	-1076	-218
Special plug	J	8	1152	190	-1152	-242
	L	5	720	119	-720	-151
Small experimental loop	B	34	4893	807	-4893	-1028

[a]Temperature excess above reference temperature, see Eq. (11), Part II.

Appendix C

ANALYTICAL STUDY AND COMPARISON OF EXPERIMENTAL AND THEORETICAL RESULTS

In examining the pressure vessel, it was deemed prudent to compare the experimental stress values for both the head and nozzle with those determined theoretically. The analytical model was a single nozzle radially attached to a spherical shell; the complete analysis of this configuration is described in ref. 3. The asymptotic solutions to the two differential equations for the spherical shell were used:

$$\frac{d^2Q_\phi}{d\phi^2} + \cot\phi \frac{dQ_\phi}{d\phi} - \cot^2\phi \, Q\phi \pm 2ik^2Q_\phi = 0 \quad .$$

The complementary solution is then[13]

$$Q_\phi = \sqrt{\phi/\sin\phi} \, (A_1 \, \mathrm{ber}' \sqrt{2} \, k\phi + A_2 \, \mathrm{bei}' \sqrt{2} \, k\phi +$$

$$+ A_3 \, \mathrm{ker}' \sqrt{2} \, k\phi + A_4 \, \mathrm{kei}' \sqrt{2} \, k\phi \quad ,$$

where Q_ϕ is the shearing force, k is a constant depending upon the shell dimensions, ϕ is the colatitude angle, and the A's are integration constants. The functions are the real and imaginary parts of the modified Bessel functions $I_0 \, (\sqrt{2i} \, k\phi)$ and $K_0 \, (\sqrt{2i} \, k\phi)$, and the prime denotes differentiation with respect to the agrument. The cylinders, or nozzles, were assumed to be semi-infinite in extent both inside and outside the pressure vessel.

For the pressure vessel, only nozzle A and the burst-slug-detection and the gas outlet nozzles are radially attached. From the experimental results, it is realistic to assume that only the burst-slug-detection nozzle and nozzle A are symmetrically loaded, since the proximity

[13]F. A. Leckie, Asymptotic Solutions for the Spherical Shell Subjected to Axially Symmetric Loading, pp. 286–297 in Nuclear Reactor Containment Buildings and Pressure Vessels, Butterworths, London, 1960.

of the head-to-body discontinuity in the vessel causes asymmetrical edge loadings for the gas outlet nozzle. Unfortunately, the presence of adjacent nozzles cannot be taken into account in the theoretical analysis of nozzle A, leaving the burst-slug-detection nozzle as one which can be adequately described by the analytical model.

Even though the mathematical model of ref. 3 was not expected to give exact results for the pressure vessel, a complete theoretical analysis was made for each nozzle-to-shell attachment. In the discussion that follows exterior nozzles refer to the nozzles exterior to the sphere, while interior nozzles refer to the nozzle extensions on the inside of the vessel. Only two types of nozzles are represented in the cluster region of the top head; hence, the total number of configurations examined was four.

Stress profiles for the exterior nozzles subjected to pressure and axial loadings are given in Figs. C.1 through C.8, while similar profiles for the interior nozzles are given in Figs. C.9 through C.16. The stress profiles for the sphere are plotted in Figs. C.17 through C.24. The data plotted on these figures for the various nozzle-sphere configurations are the stresses in the regions of nozzle A, the uphill side of nozzle B, the burst-slug detection nozzle, and the uphill side of the gas outlet nozzle. Experimental stresses for the spherical head in the regions adjacent to the burst-slug-detection and gas outlet nozzles are listed in Table B.15. The data for the regions around nozzles A and B were plotted because that area was the most crucial; in the case of the gas outlet configuration the uphill side was chosen because extraneous structural influences are a minimum there.

In Figs. C.1 and C.3 the apparent success of the mathematical model for cluster nozzles under pressure loading is misleading. The theoretical estimates are not conservative, and when compared with the results obtained in Part II indicate a maximum stress about 5000 psi too low.

An examination of Figs. C.2 and C.4 reveals that for axial loadings the theoretical analysis is probably conservative. Since axial loads produce localized stresses, theoretical thermal stresses due to localized temperature gradients on the nozzles may also be conservative.

As stated previously, the burst-slug-detection nozzle is located in a region that is not affected by other structural discontinuities. Hence, the theoretical and experimental results should be in agreement, and comparisons of data points and stress profiles are given in Fig. C.5. Some of the discrepancy can be attributed to the nonlinearity of the gage readings and to inexact positioning of the gages. Also, the product of the inverse of the characteristic length and the actual length,[4] βl, for the interior extension of the nozzle is only 2.88, which places it more in the category of a ring than that of a semi-infinite shell. The presence of the fillet reduces the experimental stresses in the discontinuity region. These same factors are also influential in the cases of the cluster and gas outlet nozzles.

An examination of Figs. C.1 through C.16 reveals that the maximum nozzle stresses always occur in the exterior portions. This is true for all critical design loadings. It may also be concluded that the mathematical model is not a valid one for use in examining the cluster region and does not give sufficiently accurate results for the other nozzles. However, for loadings of local character (axial and thermal loadings on a nozzle) the theoretical curves are reasonably accurate.

The stresses for the shell in the vicinity of the burst-slug-detection nozzle which result from an internal pressure loading are assumed to have axial symmetry. As may be seen from Fig. C.21 the peak stresses obtained from the theoretical curves equal or exceed those obtained from extrapolation of experimental results, except in the case of the meridional stress at the outer surface. The over-all agreement between theory and experiment is very good. Some of the discrepancy can be accounted for as previously cited.

The experimental stresses for the shell in the region of the gas outlet nozzle are plotted in Figs. C.23 and C.24, where the data from along the meridional line near the uphill side of the nozzle are plotted. As in the case of the burst-slug-detection nozzle, the peak pressure stresses from the theoretical curves equal or exceed those obtained from extrapolation of experimental results for all principal stresses, except the meridional stress at the outer surface. Excellent agreement exists between

the theoretical and experimental results for the meridional stress at the inner surface, but in other cases there are wide variations. For the cluster region, there is a much wider discrepancy for pressure stresses.

As noted in Part II, the maximum stresses in the head could probably be approximated. This is especially true for the outer circumferential stresses which not only are the maximum experimental stresses but also are not greatly influenced in most cases by the presence of other nearby discontinuity regions. It should be noted, however, that the maximum head stresses in the theoretical model are always less than those in the exterior nozzle in question. From this observation, together with the approximation indicated above, it was concluded that for any design loading the maximum stress always occurs in a nozzle.

List of Figures

		Page
Fig. C.1.	Principal Stresses (Theoretical) in the Exterior Control Rod or Large Experimental Loop Nozzle from 350-psig Pressure Loading, Assuming a Single Nozzle-to-Shell Attachment.	250
Fig. C.2.	Principal Stresses (Theoretical) in the Exterior Control Rod or Large Experimental Loop Nozzle from Axial Tensile Loading of 1 lb/in. Along Mean Circumference, Assuming a Single Nozzle-to-Shell Attachment.	250
Fig. C.3.	Principal Stresses (Theoretical) in the Exterior Special Plug or Small Experimental Loop Nozzle from 350-psig Pressure Loading, Assuming a Single Nozzle-to-Shell Attachment.	251
Fig. C.4.	Principal Stresses (Theoretical) in the Exterior Special Plug or Small Experimental Loop Nozzle from Axial Tensile Loading of 1 lb/in. Along Mean Circumference, Assuming a Single Nozzle-to-Shell Attachment.	251
Fig. C.5.	Principal Stresses (Theoretical) in the Exterior Burst-Slug-Detection Nozzle from 350-psig Pressure Loading, Assuming a Single Nozzle-to-Shell Attachment.	252
Fig. C.6.	Principal Stresses (Theoretical) in the Exterior Burst-Slug-Detection Nozzle from Axial Tensile Loading of 1 lb/in. Along Mean Circumference, Assuming a Single Nozzle-to-Shell Attachment.	252
Fig. C.7.	Principal Stresses (Theoretical) in the Exterior Gas Outlet Nozzle from 350-psig Pressure Loading, Assuming a Single Nozzle-to-Shell Attachment.	253
Fig. C.8.	Principal Stresses (Theoretical) in the Exterior Gas Outlet Nozzle from Axial Tensile Loading of 1 lb/in. Along Mean Circumference, Assuming a Single Nozzle-to-Shell Attachment.	253
Fig. C.9.	Principal Stresses (Theoretical) in the Interior Control Rod or Large Experimental Loop Nozzle from 350-psig Pressure Loading, Assuming a Single Nozzle-to-Shell Attachment.	254
Fig. C.10.	Principal Stresses (Theoretical) in the Interior Control Rod or Large Experimental Loop Nozzle from Axial Tensile Loading of 1 lb/in. Along Mean Circumference, Assuming a Single Nozzle-to-Shell Attachment.	254

		Page
Fig. C.11.	Principal Stresses (Theoretical) in the Interior Special Plug or Small Experimental Loop Nozzle from 350-psig Pressure Loading, Assuming a Single Nozzle-to-Shell Attachment.	255
Fig. C.12.	Principal Stresses (Theoretical) in the Interior Special Plug or Small Experimental Loop Nozzle from Axial Tensile Loading of 1 lb/in. Along Mean Circumference, Assuming a Single Nozzle-to-Shell Attachment.	255
Fig. C.13.	Principal Stresses (Theoretical) in the Interior Burst-Slug-Detection Nozzle from 350-psig Pressure Loading, Assuming a Single Nozzle-to-Shell Attachment.	256
Fig. C.14.	Principal Stresses (Theoretical) in the Interior Burst-Slug-Detection Nozzle from Axial Tensile Loading of 1 lb/in. Along Mean Circumference, Assuming a Single Nozzle-to-Shell Attachment.	256
Fig. C.15.	Principal Stresses (Theoretical) in the Interior Gas Outlet Nozzle from 350-psig Pressure Loading, Assuming a Single Nozzle-to-Shell Attachment.	257
Fig. C.16.	Principal Stresses (Theoretical) in the Interior Gas Outlet Nozzle from Axial Tensile Loading of 1 lb/in. Along Mean Circumference, Assuming a Single Nozzle-to-Shell Attachment.	257
Fig. C.17.	Principal Stresses (Theoretical) in Spherical Head Adjacent to Control Rod Nozzle from 350-psig Pressure Loading, Assuming a Single Nozzle-to-Shell Attachment.	258
Fig. C.18.	Principal Stresses (Theoretical) in Spherical Head Adjacent to Control Rod Nozzle with an Axial Loading on the Nozzle of 1 lb/in. on Mean Circumference, Assuming a Single Nozzle-to-Shell Attachment.	258
Fig. C.19.	Principal Stresses (Theoretical) in Spherical Head Adjacent to Special Plug Nozzle from 350-psig Pressure Loading, Assuming a Single Nozzle-to-Shell Attachment.	259
Fig. C.20.	Principal Stresses (Theoretical) in Spherical Head Adjacent to Special Plug Nozzle with an Axial Load on the Nozzle of 1 lb/in. on Mean Circumference, Assuming a Single Nozzle-to-Shell Attachment.	259

Page

Fig. C.21. Principal Stresses (Theoretical) in Spherical Head Adjacent to Burst-Slug-Detection Nozzle from 350-psig Pressure Loading, Assuming a Single Nozzle-to-Shell Attachment. 260

Fig. C.22. Principal Stresses (Theoretical) in Spherical Head Adjacent to Burst-Slug-Detection Nozzle with an Axial Tensile Loading on the Nozzle of 1 lb/in. on Mean Circumference, Assuming a Single Nozzle-to-Shell Attachment. 260

Fig. C.23. Principal Stresses (Theoretical) in Spherical Head Adjacent to Gas Outlet Nozzle from 350-psig Pressure Loading, Assuming a Single Nozzle-to-Shell Attachment. 261

Fig. C.24. Principal Stresses (Theoretical) in Spherical Head Adjacent to Gas Outlet Nozzle with an Axial Loading on the Nozzle of 1 lb/in. on Mean Circumference, Assuming a Single Nozzle-to-Shell Attachment. 261

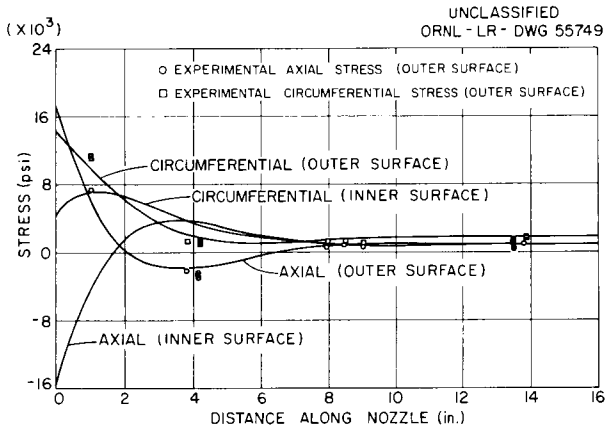

Fig. C.1. Principal Stresses (Theoretical) in the Exterior Control Rod or Large Experimental Loop Nozzle from 350-psig Pressure Loading, Assuming a Single Nozzle-to-Shell Attachment.

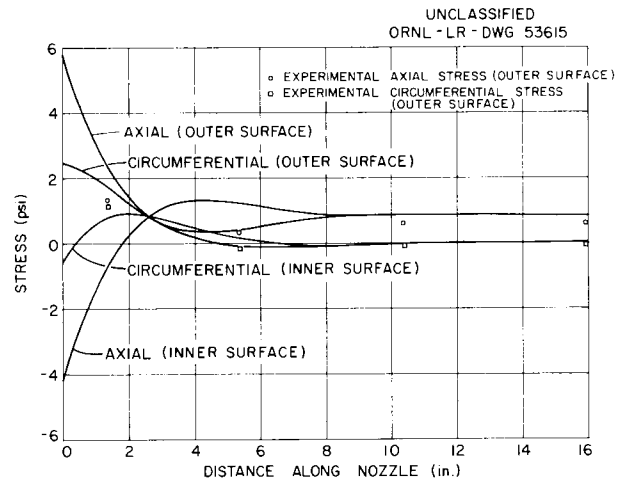

Fig. C.2. Principal Stresses (Theoretical) in the Exterior Control Rod or Large Experimental Loop Nozzle from Axial Tensile Loading of 1 lb/in. Along Mean Circumference, Assuming a Single Nozzle-to-Shell Attachment.

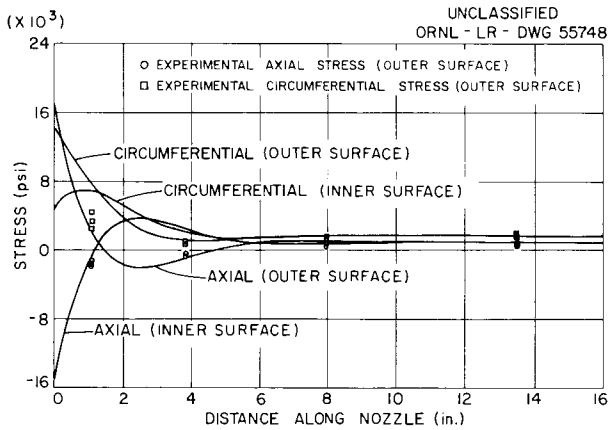

Fig. C.3. Principal Stresses (Theoretical) in the Exterior Special Plug or Small Experimental Loop Nozzle from 350-psig Pressure Loading, Assuming a Single Nozzle-to-Shell Attachment.

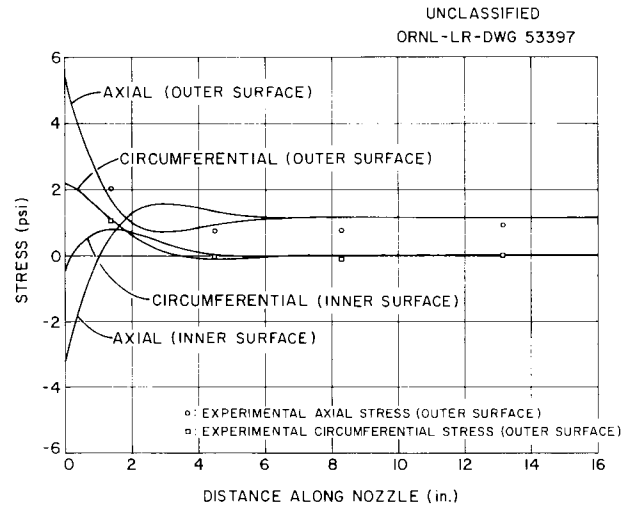

Fig. C.4. Principal Stresses (Theoretical) in the Exterior Special Plug or Small Experimental Loop Nozzle from Axial Tensile Loading of 1 lb/in. Along Mean Circumference, Assuming a Single Nozzle-to-Shell Attachment.

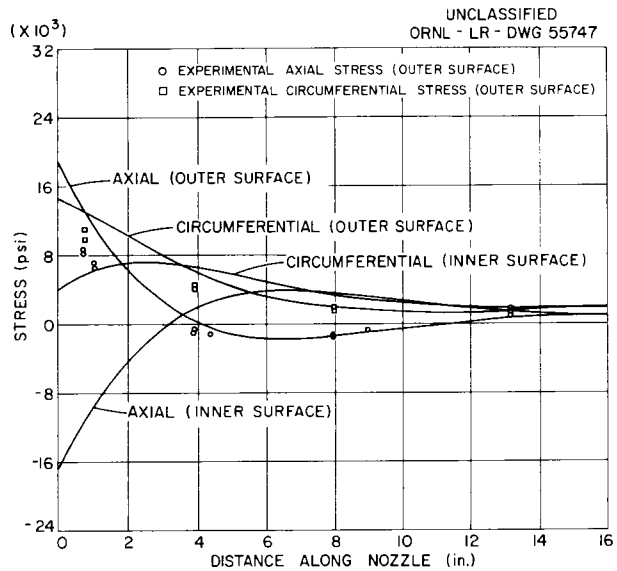

Fig. C.5. Principal Stresses (Theoretical) in the Exterior Burst-Slug-Detection Nozzle from 350-psig Pressure Loading, Assuming a Single Nozzle-to-Shell Attachment.

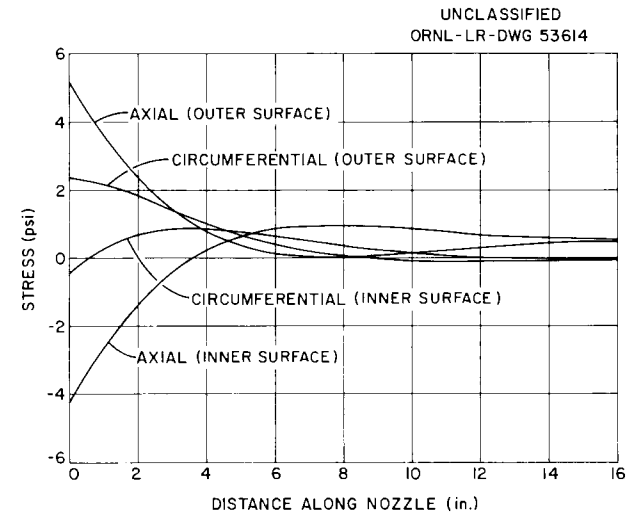

Fig. C.6. Principal Stresses (Theoretical) in the Exterior Burst-Slug-Detection Nozzle from Axial Tensile Loading of 1 lb/in. Along Mean Circumference, Assuming a Single Nozzle-to-Shell Attachment.

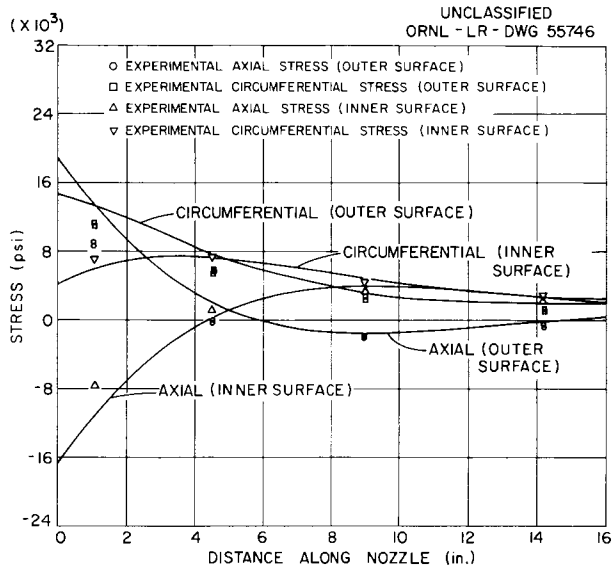

Fig. C.7. Principal Stresses (Theoretical) in the Exterior Gas Outlet Nozzle from 350-psig Pressure Loading, Assuming a Single Nozzle-to-Shell Attachment.

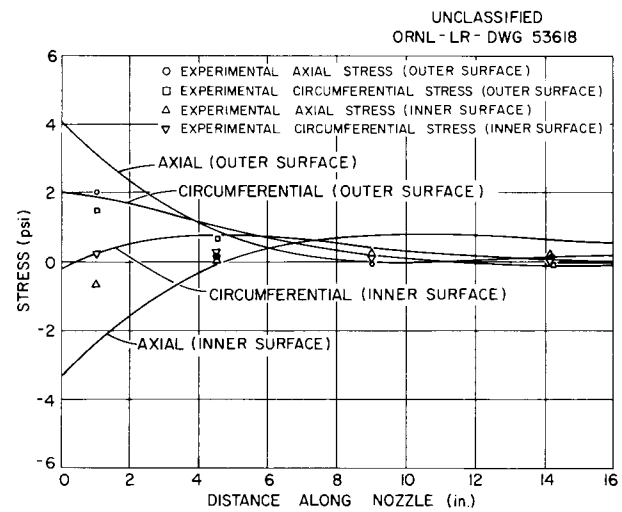

Fig. C.8. Principal Stresses (Theoretical) in the Exterior Gas Outlet Nozzle from Axial Tensile Loading of 1 lb/in. Along Mean Circumference, Assuming a Single Nozzle-to-Shell Attachment.

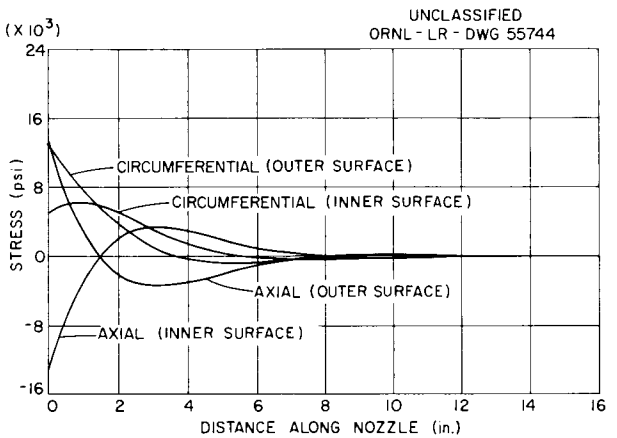

Fig. C.9. Principal Stresses (Theoretical) in the Interior Control Rod or Large Experimental Loop Nozzle from 350-psig Pressure Loading, Assuming a Single Nozzle-to-Shell Attachment.

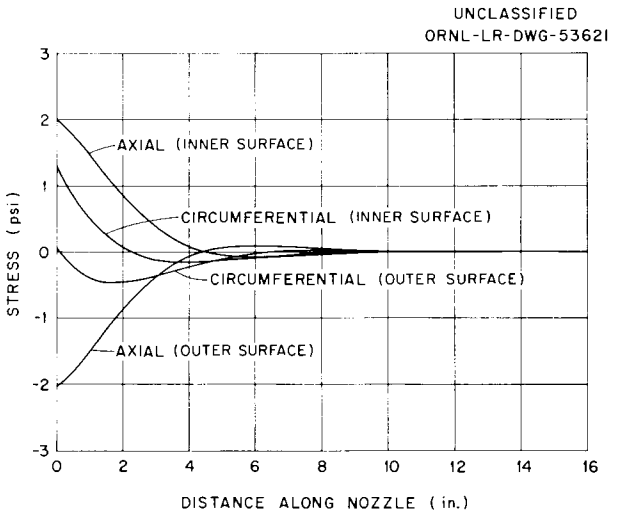

Fig. C.10. Principal Stresses (Theoretical) in the Interior Control Rod or Large Experimental Loop Nozzle from Axial Tensile Loading of 1 lb/in. Along Mean Circumference, Assuming a Single Nozzle-to-Shell Attachment.

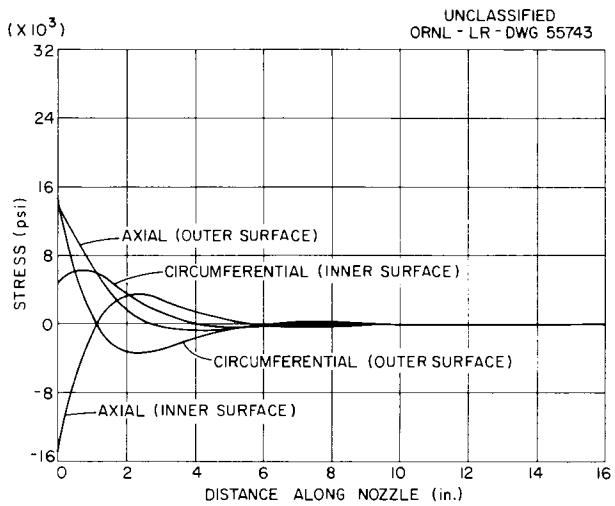

Fig. C.11. Principal Stresses (Theoretical) in the Interior Special Plug or Small Experimental Loop Nozzle from 350-psig Pressure Loading, Assuming a Single Nozzle-to-Shell Attachment.

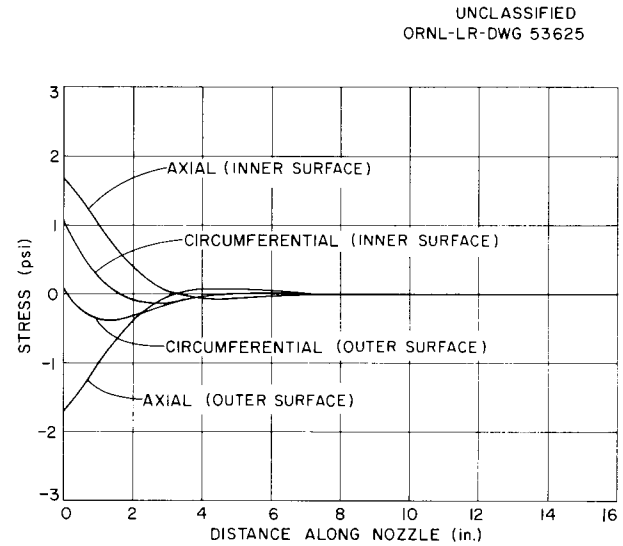

Fig. C.12. Principal Stresses (Theoretical) in the Interior Special Plug or Small Experimental Loop Nozzle from Axial Tensile Loading of 1 lb/in. Along Mean Circumference, Assuming a Single Nozzle-to-Shell Attachment.

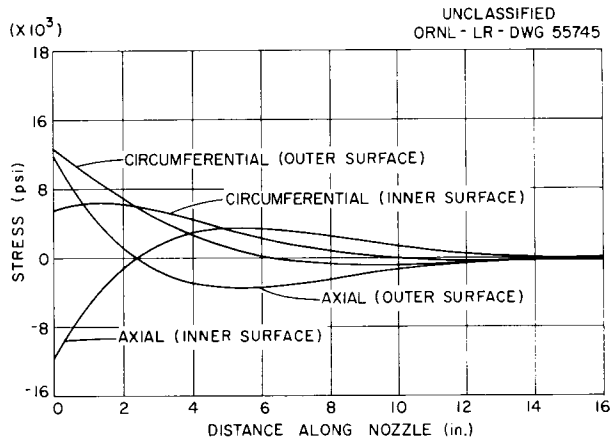

Fig. C.13. Principal Stresses (Theoretical) in the Interior Burst-Slug-Detection Nozzle from 350-psig Pressure Loading, Assuming a Single Nozzle-to-Shell Attachment.

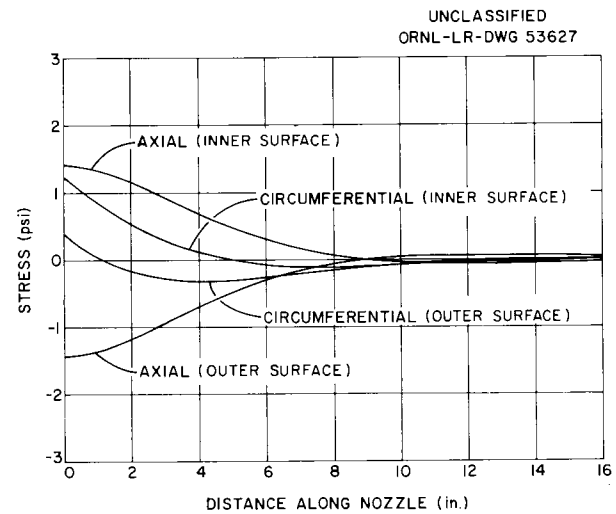

Fig. C.14. Principal Stresses (Theoretical) in the Interior Burst-Slug-Detection Nozzle from Axial Tensile Loading of 1 lb/in. Along Mean Circumference, Assuming a Single Nozzle-to-Shell Attachment.

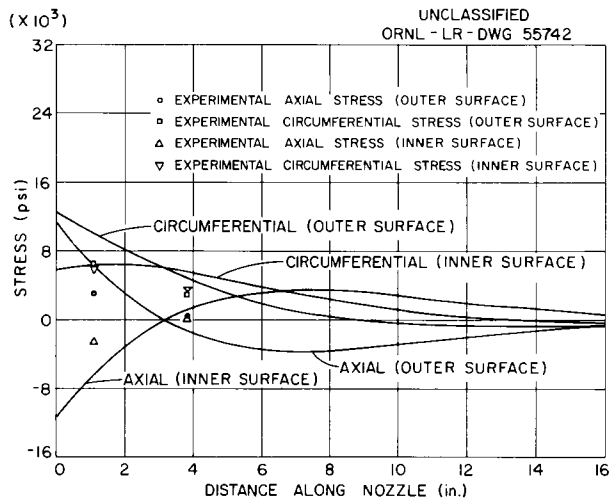

Fig. C.15. Principal Stresses (Theoretical) in the Interior Gas Outlet Nozzle from 350-psig Pressure Loading, Assuming a Single Nozzle-to-Shell Attachment.

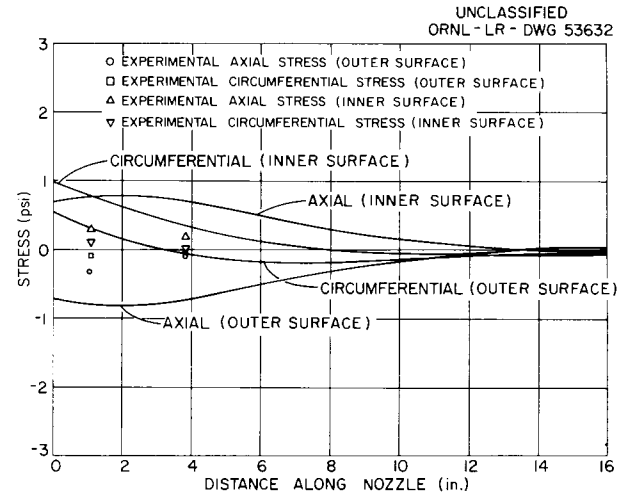

Fig. C.16. Principal Stresses (Theoretical) in the Interior Gas Outlet Nozzle from Axial Tensile Loading of 1 lb/in. Along Mean Circumference, Assuming a Single Nozzle-to-Shell Attachment.

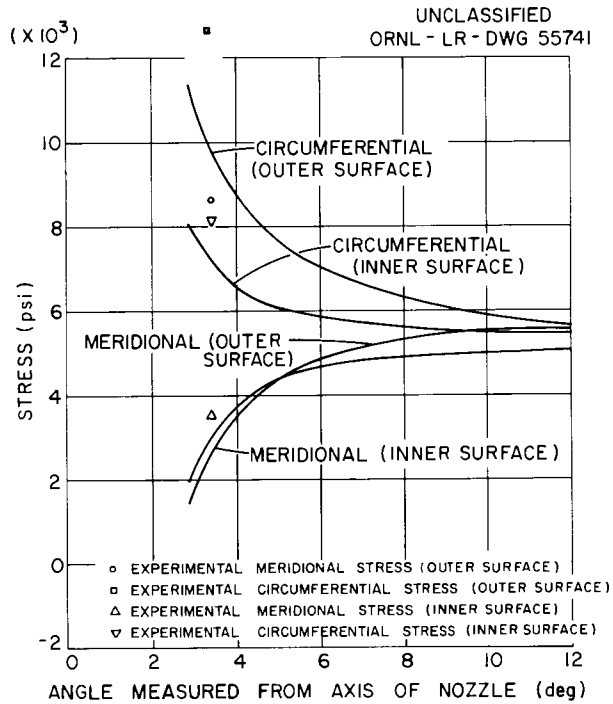

Fig. C.17. Principal Stresses (Theoretical) in Spherical Head Adjacent to Control Rod Nozzle from 350-psig Pressure Loading, Assuming a Single Nozzle-to-Shell Attachment.

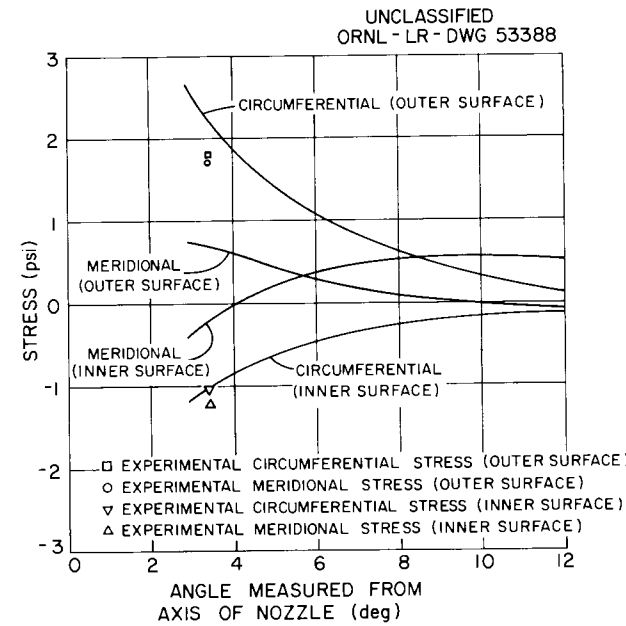

Fig. C.18. Principal Stresses (Theoretical) in Spherical Head Adjacent to Control Rod Nozzle with an Axial Loading on the Nozzle of 1 lb/in. on Mean Circumference, Assuming a Single Nozzle-to-Shell Attachment.

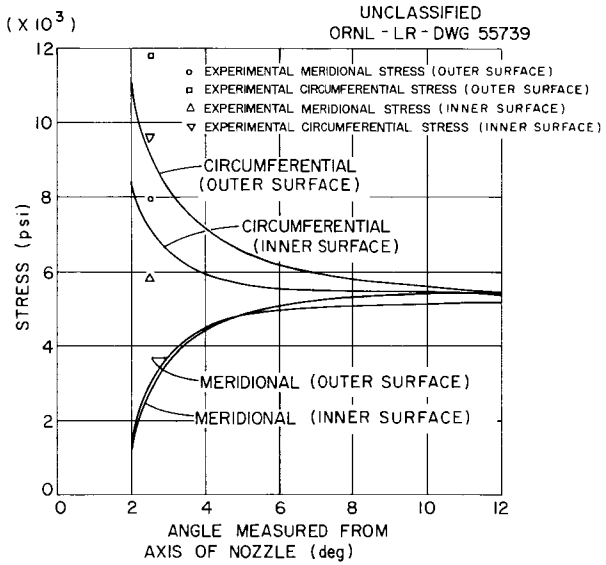

Fig. C.19. Principal Stresses (Theoretical) in Spherical Head Adjacent to Special Plug Nozzle from 350-psig Pressure Loading, Assuming a Single Nozzle-to-Shell Attachment.

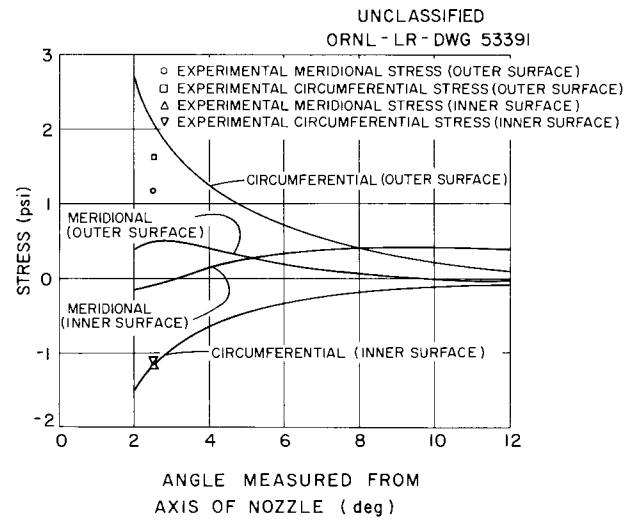

Fig. C.20. Principal Stresses (Theoretical) in Spherical Head Adjacent to Special Plug Nozzle with an Axial Load on the Nozzle of 1 lb/in. on Mean Circumference, Assuming a Single Nozzle-to-Shell Attachment.

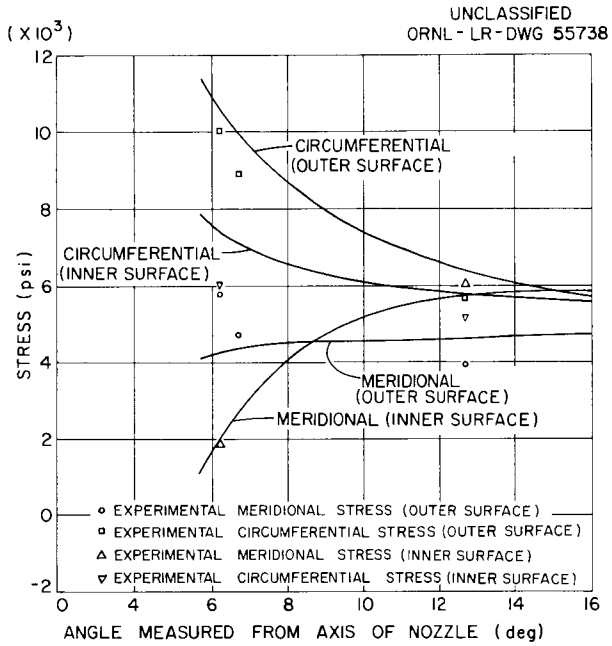

Fig. C.21. Principal Stresses (Theoretical) in Spherical Head Adjacent to Burst-Slug-Detection Nozzle from 350-psig Pressure Loading, Assuming a Single Nozzle-to-Shell Attachment.

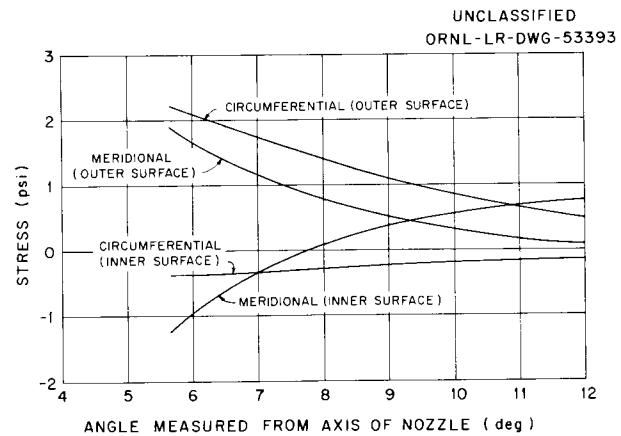

Fig. C.22. Principal Stresses (Theoretical) in Spherical Head Adjacent to Burst-Slug-Detection Nozzle with an Axial Tensile Loading on the Nozzle of 1 lb/in. on Mean Circumference, Assuming a Single Nozzle-to-Shell Attachment.

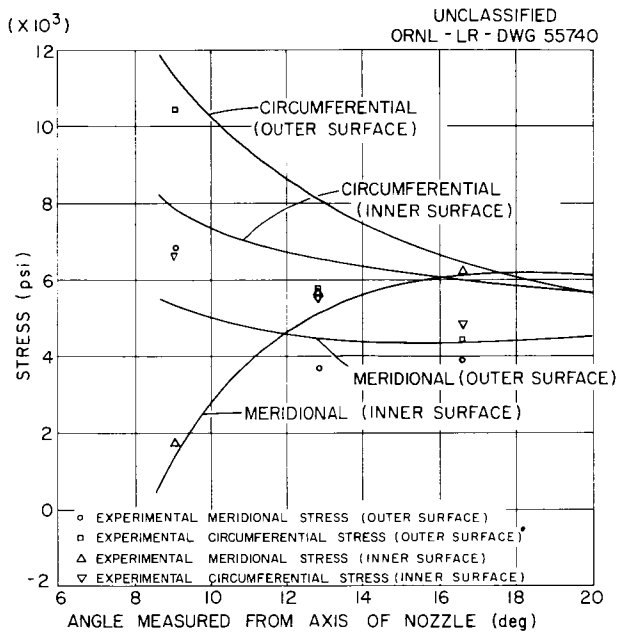

Fig. C.23. Principal Stresses (Theoretical) in Spherical Head Adjacent to Gas Outlet Nozzle from 350-psig Pressure Loading, Assuming a Single Nozzle-to-Shell Attachment.

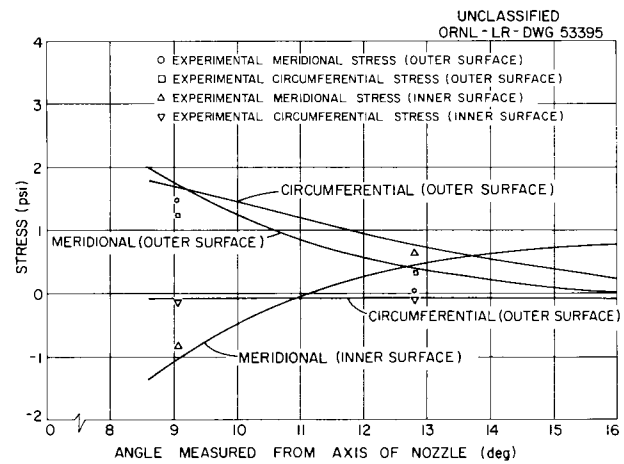

Fig. C.24. Principal Stresses (Theoretical) in Spherical Head Adjacent to Gas Outlet Nozzle with an Axial Loading on the Nozzle of 1 lb/in. on Mean Circumference, Assuming a Single Nozzle-to-Shell Attachment

ORNL-3157

UC-80—Reactor Technology
TID-4500 (16th ed.)

INTERNAL DISTRIBUTION

1. M. Bender
2. A. L. Boch
3. E. J. Breeding
4. R. H. Chapman
5. T. G. Chapman
6. R. D. Cheverton
7. J. M. Corum
8. D. A. Douglas
9. J. Foster
10. A. P. Fraas
11. C. H. Gabbard
12. D. R. Gilfillan
13-32. B. L. Greenstreet
33. P. R. Kasten
34. B. W. Kinyon
35-37. M. E. LaVerne
38. R. N. Lyon
39. H. G. MacPherson
40-41. W. D. Manly
42-51. R. L. Maxwell
52. T. J. Meador
53. S. E. Moore
54. C. A. Preskitt
55. G. C. Robinson
56. G. Samuels
57. A. W. Savolainen
58-61. L. R. Shobe
62-63. J. E. Smith
64. F. J. Stanek
65. J. R. Tallackson
66. J. R. Weir
67-86. F. J. Witt
87-156. Laboratory Records Department
157. Laboratory Records Department, ORNL R.C.
158-161. ORNL-Y-12 Technical Library, Document Reference Section
162-164. Central Research Library

EXTERNAL DISTRIBUTION

165. J. F. Bailey, University of Tennessee
166-168. W. F. Banks, Allis-Chalmers Mfg. Co.
169. E. O. Bergman, National Engineering Science Co., Pasadena, Calif.
170. C. W. Brown, University of Tennessee
171-173. P. D. Bush, Kaiser Engineers
174. A. I. Chalfant, General Atomic
175-176. D. F. Cope, AEC, ORO
177-178. R. W. Coyle, Vallecitos Atomic Laboratory
179. E. Creutz, General Atomic
180. W. E. Crowe, Los Alamos Scientific Laboratory
181-183. R. B. Duffield, General Atomic
184. E. Esztergar, Kaiser Engineers
185. E. S. Fabian, University of Tennessee
186. D. H. Fax, Westinghouse Atomic Power Division
187. C. Fisher, University of Tennessee
188. A. T. Granger, University of Tennessee
189-191. R. W. Holland, University of Tennessee
192-197. L. H. Jackson, AEC, ORO

198. T. Jarvis, Ford Instrument Co.
199. Richard Kirkpatrick, AEC, Washington
200. B. F. Langer, Bettis Plant, Westinghouse
201-202. H. Lichtenburger, General Nuclear Engineering Corp.
203. J. P. McGee, Bureau of Mines, Appalachian Experiment Station
204. R. V. Meghreblian, Jet Propulsion Laboratory
205. R. L. Miller, Kaiser Engineers
206. M. Milligan, University of Tennessee
207. S. G. Nordlinger, AEC, Washington
208. H. B. Rahner, Savannah River Operations Office
209. Corwin Rickard, General Atomic
210. S. T. Robinson, Sanderson & Porter
211. W. Satler, University of Tennessee
212. M. T. Simnad, General Atomic
213. H. L. Snider, Lockheed Aircraft Corp., Marietta, Georgia
214. Nathanial Stetson, Savannah River Operations Office
215. Donald Stewart, AEC, Washington
216. G. W. Tompkin, Mallinckrodt Nuclear Corporation
217. K. N. Tong, Syracuse University
218. Phillip L. Walker, Pennsylvania State University
219. R. E. Watt, Los Alamos Scientific Laboratory
220-221. W. L. Webb, East Central Nuclear Group, Inc.
222. C. Wilson, University of Tennessee
223. Division of Research and Development, AEC, ORO
224-825. Given distribution as shown in TID-4500 (16th ed.) under Reactor Technology Category (75 copies – OTS)